AFAPL-TR-75-43

12

HIGH POWER DENSITY FUEL CELL FOR AIRCRAFT HIGH POWER

UNITED TECHNOLOGIES CORPORATION
POWER SYSTEMS DIVISION
SOUTH WINDSOR ENGINEERING FACILITY
BOX 109, GOVERNORS HIGHWAY
SOUTH WINDSOR, CONNECTICUT 06074

MAY 1975

TECHNICAL REPORT AFAPL-TR-75-43

FINAL REPORT FOR PERIOD 1 APRIL 1972 -- 31 MARCH 1975

AIR FORCE AERO PROPULSION LABORATORY
AIR FORCE SYSTEMS COMMAND
WRIGHT-PATTERSON AIR FORCE BASE, OHIO 45433

NOTICE

When Government drawings, specifications, or other data are used for any purpose other than in connection with a definitely related Government procurement operation, the United States Government thereby incurs no responsibility nor any obligation whatsoever; and the fact that the government may have formulated, furnished, or in any way supplied the said drawings, specifications, or other data, is not to be regarded by implication or otherwise as in any manner licensing the holder or any other person or corporation, or conveying any rights or permission to manufacture, use, or sell any patented invention that may in any way be related thereto.

This final report was submitted by United Technologies Corporation, Power Systems Division, South Windsor, Connecticut under Contract F33615-72-C-1371. This effort was sponsored by the Air Force Aero Propulsion Laboratory, Air Force Systems Command, Wright-Patterson AFB, Ohio under Project Number 3145, Task Number 314521 and Work Unit 31452122 with Don R. Warnock, POE-1 as Scientist in charge. Mssrs. W. F. Bell, L. M. Handley, W. J. Maio, A. P. Meyer, J. C. Pivar, and J. K. Stedman of United's staff contributed to this work.

This report has been reviewed by the Information Office (ASD/OIP) and is releasable to the National Technical Information Service (NTIS). At NTIS, it will be available to the general public, including foreign nations.

This technical report has been reviewed and is approved for publication.

Don R. Warnock

DON R. WARNOCK,
Scientist

FOR THE COMMANDER

Donald P. Mortel

DONALD P. MORTEL
Technical Area Manager

Copies of this report should not be returned unless return is required by security considerations, contractual obligations, or notice on a specific document.

Unclassified
SECURITY CLASSIFICATION OF THIS PAGE (When Data Entered)

REPORT DOCUMENTATION PAGE

READ INSTRUCTIONS BEFORE COMPLETING FORM

1. REPORT NUMBER: AFAPL-TR-75-43	2. GOVT ACCESSION NO.
3. RECIPIENT'S CATALOG NUMBER	
4. TITLE (and Subtitle): High Power Density Fuel Cell for Aircraft High Power	5. TYPE OF REPORT & PERIOD COVERED: Final Report 1 Apr 72 – 31 Mar 75
6. PERFORMING ORG. REPORT NUMBER: FCR-0003	
7. AUTHOR(s): Alfred P. Meyer, William F. Bell	8. CONTRACT OR GRANT NUMBER(s): F33615-72-C-1371
9. PERFORMING ORGANIZATION NAME AND ADDRESS: United Technology Corporation, Power Systems Division, South Windsor Engineering Facility, Box 109, Governors Highway, South Windsor, Ct. 06074	10. PROGRAM ELEMENT, PROJECT, TASK AREA & WORK UNIT NUMBERS: Project Number 3145, Task Number 314521, Work Unit 31452122
11. CONTROLLING OFFICE NAME AND ADDRESS: Air Force Aero Propulsion Laboratory, POE-1, Wright-Patterson AFB, Ohio 45433	12. REPORT DATE: May 1975
	13. NUMBER OF PAGES: 233 (250 pp)
14. MONITORING AGENCY NAME & ADDRESS (if different from Controlling Office)	15. SECURITY CLASS. (of this report): Unclassified
	15a. DECLASSIFICATION/DOWNGRADING SCHEDULE

16. DISTRIBUTION STATEMENT (of this Report)

Approved for Public Release; Distribution Unlimited

17. DISTRIBUTION STATEMENT (of the abstract entered in Block 20, if different from Report)

18. SUPPLEMENTARY NOTES

19. KEY WORDS (Continue on reverse side if necessary and identify by block number)

20. ABSTRACT (Continue on reverse side if necessary and identify by block number)

Pratt & Whitney Aircraft has conducted an analytical and experimental program which demonstrated the feasibility of an ultra-lightweight fuel cell powerplant, with a specific weight of less than 0.5 lb/kw, for advanced aircraft applications. Full-scale single cells and 12-cell development units, the basic modular repeating subsection of which a complete powerplant is assembled, were constructed and successfully tested. Power densities up to 3000 watts/ft^2 were demonstrated; this level is almost 50 percent greater than that required for a competitive flightweight system. Endurance tests demonstrated an operating capability in excess of 600 baseline missions. Several complete power systems based on the

→OVER

DD FORM 1 JAN 73 1473 EDITION OF 1 NOV 65 IS OBSOLETE

Unclassified
SECURITY CLASSIFICATION OF THIS PAGE (When Data Entered)

409 412

as-demonstrated performance were defined. These systems included all equipment required for a flight operational installation; i.e., powerplants, a reactant supply system, and a cooling water supply system. Each offers the advantages of instant "on-off" power supply capability and modular design. Modular design provides the flexibility to meet a broad range of Air Force mission requirements without adverse impact on performance or development schedule and cost.

CONTENTS

CONTENTS (CONT'D)

ILLUSTRATIONS

ILLUSTRATIONS (CONT'D.)

ILLUSTRATIONS (CONT'D)

ILLUSTRATIONS (CONT'D.)

ILLUSTRATIONS (CONT'D.)

ILLUSTRATIONS (CONT'D.)

ILLUSTRATIONS (CONT'D.)

ILLUSTRATIONS (CONT'D.)

ILLUSTRATIONS (CONT'D.)

TABLES

TABLES (CONT'D.)

I. INTRODUCTION

The Air Force Aero Propulsion Laboratory has begun development of an ultra-lightweight fuel cell system for the supply of high-power short-duration electrical loads in advanced aircraft applications. This program was undertaken following conceptual studies which had shown a high power density fuel cell system could supply megawatts of power from a compact low weight package and offered other important advantages as well. These advantages include: capability to supply either continuous or pulsed high voltage power directly from the fuel cell; modularity of design, which provides flexibility during development and capability to easily adapt to changes in operational power output or installation requirements; quiet, vibration-free operation at low temperature; no high torques; instant on-off capability; negligible idle requirements; and long operating life.

When mission durations are short, 30 to 120 seconds, powerplant weight, not the weight of consumables, is the dominant component of total system weight. This provides a strong incentive to minimize powerplant specific weight. As a result, the program's Statement-of-Work specifically called for: "development and a demonstration of the significant features of a hydrogen-oxygen fuel cell powerplant having a specific weight of 0.5 lb/kw or less". In addition, Reference System Designs, to be used to evaluate the merits of the fuel cell at the application level, were also required. These designs were to represent a flight-ready system including all consumables and tankage required for the supply of megawatts of power for periods of seconds to minutes.

The key to achieving a powerplant weight of 0.5 lb/kw or less was a lightweight evaporatively-cooled alkaline fuel cell operated at high power density. Each of these features, lightweight cell construction, evaporative cooling, and high power density operation had been demonstrated or was being explored and developed individually in Pratt & Whitney Aircraft's technology efforts sponsored by AFAPL and the NASA Lewis Research Center. A power output of 2.0 kw/ft^2 of cell area had been demonstrated in a conventional cell in P&WA's previous AFAPL high power density fuel cell program. Lightweight cells with a weight objective of 0.75 lb/ft^2 of cell area were being developed in the NASA-LeRC program. Both programs were exploring evaporative cooling. Consequently, a specific cell weight, (lb/kw), the ratio of weight per unit of cell area (lb/ft^2) to power output per unit of cell area (kw/ft^2), of 0.375 lb/kw appeared feasible. With an allowance of 20 to 33 percent additional weight for accessory components a powerplant specific weight of 0.5 lb/kw was a reasonable goal.

Although the power system explored under this program is unique in some of its subsystem concepts and the power density at which cells are operated, it remains an electrochemical power source in which individual cells are connected in series/parallel electrical arrangements to provide the desired system power and voltage. The fundamental system element, the cell, functions as it does in all other fuel cell systems: A fuel and an oxidant react in the cell to produce electric power, waste heat, and chemical products of reaction. For this system, the fuel and oxidant (reactants) are hydrogen and oxygen respectively. Figure 1 is a schematic representation of this cell showing the overall reactions which occur at the electrodes. At the anode, hydrogen reacts with hydroxyl ions from the aqueous potassium hydroxide

electrolyte to form water and release electrons. At the cathode, oxygen reacts with electrons and water from the electrolyte to form more hydroxyl ions. Since more water is produced at the anode than is consumed at the cathode, the excess water must be removed if the cell is to operate for long periods at a time. For short periods, a few minutes or less, the water may be stored in the electrolyte. Waste heat is removed by vaporizing cooling water in compartments adjacent to the cells.

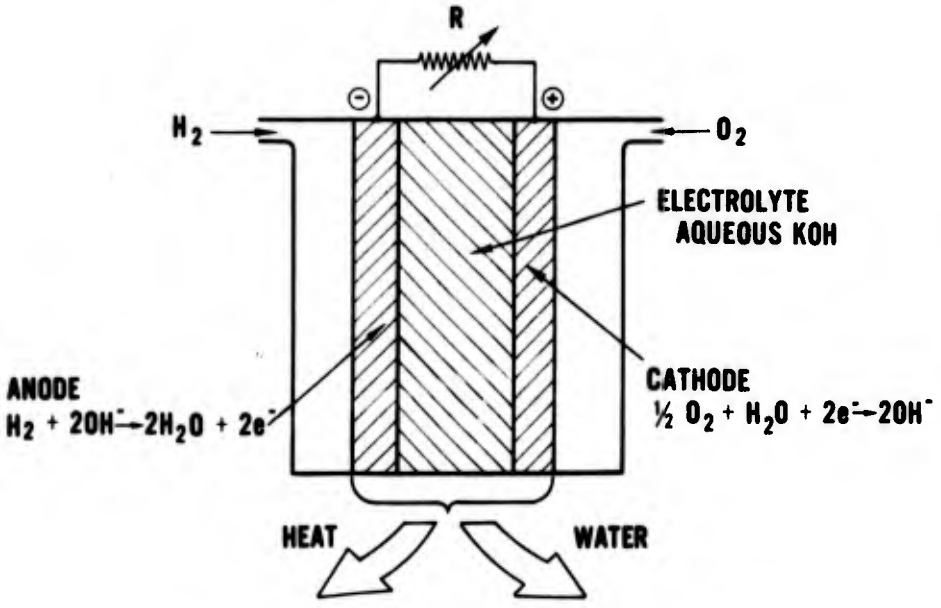

Figure 1 – Hydrogen-Oxygen Fuel Cell Concept

Physically, each cell consists of two catalyzed screen electrodes separated by a thin sheet of porous asbestos separator. The separator is soaked with an aqueous solution of potassium-hydroxide electrolyte which it retains by capillary action. Porous electrolyte reservoir plates adjacent to the anodes absorb the expansion of electrolyte caused by stored product water.

The output voltage of each cell is between 0.5 and 1.0 volt depending upon load level. To obtain high total voltage from a low unit cell voltage requires a large number of small cells. An efficient way of packaging these cells is to place several small cells in series in a single planar structure, (called a plaque), of a size that is convenient from a manufacturing standpoint. A cross section of a plaque showing the arrangement of cells is provided in Figure 2. Because the cells are electrically connected in series in a plaque, the output voltage of the plaque is equal to the product of the number of cells in the plaque and the individual cell voltages. Each plaque also contains manifold holes for reactants and coolant. Two such cell plaques are shown in Figure 3 along with a cooler which is sandwiched between them. The cooler contains the passages in which water is vaporized to cool the adjacent cell plaques. An assembly consisting of two 6-cell plaques and a cooler plaque is the basic repeating subsection of a cell stack, and is called a development unit. It contains the major structural, electrical, and thermal technology required for full size powerplants.

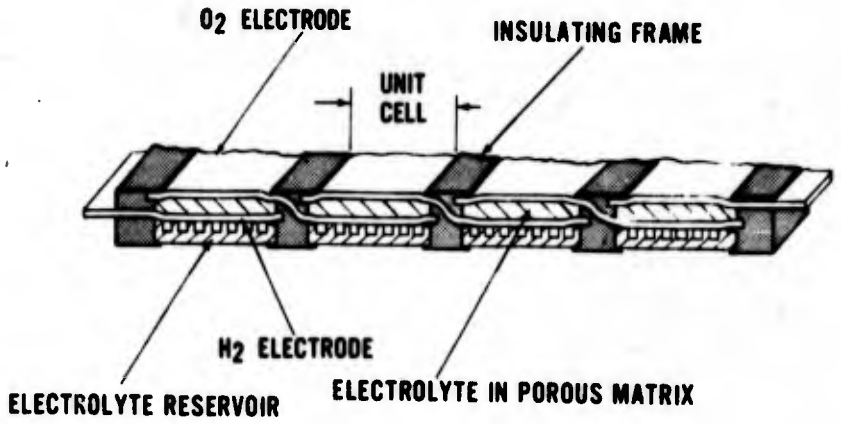

Figure 2 – Plaque Construction

TWO 6-CELL PLAQUES SEPARATED BY COOLER ASSEMBLY

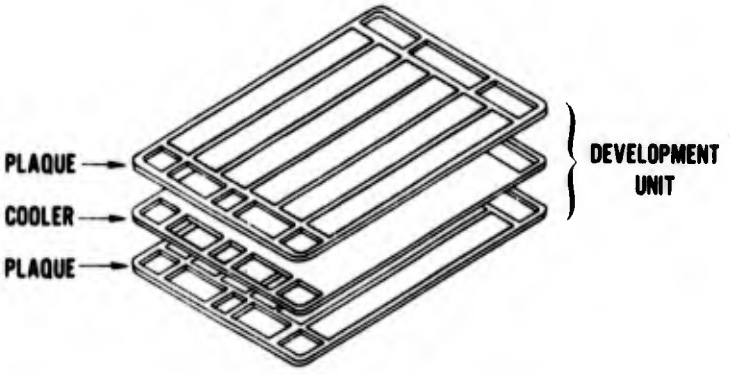

Figure 3 – Development Unit

A typical powerplant (see Figure 4) contains a stack of development units connected electrically in series. There is an accessory section on one end of the stack which houses electrical and fluid control accessories and plumbing connections to the reactant supply subsystem. Many current-voltage combinations are possible by changing to series-parallel connections between plaques. At the system level there is freedom in the series-parallel connection of powerplants. The rated output of this powerplant is 575 kw (0.575 Mw).

The program was begun using the high power density cell configuration developed in the previous AFAPL program. It was combined with the NASA-LeRC developed "strip cell" to produce a lightweight high power density cell. Simultaneously, development of lightweight evaporative coolers was begun. Eventually coolers were combined with 6-cell plaques to form development units. Development units were then tested to demonstrate perform-

ance levels required by the powerplant. Because the final powerplant is assembled of these modular units their measured weight and performance can be used to accurately verify that a powerplant with a weight of 0.5 lb/kw can be achieved.

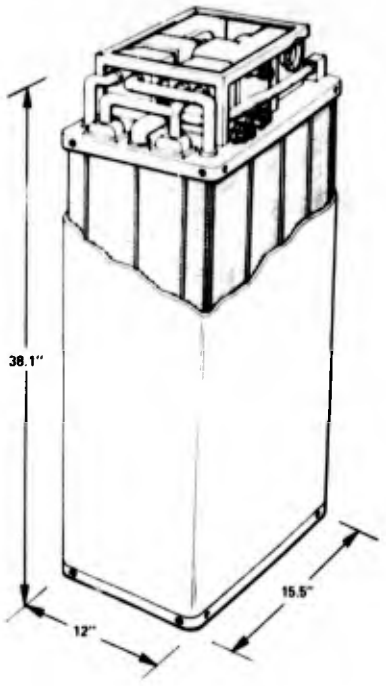

Figure 4 – 575-kw Powerplant

Several Reference System Designs, based on demonstrated performance, were prepared during the program. They were updated as Air Force mission requirements changed and as warranted by improved performance. The Reference System, Figure 5, is comprised of three major subsystems: a powerplant subsystem, a reactant supply subsystem, and a cooling water supply subsystem. The reactant supply also provides a pressure source to force cooling water from the water tank into the powerplant cooling system. The power level of the application determines the size and weight of the powerplant subsystem. The operating time determines the size and weight of the supply subsystem.

The work accomplished under this program and the conclusions reached are summarized in Section II of this report. Section III discusses the Reference System Designs in detail and presents the major analytical studies conducted in support of the development efforts. Section IV describes the development efforts beginning with single cell tests and continues through the successful testing of development units.

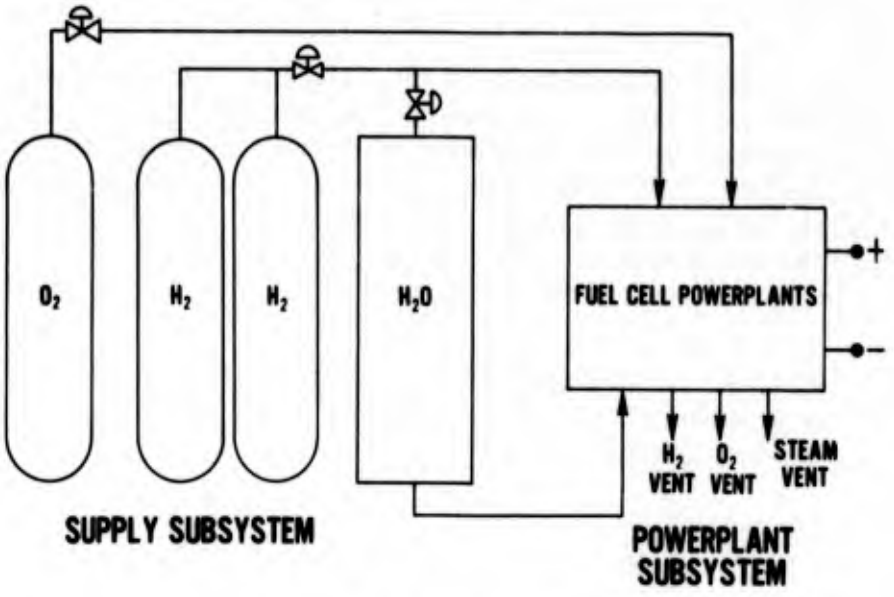

Figure 5 – Fuel Cell System Schematic

II SUMMARY

Pratt & Whitney Aircraft has conducted an exploratory program to establish a technical foundation for the development of an ultra-lightweight fuel cell power system. This system is designed for use in advanced aircraft for the supply of short-duration high-power loads. The key program objective, the demonstration by test of the feasibility of a powerplant with a specific weight of 0.5 lb/kw, was achieved. Several complete Reference System designs, for installation in advanced aircraft, were prepared based directly on the as-demonstrated test data. The primary conclusions of the program are:

1) Test demonstrations have shown that no breakthroughs are required to reduce the demonstrated hardware to prototype and then flight-ready powerplants and power systems.

2) Demonstration of power densities to 3000 watts/ft^2 has shown that the Reference System design power density of 2150 watts/ft^2 is realistic and conservative.

3) Test demonstrations have shown that the fuel cell has a useful life of at least 300 missions and probably more than 600 missions.

4) Design studies have shown that the fuel cell is competitive in advanced aircraft installations.

5) Design studies have shown that fuel cell system weight and volume do not increase rapidly as mission energy delivery and duration grow.

6) Test demonstrations and the design studies show the fuel cell possesses significant potential for development of still lighter powerplants and power systems.

Development and Demonstration Program

Development work was conducted at the cell and development unit level. The development unit is a 6-or 12-cell full-scale repeating modular subsection of a powerplant. The cell is the fundamental component of the development unit. The development approach was to progress through four successive cell configurations, each lighter then its predecessor, to reach a configuration which, when incorporated into a powerplant, would yield a weight of less than 0.5 lb/kw. As each configuration was proven, it was incorporated into a development unit and proven as a powerplant subsection. Figure 6 shows the steady development progress made during the program. The data shows cell tests demonstrated an equivalent powerplant weight of 0.42 lb/kw. This result betters the objective of 0.5 lb/kw by 16 percent. Later, when development units incorporating these successively lighter cells were tested, comparable equivalent powerplant weights were demonstrated. Each development unit was complete with manifolding and coolers as it would be assembled into a powerplant. The last development unit, based on a Configuration 3 cell, demonstrated an equivalent weight of 0.7 lb/kw. Schedule prevented incorporating the lightest cell design, Configuration 4, into a development unit. This would be accomplished as the first step in any future effort.

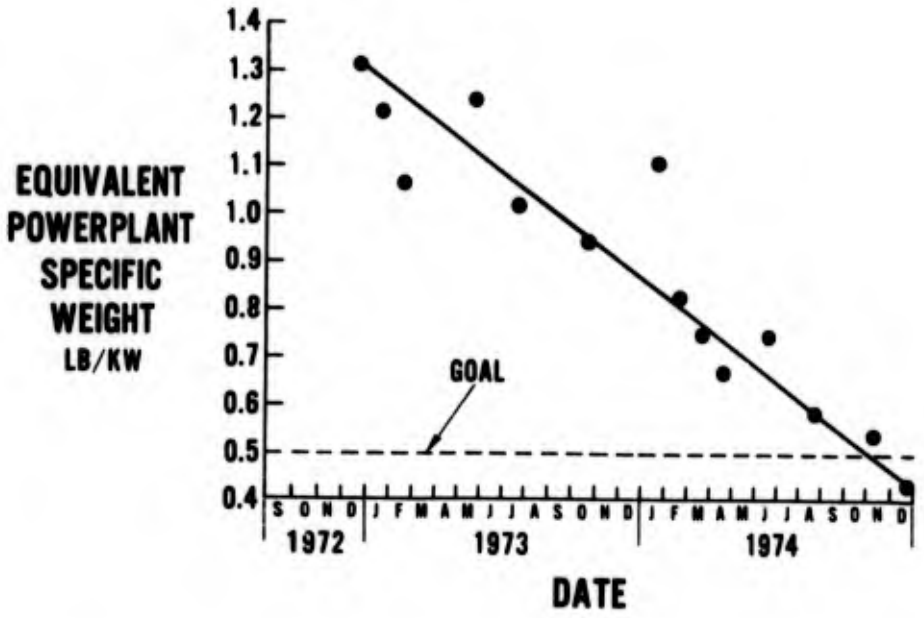

Figure 6 – Low Specific Weight Has Been Demonstrated by Cell Testing

Both the single cells and development units repeatedly demonstrated power densities at powerplant operating conditions equal to or exceeding the Reference System design power density of 2150 watts/ft^2. Figure 7 shows the performance curves demonstrated by the last three cells tested; each was of the lightest design, Configuration 4. Endurance capability was demonstrated to verify that the power system is reusable. A full-size lightweight cell was operated for more than five hours at 3000 amperes/ft^2 or higher. Half of this operation was continuous; the rest was obtained in a cycling mode of two seconds on-two seconds off. The cell completed 4600 of these cycles. The time at high power density was equivalent to 620 30-second missions. Figure 8 shows the performance history of another full-size lightweight cell subjected to 3000 cycles of three seconds on-two seconds off, for a total of 150 minutes on load (300 30-second missions). The load was set initially at 3200 amperes/ft^2. Midway through the run it was increased to 3600 amperes/ft^2. Power density on load all during the last half was above the design condition of 2150 watts/ft^2 and reached 2320 watts/ft^2 at 2400 cycles. Development units have also undergone preliminary endurance tests with good results. A full-size 6-cell plaque with cooler completed 55 missions, and a 12-cell development unit was subjected to 27 thermal cycles and 10 simulated missions.

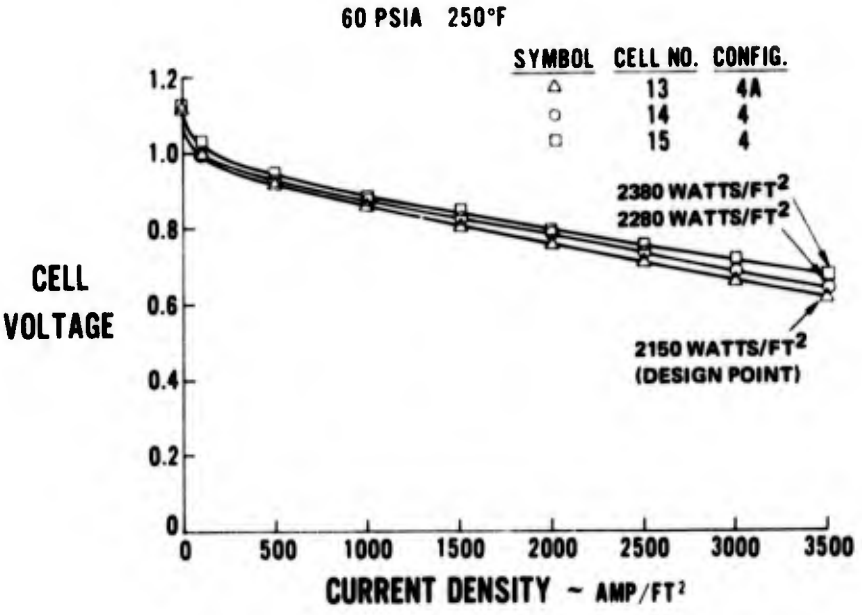

Figure 7 – Cell Power Density Has Been Demonstrated

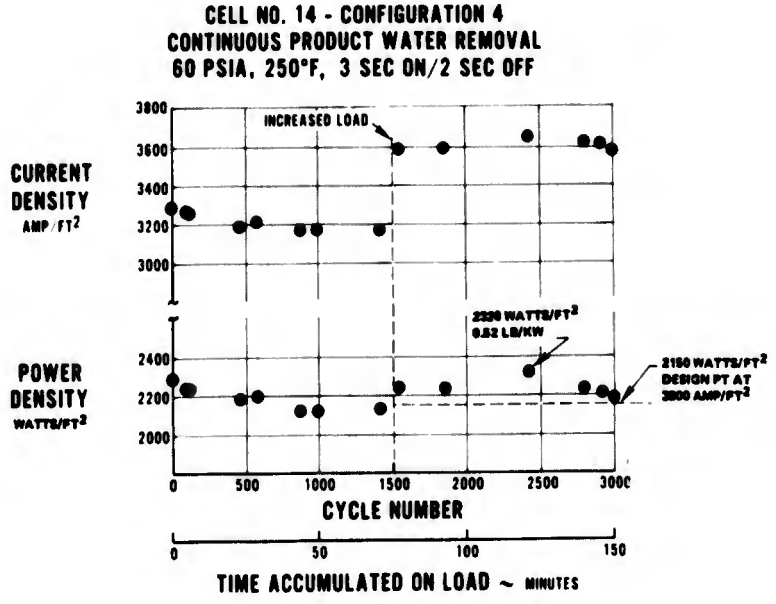

Figure 8 – Demonstration of 300-Mission Capability

Almost all of the testing has been conducted at a reactant pressure within the cell stack of 60 psia; the pressure assumed for the Reference System studies. However, higher pressure yields higher cell performance at high current density. Cell 15 was operated at a pressure of 90 psia, 50 percent higher than the design level. The results were extraordinary: much higher

power densities at relatively high voltages. Comparison of the highest performance of this cell with the baseline cell performance used in the Reference System design shows the significance of this test:

	Reference System	Cell 15
Operating Pressure, psia	60	90
Current Density, amperes/ft^2	3500	5000
Cell Voltage	0.615	0.600
Cell Power Density, watts/ft^2	2150	3000

This increase in power density could reduce powerplant weight by almost one-third. Consequently higher operating pressures are a major avenue for reduction of the Reference System weights below their already competitive levels.

Reference System Design

The Reference System designs were prepared to provide a yardstick by which to assess the benefit and potential of the fuel cell at the ultimate level – aircraft application and installation. Figure 9 shows a scale sketch of the volume envelope for one of the designs; a 4-megawatt, 30-second-duration power system. It consists of seven 575-kw powerplants, connected in series to get the desired power and voltage, and reactant and cooling water supply subsystems. To minimize the system envelope, the space between and around the hydrogen cylinders is used for cooling water storage. Hydrogen and oxygen are stored at 3000 psia. This compact rectangular arrangement is known as the Reference System and serves as a point of comparison with other system configurations. The volume of the Reference System is 42.9 cubic feet. The total weight, including reactants and cooling water, is estimated to be 2815 pounds.

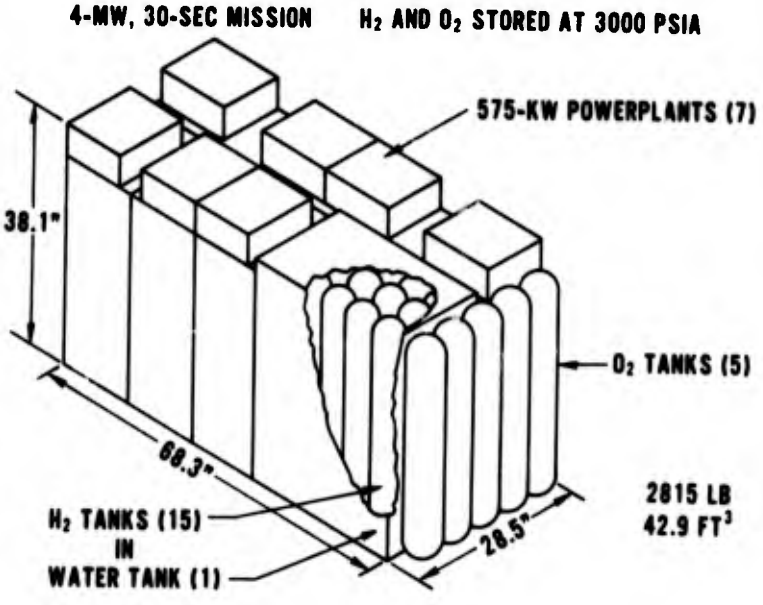

Figure 9 – Compact Packaging Arrangement

The Reference System is based on the 575-kw powerplant shown in Figure 10. This powerplant contains a stack of 195 development units connected electrically in series. There is an accessory section on one end of the stack which houses electrical and fluid control accessories and plumbing connections to the supply subsystem. The powerplant weighs 295 pounds, has dimensions of 12 x 15.5 x 38.1 inches, and occupies 4.0 cubic feet. It provides 400 amperes at 1435 volts. Other current-voltage combinations are possible by changing to series-parallel connections between plaques. At the system level there is freedom in the series-parallel connection of powerplants.

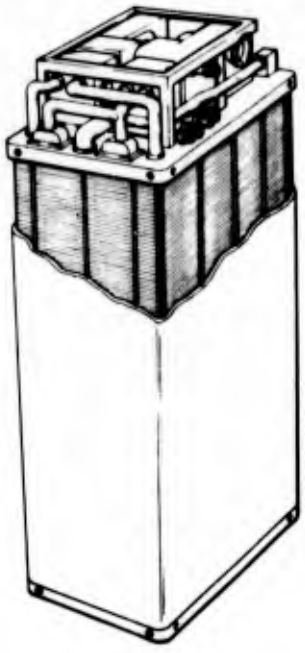

Figure 10 –
575-kw Powerplant

The fuel cell is readily adaptable to operating times longer than that of the 30-second Reference System. Figure 11 shows a typical packaging arrangement for a 4-megawatt system capable of 120 seconds of high power operation per mission. Reactants are again stored as gases at 3000 psia. Although the electrical energy supplied to the load is four times that of the Reference System, the system weight and volume are less than twice as great. Therefore energy density, both watt-hours per pound and watt-hours per ft^3, goes up by at least a factor of two as a result of the four-fold increase in mission duration. Energy density continues to improve as mission duration increases beyond 120 seconds. If Air Force mission requirements grow, the fuel cell will be able to grow with minimum impact on the host vehicle.

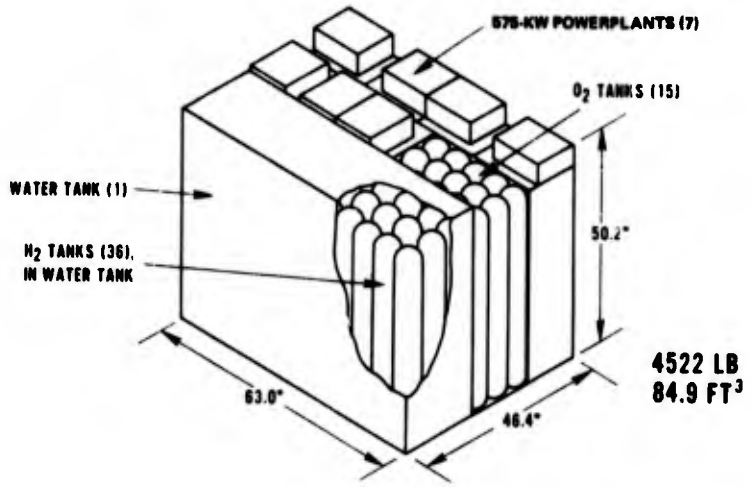

Figure 11 – Typical Packaging Arrangement for 120-Second Mission

Although differences in host vehicles may require modification of service and supply requirements, the operating characteristics of each of the systems is essentially the same. They are:

Response to Load – Instantaneous, system voltage drops to full-load power delivery voltage within a few milliseconds if load characteristics permit. Unaffected by either continuous or pulsed load.

Startup Time – 10 to 30 minutes, depends on startup power available; 35 kw required for 20-minute startup.

Idle Operation – No reactant requirement, 1 kw required to keep powerplants at operating temperature.

Refueling – Safe and rapid · Reactant tanks are removed as unit from aircraft. Requires disconnection of low pressure lines only. Water tanks refilled in situ.

Life/Maintenance – At least 300 30-second missions. System does not require removal from aircraft for maintenance within 300 mission period.

Safety – No shock hazard during servicing or after mission. Residual voltage reduced to zero by purging reactant passages with an inert gas and dissipating potential through a shunt.

Installation Flexibility – Modularity permits tailoring packaged envelope to any vehicle.

Installation Simplicity – No noise and vibration, no torques produced during operation, no high operating temperature, no significant exhaust, all permit simple installation in any vehicle.

III SYSTEM DEFINITION STUDIES

A. INTRODUCTION

The system definition studies had four objectives: 1) to prepare and maintain a Reference System Design for a 4-MW fuel cell power system, 2) to size and define the fuel cell modules of the Reference System, 3) to design the basic repeating fuel cell unit of the module to be developed under this program, and 4) to define and evaluate heat removal concepts that were alternatives to the originally proposed evaporative cooling system.

The Reference System was defined as a complete system including fuel cell modules with their associated controls, reactant storage vessels, and cooling water storage vessels. The design was based on cell performance demonstrated during the course of the program. Storage of reactants as gases and as cryogens was investigated. Packaging arrangements for an aircraft pallet installation and in a compact rectangular envelope were defined.

Fuel cell powerplants of 500 and 575-kw output were sized and designed for the Reference System. Although the 575-kw powerplant was selected for incorporation into the Reference System, both powerplants were based on the same repeating fuel cell unit, consisting of a cooler and two 6-cell plaques. As part of this work, the planforms for plaques and cooler, including their internal flow geometry, were defined, their thermal and structural characteristics were analyzed, and alternative cell configurations were evaluated.

The alternate heat rejection concept evaluated, in addition to the evaporative cooling approach originally proposed, was a ram-air cooled heat exchanger.

The work completed in each of these areas is described below.

B. REFERENCE SYSTEM DEVELOPMENT

1. Baseline Systems

Five complete fuel cell power systems tailored to specific missions and installations were developed in the course of the program. The mission requirements as defined by the Air Force Project Engineer are listed in Table I. These requirements, updated during the program as missions became better defined, reflect the current requirements of the application. Three packaging arrangements in a compact rectangular configuration and two packaging arrangements for installation in an aircraft pallet were defined. The differences between the configurations for these installations is the manner in which reactants are stored.

One packaging arrangement for each installation is based on a hydrogen storage pressure at 10,000 psi and another on a storage pressure of 3,000 psi. The oxygen storage pressure for all systems is 3,000 psi. A rectangular packaging arrangement with cryogenic reactant storage was also defined.

TABLE I

MISSION REQUIREMENTS

Power Level	4 MW
Power Delivery Period	30-120 seconds
Power Delivery Mode	Pulsed or continuous
Pulse Repetition Rate	500 pulses per second to continuous
Voltage	5000-50,000 volts
Mission Time	1-2 hours
Operating Life	300 missions
Fuel Cell Module Weight/Power Ratio	0.5 lb/kw or less
Waste Heat Rejection	Open or closed cycle

Rectangular packaging arrangements (1) and (2) with 10,000 psi and 3,000 psi hydrogen storage are shown in Figures 12 and 13. Pallet packaging arrangements (1) and (2) are shown in Figures 14 and 15. The rectangular packaging arrangement with cryogenic reactant storage is shown in Figure 16. Each package includes seven 575-kw powerplants, a reactant storage system, cooling water storage tanks, and the plumbing and cabling required to interconnect the elements of the system. The reactant and cooling water tanks are sized to provide power delivery for a reference mission of 30-seconds duration. The hydrogen storage tanks are located within the water storage tank in rectangular arrangement (2), Figure 13 to improve packaging. This feature does not appreciably improve the packaging of rectangular arrangement (1). Tables II and III present the weights and volumes of the component parts of the rectangular packages. Tables IV and V present the same data for the pallet arrangements. For both the pallet and rectangular configuration packages decreasing the hydrogen storage pressure from 10,000 to 3,000 psia has little effect on system weight or volume, see Table VI. Consequently the systems with the lower hydrogen storage pressure are recommended as baseline systems. Table VII presents the weight and volume of the compact packaging system with cryogenic storage of reactants.

These systems weights and volumes are based on operating the powerplants at a power density of 2150 WSF (0.615v at 3500 ASF). This power density was demonstrated by tests of both development units, the basic repeating unit of which the powerplant is assembled, and single cells. However, much higher power densities, up to 3000 WSF, were also demonstrated. If the powerplants were redesigned at a high power density the weights and volumes of the power system would be reduced significantly. Figure 17 shows this effect. These data are based on a fixed operating current density of 3500 ASF which implies improved individual cell voltages. Higher cell voltages can be achieved by raising operating pressure. Figure 18 shows the benefit of raising operating pressure from 60 psia to 100 psia. Based on this data, if the powerplants were redesigned at a power density of 2700 WSF, the rectangular package

system weight would be reduced by 12 percent and system volume would be reduced by 14 percent. Table VIII presents the weights and volumes of the system at both 60 and 100 psia operating pressures.

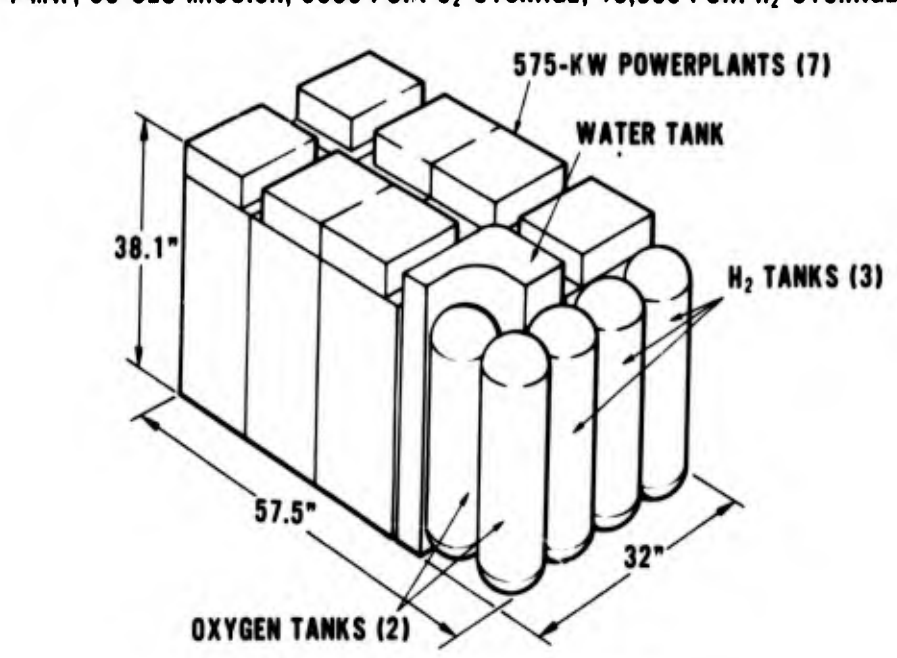

Figure 12 – Compact Packaging Arrangement (1)

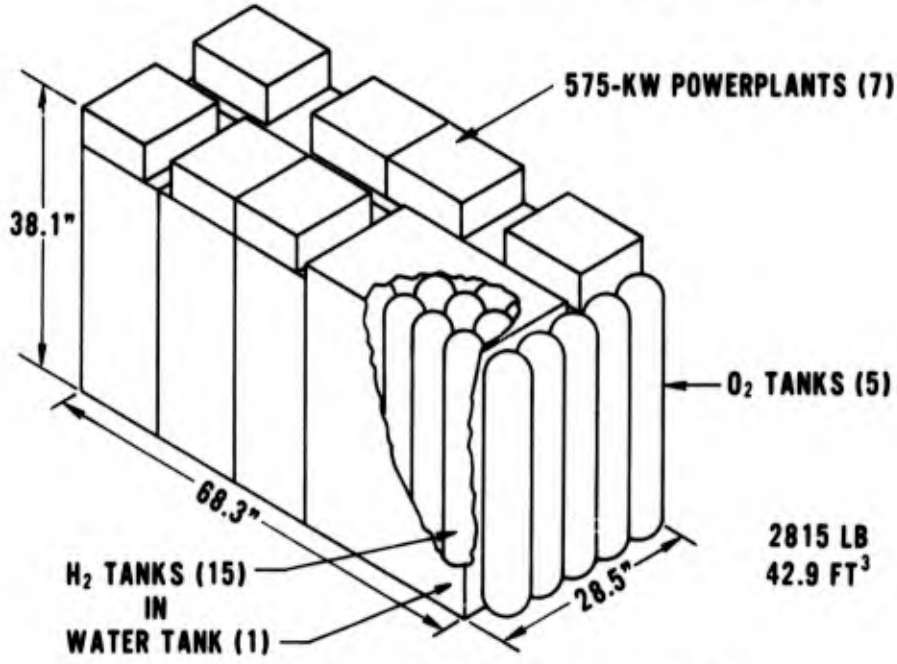

Figure 13 – Compact Packaging Arrangment (2)

4-MW, 30-SECOND MISSION, 3000 PSIA O_2 STORAGE, 10,000 PSIA H_2 STORAGE

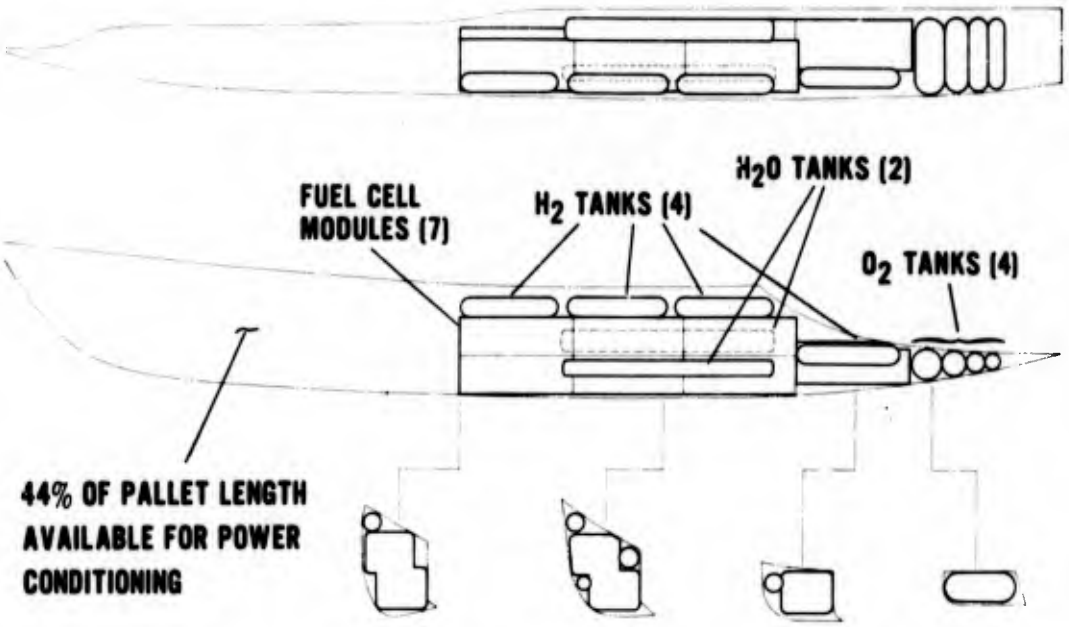

Figure 14 — Pallet Packaging Arrangement (1)

H_2 AND O_2 STORED AT 3000 PSIA

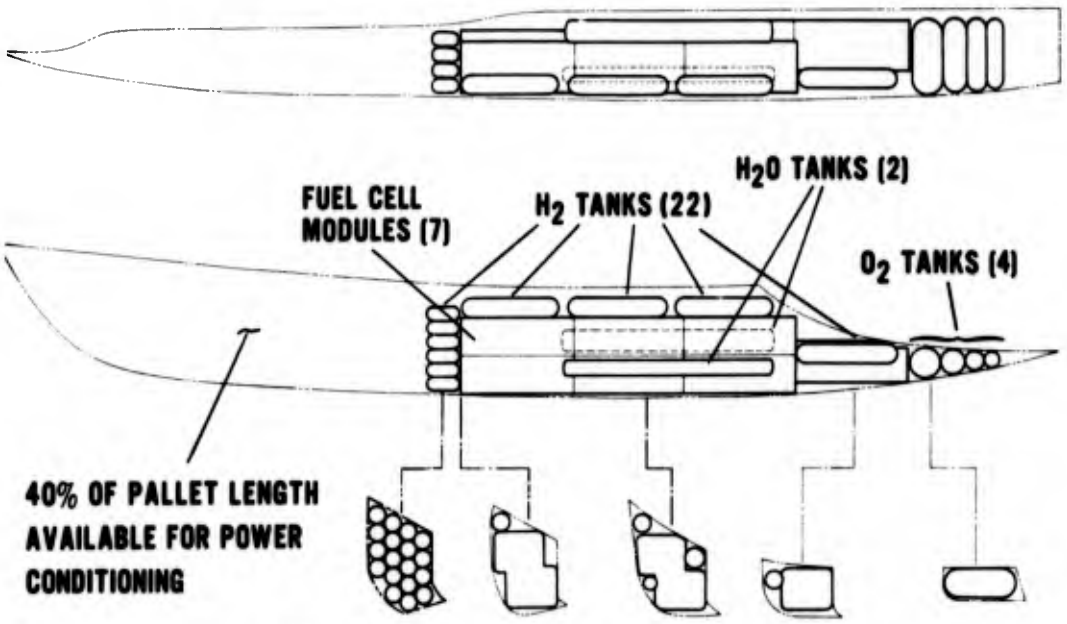

Figure 15 — Pallet Packaging Arrangement (2)

4-MW, 30-SECOND MISSION PRODUCT WATER STORED IN CELLS
CRYOGENIC REACTANT STORAGE

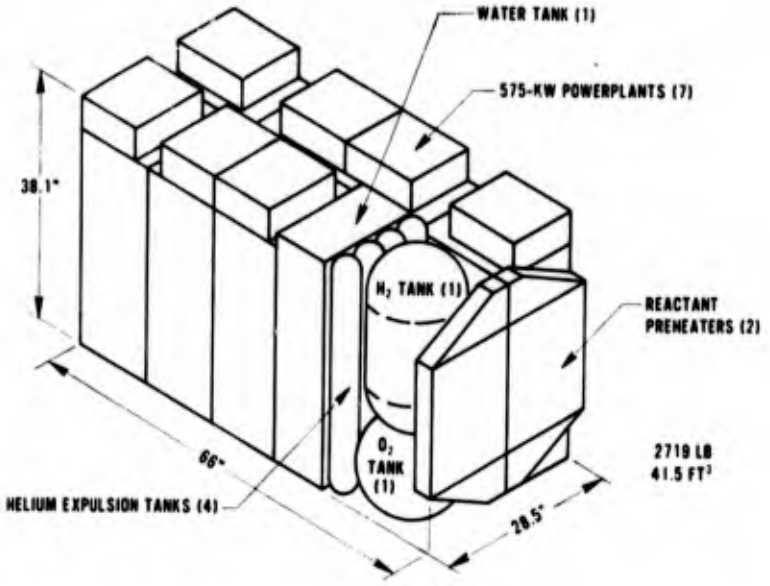

Figure 16 — Compact Packaging Arrangement

TABLE II

COMPACT PACKAGING ARRANGEMENT (1) WEIGHT AND VOLUME

4 MW, 30-SEC MISSION, 3000 PSIA O_2 STORAGE,
10,000 PSIA H_2 STORAGE

	WEIGHT LB	VOLUME FT³
SEVEN 575-KW POWERPLANTS	2070	28.0
REACTANTS AND TANKS	227	4.6
COOLING WATER AND TANKS	374	2.8
PIPING, WIRING, INSULATION, SPACE	97	5.1
TOTAL	2768	40.5

TABLE III

COMPACT PACKAGING ARRANGEMENT (2) WEIGHT AND VOLUME
(3000 psia H_2 and O_2 Storage)

4-MW, 30-SEC MISSION, H_2 AND O_2 STORED AT 3000 PSIA

	WEIGHT LB	VOLUME FT^3
SEVEN 575-KW POWERPLANTS	2070	28.0
REACTANTS, COOLING WATER AND TANKS	640	11.1
PIPING, WIRING, INSULATION, SPACE	105	3.8
TOTAL	2815	42.9

TABLE IV

PALLET PACKAGING ARRANGEMENT (1) WEIGHT AND VOLUME

4 MW, 30-SEC MISSION, 3000 PSIA O_2 STORAGE,
10,000 PSIA H_2 STORAGE

	WEIGHT (lb)	VOLUME (FT^3)
SEVEN-575 KW POWERPLANTS	2070	28.0
REACTANTS AND TANKS	232	4.8
COOLING WATER AND TANKS	437	3.0
PIPING, INSULATION, WIRING, SPACE	117	24.5
TOTAL	2856	60.3

TABLE V

PALLET PACKAGING ARRANGEMENT (2) WEIGHT AND VOLUME
(3000 psia H_2 and O_2 Storage)

4 MW, 30-SEC MISSION
H_2 AND O_2 STORED AT 3000 PSIA

	WEIGHT (LB)	VOLUME (FT^3)
SEVEN 575-KW POWERPLANTS	2070	28.0
REACTANTS AND TANKS	196	7.5
COOLING WATER AND TANKS	437	3.0
PIPING, INSULATION, WIRING, SPACE	131	26.4
TOTAL	2834	64.9

TABLE VI

EFFECT OF PRESSURE ON SYSTEM WEIGHT AND VOLUME

4-MW, 30-SEC MISSION H_2 AND O_2 STORED AT 3000 PSIA

REACTANT PRESSURE AT CELLS, PSIA	POWER DENSITY, W/FT^2	SYSTEM WEIGHT, LB	SYSTEM VOLUME, FT^3
60	2150	2815	42.9
100	2700	2470	37.0

INCREASE IN PRESSURE TO 100 PSIA RESULTS
IN 12% WEIGHT SAVING, 14% VOLUME SAVING

TABLE VII

COMPARISON OF 4-MEGAWATT SYSTEMS

PACKAGING	MISSION DURATION, SEC	GAS STORAGE PRESSURE, PSIA H_2	GAS STORAGE PRESSURE, PSIA O_2	SYSTEM WEIGHT, LB	SYSTEM VOLUME, FT^3
RECTANGULAR	30	10,000	3,000	2768	40.5
↓	↓	3,000	↓	2815	42.9
PALLET	↓	10,000	↓	2856	60.3
↓	↓	3.000	↓	2834	64.9

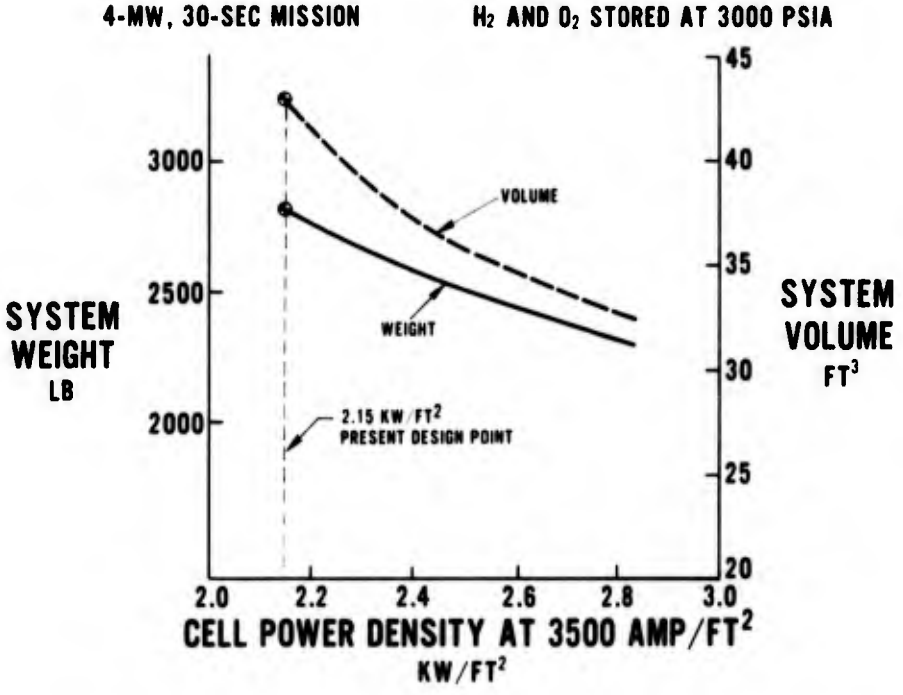

Figure 17 — Effect of Power Density on System Weight and Volume

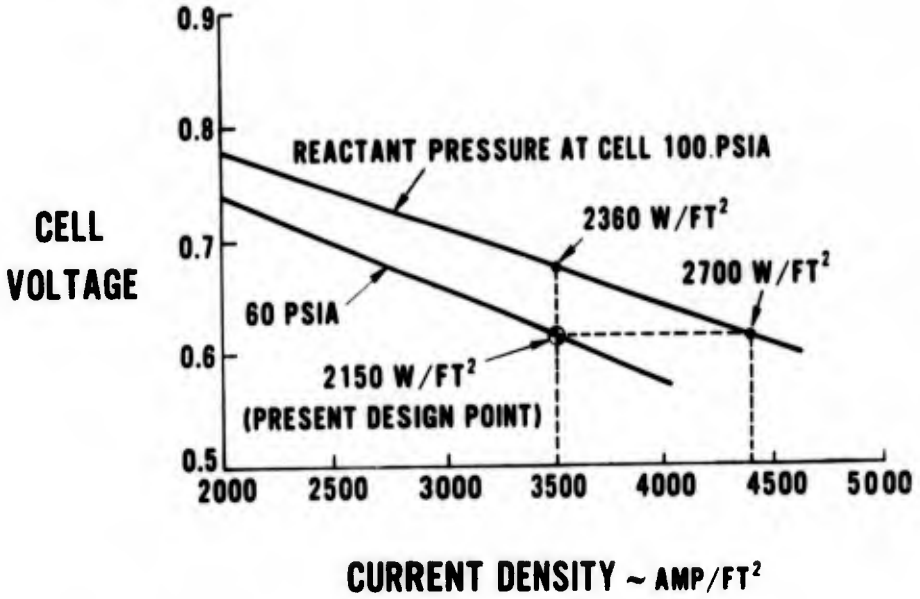

Figure 18 – Predicted Effect of Pressure on Cell Performance

TABLE VIII

WEIGHT AND VOLUME

CRYOGENIC REACTANT STORAGE WITH He PRESSURIZATION

	WEIGHT LB	VOLUME FT³
SEVEN 575-KW POWERPLANTS	2070	28.0
REACTANTS AND TANKS	143	4.2
COOLING WATER AND TANKS	395	2.8
PIPING, WIRING, INSULATION, SPACE	111	6.5
TOTAL	2719	41.5

The operating characteristics of all of the systems are the same. They are summarized in Table IX. The powerplants are started by turning on their coolant pumps which circulate hot water through them to bring them to operating temperature. The water is heated by electrical heaters located in the coolant flow system of each powerplant. The total power required during startup for the pumps and heaters is about 35 kw. Startup requires less

than 20 minutes, and shorter times are possible by increasing the power level during startup. Once the powerplants are at operating temperature and the reactant valves are opened, power is instantaneously available.

TABLE IX

POWER SYSTEM OPERATING CHARACTERISTICS

GROUND TURN-AROUND ~ 20-30 MINUTES

- RECONDITION CELL STACK WITH GROUND CART
- REFILL H_2O TANK
- REPLACE REACTANT TANKS
- BRING POWER SYSTEM TO 250°F OPERATING TEMPERATURE
  - 35 KW TO PUMPS AND HEATERS

IDLE (READY STANDBY) ~ AS LONG AS REQUIRED

- MAINTAIN OPERATING TEMPERATURE
  - 1-2 KW TO PUMPS AND HEATERS (TRADE-OFF AGAINST INSULATION VOLUME)

OPERATION ~ LIMITED ONLY BY REACTANT SUPPLY

- SELF-CONTROLLED — LOAD DEMAND

SHUTDOWN ~ INSTANTANEOUS

- DISCONNECT POWER TO PUMPS AND HEATERS

Turn-around between missions requires only replenishment of reactants and cooling water, and removal of product water accumulated within the powerplants. It can be completed within 20 to 30 minutes. Product water, stored in the powerplant during a mission, is removed by circulating a dry inert gas; e.g., nitrogen, through the powerplants into which the product water evaporates. The dry gas is supplied by a ground cart which incorporates a recirculating system that dries the moist gas leaving the powerplants and continuously returns it to the powerplants until all product water has been removed. Reactants, and the helium for pressurizing the cryogens, are replenished by removing the empty storage tanks from the aircraft and replacing them with full ones. This approach appears to be the safest and fastest method for resupplying reactants. However the tanks can also be refilled directly from GSE without being removed if that were preferred. The water tanks are refilled directly from a ground cart; they are not removed from the aircraft. In the case of rectangular arrangment (2) the hydrogen and water tank would be removed as a unit. Water replenishment could be carried either on-board or off the aircraft.

The powerplant can remain in an idle condition, immediately ready to supply power, as long as is required by the mission. During this period 1 to 2 kilowatts of electrical power are required to keep the powerplants at operating temperature. No reactants are consumed while the power system is on ready standby.

Operation of the power system, while idling or supplying power, is completely automatic and self-controlled. No monitoring of the system by the aircrew is required. Delivery of power is on demand. Response to an electrical load is instantaneous. If the switch and the impedance characteristics of the load permit, the voltage drops within a few tens of microseconds to the full-load voltage of the system and remains constant for the duration of the load. The fuel cell system is insensitive to whether the load is pulsed or continuous. During operation reactants are consumed, cooling water is vaporized and vented overboard, and product water is stored in the electrolyte. After completing the mission, the reactant supply valves are closed.

The voltage of the system can be reduced to zero by flushing the reactant gas passages in the powerplant subsystem with an inert gas and dissipating the cell stack potential through a resistor. This can be done immediately after use or upon returning to the base of operations. It eliminates any safety hazard due to shock during further operations or servicing.

Shutdown of the system is instantaneous. Power is removed from the pumps and heaters allowing the powerplants cool to ambient conditions. No conditioning or monitoring of any kind is required during the shutdown process. The powerplants can be restarted from any point in the cooldown. If restarted before they have completely cooled, the powerplants will require a shorter time to reach operating temperature than if they had been started from an ambient condition.

The powerplant upon which each system is based is shown in Figure 19. It has a rated output of 575 kw and weighs 295 pounds. Its dimensions are 12 x 15.5 x 38.1 inches, and has a volume of 4.0 cubic feet. It provides 400 amperes at 1435 volts. Other current-voltage combinations are possible by changing its internal electrical arrangement.

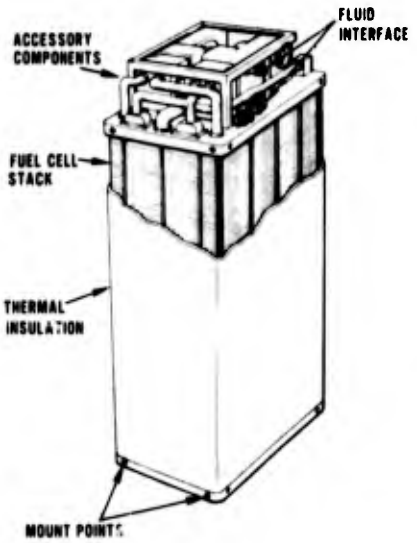

WEIGHT AND VOLUME

• STACK	260 LB	3.6 FT³
• COMPONENTS	25	0.4
• MISC	10	
TOTAL	295 LBS	4.0 FT³

PERFORMANCE

- MAXIMUM VOLTAGE — 1435 VOLTS
- CURRENT — 400 AMPS
- H_2 FLOW — 0.02 LB/SEC
- O_2 FLOW — 0.17 LB/SEC
- H_2O FLOW — 0.78 LB/SEC

Figure 19 – 575-kw Powerplant Forms Basis of Fuel Cell Power

The powerplant consists of two major subassemblies a power section and accessory section. The power section is a stack of 195 development units connected in series. The accessory section includes the electrical and fluid control components (pumps, regulators, and flow valves) and plumbing connections to the consumable's supply subsystems. The accessory section component designs are based directly on those of the PC15 powerplants developed for the Navy and the PC17 powerplant being developed for the Space Shuttle.

The powerplant design is based on a performance level of 0.615 volts at 3500 ASF, i.e. a power density of 2150 WSF, at an operating temperature of 250°F and reactant pressure of 60 psia. This performance level, at these operating conditions, was demonstrated repeatedly during this program in tests of both single cells and full-sized development units. At a rated power delivery of 575 kw, each powerplant has reactant and cooling water consumption rates of 0.02 lb/sec. of hydrogen, 0.17 lb/sec. of oxygen and 0.78 lb/sec. of water.

The flow schematic for the powerplant, including all the components required for control and operation of the unit, is shown in Figure 20. Both reactant flow paths are straight-through dead ended systems, neither reactant is recirculated. The H_2-O_2 regulator reduces reactant supply pressure to working pressure and supplies reactant to the powerplant on demand. The cooling water system however does have a recirculation loop. As explained above, during startup liquid water is circulated through a heater and then through the stack to heat the powerplant. During normal operation liquid water is admitted to the stack and partially flashed to steam. The steam/water mixture is separated by the pump/separator. Vapor is vented overboard and the liquid water is returned to the stack. Additional water, from the cooling water tanks, is admitted to the loop through the water reglulator as necessary to make-up for the steam that has been vented. The circulation loop is also used to maintain the powerplant at operating temperature during periods of operation at idle conditions. During this period warm water, heated by the start/idle heater, is circulated through the powerplants.

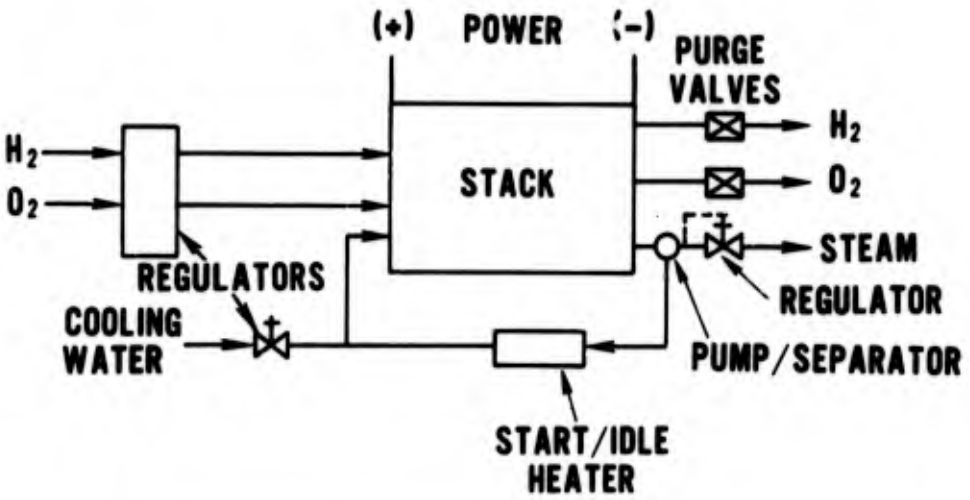

Figure 20 – Powerplant Schematic for High Power Mission

Product water generated during the mission is stored within the individual cell assemblies of each powerplant. Each cell incorporates a porous electrolyte reservoir plate which absorbs the expansion of electrolye caused by the generation of product water.

The design criteria for and characteristics of the hydrogen storage tanks included in the pallet and compact rectangular packages are presented in Table X. The tank design is based on information supplied by Ardé, Inc. Each tank is a composite vessel, consisting of a glass fiber reinforced shell and a cryoformed type 301 stainless steel liner, designed for operation at 10,000 psia. The liner is designed for a zero stress level at maximum storage pressure to avoid hydrogen induced material degradation. A detailed description of the pallet tanks is presented in Table XI.

TABLE X

HYDROGEN REACTANT STORAGE TANK DESIGN CHARACTERISTICS

- 4 CYLINDRICAL TANKS WITH HEMISPHERICAL ENDS
- STORAGE PRESSURE - 3000 OR 10,000 PSIA
- MATERIAL
  - GLASS FIBER REINFORCED SHELL SURROUNDING VACUUM-MELT CRYOFORM
  - TYPE 301 STAINLESS STEEL LINER (GFR-ARDÉ FORM)
- DESIGN CRITERIA
  - $\frac{PV}{W} = 0.26 \times 10^6$ IN. BASED ON INFORMATION SUPPLIED BY ARDÉ, INC.
  - STAINLESS STEEL LINER DESIGNED FOR ZERO STRESS AT OPERATING PRESSURE TO AVOID H_2-INDUCED MATERIAL DEGRADATION

TABLE XI

PALLET HYDROGEN TANK DESCRIPTION

PALLET ARRANGEMENT (1), 10,000 PSIA STORAGE

- NO. OF TANKS 4
- INTERIOR VOLUME 904.8 IN^3/TANK
- TANK I.D. 6.0 IN.
- TANK WALL THK. LINER 0.020 IN.
  SHELL 0.355 IN.
- TANK LENGTH 34 IN.

PALLET ARRANGEMENT (2), 3000 PSIA STORAGE

- NO. OF TANKS: 4 LARGE
  18 SMALL
- INTERIOR VOLUME: LARGE = 1078 IN^3/TANK
  SMALL = 239 IN^3/TANK
- TANK I.D.: LARGE = 6.57 IN.
  SMALL = 5.50 IN.
- TANK WALL THICKNESS: LINER = 0.020 IN.
  SHELL: LARGE = 0.07 IN.
  SMALL = 0.06 IN.
- TANK LENGTH: LARGE = 34 IN.
  SMALL = 12 IN.

Table XII presents design criteria for the oxygen storage vessels used in the pallet. These tanks are each of a different diameter for improved packaging. They are cryoformed type 301 stainless steel based on existing Ardé, Inc. designs. Storage pressure is 3,000 psia. The same storage pressure and tank designs were used for the oxygen storage vessels in the rectangular power system package.

TABLE XII

OXYGEN STORAGE VESSEL DESIGN

DESIGN CHARACTERISTICS

- VARIABLE SIZE CYLINDRICAL TANKS (HEMISPHERICAL ENDS) TO FIT POD CONFIGURATION
- STORAGE PRESSURE - 3000 PSIA
- MATERIAL — VACUUM-MELT CRYOFORM TYPE 301 AGED STAINLESS STEEL (ARDÉ FORM)
- DESIGN CRITERIA — ULTIMATE STRESS = 300 KSI
  — SAFETY FACTOR — ULTIMATE = 2.25

TANK DESCRIPTION

TANK	INTERIOR VOLUME (IN^3)	I.D. (IN)	WALL THK (IN)	LENGTH (IN)
1	1618.5	9.5	0.11	26.0
2	891.6	7.0	0.08	25.5
3	650.3	6.0	0.07	25.0
4	365.8	4.5	0.05	24.5

Figure 21 shows how the pallet oxygen storage tanks are arranged, with valves, regulators, and disconnects, into a quickly replaceable gas supply package. It also incorporates provision for onboard refilling of the tanks if that is desireable. By incorporating a regulator in the tank package the quick disconnect connections made by ground service personnel are all low pressure. The compact rectangular package oxygen storage systems are designed with the same features.

The characteristics of the water storage tank for the pallet power system package are presented in Table XIII. These tanks pressurized to a maximum of 30 psia for water expulsion, are designed of stainless steel. The water storage tanks used in the compact packaging arrangement are designed of stainless steel to withstand an operating pressure of 30 psia. They are internally-stayed right-rectangular solids.

Total system schematics for the pallet packages, showing all reactant and water lines between the hydrogen storage packages, the oxygen storage package, the water tanks, and the power-plants are shown in Figures 22 and 23. The hydrogen storage systems are broken into separate units because they package more effectively than a single unit in the space available in the pallet. Each of these units incorporate the same safety and handling features that are designed into the oxygen system. The compact rectangular packages are plumbed and arranged in a similar manner.

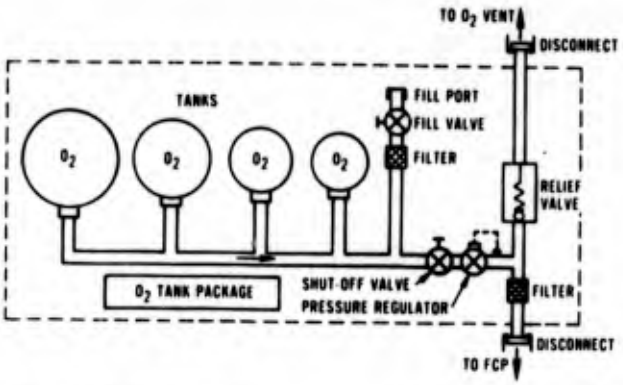

- COMPONENT PACKAGING AND DISCONNECTS PERMIT RAPID REMOVAL FROM AIRCRAFT BETWEEN MISSIONS
- MANUAL VALVES ALLOW EASY REFILLING OF TANKS WITH PACKAGE IN OR OUT OF AIRCRAFT
- SLIP TYPE DISCONNECTS PROTECT AGAINST GENERATION OF METAL CHIPS ASSOCIATED WITH SCREW TYPE FITTINGS
- 10 MICRON FILTERS PREVENT FOREIGN PARTICLES FROM ENTERING SYSTEM
- RELIEF VALVE PROTECTS AGAINST OVERPRESSURE CAUSED BY REGULATOR FAILING OPEN

Figure 21 – Oxygen Storage Package Schematic

TABLE XIII

PALLET COOLING WATER STORAGE VESSELS

DESIGN CHARACTERISTICS

- 2 CYLINDRICAL TANKS WITH DOMED ENDS
- STORAGE PRESSURE = 30 PSIA (O_2 PRESSURIZED)
- MATERIAL — STAINLESS STEEL
- DESIGN CRITERIA — ULTIMATE STRESS = 65 KSI
  — SAFETY FACTOR >> 2.25

TANK DESCRIPTIONS

TANK	INTERIOR VOLUME (IN^3)	I.D. (IN)	WALL THK. (IN)	LENGTH (IN)
1	3225.1	7.5	0.109	73
2	1580.2	5.25	0.109	73

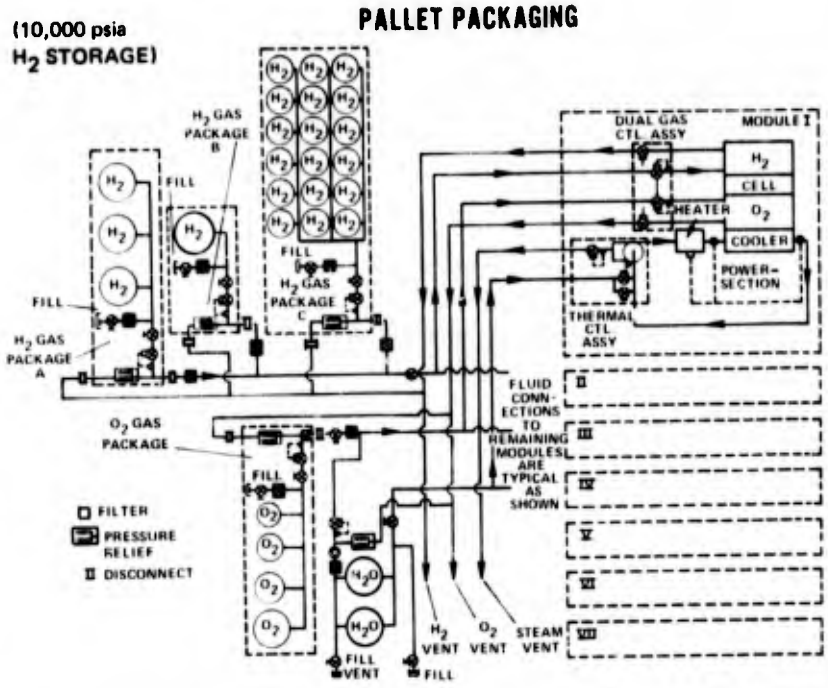

Figure 22 — Fuel Cell Power System Schematic, Pallet Packaging Arrangement (1)

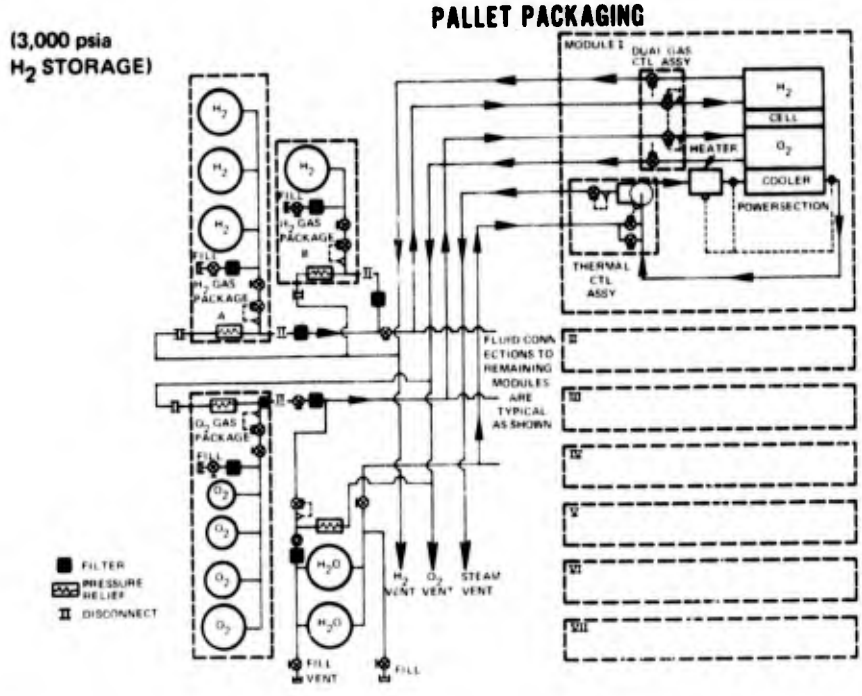

Figure 23 — Fuel Cell Power System Schematic, Pallet Packaging Arrangement (2)

The design criteria and characteristics of the cryogenic hydrogen and oxygen storage tanks are present in Tables XIV and XV respectively. The helium storage tanks are also of aluminum construction and are designed for a storage pressure of 3000 psi with a factor of safety of 2.25 based on ultimate stress. Figure 24 shows the arrangement of and interconnections between the cryogenic storage vessels and the fuel cell modules.

TABLE XIV

CRYOGENIC HYDROGEN STORAGE VESSELS

DESIGN CHARACTERISTICS

- STORAGE CONDITIONS: SATURATED LIQUID AT 55°R (PRESSURE ≃ 130.7 PSIA)
- CYLINDRICAL TANK WITH HEMISPHERICAL ENDS
- He PRESSURIZATION
- MATERIAL
  - INNER LINER: 6063-T6 ALUMINUM
  - INSULATION: LINDE S1-12 SUPER INSULATION AT 10^{-3} TORR
  - OUTER SHELL: 6063-T6 ALUMINUM
- DESIGN CRITERIA
  - ULTIMATE STRESS = 60 KSI
  - ULTIMATE SAFETY FACTOR = 2.25

TANK DESCRIPTION

- NO. OF TANKS = 1
- INTERIOR VOLUME = 2530 IN^3
- TANK DIMENSIONS:
  - I.D. = 12.5 IN.
  - WALL THICKNESS:
    - LINER = 0.03 IN.
    - INSULATION = 0.06 IN.
    - SHELL = 0.03 IN.
  - TANK LENGTH = 25 IN.

TABLE XV

CRYOGENIC OXYGEN STORAGE VESSELS

DESIGN CHARACTERISTICS

- STORAGE CONDITIONS: SATURATED LIQUID AT 212°R (PRESSURE ≃ 130.7 PSIA)
- CYLINDRICAL TANK WITH HEMISPHERICAL ENDS
- He PRESSURIZATION
- MATERIAL
  - INNER LINER: 6063-T6 ALUMINUM
  - INSULATION: LINDE S1-12 SUPER INSULATION AT 10^{-3} TORR
  - OUTER SHELL: 6063-T6 ALUMINUM
- DESIGN CRITERIA
  - ULTIMATE STRESS = 60 KSI
  - ULTIMATE SAFETY FACTOR = 2.25

TANK DESCRIPTION

- NO. OF TANKS = 1
- INTERIOR VOLUME = 1108 $IN.^3$
- TANK DIMENSIONS:
  - I.D. = 12.5 IN.
  - WALL THICKNESS:
    - LINER = 0.03 IN.
    - INSULATION = 0.024 IN.
    - SHELL = 0.03 IN.
  - TANK LENGTH = 13.4 IN.

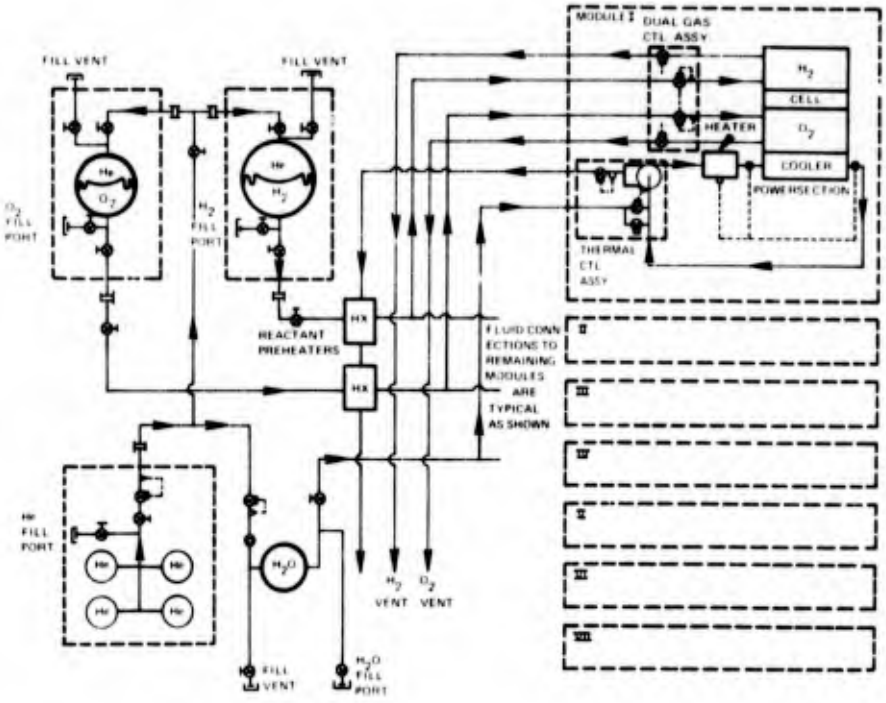

Figure 24 – Compact Packaging Arrangement Schematic, Cryogenic Reactant Storage

2. Mission Growth

The fuel cell is readily adaptable to mission durations longer than the 30-second reference mission. In fact, increasing mission length and energy delivery dramatically improves the fuel cell system's energy density. For example, data for the rectangularly packaged system shows increasing mission length (and energy delivery) by a factor of four, to 120 seconds, increases system weight by less than a factor of two and system volume doubles. See Table XVI. In order to increase mission duration, only the consumable's storage tanks need be increased. Figure 25 shows how additional tankage can be added to the baseline compact rectangular system for a mission duration of 120 seconds. This system is identical to the 30-second mission system except for the additional tankage. The added tankage is designed using the same criteria and characteristics used for the baseline systems.

Figures 26 and 27 show how the compact rectangular system's weight and volume vary with mission duration. Figure 26 depicts systems with two different criteria for design of the electrolyte reservoir plates (ERP's) incorporated into the individual cell assemblies. Product water is stored in the ERP's as it is produced. The solid lines represent a system in which the ERP's are large enough to store only the water produced during a mission of the length selected on the abscissa of the curve. The dashed lines represent a system where the ERP's are sized for a mission of 120 seconds duration regardless of the actual mission length selected on the abscissa of the curve. Consequently, in this case, the ERP's are larger than necessary for all missions shorter than 120 seconds. Figure 16 compares the weight and volume of a

system using ERP's, sized for a selected mission length for water storage, with a system in which product water is evaporated into a vented hydrogen stream. In the second system the weight and volume saved by decreased ERP size is offset by additional hydrogen and hydrogen storage vessel weight and volume.

TABLE XVI

COMPARISON OF 4-MEGAWATT SYSTEMS

PACKAGING	MISSION DURATION, SEC	GAS STORAGE PRESSURE, PSIA H_2	GAS STORAGE PRESSURE, PSIA O_2	SYSTEM WEIGHT, LB	SYSTEM VOLUME, FT^3
RECTANGULAR		3,000	3,000	2815	42.9
PALLET				2834	64.9
RECTANGULAR	120			4522	84.9

4-MW, 120-SECOND MISSION
PRODUCT WATER STORED IN CELLS
REACTANTS STORED AT 3000 PSIA

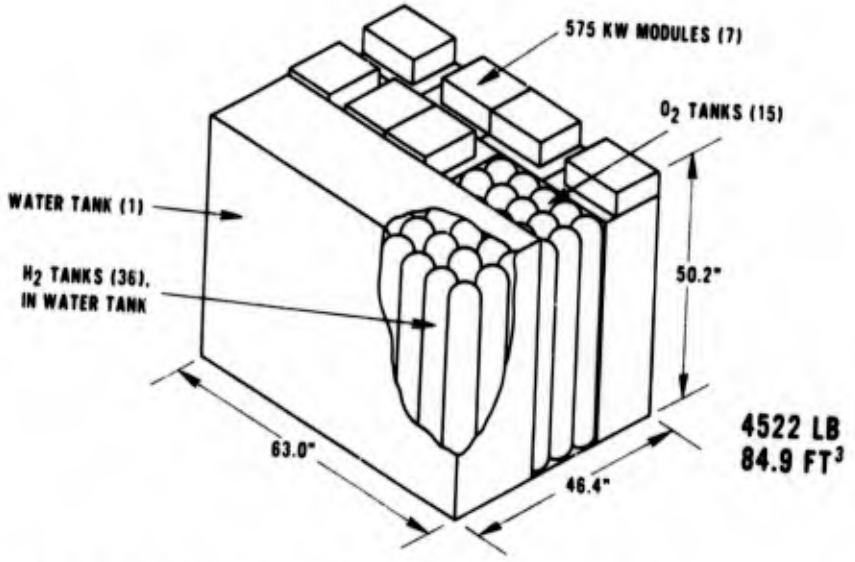

Figure 25 – Compact Packaging Arrangement for Mission Growth

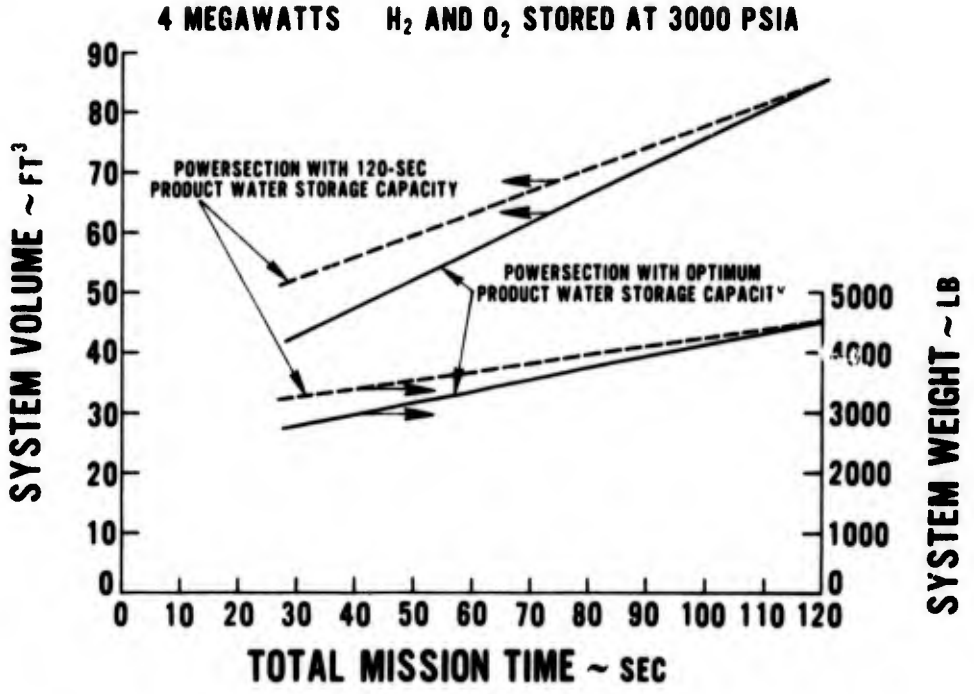

Figure 26 – Mission Growth Characteristics

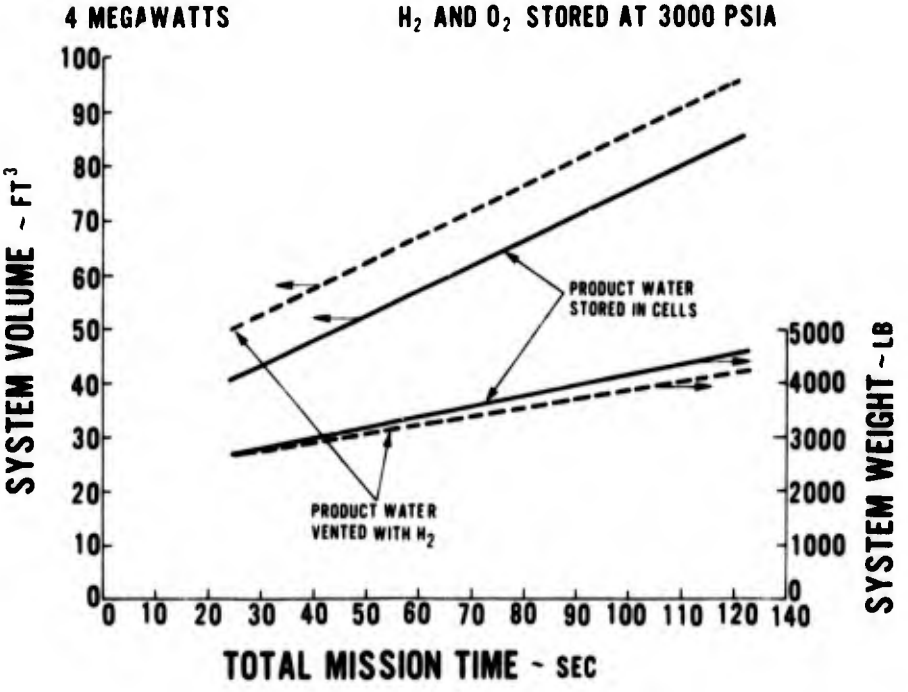

Figure 27 – Mission Growth Characteristics

C. MODULE AND DEVELOPMENT UNIT SIZING

1. Objectives

The objective of these studies was the definition and design of the fuel cell unit for development under this program. This unit, the development unit, is the basic repeating fuel cell section of which the stack for a complete full-size powerplant is assembled. Factors which influenced the design of the development unit and its individual elements were defined and analyzed. Based on these analyses a unit consisting of two 6-cell plaques and an evaporative cooler was selected for development. The primary studies resulting in this choice are presented below. All studies were reviewed with the Air Force Project Engineer as the development unit design was defined.

2. Selection of Repeating Unit and Cell Concept

Two design concepts were considered as candidates for the high power density fuel cell repeating unit. One was based on an arrangement in which current is transferred from cell to cell through the plates which separate individual cells and incorporate cavities for reactant supply and coolant flow. This arrangement is referred to as a "series" stack. The other concept was one in which several cells are arranged in multicell plaques, so that current is transferred from cell to cell in the plane of the plaque and from plaque to plaque via interplaque connections that are made external to the stack. This concept is referred to as a "plaque" stack. The two concepts are shown in Figure 28. Powerplant weights were established based on each of these stack concepts with the conclusion that: (1) A series stack powerplant could be developed that would meet the program weight goals and (2) A plaque stack powerplant could be developed that would be approximately 20 percent lighter than goal weight. Consequently since the development effort required for either approach was judged to be the same, the plaque stack concept was selected for development. It offered: (1) A superior weight potential to the series stack and/or (2) provided a weight margin in the event development was more difficult than anticipated.

The powerplant weight comparisons are presented in Table XVII. To establish these weights a functional and design analysis of both concepts was made. Figure 29 shows the functional elements of the repeating fuel cell unit of which each stack is assembled. Figures 30 and 31 show the functional requirements of each element of the plaque and series stacks, respectively. The operating conditions for each stack are the same and were based on an overall reference powerplant and system analyses summarized in Figure 32. The detailed cross sections used for a weight comparison of the stacks are shown in Figure 33. The detailed elements of the plaque stack are shown in Figures 34, 35, and 36 and in Figures 34 and 37 for the series stack. The design and sizing of the details were based on the assumptions and analyses presented in Tables XVIII through XXII. The planforms of the two stacks are shown in Figure 38. The assumptions and analyses used to define the planforms are presented in Tables XXIII through XXV. This work was the subject of a design review with the Air Force Project Engineer at AFAPL, early in the program, and was the basis of selecting the development unit designs selected for fabrication and testing.

PLAQUE

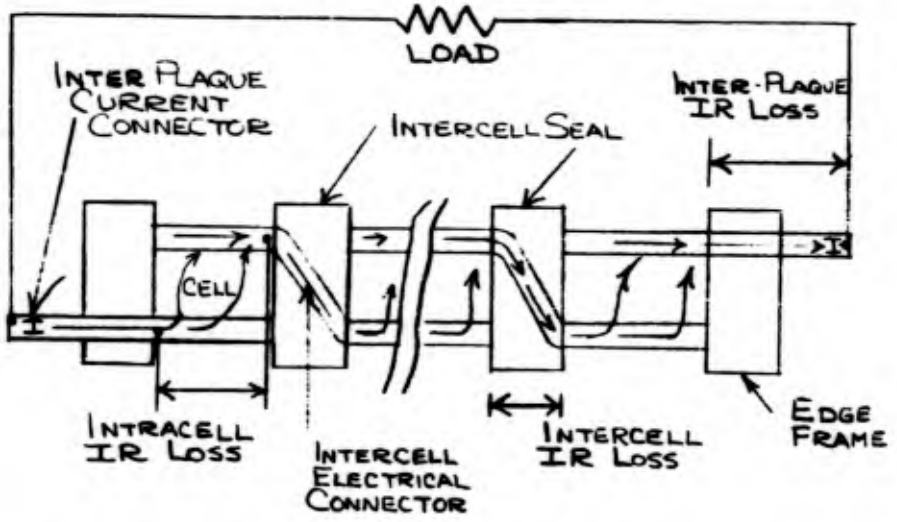

- CURRENT FLOWS THROUGH ELECTRODES PARALLEL TO PLANE OF CELL
- INTER CELL CURRENT TRANSFER IS THROUGH INTERCELL SEAL
- INTER-PLAQUE CURRENT TRANSFER IS THROUGH PLAQUE EDGE FRAME AND EXTERNAL CONNECTION

SERIES

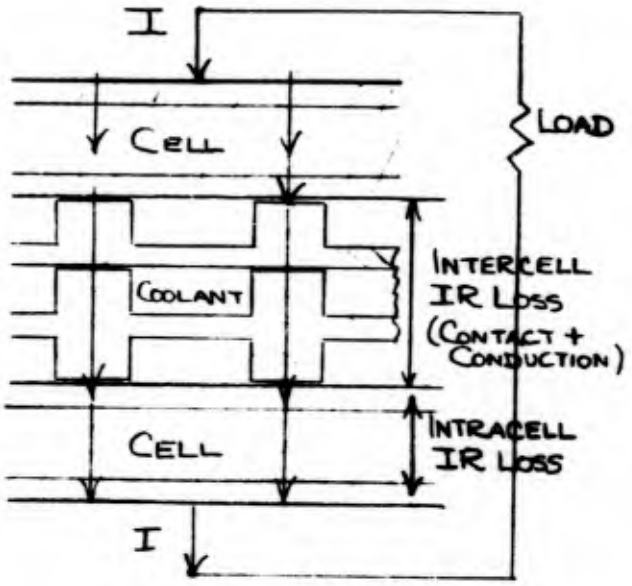

- CURRENT FLOWS THROUGH STACK PERPENDICULAR TO PLANE OF CELLS
- INTER-CELL CURRENT TRANSFER IS THROUGH COOLERS AND FLUID FLOW FIELDS

Figure 28 – Candidate Cell Stack Concepts

TABLE XVII

COMPARISON OF POWERPLANT WEIGHTS

PLAQUE			SERIES		
STACK:		151	STACK:		208
CELLS	66		CELLS	62	
ERP/H_2 PLATE	23		COOLING PLATE & FLOW FIELD ASSY'S	141	
O_2 FIELD & PLATE/ H_2O-STEAM FIELD	55		END PLATES & TIE BOLTS	5	
END PLATES AND TIE BOLTS	7				
COMPONENTS		68	COMPONENTS		68
MODULE WEIGHT-LBS.		219			276
WGT GOAL-LBS (0.5 LBS/KW)		275			275
DEVELOPMENT MARGIN - LBS.		56			-1

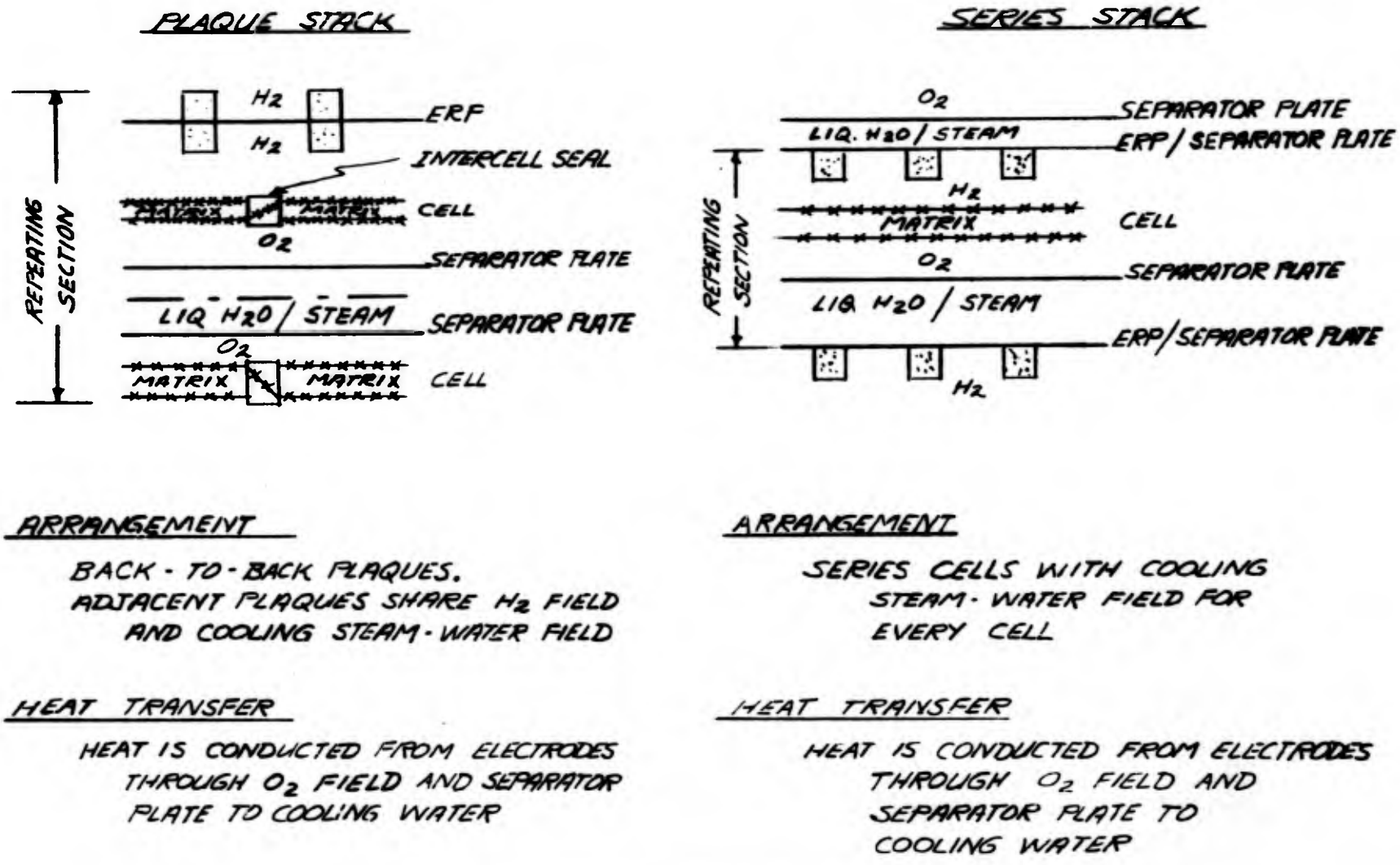

Figure 29 — Functional Elements of Repeating Section of Stack

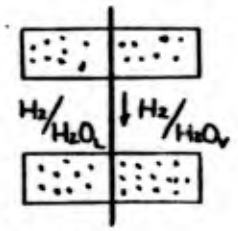

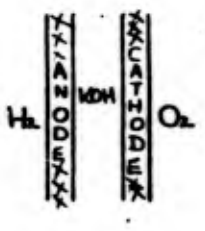

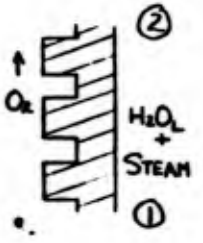

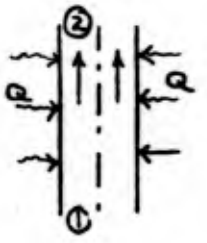

	ERP-H_2 PLATE	CELL	O_2 FIELD & PLATE	LIQ. H_2O/STEAM FIELD
	• PROVIDES 0.30 IN^3/FT^2 KOH RESERVOIR • FORMS H_2 FLOW FIELDS • ELECTRICALLY INSULATES ADJACENT PLAQUES • ELECTRICALLY INSULATES ADJACENT CELLS	• PROVIDES ELECTRO-CHEMICAL REACTION SITES	• FORMS SEPARATOR BETWEEN O_2 & COOLING WATER • FORMS O_2 FLOW FIELD • ELECTRICALLY INSULATES ADJACENT CELLS & ADJACENT PLAQUES • CONDUCTS 4470 BTU/HR-PLAQUE HEAT FROM CELL TO WATER/STEAM FIELD	• FORMS FLOW FIELD FOR COOLING WATER/STEAM • IMPOSES 5.2 PSI ΔP (10°F ΔT) IN STEAM FIELD REQUIRED FOR CELL ELECTROLYTE VOLUME CONTROL
OPERATING TEMPERATURE °F NOM	150 - 290	280-290 NORMAL 160 STANDBY	150 - 290	245 - 255
FLUID PRESSURES PSIA NOM	45/45	45/45	45/① 32.5 ② 27.3	① 32.5 ② 27.3
FLOW ~LB/HR-FIELD	IN : 0.690 H_2 + 2.319 H_2O_L OUT: 0.518 H_2 + 3.841 H_2O_V COUNTER TO COOLANT		IN : 1.351 O_2 OUT: —	IN : 16.622 H_2O_{LIQ} OUT : 8.756 H_2O_{LIQ} + 7.866 H_2O_{VAP}

• ALLOWABLE ΔT FROM CELL TO STEAM ~ 35 °F

Figure 30 — Functional Requirements of Plaque Stack

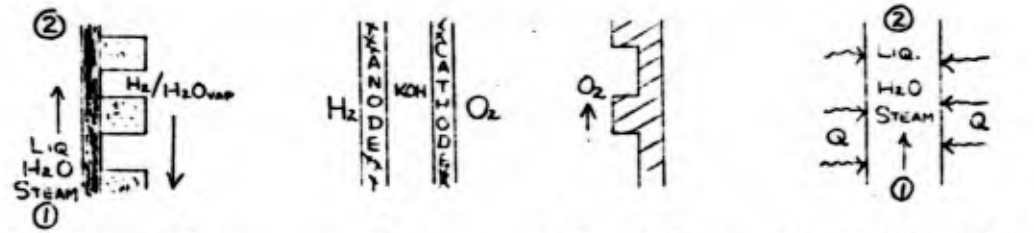

ERP/H_2-H_2O PLATE	CELL	O_2 FIELD/ PLATE	LIQ. H_2O/STEAM FIELD
• PROVIDES 0.30 IN^3/FT^2 KOH RESERVOIR • FORMS H_2 FLOW FIELD • CONDUCTS CURRENT FROM CELL TO CELL • CONDUCTS HEAT FROM CELL TO WATER	• PROVIDES ELECTRO-CHEMICAL REACTION SITES	• CONDUCTS HEAT FROM CELL TO WATER (745 BTU/HR-CELL) • SEPARATES O_2 FROM WATER • FORMS O_2 FLOW FIELD • CONDUCTS CURRENT FROM CELL TO CELL	• FORMS FLOW FIELD FOR COOLING H_2O_L/ STEAM • IMPOSES 3.2 PSI ΔP (10°F ΔT) IN STEAM FIELD—REQUIRED FOR ELECTROLYTE VOLUME CONTROL • CONDUCTS CURRENT FROM CELL TO CELL
OPERATING TEMPERATURE—°F—NOM	150 - 290	280-290 NORMAL 160 STANDBY	150 - 290	245 - 255
FLUID PRESSURES PSIA NOM.	① 32.5 ② 27.3 / 45	45 / 45	45	① 32.5 ② 27.3
FLOW ~LB/HR-FIELD	IN : 0.115 H_2 + 0.387 H_2O_V OUT: 0.056 H_2 + 0.640 H_2O_V COUNTER TO COOLANT		IN : 0.225 O_2 OUT: —	IN : 3.770 H_2O_{LIQ} OUT: 1.460 H_2O_{LIQ} + 1.310 H_2O_{vap}

• ALLOWABLE ΔT FROM CELL TO STEAM ~ 35°F

Figure 31 — Functional Requirements of Series Stack

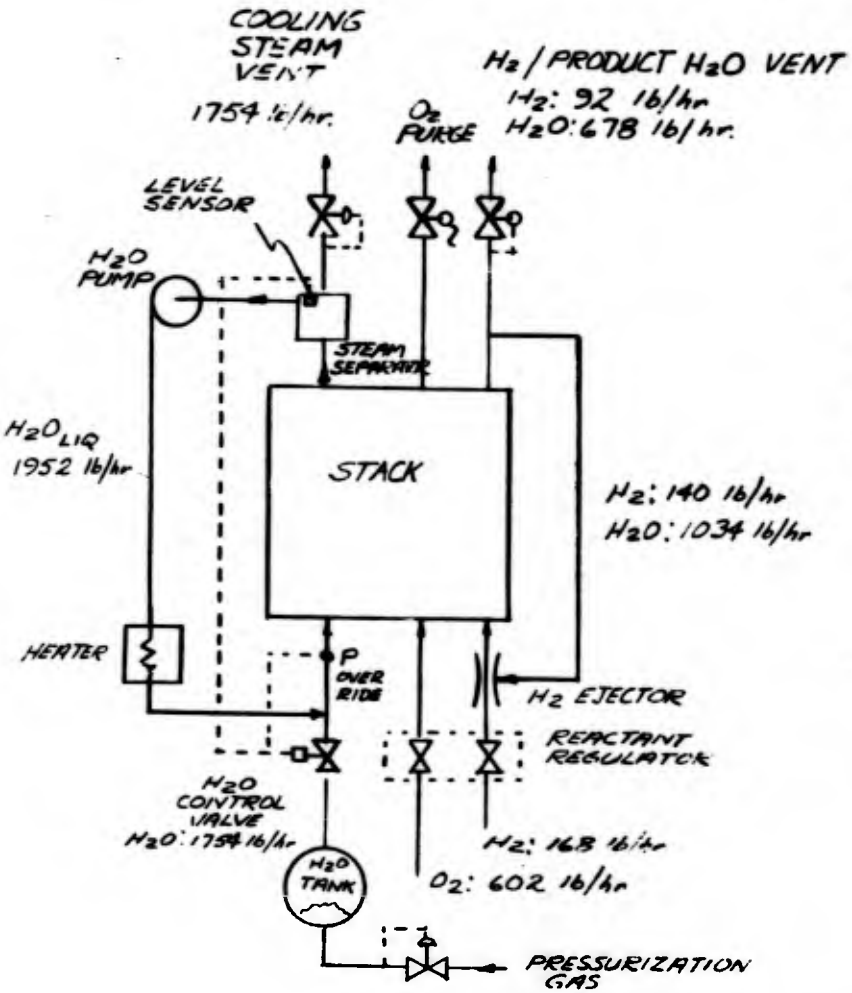

MODULE OPERATING CONDITIONS

POWER = 550 KW GROSS

VOLTAGE = UP TO 1600 VOLTS

CELL TEMPERATURE = 280° - 290° F

REACTANT PRESSURE = 45 PSIA

ELECTROLYTE CONCENTRATION = 45-50 W% KOH

H_2 RECYCLE RATIO = 7 $\frac{\text{LBS TOTAL RECYCLE}}{\text{LB } H_2 \text{ INLET}}$

TOTAL EXPENDABLES = LB/KW HR GROSS

- H_2 REACTED = 0.138
- H_2 VENTED = 0.178
- O_2 REACTED = 1.09
- H_2O COOLING = 3.19

CELL PERFORMANCE = AVERAGE OF 0.60 V/C AT 3000 ASF (1800 MSF) AT MODULE LOAD TERMINALS

Figure 32 — Reference Powerplant Operating Conditions

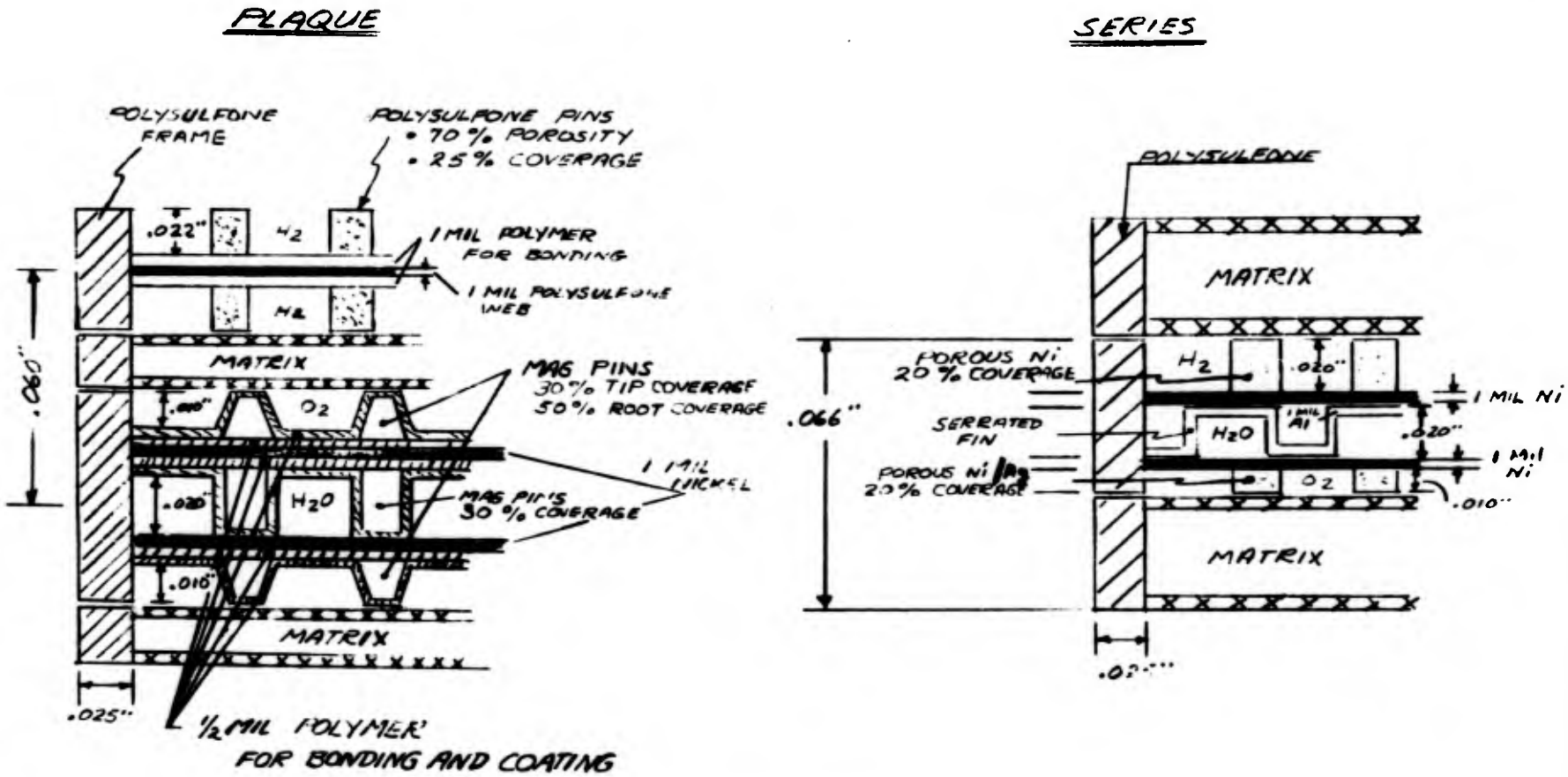

Figure 33 — Stack Cross Section

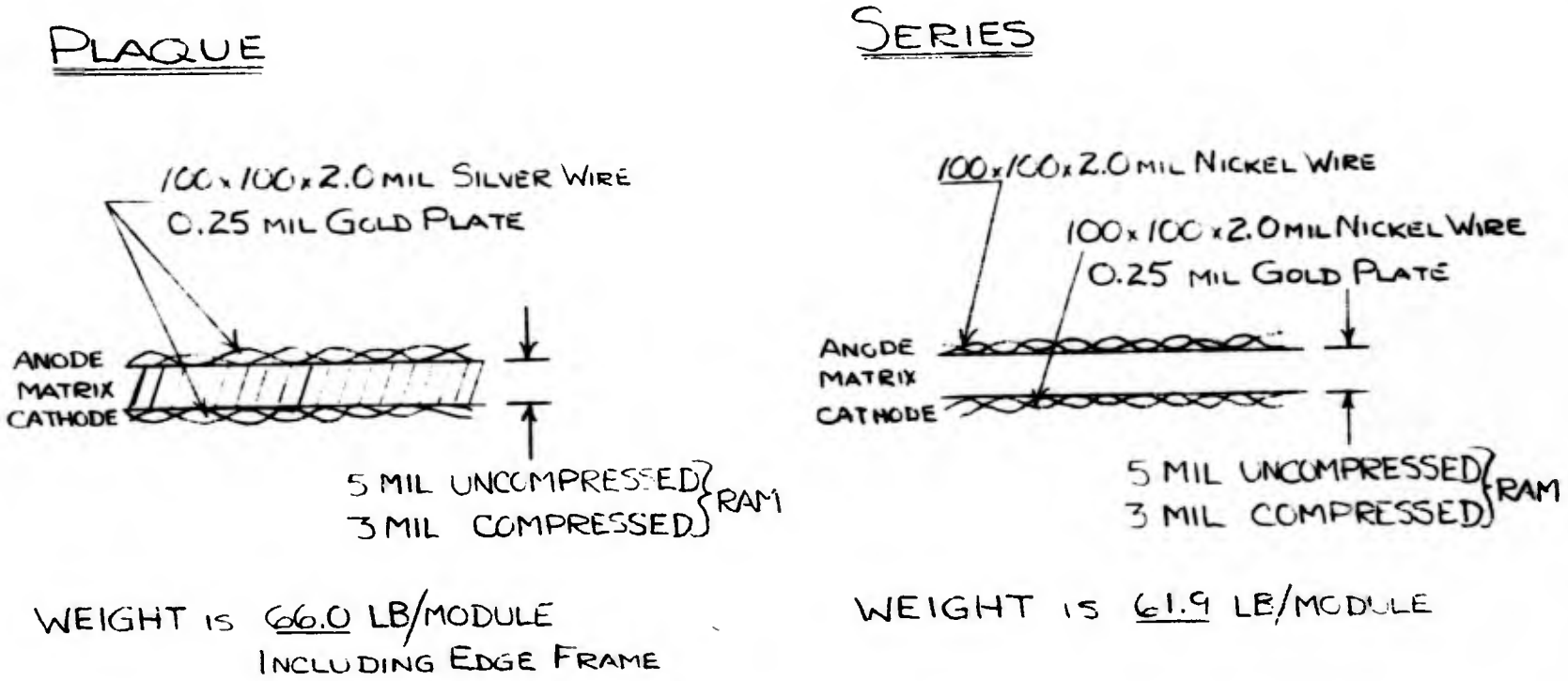

Figure 34 – Cell Cross Sections

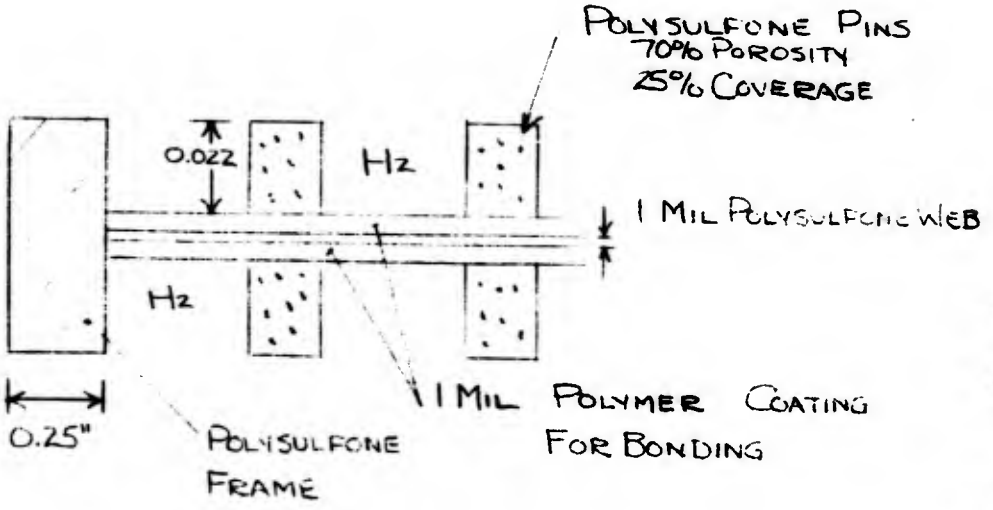

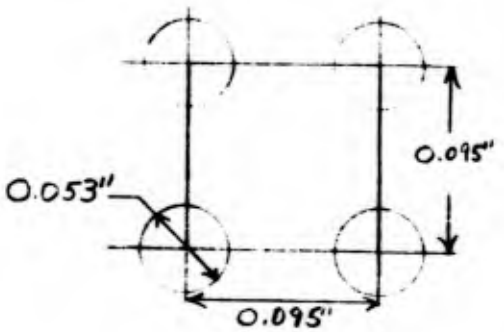

Fiugre 35 — Plaque - ERP/H_2 Plate

- WEIGHT IS 22.6 lb/MODULE
- ALTERNATE CONFIGURATIONS MAY BE DERIVED FROM ABOVE CONFIGURATION BY CHANGING FOLLOWING PARAMETERS
  1) PIN COVERAGE
  2) PIN PITCH
  3) WEB MATERIAL OR THICKNESS
- POROUS POLYSULFONE PINS
  - ELECTROLYTE RESERVOIR
  - Hz FLOW FIELD SUPPORT
- POLYSULFONE WEB
  - HOLDS PINS IN POSITION DURING ASSEMBLY - NO OTHER STRUCTURAL REQUIREMENT
  - IMPERVIOUS TO KOH TO PREVENT SHORTING THROUGH ELECTROLYTE IN BACK-TO-BACK PINS
- POLYMER COATING
  - BONDS POROUS PINS TO WEB

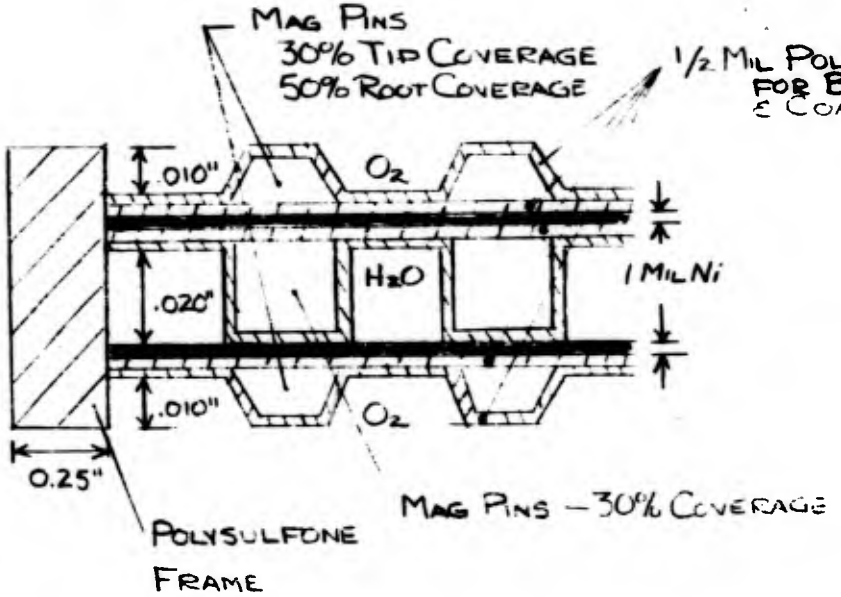

- ½ MIL POLYMER BONDS PINS TO WEB. ADDITIONAL ½ MIL PROTECTS PINS AND ELECTRICALLY INSULATES PLAQUE-TO-PLAQUE AND PLAQUE-TO-H_2O
- 1 MIL NICKEL WEB DISTRIBUTES HEAT BEFORE PASSING THROUGH WATER AND PROVIDES STRUCTURAL CAPABILITY
- PIN TYPE H_2O FLOW FIELD PROVIDES MORE DESIRABLE MECHANICAL LOAD TRANSMISSION THAN PLASTIC MESH
- WEIGHT IS 55 lbs/MODULE

Figure 36 — Plaque - O_2 Field and Plate/Liquid H_2O/Steam Field

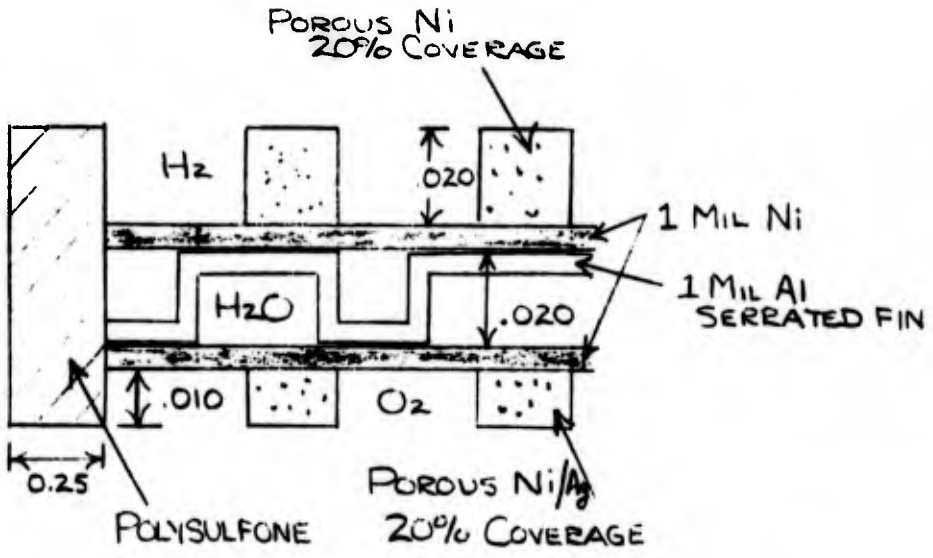

- WEIGHT IS 141 lb/MODULE FOR COOLING EVERY CELL
- H_2O/STEAM FIELD NOT ELECTRICALLY INSULATED
- 1 MIL NICKEL WEB REQUIRED FOR 18 PSI REACTANT-TO-STEAM CROSS PRESSURE

Figure 37 -- Series - O_2 Field and Plate/Liquid H_2O - Steam Field/ERP-H_2 Plate

TABLE XVIII

HYDROGEN FLOW FIELD AND PORT DEFINITION

- ASSUMPTIONS
  1. ΔP ALLOCATION BASED ON EJECTOR CAPABILITY (ΔP(STACK))~1/2 ΔP(SYSTEM))
  2. 20 MIL MINIMUM FIELD DEPTH LIMITED BY TOLERANCE EFFECTS ON FLOW DISTRIBUTION

- ANALYSIS
  1. PIN FIELD ΔP BASED ON COMPACT HEAT EXCHANGERS (KAYS & LONDON)
  2. KNOWN QUANTITIES - FLOW RATES, FLOW PROPERTIES, FIELD AND PORT ΔP

- RESULT

  (H_2 PORT AND FIELD CONFIGURATION)

  PLAQUE - 25% PIN COVERAGE - 22 MIL DEPTH

  SERIES - 25% PIN COVERAGE - 20 MIL DEPTH

TABLE XIX

ERP VOLUME REQUIREMENT

- ASSUMPTIONS
  - NORMAL OPERATING CONCENTRATIONS BASED ON NOMINAL TEMPERATURE AND EQUILIBRIUM WATER VAPOR PRESSURES AT CELL H_2 INLET AND EXIT
  - NOMINAL TEMPERATURES AND PRESSURES
  - STANDBY TEMPERATURE = 160°F
  - NO PRODUCT WATER REMOVED DURING HEATUP FROM STANDBY TO OPERATING TEMPERATURE
- ANALYSIS
  - KNOW ELECTROLYTE PROPERTIES AND ELECTROLYTE VOLUME OF ANODE, CATHODE, AND MATRIX

    CALCULATE:
    - VOLUME OF H_2O PRODUCED DURING HEATUP FROM STANDBY TO OPERATING TEMPERATURE
    - CHANGE IN ELECTROLYTE VOLUME DUE TO NORMAL OPERATING CONCENTRATION VARIATION
- RESULT
  - ERP VOLUME REQUIREMENT OF 0.30 IN^3 VOID VOLUME/FT^2 CELL AREA

TABLE XX

O_2 SEPARATOR PLATE WEB STRUCTURAL ANALYSIS

- ASSUMPTIONS
  1. UNIFORMLY-LOADED, FIXED-END BEAM WITH LENGTH EQUAL TO PIN PITCH
  2. NO FACTOR-OF-SAFETY
  3. NOMINAL PRESSURES
  4. PINS OF OPPOSING FIELDS ALIGN PREVENTING ADDITIONAL MOMENTS ON WEBS
- ANALYSIS
  1. BASED ON FORMULAS FOR STRESS AND STRAIN (ROARK)
  2. KNOWN QUANTITIES - WEB MATERIAL YIELD STRENGTH, PIN PITCH, CROSS-PRESSURE
- RESULTS

  WEB THICKNESS - 1 MIL NICKEL

TABLE XXI

THERMAL ANALYSIS

- ASSUMPTIONS

  1. NEGLECT FORCED CONVECTION EFFECTS ON BOILING FILM COEFFICIENT

- ANALYSIS

  1. ONE-DIMENSIONAL CONDUCTION HEAT TRANSFER
  2. O_2 WEB FIN EFFECTIVENESS ESTIMATES BASED ON COMPACT HEAT EXCHANGERS
  3. BOILING FILM COEFFICIENTS BASED ON POOL BOILING CORRELATIONS IN PRINCIPLES OF HEAT TRANSFER (KREITH)
  4. KNOWN QUANTITIES - THERMAL CONDUCTIVITIES, HEAT FLUX, ALLOWABLE ΔT

- RESULTS

  (O_2 FLOW FIELD HEAT TRANSFER CONFIGURATION)

  PLAQUE - TRUNCATED, CONICAL MAG PINS (30-50% COVERAGE) WITH 1/2 MIL POLYSULFONE COATING

  SERIES - 20% COVERAGE, POROUS NI/Ag PINS

TABLE XXII

STEAM FLOW FIELD AND PORT DEFINITION

- ASSUMPTIONS
  1. 20 MIL MINIMUM FIELD DEPTH LIMITED BY TOLERANCE EFFECTS ON FLOW DISTRIBUTION
  2. MEAN GAS AND LIQUID FLOWS ASSUMED FOR ΔP CALCULATION

- ANALYSIS
  1. BASED ON MARTINELLI'S METHOD FOR TWO-PHASE FLOW. EQUATIONS FOR SUPERFICIAL ΔP'S GIVEN IN COMPACT HEAT EXCHANGERS
  2. KNOWN QUANTITIES - FLOWS, FLOW PROPERTIES, FIELD ΔP

- RESULT

  (STEAM FLOW FIELD CONFIGURATION)

  PLAQUE - 30% PIN COVERAGE - 20 MIL DEPTH

  SERIES - 20 MIL ALUMINIMUM CORRUGATION

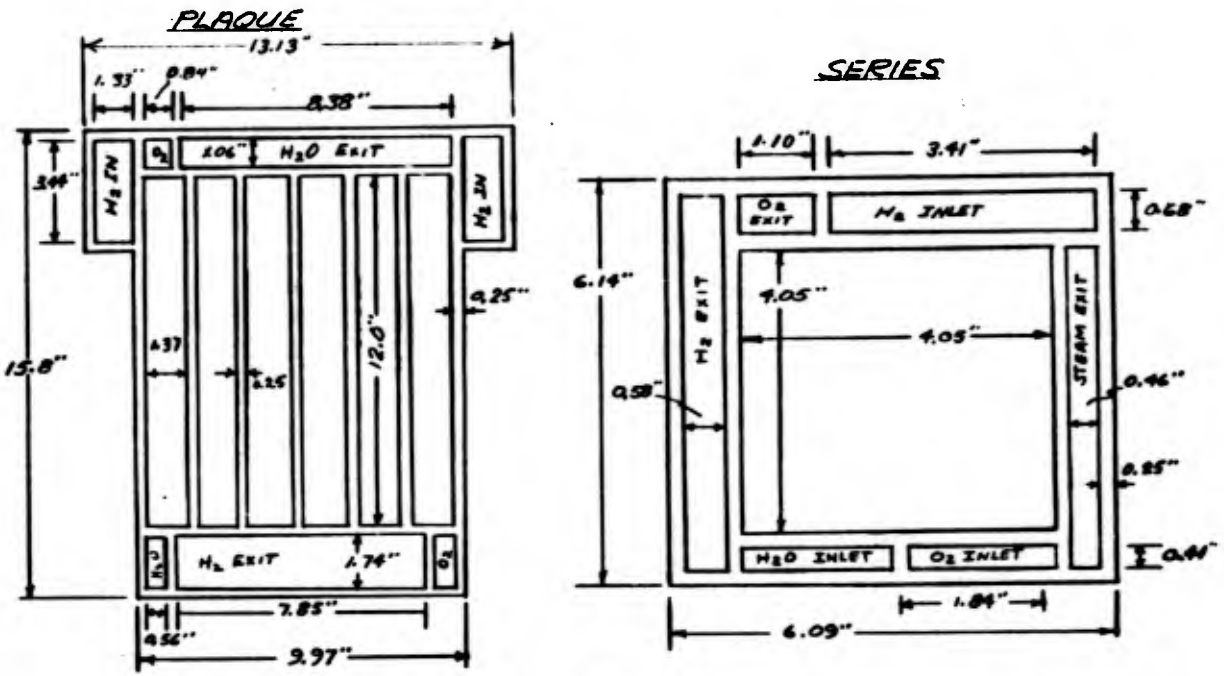

1 STACKS PER 550 KW MODULE - - - - - - - - 4

13.1" X 15.8" X ≈ 32" LONG - - - - STACK SIZE - - - - - - 6.1" X 6.1" X ≈ 44" LONG

2676 IN 446 PLAQUES - - - - NUMBER OF CELLS - - - - - - - - 2676

- PLAQUE HAS LESS EDGE FRAME PER UNIT ACTIVE CELL AREA
- SERIES HAS LESS TOTAL ELECTRODE PERIMETER SEAL AREA PER UNIT ACTIVE CELL AREA
- ALL FOUR EDGES OF SERIES AVAILABLE FOR MANIFOLDS
- TWO EDGES OF PLAQUE AVAILABLE FOR MANIFOLDS

Figure 38 — Stack Planforms

TABLE XXIII

HYDROGEN AND STEAM MANIFOLD SIZE

- ASSUMPTIONS

  1. MANIFOLD LOSSES ≈10% OF ALLOCATED FIELD ΔP. BASED ON FLOW DISTRIBUTION CONSIDERATIONS.

  2. MANIFOLD LOSSES ESTIMATED BY CONSIDERING MOMENTUM LOSSES ONLY AND NEGLECTING MANIFOLD FRICTION. BASED ON STACK DESIGN EXPERIENCE

- ANALYSIS

  1. BASED ON P&WA/U-CONN SEMI-EMPERICAL CORRELATIONS

  2. KNOWN QUANTITIES - FLOW RATE; FLOW PROPERTIES; FIELD ΔP

- RESULT - HYDROGEN AND STEAM MANIFOLD AREAS

	PLAQUE	SERIES
H_2 INLET	9.2 IN^2	2.3 IN^2
H_2 EXIT	13.6	3.4
STEAM	8.9	2.2

TABLE XXIV

OXYGEN AND WATER MANIFOLD SIZE

- ASSUMPTION - MANIFOLD AREA NOT CRITICAL FOR DEAD-ENDED FLOWS

- RESULT - CHOOSE MANIFOLD AREA PER AVAILABLE SPACE - 0.75 TO 1.0 IN^2 EACH

TABLE XXV

PLANFORM DEFINITION

- PLAQUE STACK

  1. CELL ASPECT RATIO SAME AS LeRC - 12" X 1.37"
  2. 6-CELLS PER PLAQUE - SAME AS LeRC
  3. 1/4" - EDGE FRAME FOR GAS SEAL AND I/C SEAL
  4. ONE STACK PER MODULE - ≈32" STACK LENGTH
  5. ONLY TWO EDGES OF PLANFORM AVAILABLE FOR MANIFOLDS. OTHER TWO EDGES REQUIRED FOR INTER-PLAQUE ELECTRICAL CONNECTION

- SERIES STACK

  1. SQUARE ACTIVE AREA - MINIMIZE PERIMETER FOR GIVEN AREA - 4.05" X 4.05"
  2. 1/4" - EDGE FRAME FOR GAS SEAL
  3. FOUR STACKS PER MODULE - MORE REASONAPLE STACK LENGTH (≈172" FOR 1-STACK OR ≈44" FOR 4-STACKS)
  4. RECTANGULAR SHAPED PLANFORM WITH MANIFOLDS ON ALL EDGES - EASIER TO PORT FIELDS AND SIMPLE ENDPLATE GEOMETRY

3. Selection of Cell Area

A study of cell size was conducted to define a preferred cell area. The objective was to select an area which would be compatible with a broad range of powerplant power and voltage ratings to provide flexibility in meeting the application requirements. It was concluded that for maximum power and voltage flexibility development efforts should concentrate on a small cell with an area of 14 to 21 $in.^2$. Because a cell with an area of 16.4 $in.^2$ was being developed, under a program sponsored by the NASA Lewis Research Center, this size was selected for use in this program. This choice provided the Air Force with economies in manufacturing tooling, processes, and methods without compromise in size.

A fuel cell system power output of 4.4 MW was assumed in the study to determine the preferred cell size. This power output was selected by the Air Force for this study. Other parameters considered included the system output voltage level and the power output of individual fuel cell modules contained in the system. Two ranges of system voltage levels (400 to 600 and 10,000 to 15,000 volts) and two module power levels (550 and 1100 kw) were studied. Figure 39 shows the relationship between these parameters. For the low voltage range, the individual modules are electrically connected in parallel to provide the desired system output voltage while for the high voltage range they are connected in series. The figure shows that a cell size of 14 to 21 $in.^2$ is necessary for the high voltage system and is independent of module power since all the cells are connected in series. A larger cell size is required for the low voltage systems with 550 and 1100-kw modules. In this case, cell size is proportional to module power. However, the effect of a larger cell can be achieved by connecting smaller cells in parallel. In fact, a 550-kw low voltage module can be achieved with three cells of the smaller size required for the high voltage system connected in parallel. Consequently the smaller area cell is suitable for either high or low voltage systems and provides maximum power and voltage flexibility.

4. Optimization of Substrate Plating Thickness

A parametric study was performed to determine the optimum thickness of substrate plating. As substrate plating thickness is increased electrical resistance and losses in the substrate decrease, increasing the net power delivered by a unit area of electrode. However the weight of the unit area electrode increases, as plating thickness increases, offsetting some of the gain when specific weight, lb/kw, is considered. The study utilized experimental values of resistivity obtained from bench test data prior to actual strip-cell testing. Figure 40 shows cell performance predicted at 3000 ASF for variations of plating thickness about the nominal 0.5-mil plating on the electrode area of standard substrates. A 1.0-mil plating is assumed for the intercell and interplaque connection in all cases. The predicted average loss for 0.5-mil plating was 90 mv or 270 WSF, although, subsequent cell testing has shown considerably lower losses. Figure 41 shows the combined effect of weight and performance increase. The power level was held constant and plaques were added or subtracted as performance varied with plating thickness. Curves are shown for a variation in cell weight (lb/ft^2) representing a range of different cell constructions with electrode substrate weight excluded. Two conclusions are evident; (1) 0.5- mil plating is close to the optimum for all levels cell weight, and (2) the optimum is essentially flat over quite a range of plating thickness. As a result 0.5-mil thick substrate plating was selected for the cells fabricated in this program.

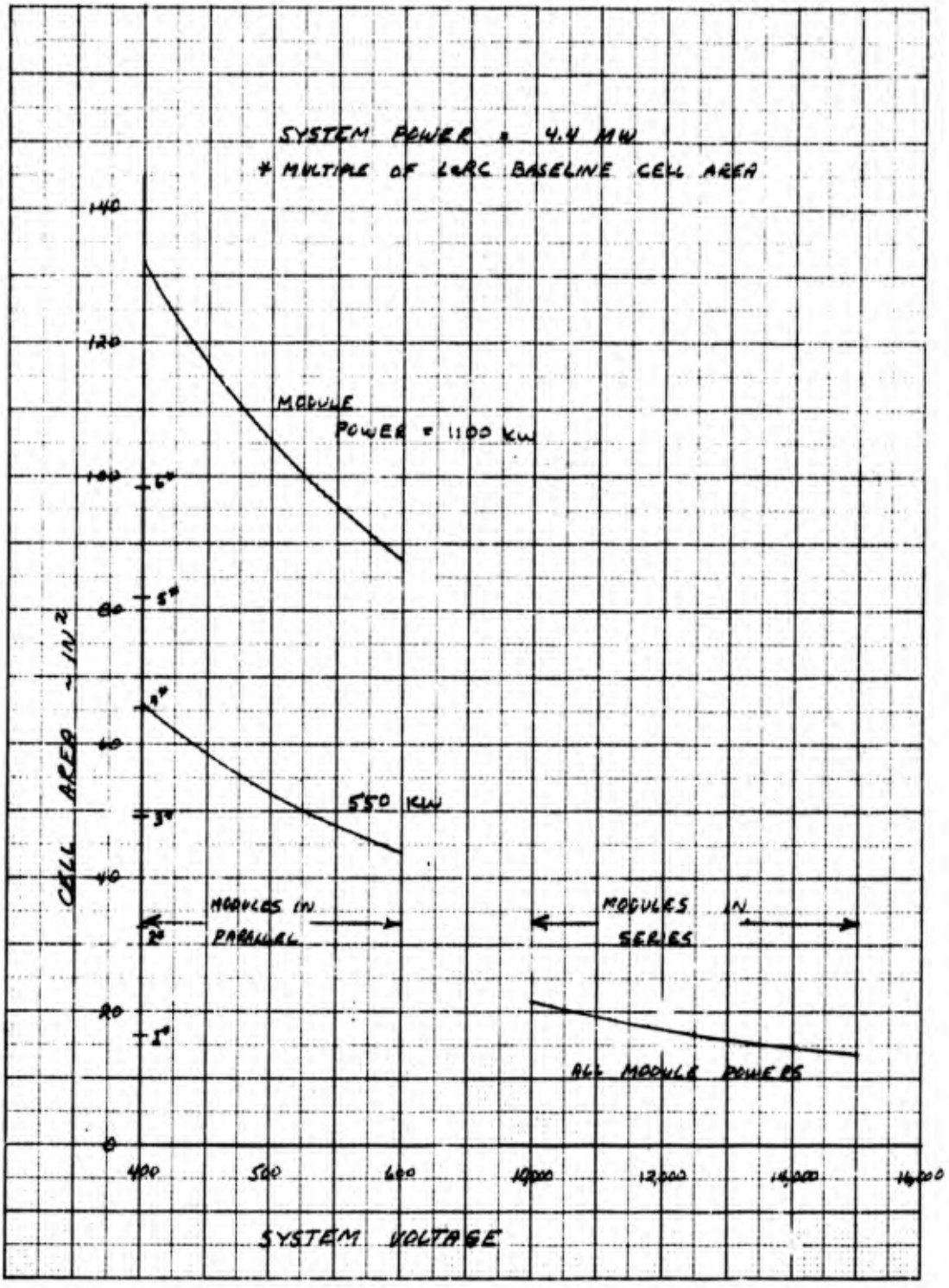

Figure 39 – Cell Area vs. System Voltage

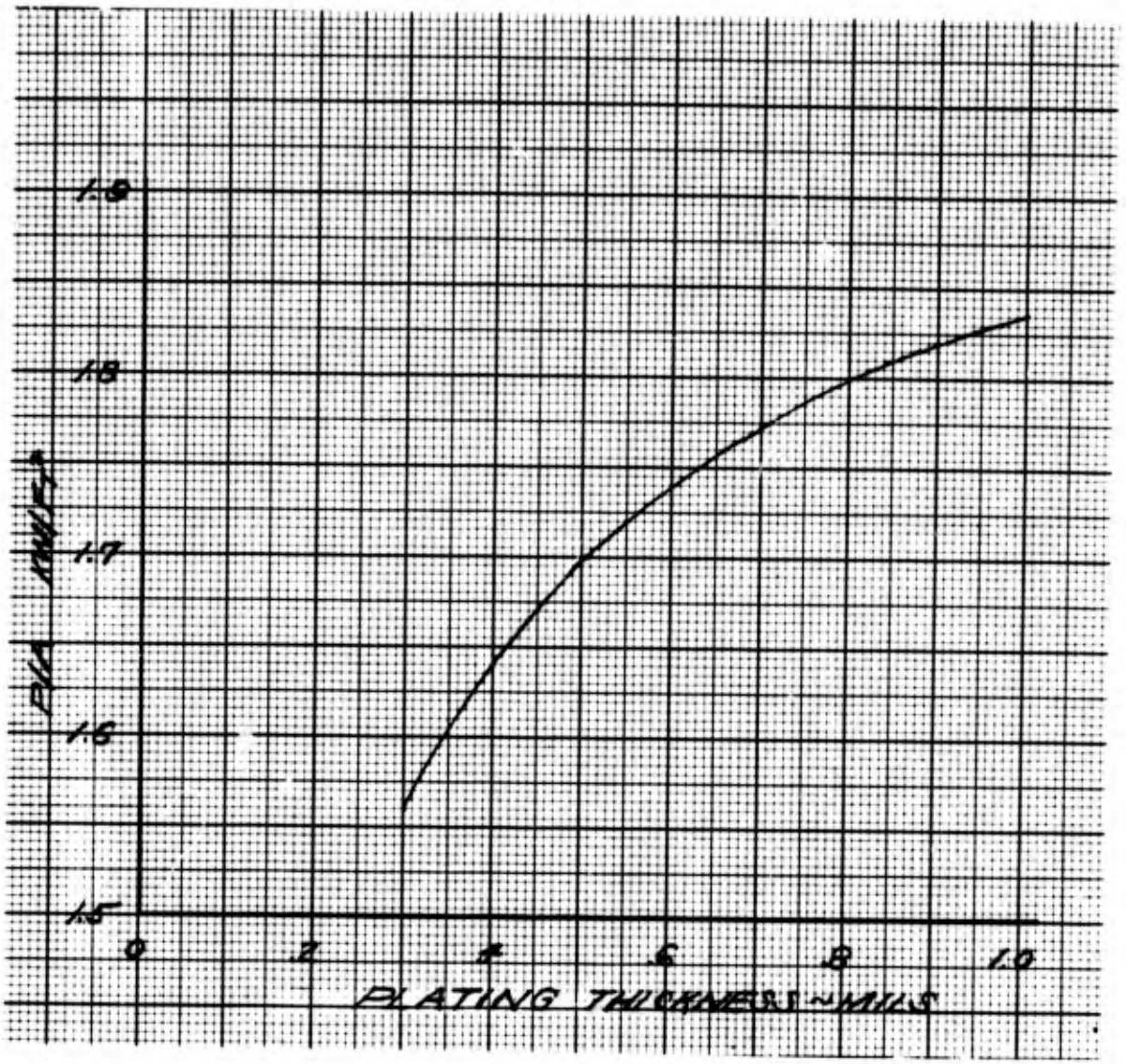

Figure 40 – Improved Cell Power Output at 3000 ASF for Variations in Electrode Substrate Plating Thickness

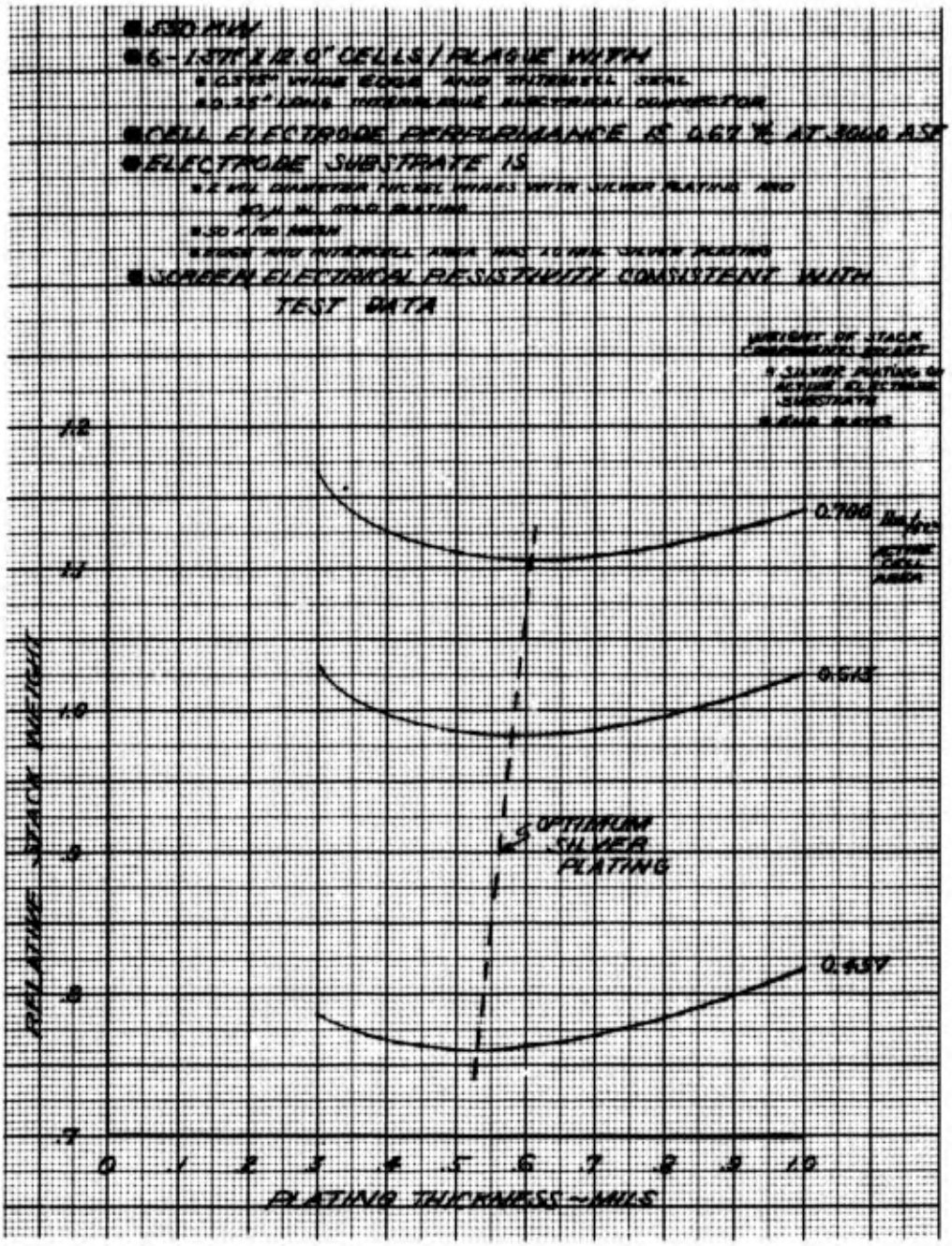

Figure 41 — Effect of Substrate Plating Thickness on Stack Weight

5. Definition of Improved Planform

During the Design Review of the High Power Density Stack at AFAPL, including the plaque planform shown above in Figure 38, it was recommended that all manifolds be located in the area at the ends of the cells, rather than in the area parallel to the major dimension of the cells. This change permits maximizing the width of the plaque-to-plaque connections along the major cell dimension to decrease IR and I^2R losses. The revised planform is shown in Figure 42 and the flow geometries for each fluid are shown in Figure 43. Pressure drop estimates for these flow geometries were made and were judged to be acceptable, the results were:

Fluid	Press. Loss (psi)	Field Geometry
Hydrogen	1.9	25-mil depth-50 percent free area
Oxygen	0.75	15-mil depth-50 percent free area
Water/Steam	8.0	25-mil depth-50 percent free area

In addition, thermal studies were conducted to define the differential between the cell temperature and the bulk temperature of the water/steam mixture. The result indicated the temperature differential would be less than 40°F. Appendix A presents the assumptions made in these analyses, parametric data developed for the analyses, and sample calculations for two cooler geometries.

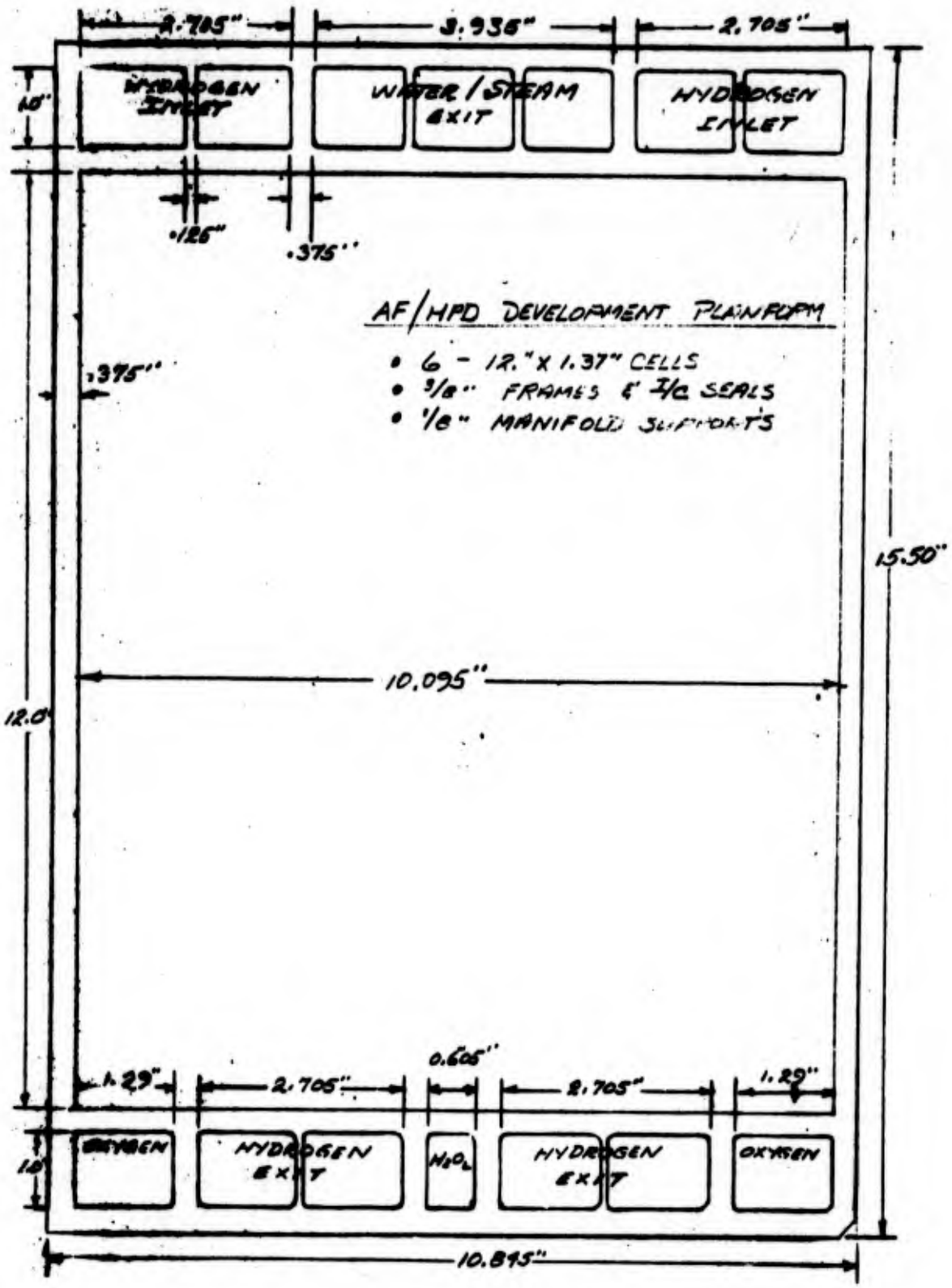

Figure 42 — Improved Plaque Planform

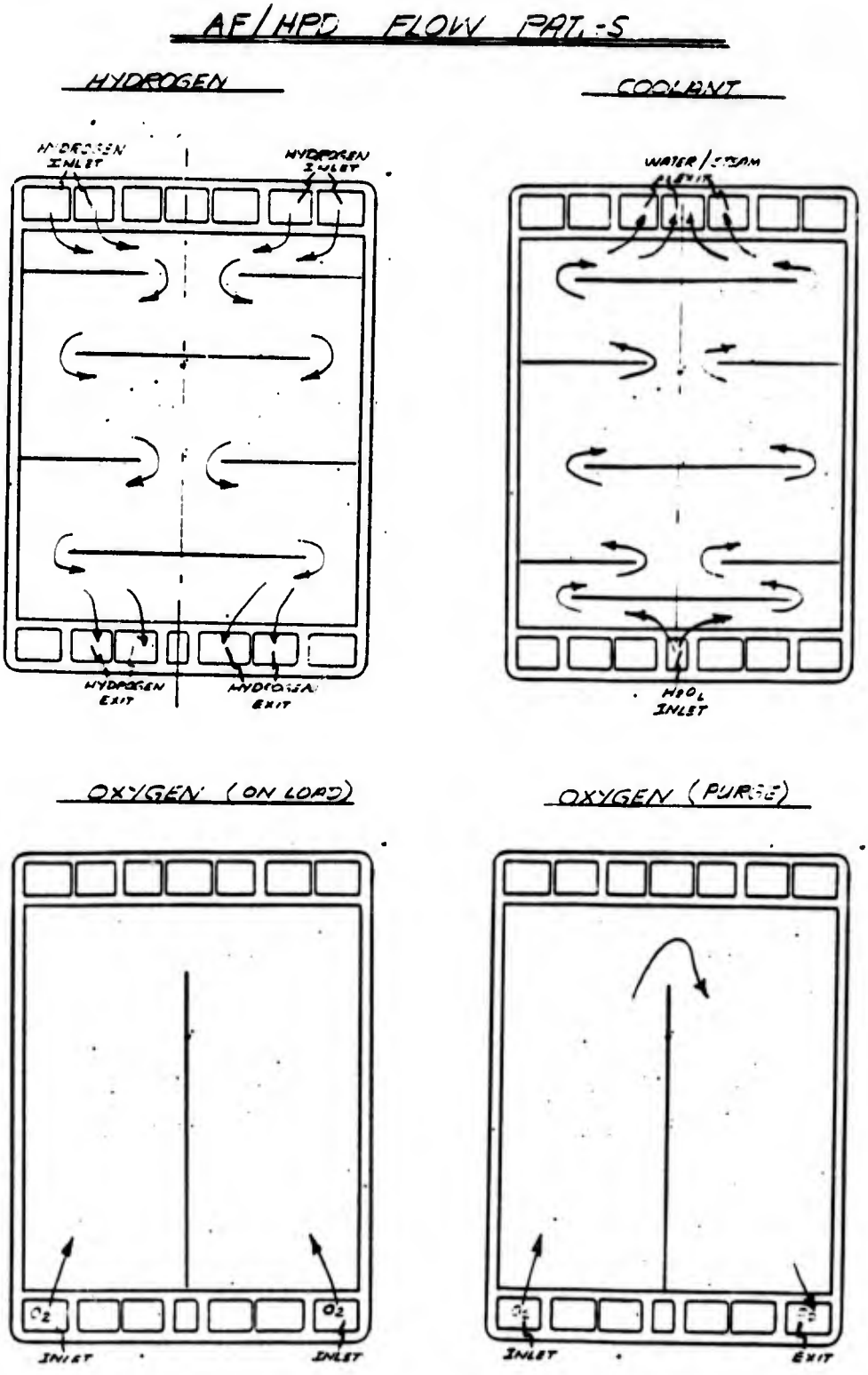

Figure 43 – Flow Field Geometry for Improved Planform

6. Subsystem Analysis

Selection of Cooling Subsystem Concept

The high power density stack is evaporatively cooled. This approach ensures uniform cooling of the cells at the high heat flux at which the coolers operate. Control of the back-pressure imposed on the cooler sets the temperature at which the evaporation occurs and, in turn, the cell temperature. Two approaches to cooler design were considered. They are illustrated in Figure 44. In both coolers evaporation of water to steam occurs within the stack. Water is pumped into the stack into cavities adjacent to the oxygen electrode. In the first approach as steam is generated it passes through a porous hydrophobic membrane, which prevents liquid water from leaving the cooler, and passes from the stack into an external condenser. It can also be vented overboard. In the second approach steam and water flow from the stack to an external dynamic separator where the steam and water are separated. The water is returned to the stack and the steam can be condensed or vented overboard.

Analysis of both approaches resulted in the comparison presented in Table XXVI. A cooling system based on external steam/water separation was selected for development. This choice was made because:

1) A system weight saving of 0.7 lb/kw, or 14 percent of the system goal, could be achieved.

2) Development risk was lower because the state of development of dynamic separator was judged higher than the internal separator membrane, and,

3) The stack design was less complex and required fabrication of fewer pieces.

The pump/separator design used for the comparisons is shown in Figure 45. It consists of a perforated disc separator section which slings liquid to the outside while steam passes axially through the unit. The water flows from the periphery of the separtor, through a check valve, into the pump which returns it to the stack. This design is based on experience with pump/separators designed and developed for undersea and space powerplants.

- INTERNAL

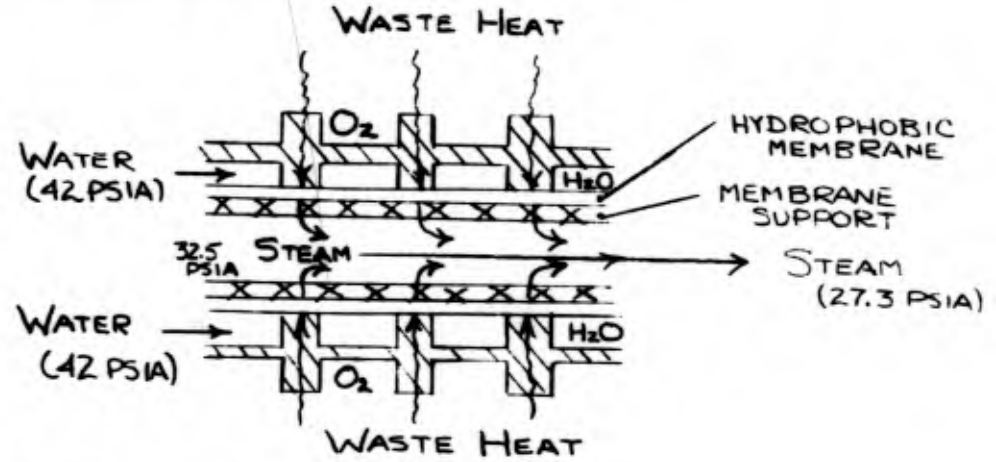

WEIGHT FOR ELEMENTS SHOWN

0.16 lb/kw

- EXTERNAL

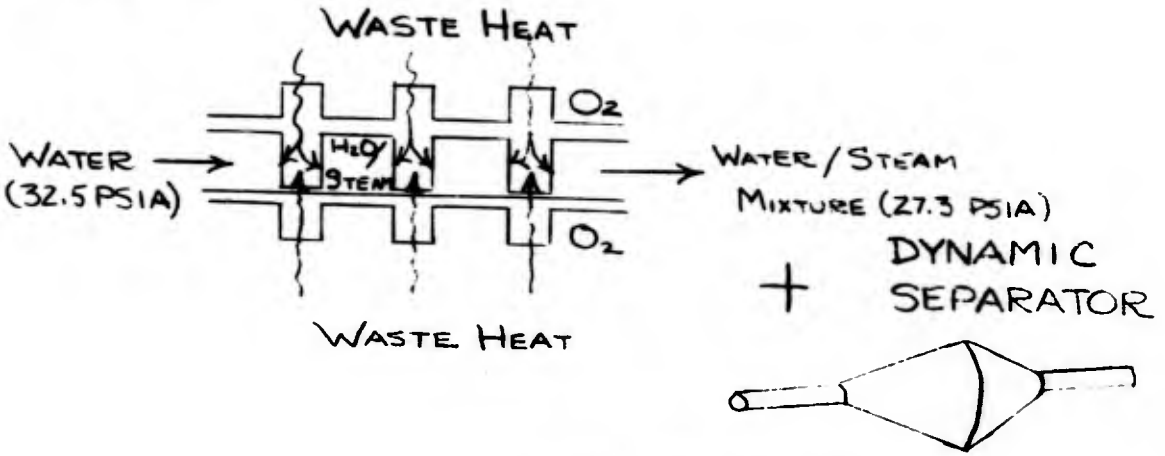

0.09 lb/kw

Figure 44 — Steam Separator

TABLE XXVI

COMPARISON OF STEAM SEPARATION OPTIONS

INTERNAL	EXTERNAL
• WEIGHT: 0.16 lb/KW (stack elements)	• WEIGHT: 0.09 lb/KW (stack elements plus separator) 14% WEIGHT SAVINGS
• REQUIRES HYDROPHOBIC STEAM SEPARATOR INSIDE STACK THAT:	• REQUIRES MECHANICAL STEAM - WATER SEPARATOR OUTSIDE STACK TO SEPARATE 1754 LB/HR STEAM FROM 1952 LB/HR LIQUID WATER. MECHANICAL SEPARATOR CONCEPT BASED ON H_2-H_2O SEPARATORS IN SPACE AND UNDERWATER POWER-PLANTS.
• SEPARATES 5.75 LBS STEAM/HR-FT^2 MEMBRANE FROM LIQUID WATER	
• WITHSTANDS $\approx$15 PSI CROSS PRESSURE DIFFERENTIAL. (ΔP REQUIRED TO PRECLUDE WATER BOILING IN WATER FLOW FIELD)	
• BASED ON LeRC EXPERIENCE BUT MUST HAVE 8 TIMES GREATER FLOW AND ΔP CAPABILITY	• REQUIRES O_2-COOLANT SEPARATOR PLATE TO WITHSTAND $\approx$18 PSI CROSS PRESSURE DIFFERENTIAL.
• REQUIRES O_2-COOLANT SEPARATOR PLATE TO WITHSTAND $\approx$3 PSI CROSS PRESSURE DIFFERENTIAL	
• REQUIRES SEPARATE STACK FLOW FIELD AND MANIFOLD FOR LIQUID COOLING WATER AND STEAM	• REQUIRES ONE STACK FLOW FIELD AND MANIFOLD FOR BOTH LIQUID COOLING WATER AND STEAM

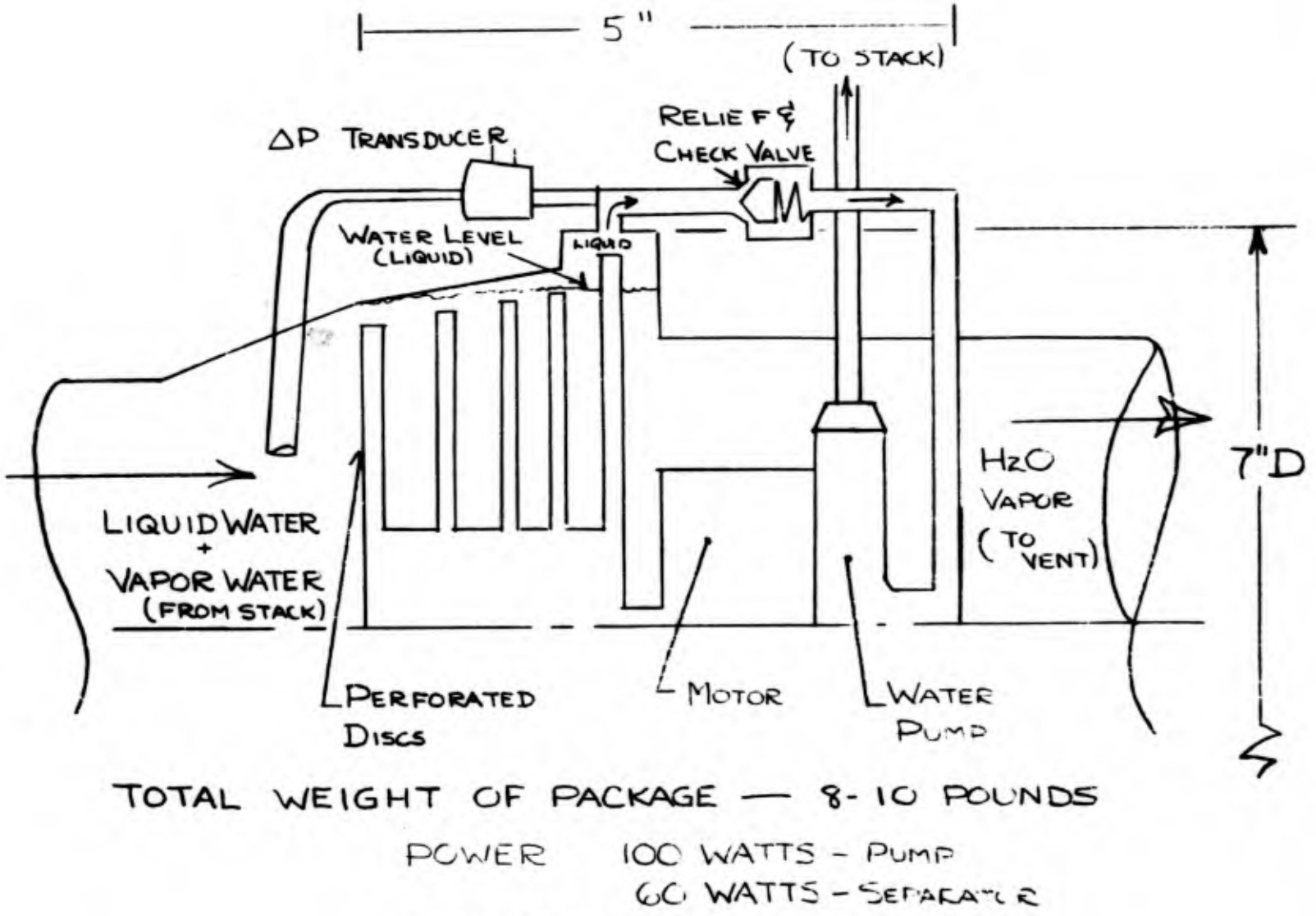

Figure 45 – External Steam Separator/H_2O Pump

D. ALTERNATE HEAT REJECTION SYSTEM

In the baseline high power density heat rejection system the water which is evaporated to steam is vented overboard. A system in which the water is condensed and returned to the powerplants was considered as an alternative to the baseline. In this system a ram-air heat exchanger is used to condense the steam generated within the powerplants. The objective was to determine whether the closed system, in which water is recirculated, might be lower in weight than the open system. For this study a mission of 2 minutes duration with a power delivery of 4 MW was considered. For the open cycle cooling system this mission requires 450 pounds of cooling water.

The design and evaluation of the ram-air heat exchanger was conducted by the Hamilton Standard Division of United Aircraft Corporation. Hamilton Standard was selected because it has designed and supplied heat exchangers for many airborne applications. The study covered a range of speeds from Mach 0.5 to 0.9 and altitudes from 15,000 to 45,000 ft. Core weights and frontal areas, drag penalties, and estimates of ducting weights were made. The results are summarized in Hamilton Standards Design Study No. 294 "Fuel Cell Condenser Study", January 10, 1973, which is included as Appendix B of this report.

The conclusion is that no weight saving would be achieved by incorporating a ram-air heat exchanger into the system for water vapor recovery. In fact, for a two-minute mission, the weight of the condenser core and its associated ducting and propulsive fuel, to overcome increased drag, would approach 700 pounds. An addition weight penalty for the ram scoop, retracting mechanism, and overboard louvers should be added to this figure to define a complete system weight. These weights were not defined because, based on the weight of the partial system, it was apparent this approach provided no weight advantage.

IV DEVELOPMENT EFFORTS

A. INTRODUCTION

The key technical objective of the development effort was demonstration of the feasibility of a multimegawatt fuel cell powerplant with a specific weight of 0.5 lb/kw or less. Achievement of this objective was approached as a three part problem: 1) Developing a cell configuration which could operate at the highest power density possible, 2) developing stack components of the least possible weight per unit area, and 3) combining these stack compomponents and the advanced cell configuration into development units which were the basic repeating sections of a fullsize powerplant stack. Each of these steps built upon experience and hardware developed by P&WA under previous Air Force and NASA-sponsored programs. P&WA had begun development of a high power density cell in a program to develop a "Dual-Mode High Power Density Fuel Cell Power System" under Air Force Contract F33615-70-C1134. This program had as its objective a fuel cell powerplant that could operate in two modes: when it supplied a nominal power output, and operated at low cell current and power densities, it was cooled by a circulating liquid, but when it supplied peak power, at many times the nominal power current and power densities, it was cooled by evaporating water within the cell stack. This work provided both a starting point in terms of a candidate high power density cell configuration and an evaporative cooling concept require for the high power density powerplant.

Steps (2) and (3) were based on work performed by P&WA for the NASA Lewis Research Center under Contract NAS3-15339. This work, aimed at developing advanced lightweight fuel cells, provided background in lightweight materials and designs and also in evaporative cooling concepts.

To achieve low weight this program used plastics for all cell and stack structural elements and had developed a lightweight planar arrangement of six cells called a plaque. Each of the six cells in a plaque, see Figure 46, measured 1.375 in. x 12 in. Current transfer from cell to cell is in the plane of the plaque through the molded intercell seals. This concept eliminates the need for conducting current from cell-to-cell through the separators used between cells. With the need for electrical conductivity eliminated these cell separators can be made of plastic, significantly reducing the weight of the major structural elements of a stack. Plaque-to-plaque transfer of current is achieved by interconnections made to the screens which extend beyond the edge of the stack. With this background steps (1) and (2) were undertaken concurrently: Step (3) began as success was achieved in the first efforts. Each of these activities is described in the sections which follow.

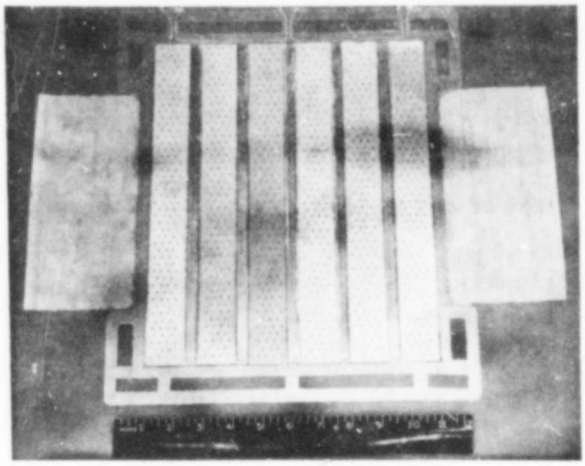

Figure 46 – Six-Cell Plaque

B. SINGLE CELL CONFIGURATION AND PERFORMANCE IMPROVEMENT

The objective of this task was to develop an improved cell in the strip configuration (1.375 in. x 12 in.) that could be incorporated into a lightweight plaque and could operate at a power density of at least 2000 watts per square foot. The approach was to improve the cell by reducing the losses in the individual elements of the cell. This included investigating the preparation and loading of catalysts, to reduce activation polarization; improving current collection and conduction, to reduce ohmic losses; and improving and thinning matrices, to reduce ionic losses.

Initial experimentation and development was conducted with the 4 in. x 4 in. cell configuration developed under the "dual-mode" cell program. As the configuration was improved strip cell development was begun. This led to a baseline strip cell which was improved through a series of configurations to a unit that was operated up to 3000 watts per square foot. The weight of a stack based on this cell design, designated Configuration 4, was 0.45 lb/kw, if a cell power density of 2150 watts per square foot was assumed. This power density was the baseline power density used in the design of the powerplants and power system described in Section III. If the cell were to be operated at higher power densities, closer to the maximum demonstrated, the specific weight of the stack would be correspondingly reduced.

Table XXVII summarizes the testing of the 4 in. x 4 in. cells at the beginning of the development program. Ten tests were conducted in all, including initial cooling system and test stand operation verifications. Beginning with Cell 5, a power density of more than 2000 WSF was demonstrated.

TABLE XXVII

HIGH POWER DENSITY SINGLE CELL TEST SUMMARY

Cell No.	Rig No.	Features	Max. Demon. Power Density (watts/ft^2)	No. Starts	Total Load Time (hrs)	3000 ASF Load Time (hrs)
1	38127-1	Dummy cell for cooler check-out	D.N.A.	D.N.A.	D.N.A.	D.N.A.
2	38127-2	Standard Platinum Catalyst Electrodes 100-Mil Nickel ERP	1260	4	7.1	0.6
3	38127-3	Standard Platinum Catalyst Electrodes 100-Mil Nickel ERP	1410	2	3.7	0.2
4	38127-4	Au/Pt Cathode, High Sinter Temp (635°F) Anode, 30-Mil Nickel ERP	1884	5	20.8	3.1
5	38127-5	Au/Pt Cathode, 635°F Anode, 30-Mil Nickel ERP	2118	9	47.4	19.3
6	38127-6	Au/Pt Cathode, 635°F Anode, 30-Mil Nickel ERP, No Cathode Support Screen	437	1	2.5	0
7	38127-7	Au/Pt Cathode, Standard Platinum Anode (590°F), 30-Mil Nickel ERP	2140	3	16.2	5.1
8	38127-8	Same as 7	1980	1	6.2	3.2
9	38127-9	Au/Pt Cathode, 635°F Anode, 30-Mil-Ni ERP, 5-Mil Matrix	2559	4	17.7	6.0
10	38127-10	Same as 9	2290	3	18.1	2.0

Table XXVIII summarizes the testing of the 15 strip cells that led to the lightweight Configuration 4 cell that operated well above goal power density.

Although the first strip cells were not strictly Configuration 1 or 2 a gradual progression of lightening cell construction was made throughout this development activity. Table XXIX presents a weight breakdown for each configuration and the equivalent weight of a stack based on that configuration if operated at 2150 WSF. The physical differences which account for the weight differences in the configurations are discussed as part of the single cell tests in which they were proven. In the course of the program, electrode structures and characteristics were improved. When a new electrode structure was first developed it was usually fabricated in the laboratory by engineers and technicians and is referred to as a "lab" electrode. When it was decided to use this type of electrode repeatedly, the processes for its manufacture were transferred to P&WA's semi-production electrode manufacturing operation. It was then fabricated by shop personnel and is referred to as a "shop" electrode. Each strip cell test is described in the section which follows. This section also discusses each of the ten 4 in. x 4 in. single cell tests.

The test discussions often refer to procedures P&WA has developed for diagnosis of a cells operating condition. These procedures are described here for reference.

Performance Calibration: Voltage-current characteristics generated to 3000 ASF and higher. Taken periodically, the performance calibration changes with time and is a valuable tool in determining the type and extent of any decay mechanisms. This is especially true of the semi-log representations of the performance data on an IR free basis which are commonly described as Tafel plots.

Tafel Plots: The Tafel region refers to the low current density portion of a performance calibration. In this region, anode and ohmic polarizations are minimal or correctable so the cell voltage is essentially cathode activation limited performance. The Tafel region extends from approximately 1 ASF to a level where diffusion losses become significant, 10 to 100 ASF, which is a function of operating temperature and pressure. In the Tafel region, the semi-log voltage-current curve should be a straight line, with a slope characteristic of the catalyst/reactant combination and a level proportional to the cathode activation.

Departures from this slope are an indication of parasitic loads, either internal cell shorting or gas crossover. Thus, the Tafel slope is a useful diagnostic tool in assessing the life expectancy of an operating cell. Changes in the levels of Tafel data are also a useful tool, since they indicate changes in the activity of the catalyst, either through changes in the number of active catalytic sites or structural modifications (e.g., recrystallization), changing the effective catalyst active area.

The so-called Tafel plot is also a useful diagnostic tool at current densities above the Tafel region. At these current densities, typical of operating cells, internal resistance (IR) corrections are required. When the cell performance is thus corrected, changes in the shape of the curves can be interpreted as changes in the diffusion characteristics of the electrodes. In this region, transport limitations are encountered if the electrode structure is not adequate for

delivery of reactants or removal of product water. For example, diffusion problems can be related to flooding of the Teflon microscopic pores in a wet proofed electrode, or to increased concentration gradients in a heavily carbonated cell. While the semi-log performance plots alone do not distinguish such possible causes or even anode from cathode losses, they are valuable tools, in conjunction with previous experience and post-test analysis, in evaluating any performance decay trends.

TABLE XXVIII

HIGH POWER DENSITY STRIP CELL TEST SUMMARY

Cell No.	Rig No.	Features	Cell Stack Design Specific Weight (lbs/kw) @ 2150 WSF	Max. Demon. Power Density (watts/ft^2)	No. Starts	Total Load Time (hrs)	3000 ASF Load Time (hrs)
1	38239-1	Anode: Au Screen PPF 590°F Cathode: AuPt on Au Screen ERP: 30 Mil Ni	0.96	1620	3	6.8	2.4
2	38239-2	Anode: 1/2 Mil Ag Screen 590°F PPF Cathode: AuPt on 1/2-1.0 Mil Ag Screen ERP: 30 Mil Ni	0.96	1740	1	7.9	6.0
3	38239-3	Anode: 1/2 Mil Ag Screen 635°F PPF Cathode: Standard ERP: 20 Mil Ni	0.92	2040	2	7.2	1.5
4	38239-4	Anode: 1/2 Mil Ag Screen 635°F PPF Cathode: AuPt on 1/2 Mil Ag Screen ERP: 30 Mil Ni	0.96	1710	2	7.7	0.1
5	38239-5	Anode: STD on 50 x 100 Cathode: STD on 50 x 100 ERP: 20 Mil Ni	0.82	1880	3	9.7	3.8

TABLE XXVIII (CONT'D)

HIGH POWER DENSITY STRIP CELL TEST SUMMARY

Cell No.	Rig No.	Features	Cell Stack Design Specific Weight (lbs/kw) @ 2150 WSF	Max. Demon. Power Density (watts/ft^2)	No. Starts	Total Load Time (hrs)	3000 ASF Load Time (hrs)
6	38518-6	Electroformed Ni Cooler (Config. 2)	0.73	1940	2	6.0	0.3
7	38519-7	30 Mil Polysulfone ERP (Config. 3)	0.65	815	2	9.1	0
8	38520	Configuration 3	0.64	1270	3	18.7	0
9	38521	Configuration 3	0.64	1818	2	10.4	0.1
10	38522	Configuration 3	0.64	2030	4	24.1	1.1
11	38523	Configuration 4 (UEA from S/C No. 10)	0.47	1695	3	11.4	0.1
12	38667	Configuration 4	0.45	1406	1	1.2	0
13	38722	Configuration 4 (10-mil matrix)	0.48	2150	6	23.0	5.1
14	38788	Configuration 4	0.45	2320	2	8.4	2.5
15	38806	Configuration 4	0.45	3000	2	5.6	0.1

TABLE XXIX

HIGH POWER DENSITY REPEATING UNIT WEIGHT ESTIMATES

Item	Configuration 1	Configuration 2	Configuration 3	Configuration 4
2 - 6 Cell Plaques				
Substrates	†0.30 lbs (100x100 Mesh)	†0.23 lbs (50x100 Mesh)	†0.23 lbs	†0.23 lbs
Catalyst	†0.12	†0.11	†0.11	†0.11
Matrix	†0.06 (10-Mil RAM)	†0.06	†0.06	0.03
Electrolyte	0.10	0.10	0.10	0.06
Frame	0.11 (Epoxy/Fiberglass 5-Mils Pinch)	0.11	0.11	0.09
	0.69 lbs	0.61 lbs	0.61 lbs	0.52 lbs
H_2 Flow Field/ERP				
Field Insert	0.14 (Polysulfone)	†0.18 (Astrel)	†0.18	0.09 (Plated Porous Polysulfone ERP/H_2 Flow Fields 0.025 Field Depth)
Field Frame	0.16 (Epoxy/Fiberglass)	†0.16	†0.16	
ERP	†0.67 (30-Mil Ni)	†0.47 (20-Mil Ni)	†0.17 (20-Mil Polysulfone)	0.11 (Epoxy/Fiberglass Frame)
Electrolyte	0.084	0.05	0.01	0.01
ERP Frame	0.21 (Epoxy/Fiberglass)	0.14	0.14	
	1.26 lbs	1.00 lbs	0.66 lbs	0.21 lbs
Coolant Flow Field				
Field Insert	0.09 (Polysulfone)	†0.11 (Astrel)	†0.11	0.07 (Unplated Porous Polysulfone 20-Mil Flow Field)
Frame	0.09 (Epoxy/Fiberlass)	†0.09	†0.09	0.09 (Epoxy/Fiberglass Frame)
	0.18 lbs	0.20 lbs	0.20 lbs	0.16 lbs
O_2 Field Separator				
Plate Assembly		Option B	Option B	Option B
Field Insert	†0.27 (Ni-plated Magnesium)	†0.16 (Electroformed Ni Without Backfill)	†0.16	†0.16
Separator	0.23 (3-Mil Ni)	0.08 (1-Mil Ni)	0.08	0.08
Frame	0.11 (Epoxy/Fiberglass)	†0.15	†0.15	†0.15
Dielectric	0.08 (FEP)	0.04 (Epoxy/Fiberglass)	0.04	0.04
	0.69 lbs	0.43 lbs	0.43 lbs	0.43 lbs
Repeating Unit Weight	2.82 lbs	2.14 lbs	1.89 lbs	1.32 lbs
Lbs/kw at 2.15 kw/ft^2	0.95	0.73	0.64	0.45

†Actual Weights

Internal Resistance (IR): Internal resistance or ohmic polarization losses are unavoidable in any cell. However, they can be minimized by matrices with high porosity and correct assembly to insure proper cell compression. In the strip cell with edge current collection, there are also resistance losses in the electrode substrates and edge frames which are measured together with the conventional ohmic loss. IR measurements are taken periodically to insure that the initial assembly is correct and that the correct cell compression is being maintained.

IR measurements are taken by the current interruption technique. Typically, a 100 ASF load is interrupted and the resulting step change in voltage is measured on a Tektronix Type 545 oscilloscope. Since other polarizations have a long response time, the step change is a direct measure of internal cell resistance.

Dilute Oxygen Diagnostic Test: Although the Tafel and IR tests give good indication of relative cathode-matrix-anode losses at low current densities, they cannot be used to distinguish cathode and anode losses in the diffusion region, the area of operational interest. This technique permits identification of anode and cathode losses in the diffusion region by running performance sweeps on 20 percent oxygen/80 percent nitrogen and on pure oxygen. It is based on the fact that cathode performance is proportional to the partial pressure of oxygen. A graphical procedure based on this relationship, illustrated in Figure 47, allows determination of individual electrode performance.

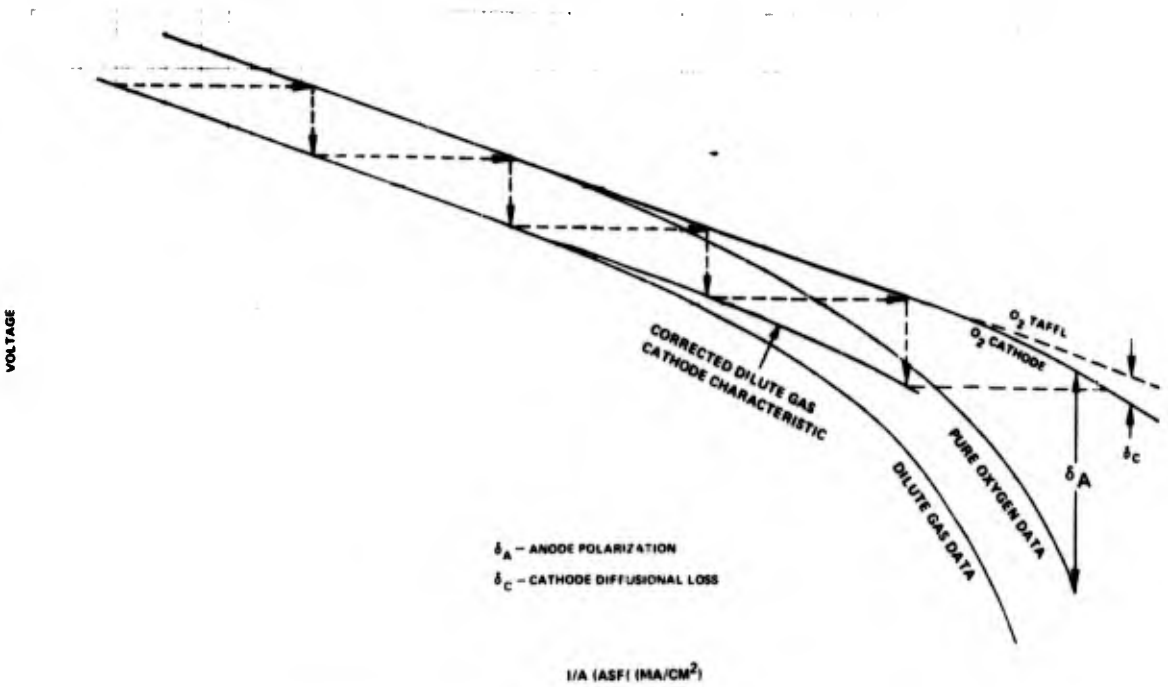

Figure 47 – Dilute Gas Diagnostic Method

A point in the activation region is selected on the dilute gas (20 percent oxygen) data curve and the current is multiplied by 5, the ratio of oxygen partial pressures. The corrected point is plotted and compared to the oxygen data curve; if the point falls on the oxygen curve, no anode polarization has occurred. When a deviation occurs between the corrected point and the actual oxygen curve, the deviation is attributed to anode polarization. A correction is then made up to the 20 percent oxygen curve corresponding to this amount of anode polarization and the procedure is repeated.

When the true oxygen polarization curve is obtained, the difference between this curve and the generated oxygen data is anode loss. The deviation of the corrected cathode performance curve from the oxygen Tafel line is normally attributed to diffusional loss.

This approach does not separate anode losses into such categories as poisoning, flooding, concentration polarization and undescribed resistance but it does clearly show which electrode has the major effect on cell performance.

Off-Design Tolerance: If a cell is improperly filled, or if the contact between the ERP and cell is inadequate, the off-design tolerance characteristics of the cell will depart from the normal value. Off design tolerance data can be generated in various ways. In the high power density cells the most convenient method is to vary the dew point of the inlet hydrogen gas. This in turn changes the volume of the electrolyte causing a transfer of electrolyte between the cell and ERP.

Post-Test Analysis: All cells are subjected to post-test analysis. This includes visual (and microscopic) examination of components for observable changes in physical properties, structural defects, or peculiar deposits. Because of the importance of electrode performance in this program cells are analyzed in the laboratory for electrode structural changes such as catalyst recrystallization and flooding. Tests such as this are done by the floating half-cell method, electrolyte take-up measurements, and photomicrographs.

1. Development and Testing of 4 inch x 4 inch Cells

Cell 1 – The objective of this test was to verify proper operation of the cooling system to be used for high power density single cell testing. This cooling system, together with a hydrogen and an oxygen reactant supply system, comprise the test stand used for high power density tests. A schematic of the test stand is shown in Figure 48. The cooling system supplies heated water to the cell, where cooling is accomplished by partially boiling the water in a cavity adjacent to the cathode. The steam-water mixture flows from the cell into a condenser and is condensed to water. The pump returns the water through a trim-heater to the cell. The boiling temperature is controlled by setting a selected back pressure on the condenser with the nitrogen blanket regulator. The cooling system was evaluated using a dummy "dual-mode" cell with a heater pad simulating fuel cell heat loads. Temperatures were measured, within the water-steam cavity next to the heater pad, initially at a heat flux of 6700 BTU/hr/ft^2 (equivalent to 3000 ASF at 0.63 volts per cell) over a range of steam qualities.

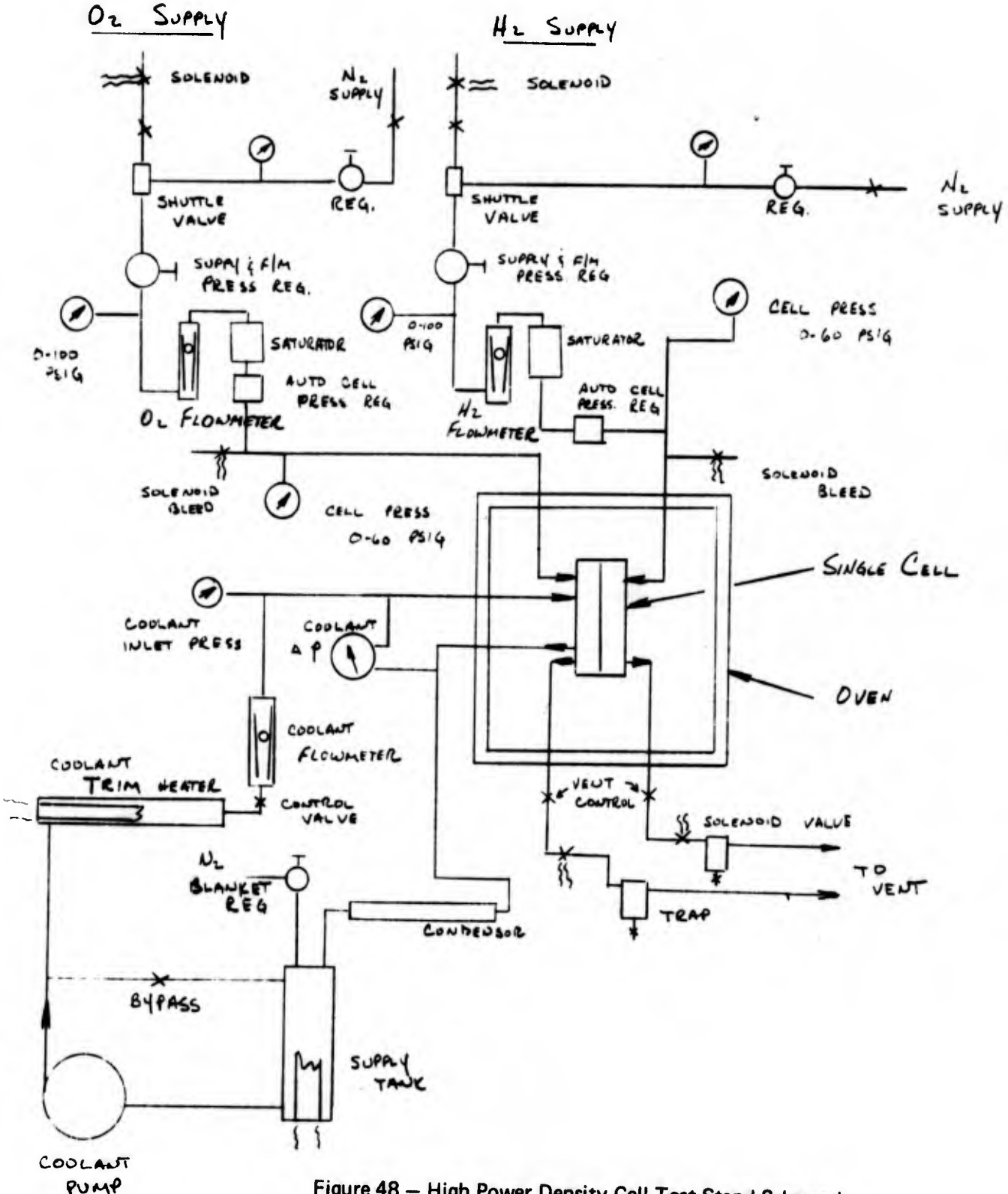

Figure 48 — High Power Density Cell Test Stand Schematic

Then the heat flux was increased by a factor of 1.5 to 10,000 BTU/hr/ft^2. The system back pressure was set to maintain a 250°F temperature on the thermocouple located between the magnesium cooling plates. The pressure drop was measured and compared to the predicted values. Isothermal operation (temperature gradient from cell inlet to exit was less than 2°F) at 250°F was obtained over the following range of conditions:

System Pressure (PSIA)	Applied Heat Flux (BTU/hr/ft^2)	Steam Exit Quality (%)	Measured Delta P (PSI)	Estimated Delta P (PSI)
29.7	6700	16	0.80	0.76
29.7	6700	32	0.65	0.60
29.7	6700	73	0.60	0.43
29.7	10000	40	1.00	0.87

These results indicated that the loop could maintain proper thermal conditions and would provide cooling at all heat-flux values anticipated in the development program.

Cell 2 – Test stand and cell checkout was initiated with the operation of Cell 2. This cell was a "dual mode" 4 inch x 4 inch cell with standard platinum catalyst electrodes a 10-mil thick reconstituted asbestos matrix, and 100-mil nickel electrolyte reservoir plate, (ERP), see Figure 49. Magnesium separator plates, of the type used to build the "dual mode" breadboard demonstrator, stack, see Figure 50, were also used with this cell to provide reactant and cooling cavities. Test stand checkout and cell operation was conducted at 220°F and at an operating pressure of 40 psia. A total time of 25 minutes at 3000 ASF and over one hour above 2500 ASF was accumulated on this cell. Testing was terminated by failure of a saturator that prevented establishing conditions to permit operation at the proposed design temperature of 250°F. Performance data generated during the testing is shown in Figure 51. Operation of the test stand cooling system for high power density cell testing appeared satisfactory.

Cell 3 – This cell, like Cell 2, was constructed with standard platinum electrodes and a 100-mil nickel ERP and a 10-mil thick matrix. The successful testing of this cell completed initial assembly, hardware, and stand checkout. The test emphasized operation at 250°F and established procedures for diagnostic and calibration tests. Testing included steady state operation at 250°F, measurements of cell Internal Resistance (IR), and low current density calibrations (Tafel plots).

Cell 4 – This cell test was the first to evaluate a gold/platinum (Au/Pt) cathode, an improved platinum anode, and a 30-mil thick ERP. The improved electrodes used in this cell were developed in other concurrent advanced cell development programs P&WA was conducting. The matrix was 10-mil thick reconstituted asbestos. Power density exceeding 1800 WSF was obtained in a 2½ hour steady-state run at 3000 ASF. The performance demonstrated in this test is shown in Figure 52. Total load time on the cell was 20.8 hours with 8.8 hours at 2500 ASF or above. Anode and cathode limiting current diagnostic test procedures were developed. The limiting current data is shown in Figures 53 and 54. Limiting current is a

measurement of the diffusivity limit of the electrode. It occurs when the reactant concentration at the electrodes reaction sites approaches zero. The limiting current measurements provide information on the electrode structure and internal losses.

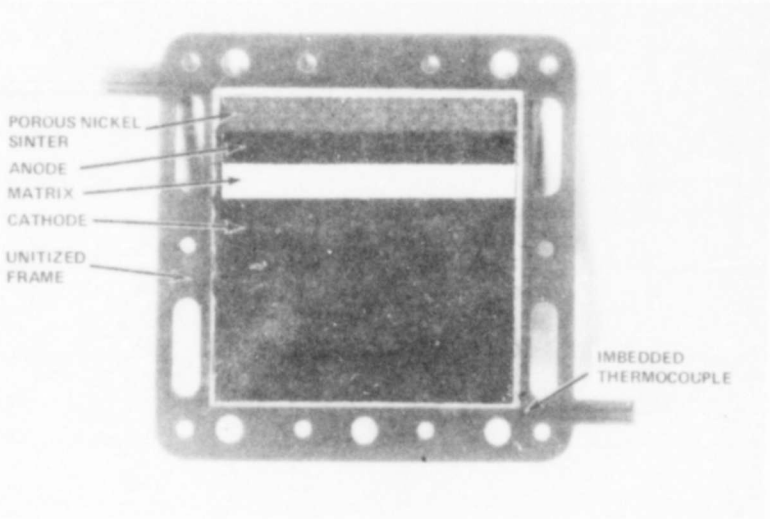

Figure 49 – "Dual Mode" 4 In. x 4 In. Cell

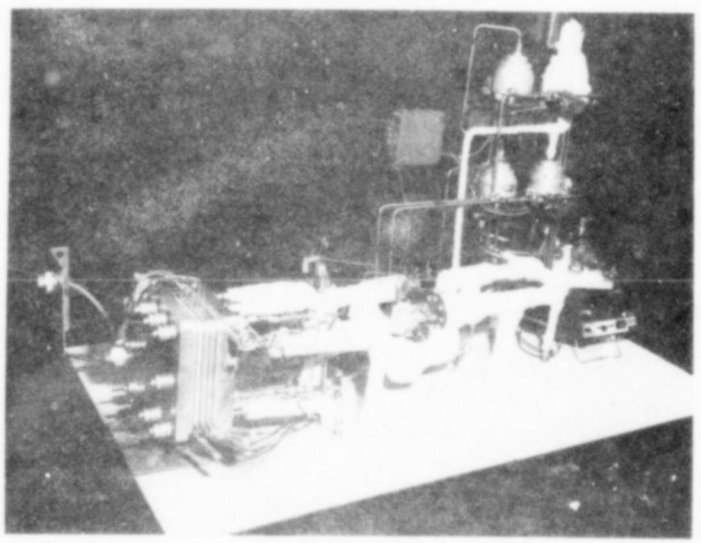

Figure 50 – Dual Mode Breadboard Demonstrator

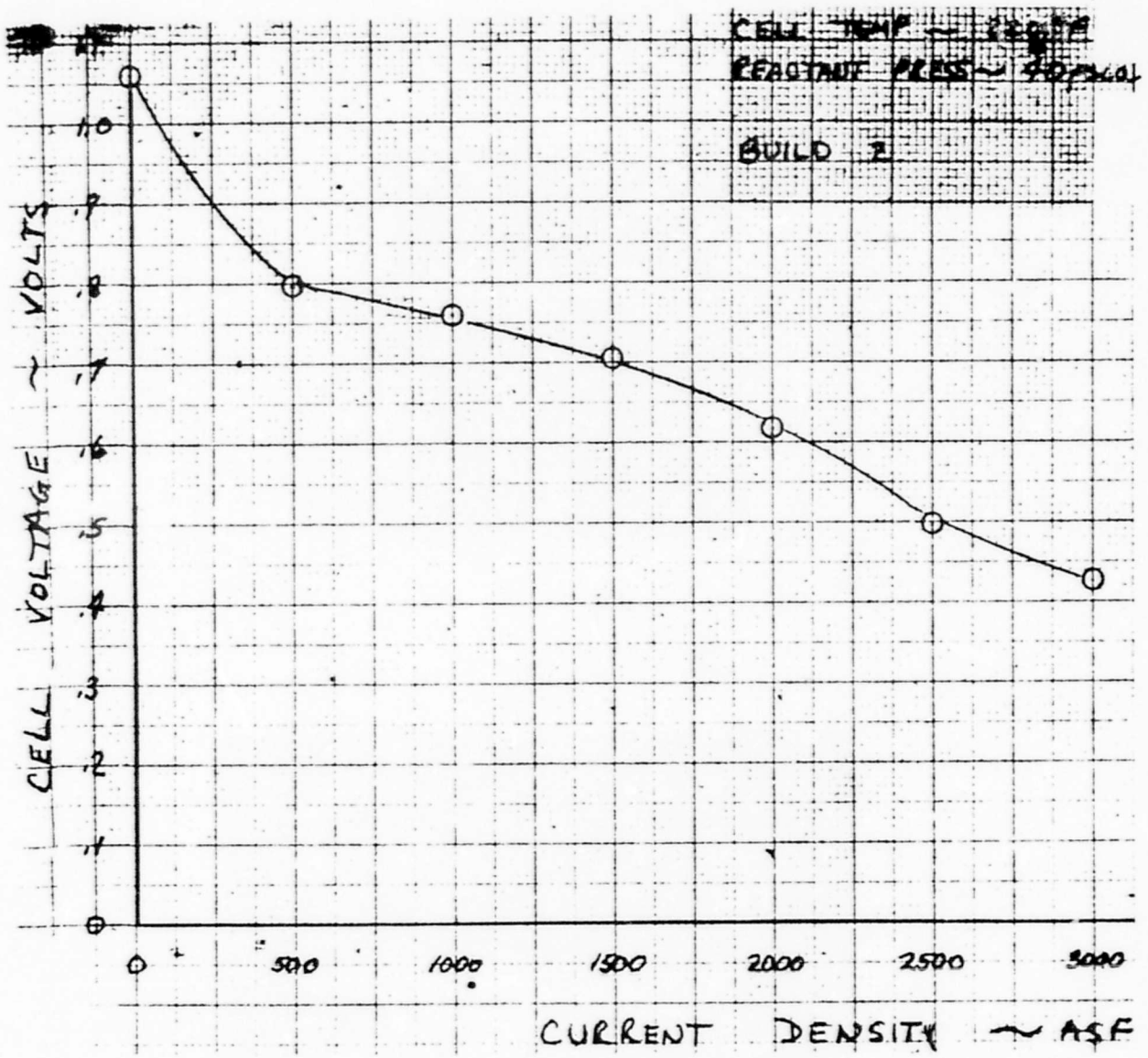

Figure 51 — Cell 2, Performance Calibration to 3000 ASF

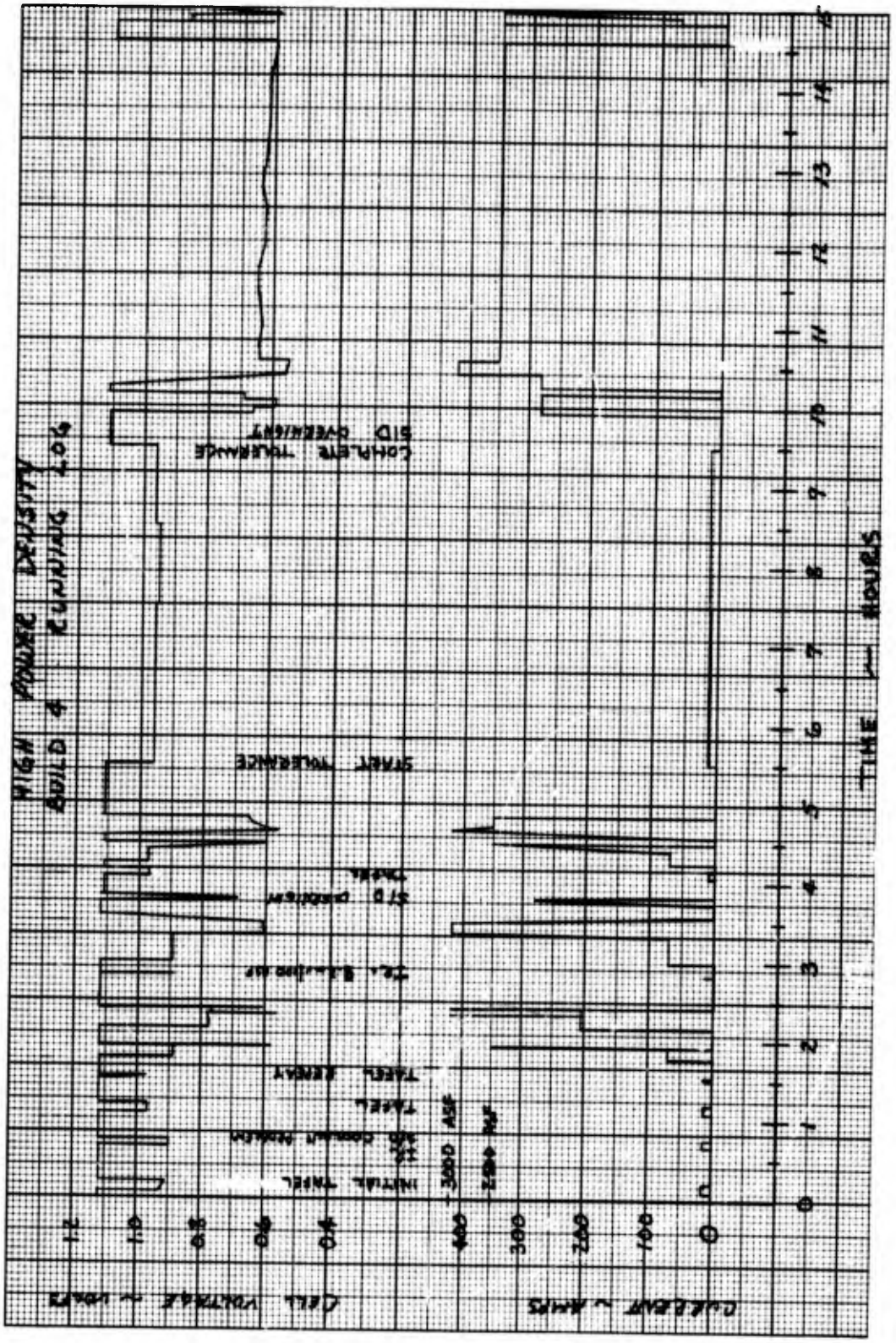

Figure 52 – Cell 4, Performance History

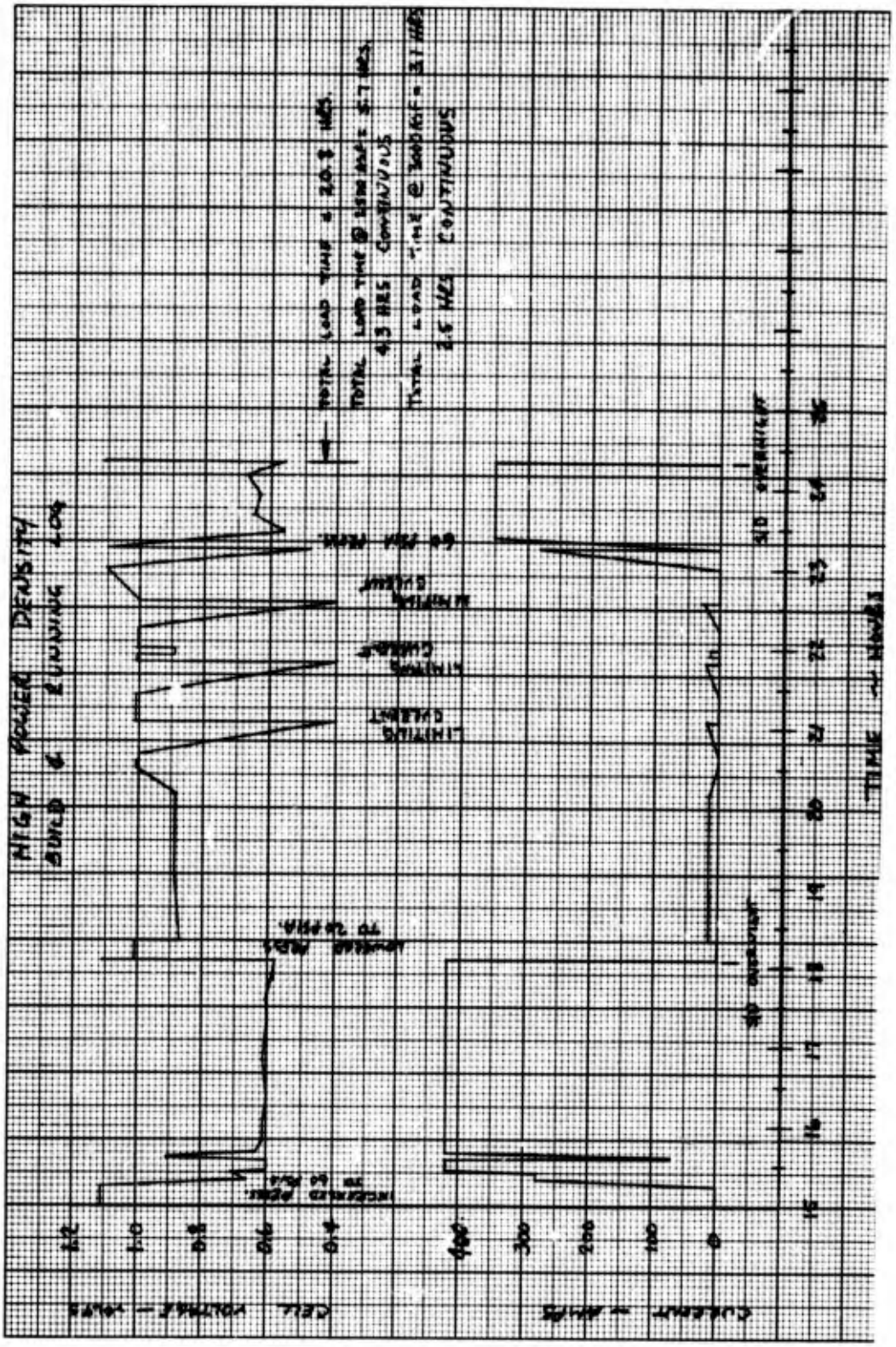

Figure 52 — Cell 4, Performance History (Continued)

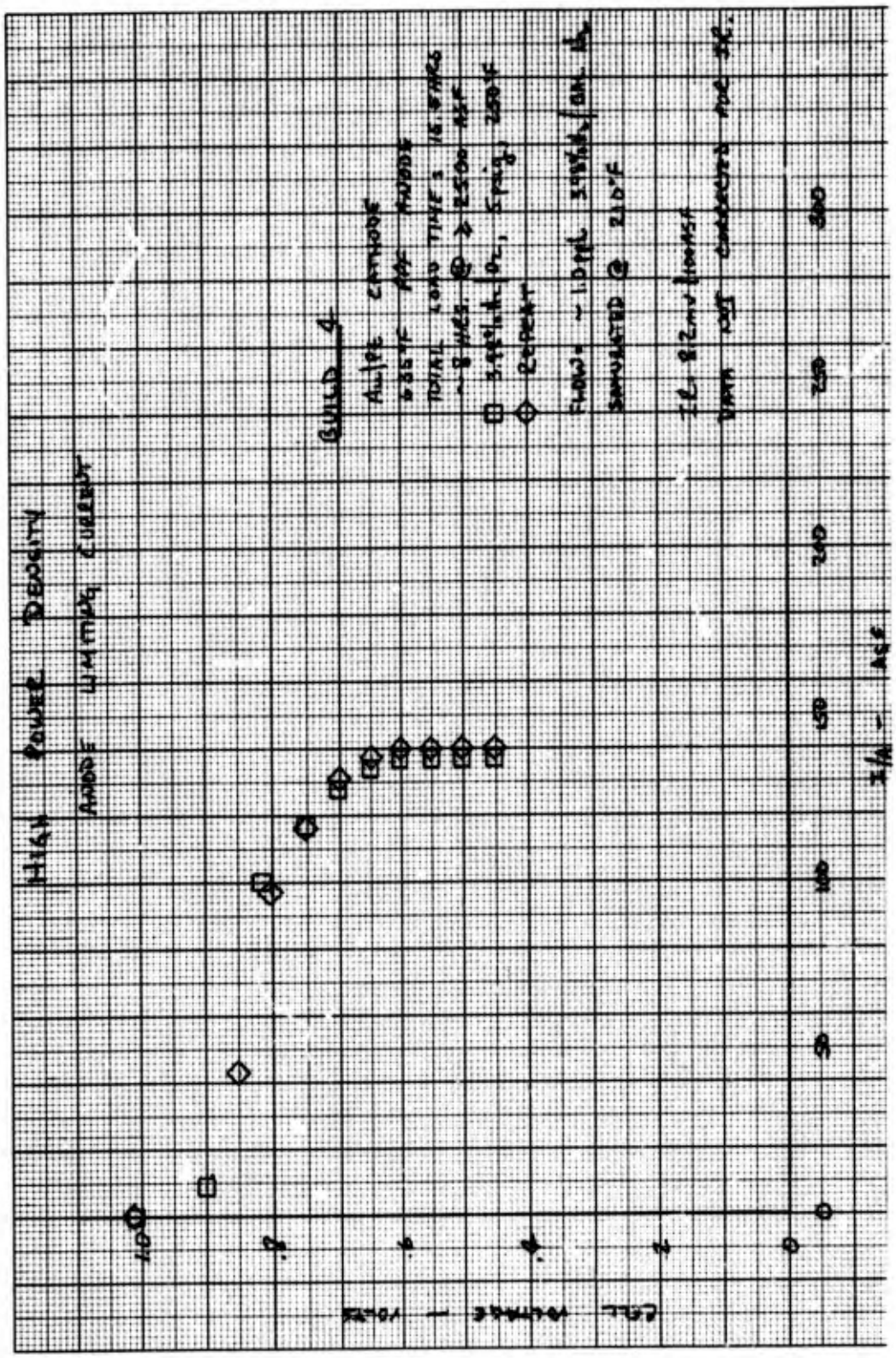

Figure 53 — Cell 4, Anode Current Limit Data

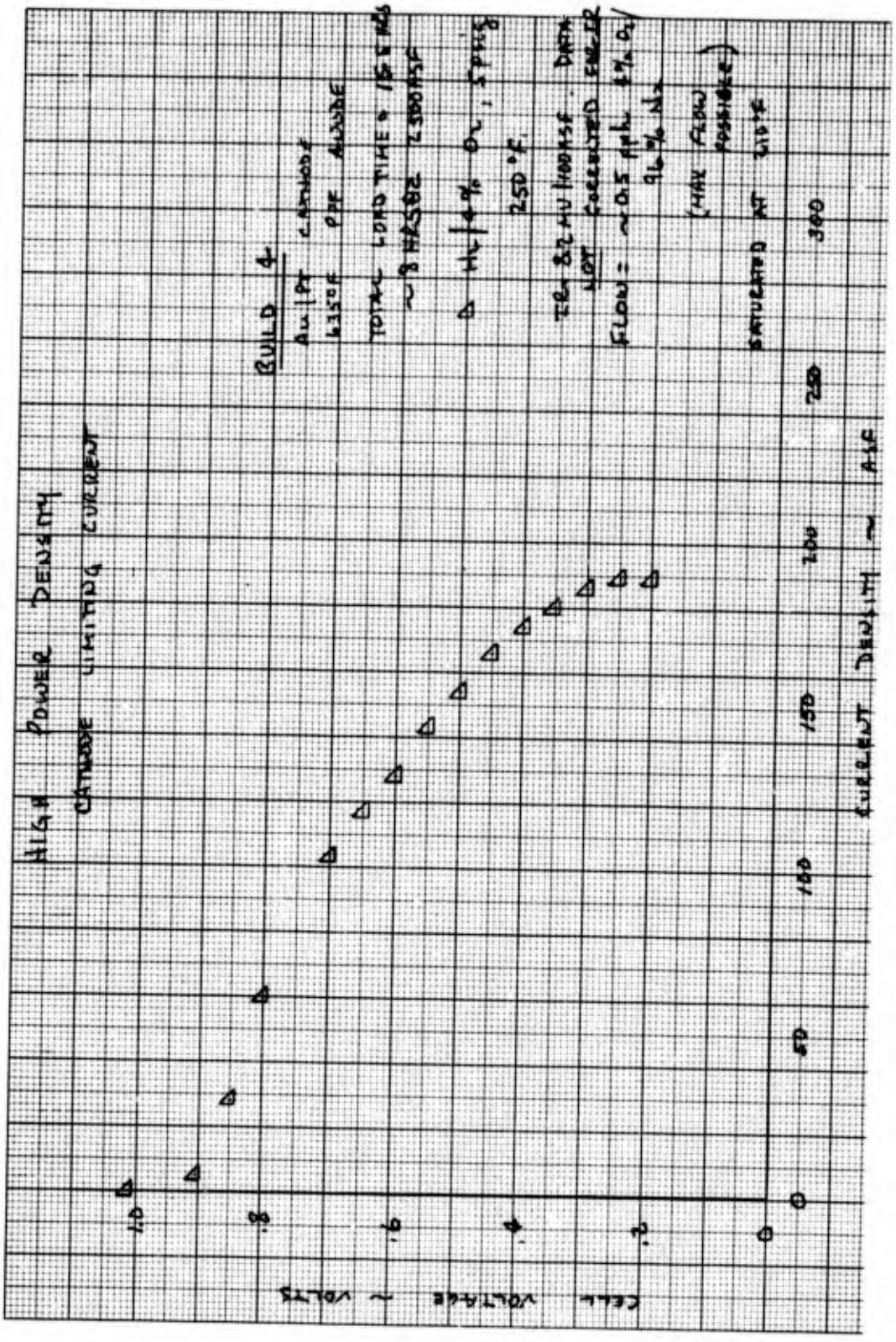

Figure 54 – Cell 4, Cathode Current Limit Data

The limiting currents on Cell 4's electrodes were measured at low pressure, to achieve an actual limit within test stand capability. They were then corrected up to a 40 psia reactant pressure and found to be 34,000 ASF for the gold/platinum cathode and 20,600 ASF for the improved platinum anode. The correction involves ratioing the current by the reactant partial pressure ratio. These limiting current values indicate that the electrodes in Cell 4 were capable of carrying much higher than 3000 ASF and that the variation in performance during high power density operation was probably due to off-optimum water management conditions.

Cell 5 – This cell was a duplicate of Cell 4. It was constructed with a gold/platinum cathode an improved platinum anode, a 10-mil reconstituted asbestos matrix, and a 30-mil nickel ERP. Its test objectives were to determine the repeatability of the performance of gold/platinum cells at 3000 ASF, to optimize operating conditions, and to run endurance at 3000 ASF. The results of initial perfcrmance calibrations at 20, 40, and 60 psia are shown in Figure 55. A comparison of this data with that of Cell 4 is shown in Figure 56. These curves show that the cells had essentially identical 60 psia-IR corrected performance and differed by only 36 mv at the 40 psia, - 3000 ASF loads. Considering the uncertainty of IR measurements, which are taken at 100 ASF and extrapolated to 3000 ASF, this was considered to be excellent repeatability. The 60 psia performance was the highest fuel cell performance obtained to date on full size hardware; 0706 v at 3000 ASF or 2118 WSF.

Dew point optimization tests were run next. The results, shown in Figure 57, demonstrate that the normal hydrogen and oxygen dew points were at or near the optimum for 250°F cell operating temperatures. The data also shows that the range of optimum operation is considerably narrowed at the higher current densities.

Following the dew point optimization tests, a 3000 ASF endurance program was started. A total of 10 hours continuous running was completed, followed by an additional 6.5 hours the next day. Figure 58 is a running log of the endurance testing. During the 16.5 hours at 3000 ASF 3 hours of running with dry oxygen and 1.5 hours with 220°F dew point oxygen were conducted with no noticeable effect on cell performance. Total load time on the cell was 47.4 hours including 19.3 hours at 3000 ASF.

Cell 6 – In this cell, matrix pinch was set without the additional cathode support screen used in all previous cells. The proper pinch was set by adjustment of the frame thickness. Otherwise, the cell was similar to previous Cells 4 and 5 with a gold/platinum cathode, improved anode, 30-mil nickel ERP, and 10-mil asbestos matrix.

Although this cell's IR was comparable to earlier cells, 8.2, 5.2, 8.0 mv on Cell 4, 5, and 6, respectively, performance was low at 100 ASF and unstable above 500 ASF, see Figure 59.

A post-test analysis indicated that the anode and cathode of Cell 6 were good. Therefore, the relatively poor performance of Cell 6 was attributable to the poor electrode support (9 percent nubbin coverage) which caused high current collection losses in this cell configuration. All further testing of 4 inch x 4 inch cells incorporated the additional support screen. This result is consistent with eariler high power density testing and was confirmed by experience in other programs.

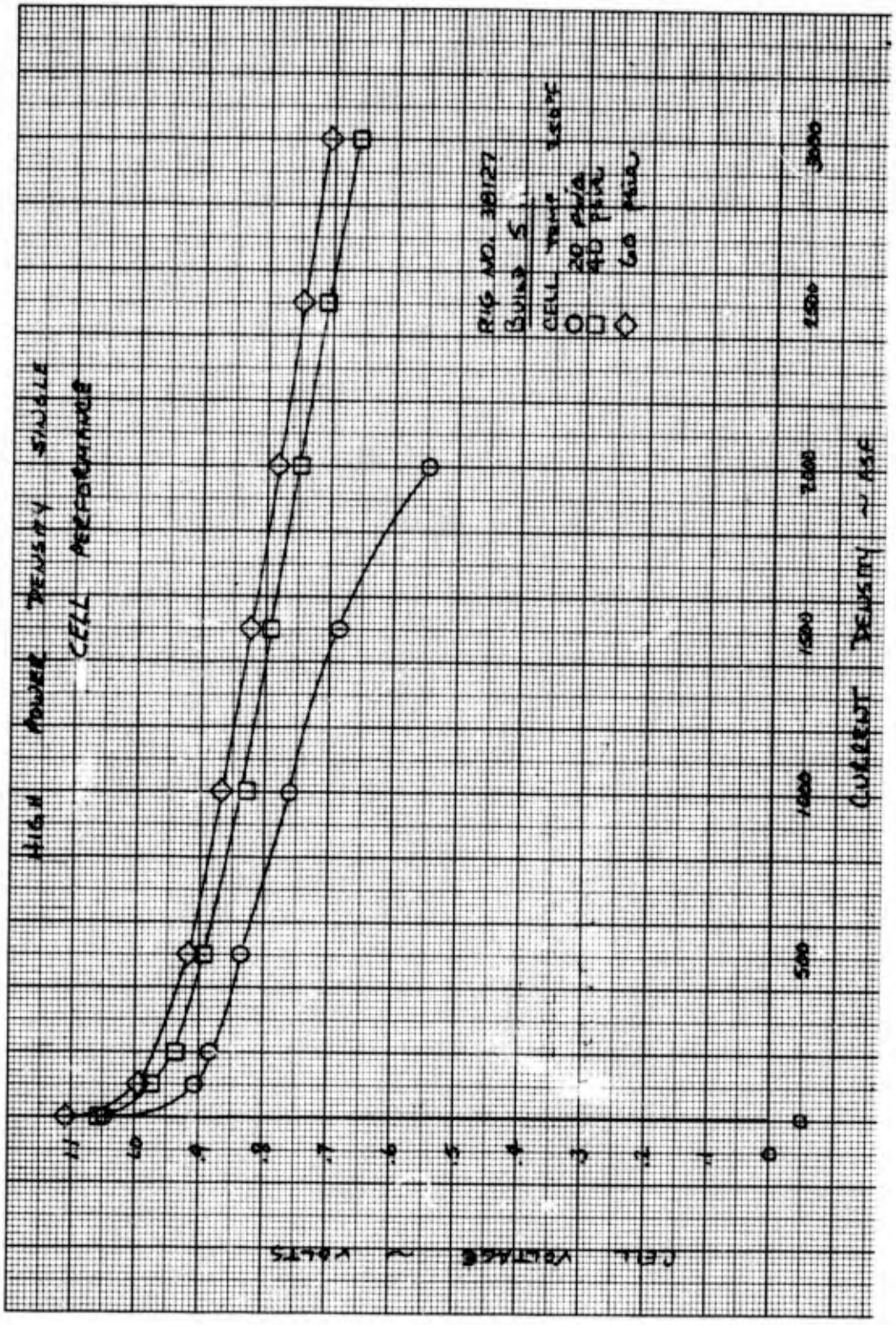

Figure 55 – Cell 5, Initial Performance Calibrations

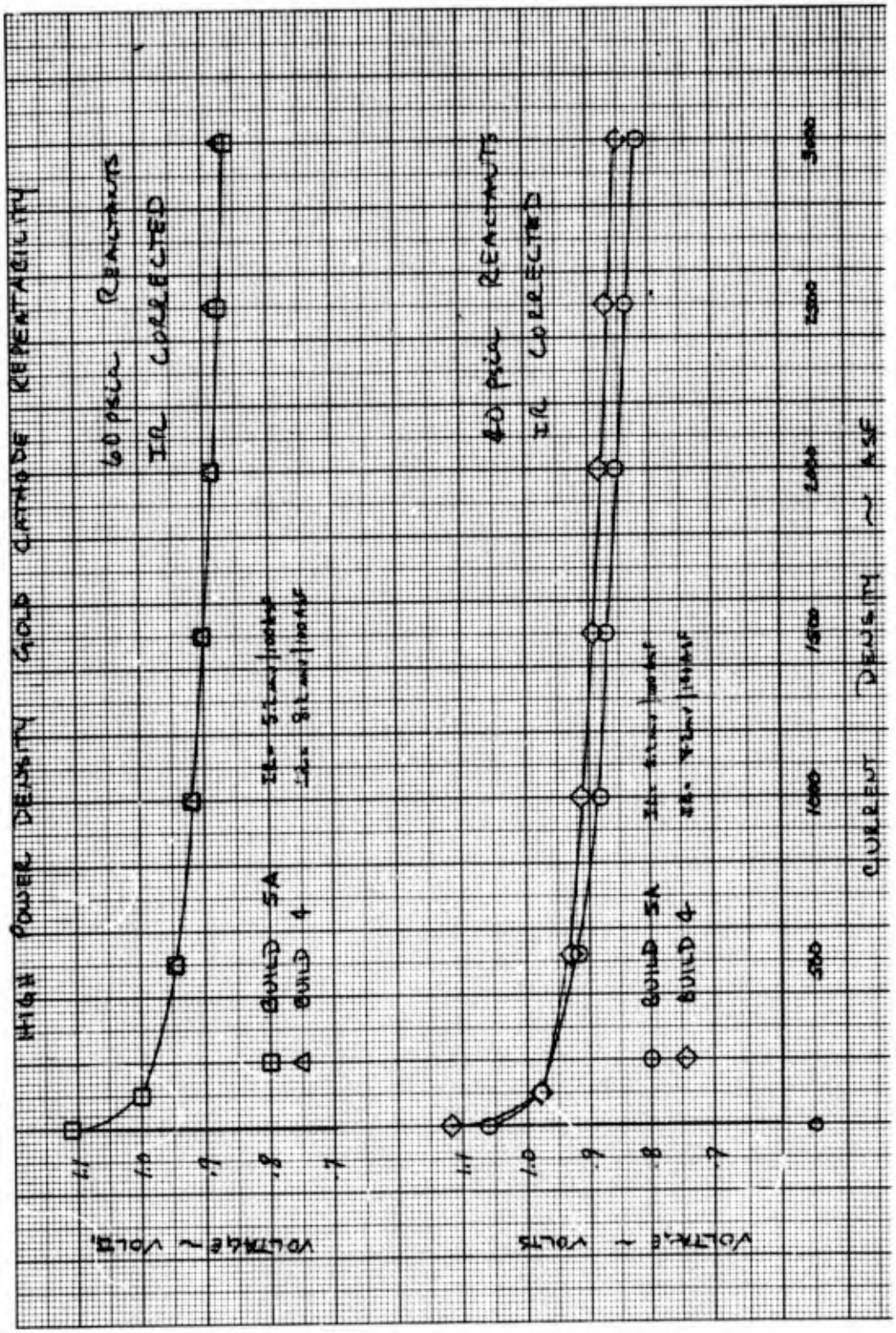

Figure 56 — Cell Performance Repeatability Evaluation Data

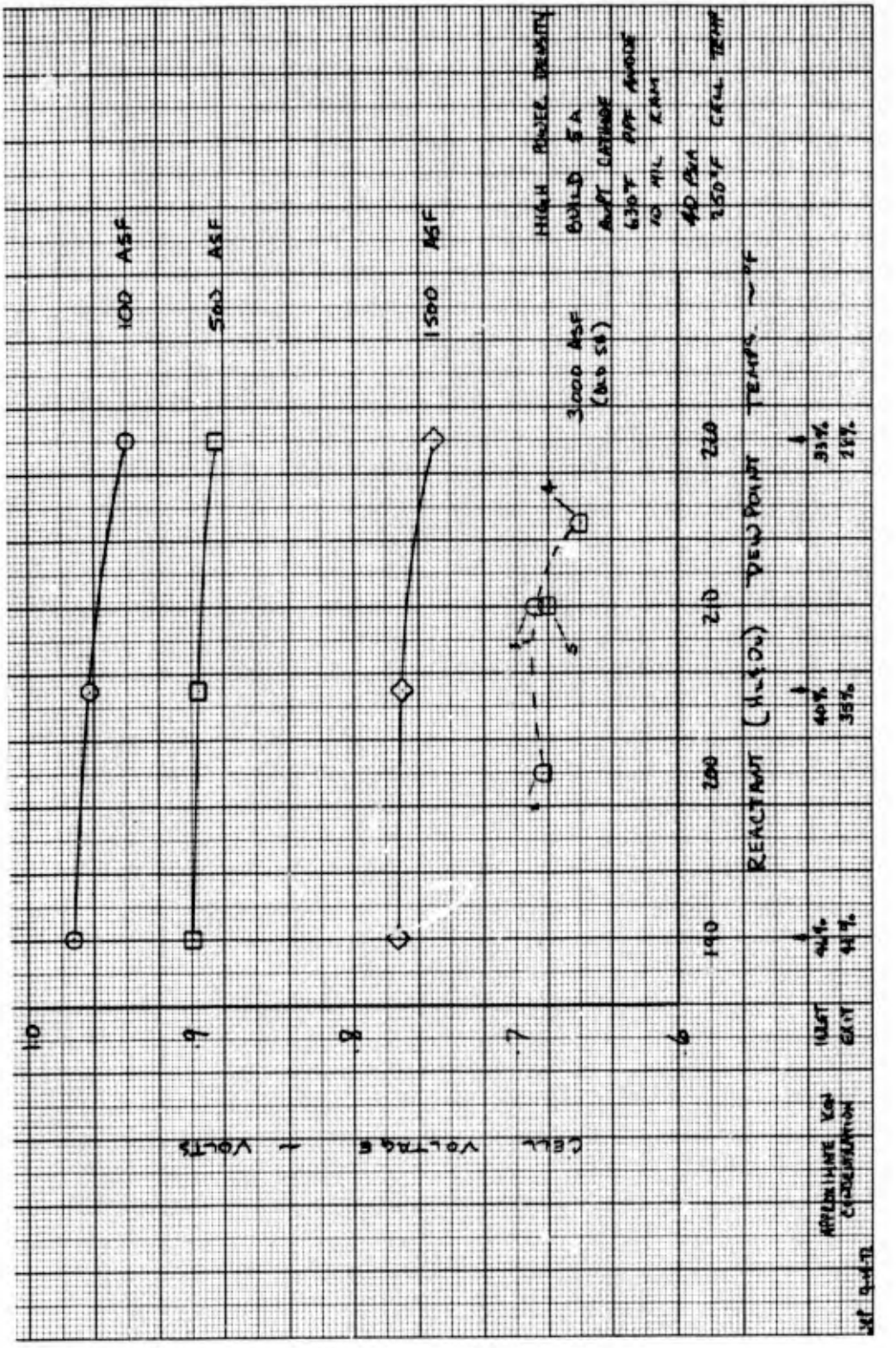

Figure 57 – Cell 5, Dew Point Tolerance Data

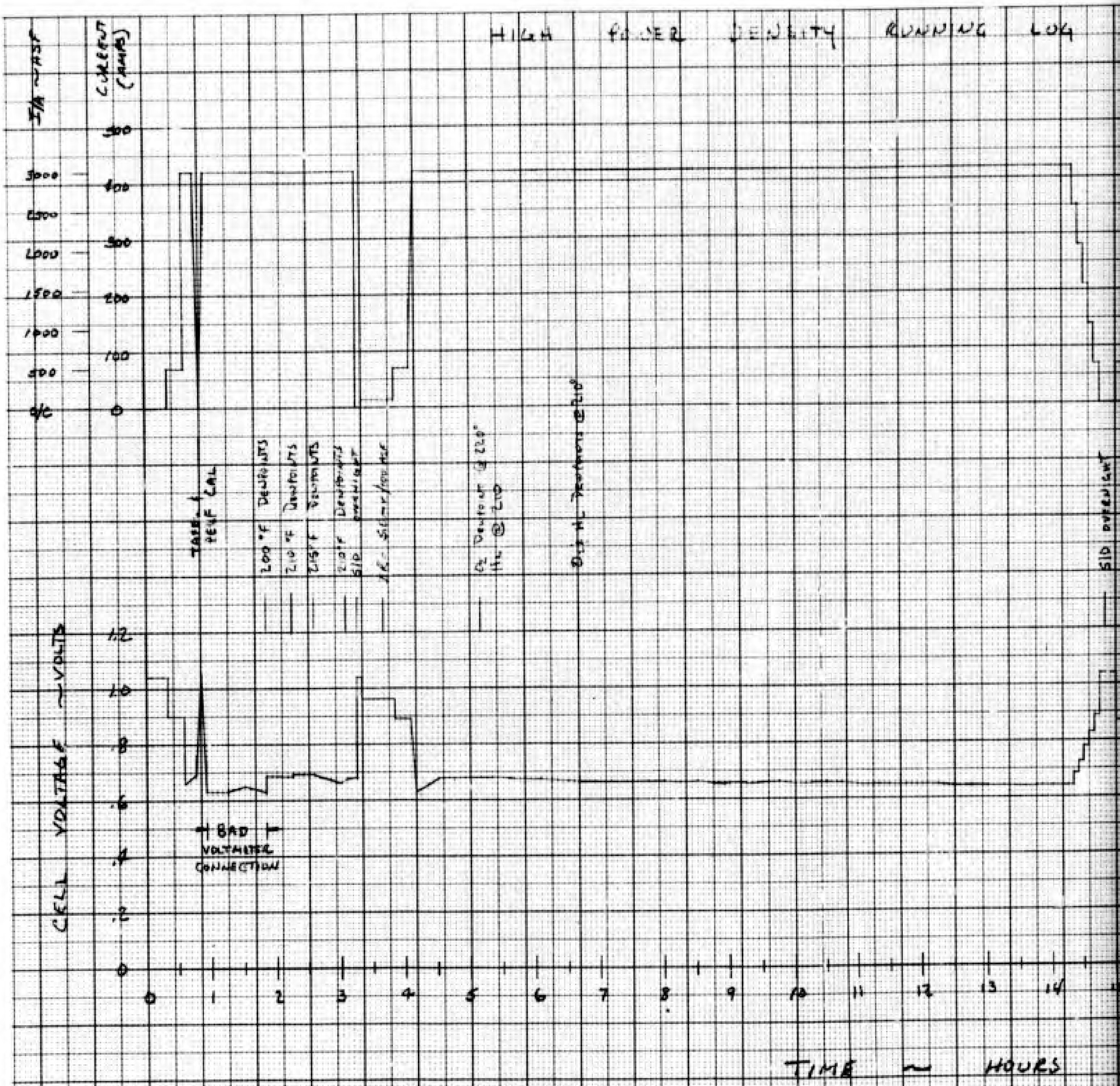
HIGH POWER DENSITY RUNNING LOG
I/A ~ ASF
CURRENT (AMPS)
CELL VOLTAGE ~ VOLTS
BAD VOLTMETER CONNECTION
200 °F DEWPOINTS
210 °F DEWPOINTS
S/D OVERNIGHT
TIME ~ HOURS

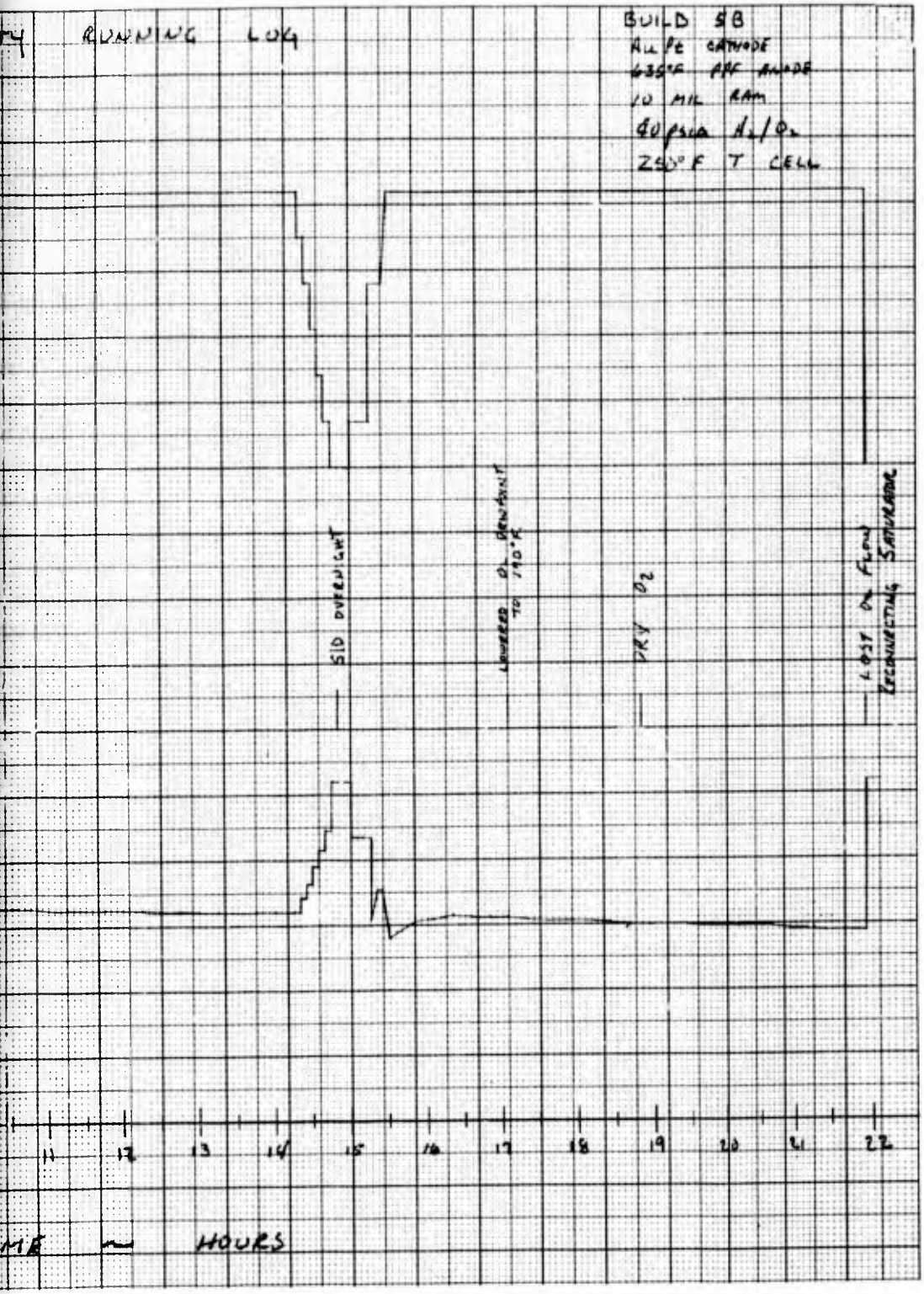

Figure 58 — Cell 5, Performance History

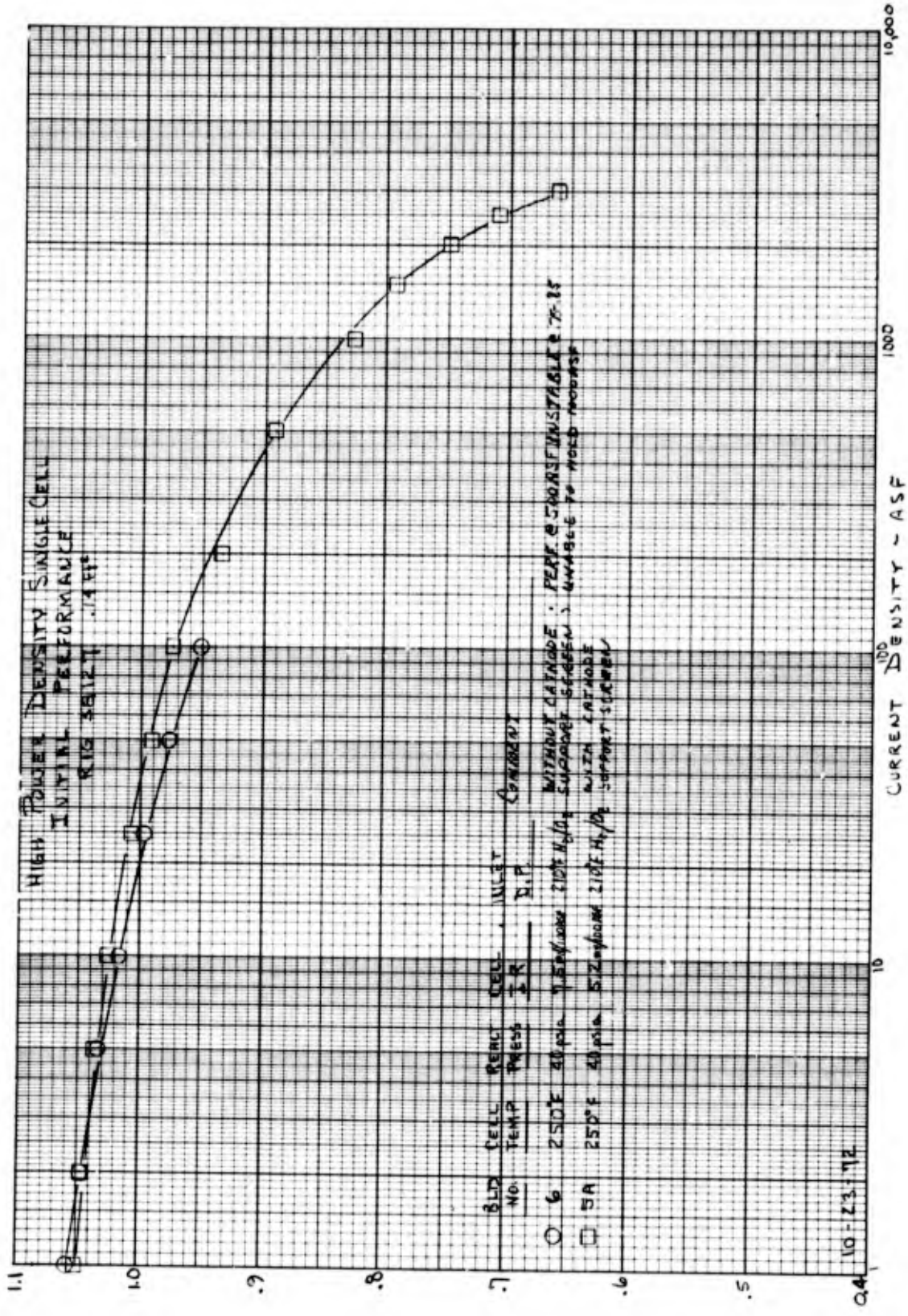

Figure 59 — Cell 6, Initial Performance Calibrations

Cell 7 – Cell 7 was constructed with a standard platinum catalyst anode, as opposed to the high-sinter temperature (635°F) improved anode of Cells 4, 5 and 6. The test objectives of this build were to evaluate the performance level, dew point tolerance, and endurance characteristics of the standard platinum anode. Otherwise this cell was similar to previous cells with a 10-mil asbestos matrix and a 30-mil nickel ERP. The use of standard anodes in the multicell plaque configuration would simplify electrode manufacture, since the standard anode and the gold/platinum cathodes are sintered at the same temperature (590°F).

Initial performance data taken at 40 and 60 psia is shown in Figure 60, along with the performance characteristics of Cell 5. The 60 psia performance was the highest fuel cell performance obtained to date: 0.713 v at 3000 ASF or 2140 WSF. Cell IR was 5.0 mv at 100 ASF comparable to the 5.2 mv obtained on Cell 5.

Figure 61 shows the effect of average cell electrolyte concentration on performance at 1500 and 3000 ASF, with a comparison of data from Cell 5. Normal dry side (lower dew points) and wet side (higher dew points) response was obtained at 1500 ASF. The voltage obtained during dry side operation at 3000 ASF was lower than normal, and by comparison, poorer than that of Cell 5. The loss of performance resulting from dry side operation at 3000 ASF was unrecoverable. The cell continued to decay and was shut down and refilled with electrolyte.

Endurance testing at 3000 ASF began after refill. Restart performance at 3000 ASF was some 25 mv lower than the peak level. During 1.4 hours of continuous operation at 3000 ASF, the cell decayed to 0.472 v.

Post-test analyses were performed on the anodes of Cells 5 and 6 (635°F sintered anodes) and Cell 7 (590°F sintered anode). Figure 62 shows the floating half-cell test results. The standard, low temperature sintered anode suffered considerable decay, while the higher temperature sinter anodes were unchanged. The anode from Cell 7 was visibly flooded after the high current test. From these results, it was reasoned that the relatively high temperature and high current density operating conditions caused accelerated flooding in the low-sinter temperature anodes, which in turn resulted in high performance decay. This hypothesis is consistent with the electrode model developed by P&WA. By sintering electrodes above 621°F (where the Teflon binder changes from a crystalline to an amorphous state), the electrodes become more hydrophobic and resistant to film flooding.

Cell 8 – This cell was of identical construction to Cell 7. The purpose of this test was to obtain confirmation of the previous result with the low-sinter temperature anode. The initial performance of Cell 8 compared to Cells 5 and 7, is shown in Figure 63. During continuous operation at 3000 ASF, the cell did attain a peak of 0.660 v, followed by a high decay similar to Cell 7. Attempts to recondition the cell at lower current density were unsuccessful, and testing was terminated.

A post-test analysis of Cell 8's electrodes indicated the anode to have high polarization (115 mv at 100 ASF) due to flooding, similar to the post-test results of Cell 7's anode. Therefore, all subsequent high power density cells were fabricated with the high-sinter temperature (635°F) anode.

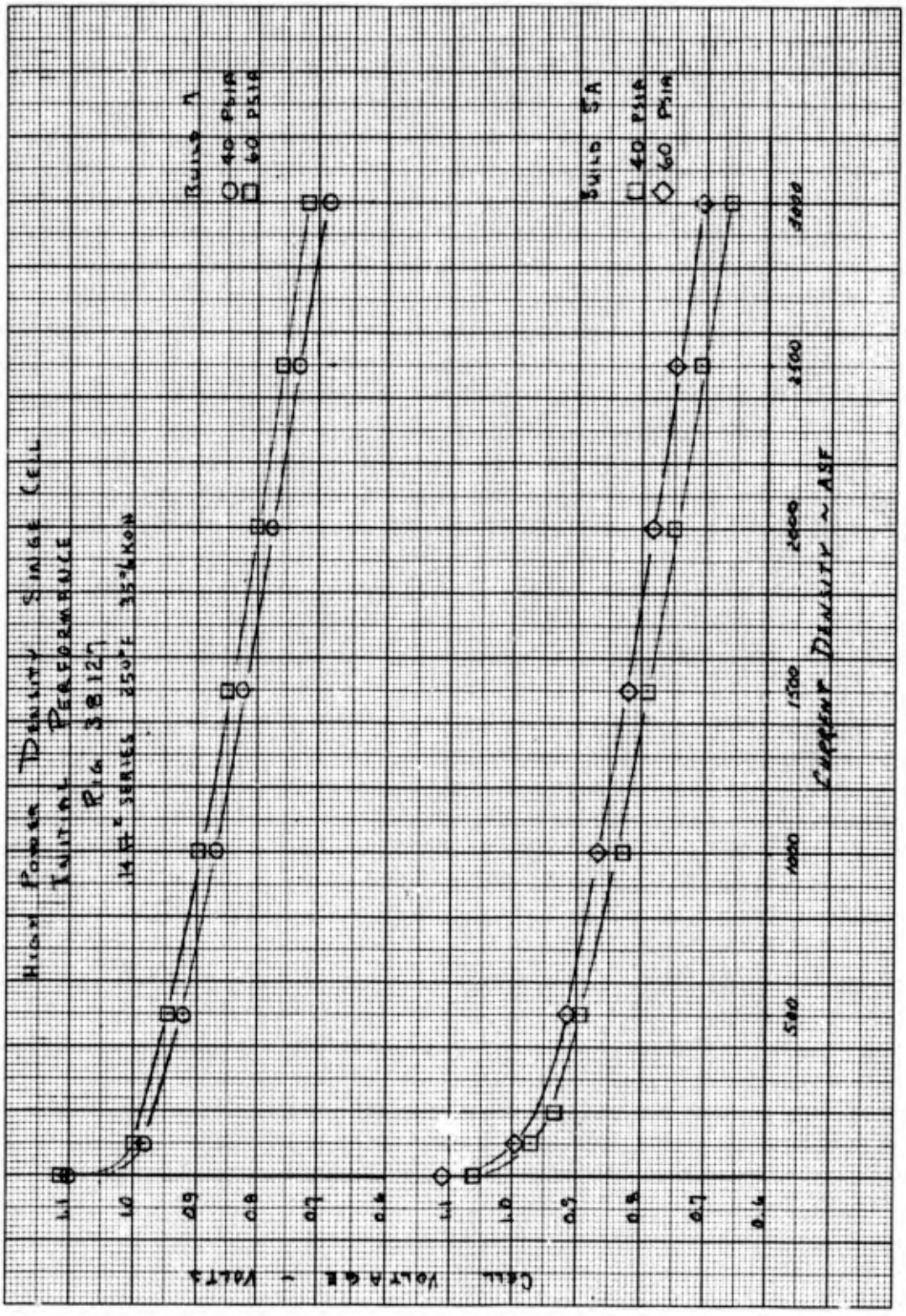

Figure 60 — Cell 7, Initial Performance Calibrations

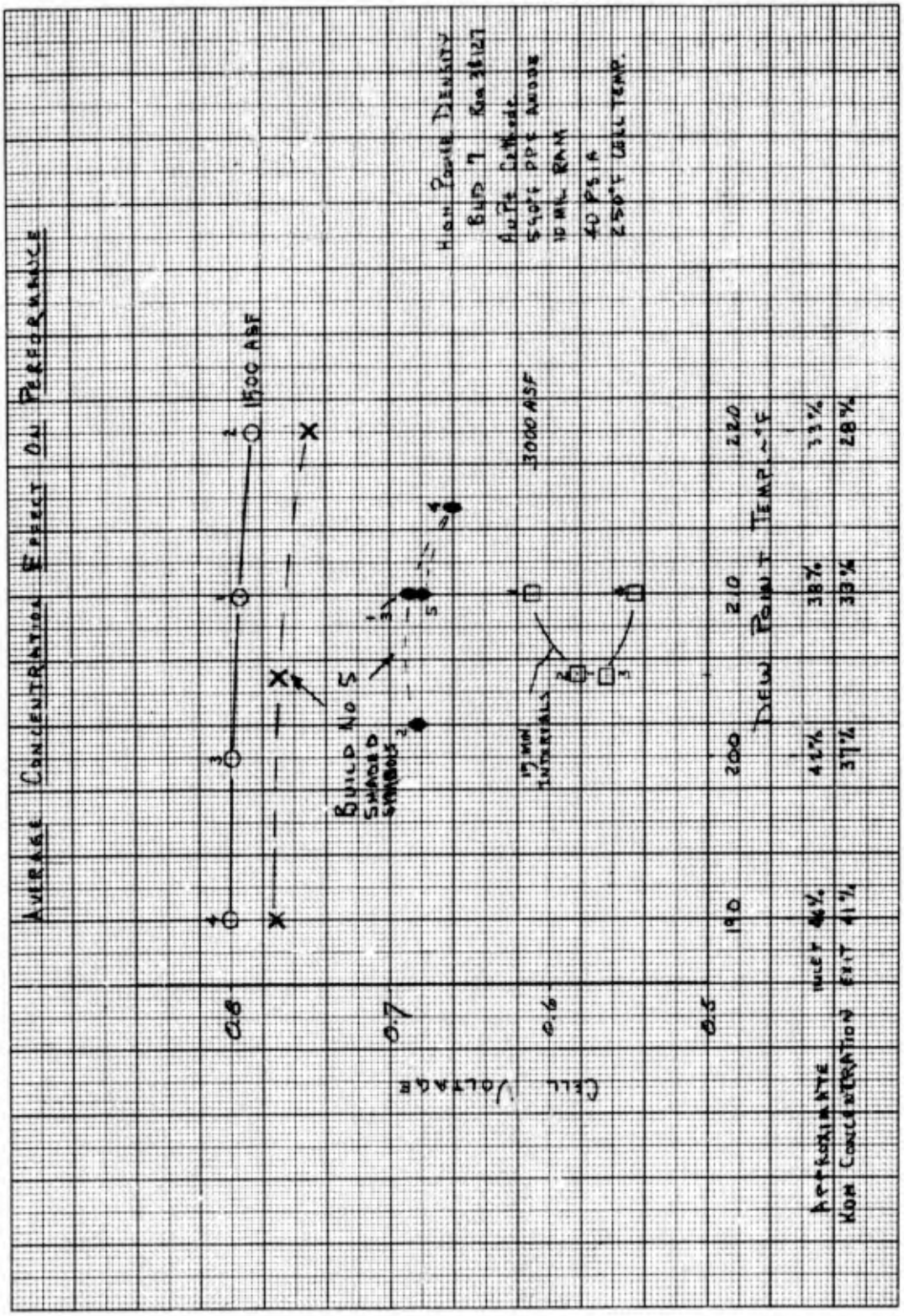

Figure 61 – Cells 5 and 7, Dew Point Tolerance Data

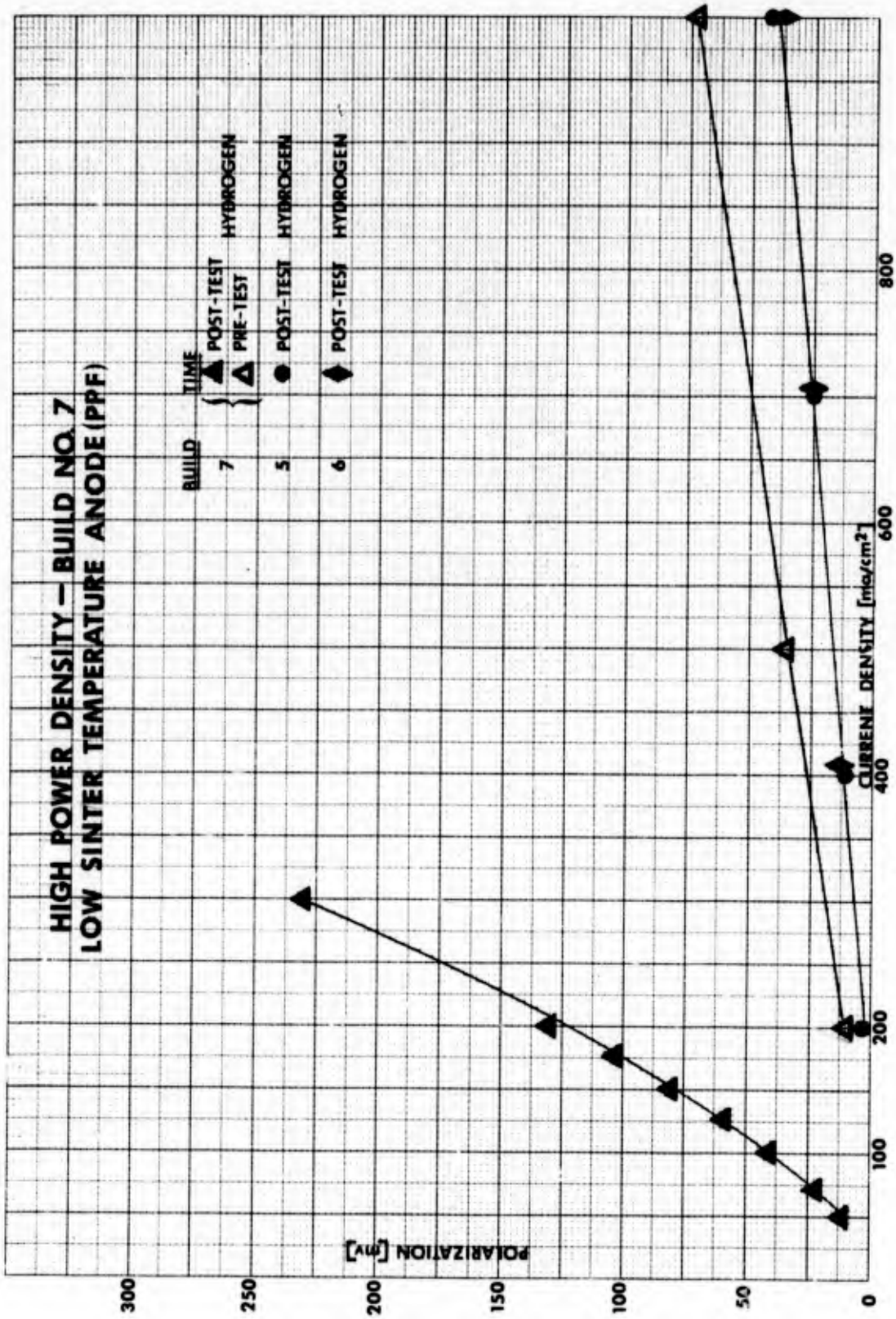

Figure 62 -- Floating Half Cell Test Results

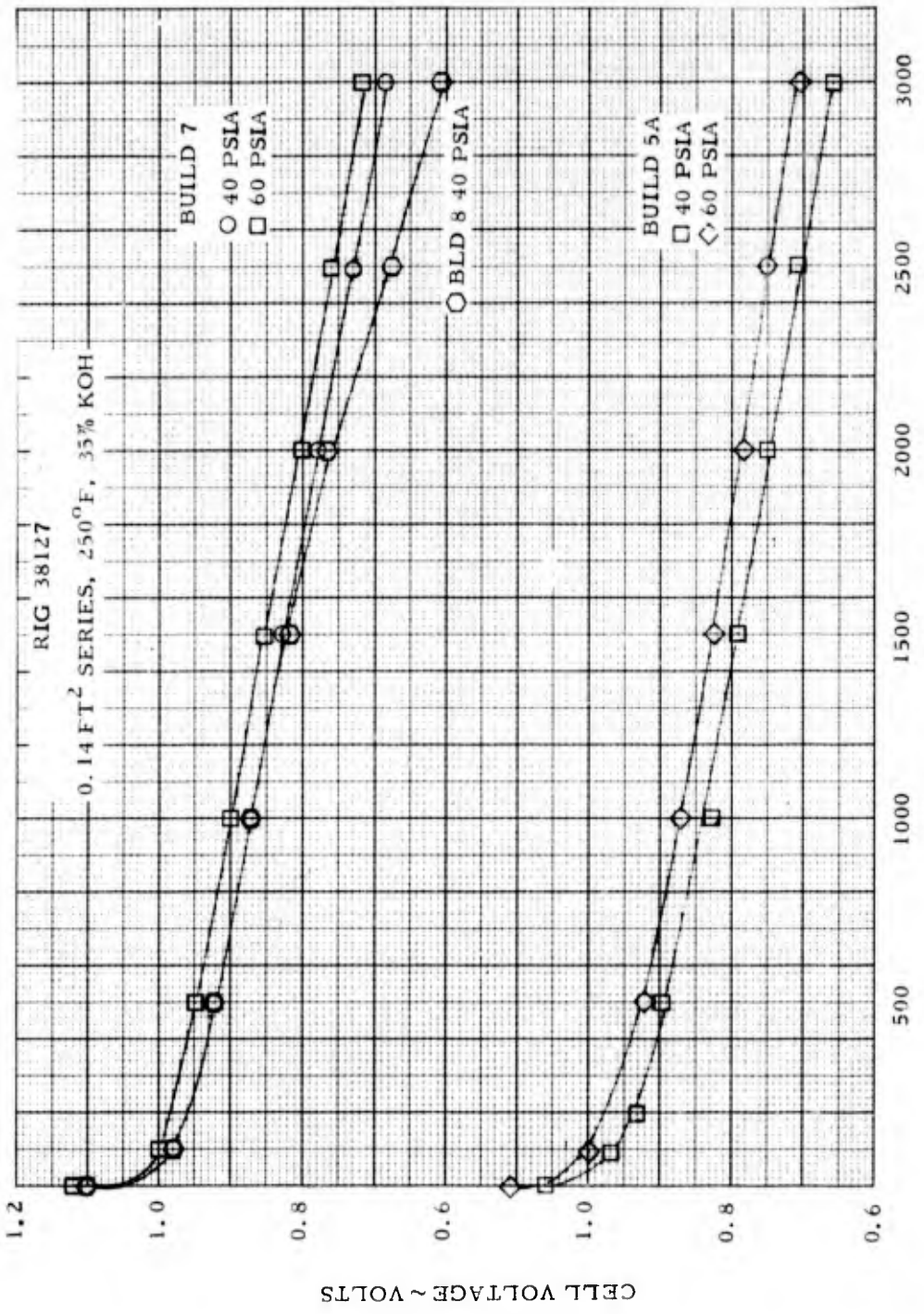

Figure 63 – Cell 8, Initial Performance Calibrations

Cell 9 – This cell was constructed with a nominal 5-mil reconstituted asbestos matrix, as opposed to the 10-mil matrix used on previous cells. Matrix pinch of 3 mils was set with an additional cathode support screen. Other components were the high-sinter temperature (635°F) anode, gold/platinum cathode, and 30-mil nickel electrolyte reservoir plate. The primary test objective was to evaluate the thinner matrix at high power density operation. A thinner matrix would improve performance by lowering cell IR and also permit a weight reduction because the electrolyte reservoir plate could be proportionately smaller.

Initial and refill performance for Cell 9 are shown in Figure 64. The performance on original fill was relatively poor, with high decay at 3000 ASF. After refill, the cell was redesignated 9A and attained the best performance to date. At 250°F/40 psia /210°F dew point, the cell ran for 1.0 hour with performance of 0.740 v at 3000 ASF, (2210 WSF) followed by a 15 second spike to 0.701 v at 3650 ASF (2550 WSF). At 60 psia, performance reached 0.760 v at 3000 ASF (2280 WSF) but conditions could not be optimized for continuous operation because the test stand hydrogen saturator could not maintain the desired dew point.

Cell IR was 3.6 to 4.0 mv at 100 ASF, consistent with the thinner matrix. Previous cells with a 10-mil matrix have demonstrated cell IR's from 5.0 to 8.0 mv at 100 ASF. The relatively low performance on the original run is attributable to an incomplete electrolyte fill.

Final testing of this cell was conducted to determine the cell voltage response to load transients to and from high power density. Figure 65 shows the effect of load transients between 500 ASF and 2500 ASF and also between 114 ASF and 2000 ASF. Cell performance remained stable following the transients and no apparent problems resulted.

Following the load transients, testing was terminated to permit modifications to the test facility. A higher temperature oven and larger hydrogen saturator, to permit a wider range of operating conditions, were installed specifically for higher hydrogen dew points and higher cell operating temperatures.

Cell 10 – The primary test objective of this cell was to evaluate high power density operation at temperatures above the nominal 250°F condition of previous cells. Cell construction was identical to Cell 9, with a nominal 5-mil asbestos matrix. Other components were a high-sinter temperature (635°F) anode, a gold/platinum cathode and a 30-mil nickel ERP.

The cell demonstrated the best performance of the series cells, 0.765 v at 3000 ASF (2290 WSF) at 250°F/40 percent KOH/45 psia. A comparable performance was attained at 290°F/ 47.5 percent KOH/45 psia, but instability prevented continuous operation at 3000 ASF.

No increase in performance resulted from elevated temperature operation to 290°F. A total of 14.0 load hours was obtained above 250°F, with 7.3 continuous hours at 290°F.

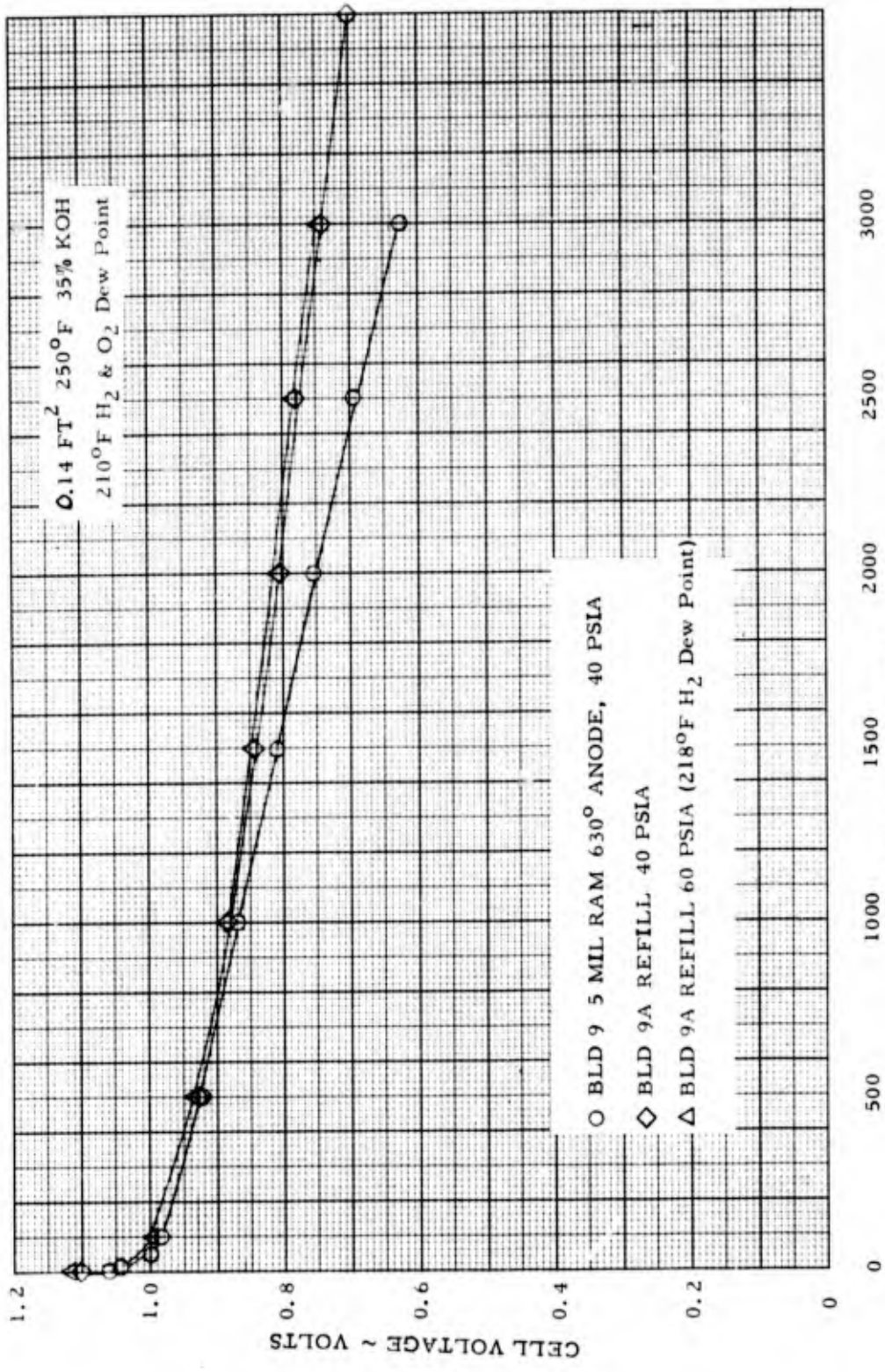

Figure 64 — Cell 9, Performance Calibrations

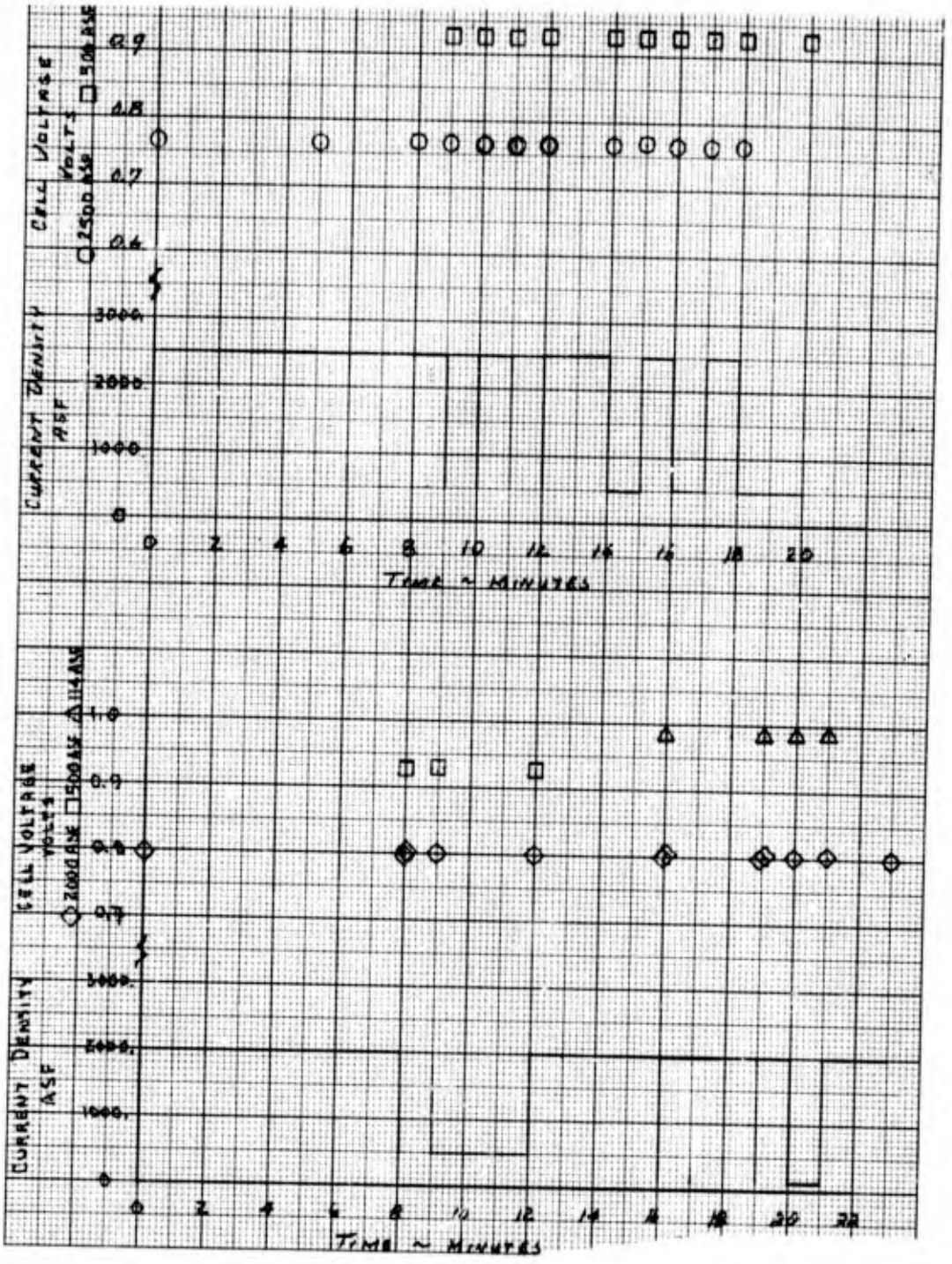

Figure 65 – Cell 9, Load Transient Capability

The lack of improvement in performance observed with the increase in temperature can be attributed to a decrease in oxygen partial pressure resulting from a change in water vapor pressure necessary to maintain a constant electrolyte concentration. The oxygen partial pressure effect was verified at 265°F by increasing the reactant pressure to offset the change in water vapor pressure. The performance at 265°F/49 psia/214°F dew point agreed closely with the final performance at 250°F/45 psia/200°F dew point, see Figure 66.

No gross detrimental effects to the electrodes of Cell 10 resulted from operation at elevated temperatures and high current density. Half-cell post-test performance results indicated the cathode to be superior and the anode comparable to the post-test results of previous Cell 5. Cell 5 ran a total of 47.4 hours at 250°F, accumulating 19.3 hours at 3000 ASF.

2. Development and Testing of Strip Cells

Development and testing of strip cells was begun, to verify methods for their fabrication and test, before single cell testing was complete. This permitted incorporation of the candidate cell configuration the single cell development had produced into strip cells shortly after it had been selected.

Strip Cell 1 – The objective of the testing of Strip Cell 1 was to evaluate the modifications made to the NASA-Lewis strip cell design for high current density operation and to obtain experience in operating strip cells at high current density.

Strip Cell 1 contained a gold/platinum cathode (Au/Pt), an anode of standard platinum catalyst fabricated on a 0.5-mil thick gold plated 100 x 100 mesh nickel screen, a 10-mil reconstituted asbestos matrix, and a 30-mil nickel ERP. The unitized electrode assembly (UEA), the above elements, except the ERP, bonded into an epoxy/fiberglass frame, was fabricated by the laminated unitization method illustrated in Figure 67. This is the standard method by which P&WA fabricates UEA'S for undersea and space powerplants. The several cell components together with layers of precut epoxy-impregnated fiberglass cloth are laid-up and placed between heated platens in a press. The platen temperature is set to soften, bond, and cure the fiberglass impregnated layers and the cell elements into a solid unit. In order to reduce IR losses and frame heating when operating at high current density, a 1-mil perforated nickel foil was bonded into the UEA, in the area of the frame, to supplement the conductivity of the screen. The cell was cooled with an evaporative water cooler. A cross-section of the UEA and of the UEA as assembled into a single cell test fixture is shown in Figure 68. The cell also contained several voltage taps located as shown in Figure 69 to permit determination of the IR losses in the electrode substrate screen and supplementary foil. The cell, as it went to test, is shown in Figure 70.

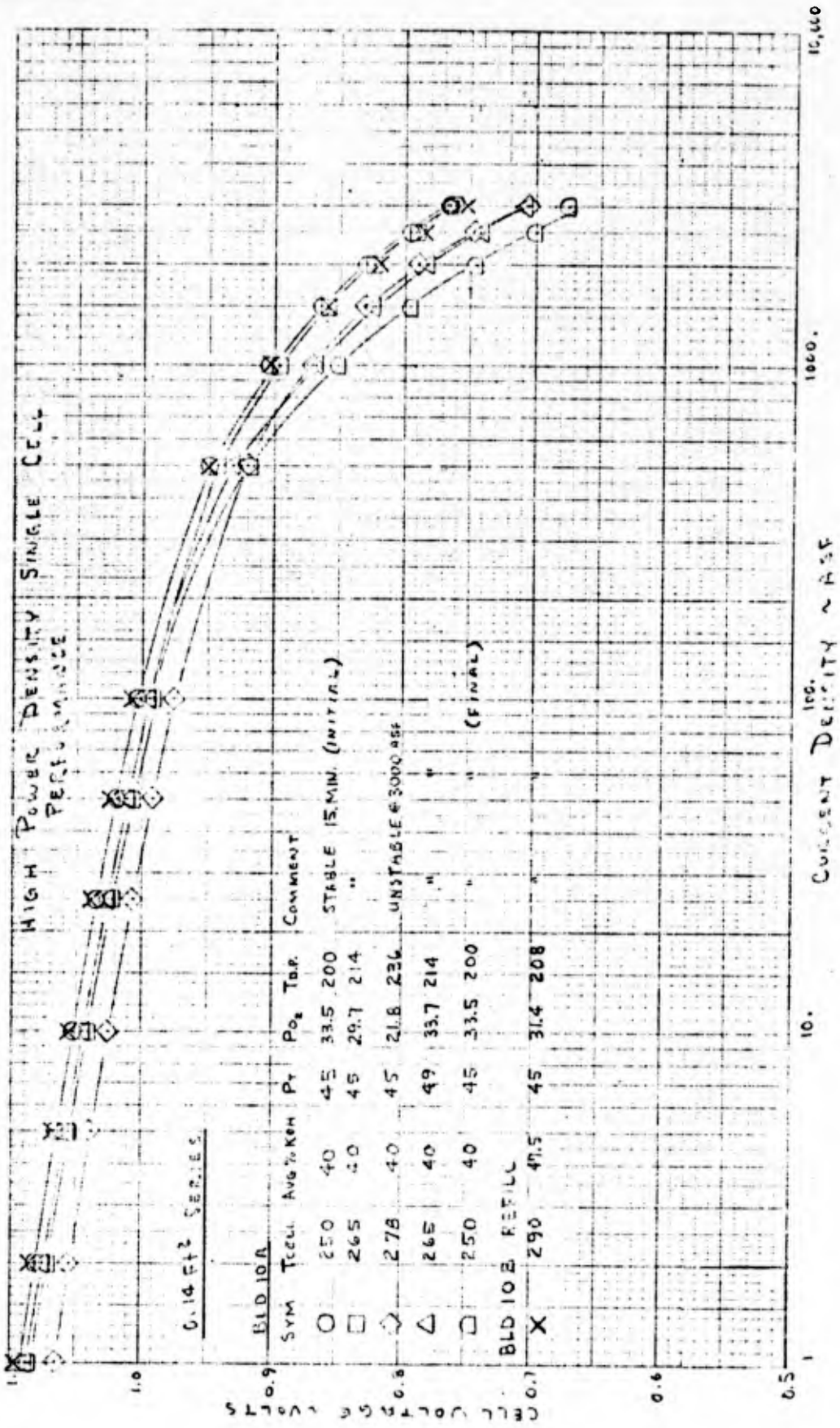

Figure 66 — Cell 10, Performance Calibrations

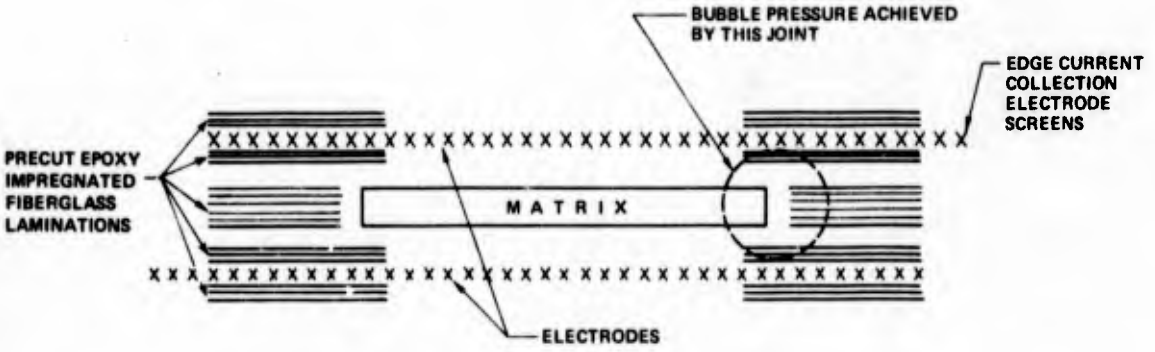

Figure 67 – Laminated Unitization Lay-Up

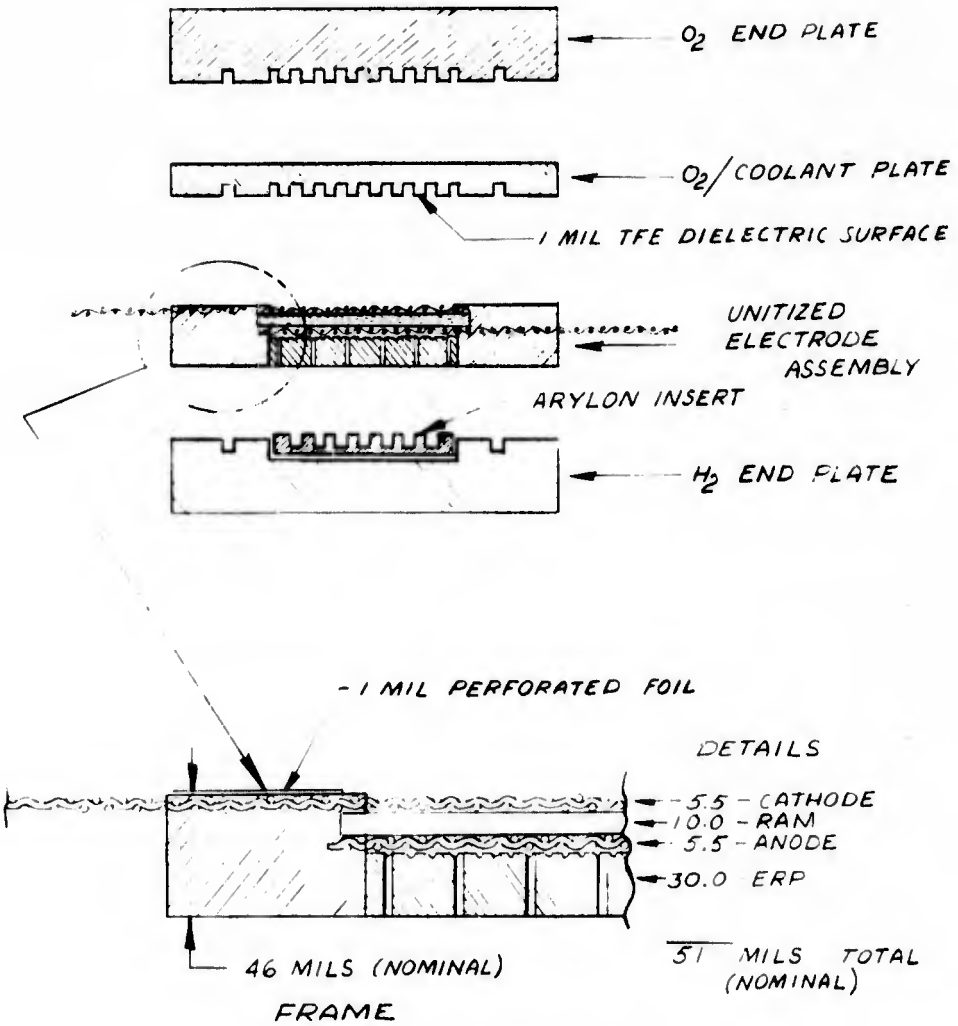

Figure 68 – Strip Cell Schematic

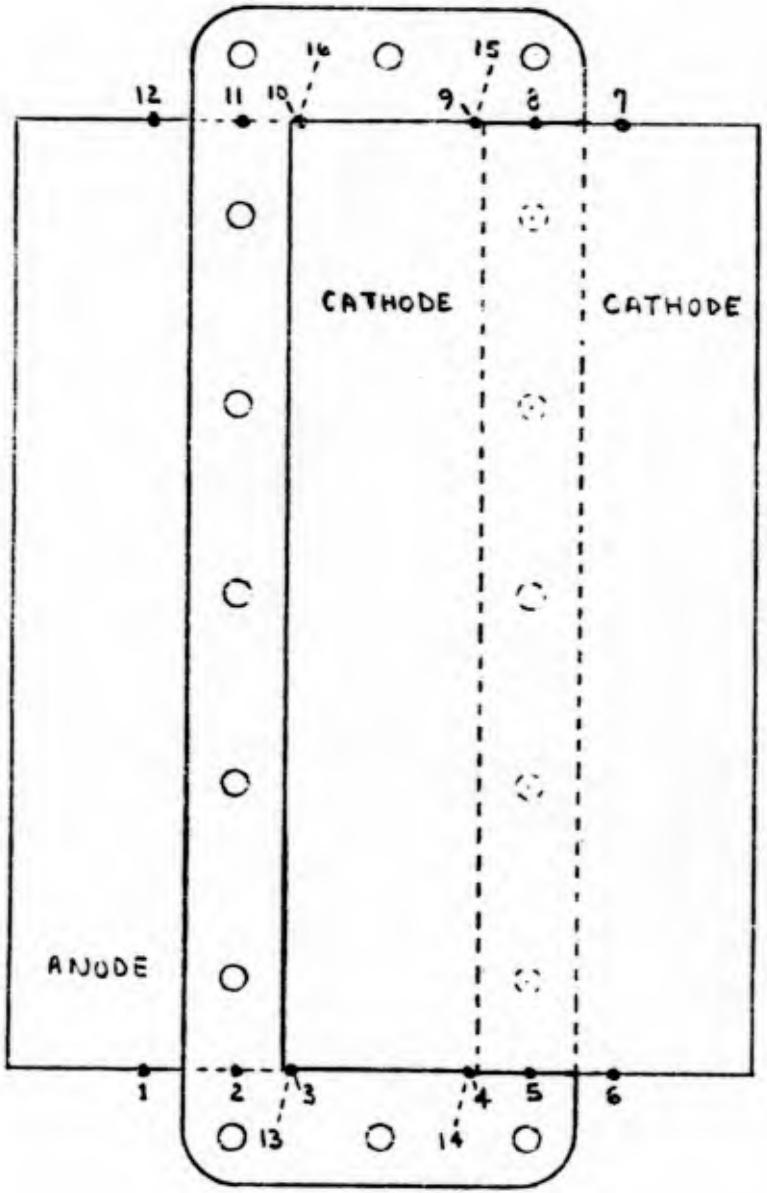

VOLTAGE No.	TAP LOCATIONS	VOLTAGE MEASURED
1	4-13	0,541 ("CELL VOLTAGE")
2	4-14	0.580
3	3-14	0.723
4	4-9	0.045
5	6-1	0.216
6	—	—
7	—	—
8	—	—

Figure 69 — Strip Cell 1, Voltage Tap Locations

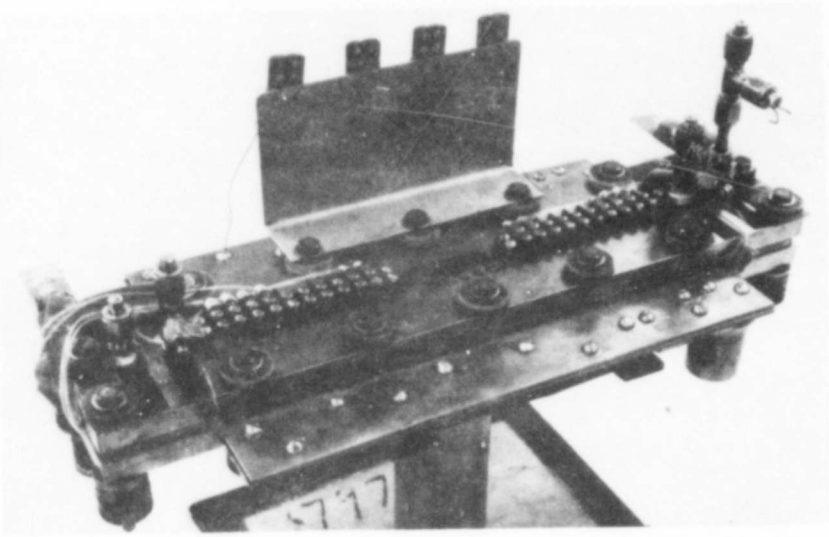

Figure 70 – Assembled Strip Cell 1

Initial internal cell performance is shown in Figure 71. This performance is the voltage measured from tap 4-13 and does not include IR losses through the frame. The cell was run for a total of 6.8 hours load time with 2.4 hours accumulated at 3000 ASF. The voltage taps shown in Figure 69, allowed determination of cell substrate losses and current density variation across the active area of the cell. The voltages shown in Figure 69 were recorded at 3000 ASF. The cathode substrate loss of 143 mv (Voltage No. 3 minus Voltage No. 2) compared favorably with analytically predicted losses. Current density variation, calculated based on local voltages, was found to be 2400 ASF to 3600 ASF in the plane of the cell from edge to edge. A total decay rate of 0.2 volts was observed during the test and was believed to result from the use of a low-sinter temperature anode and non-optimized operating conditions. The testing of this cell provided substrate loss data to permit improving the design of future cells and revealed no problems which would prevent the use of the NASA-LeRC type strip cells in subsequent testing.

Strip Cell 2 – Strip Cell 2 was constructed with a gold/platinum cathode on a nickel screen with two thicknesses of silver plating, specifically, a 0.5-mil silver plating in the active area and a 1.0-mil silver plating in the frame area. The additional plating was added in the frame area to supplement conductivity based on the substrate voltage tests made in operating Strip Cell 1. The anode was a standard platinum electrode on 0.5-mil silver plated nickel screen. The assembled cell was otherwise identical to Strip Cell 1. The objective of testing this cell was to measure substrate losses in the active and frame areas to substantiate the selection of these plating thicknesses. The selection of the plating thicknesses was based on optimization studies of weight versus resistance losses discussed in Section IIIC under Optimization of Substrate Plating Thickness. The cell was instrumented with voltage taps to permit the evaluation of the substrate as shown in Figure 72.

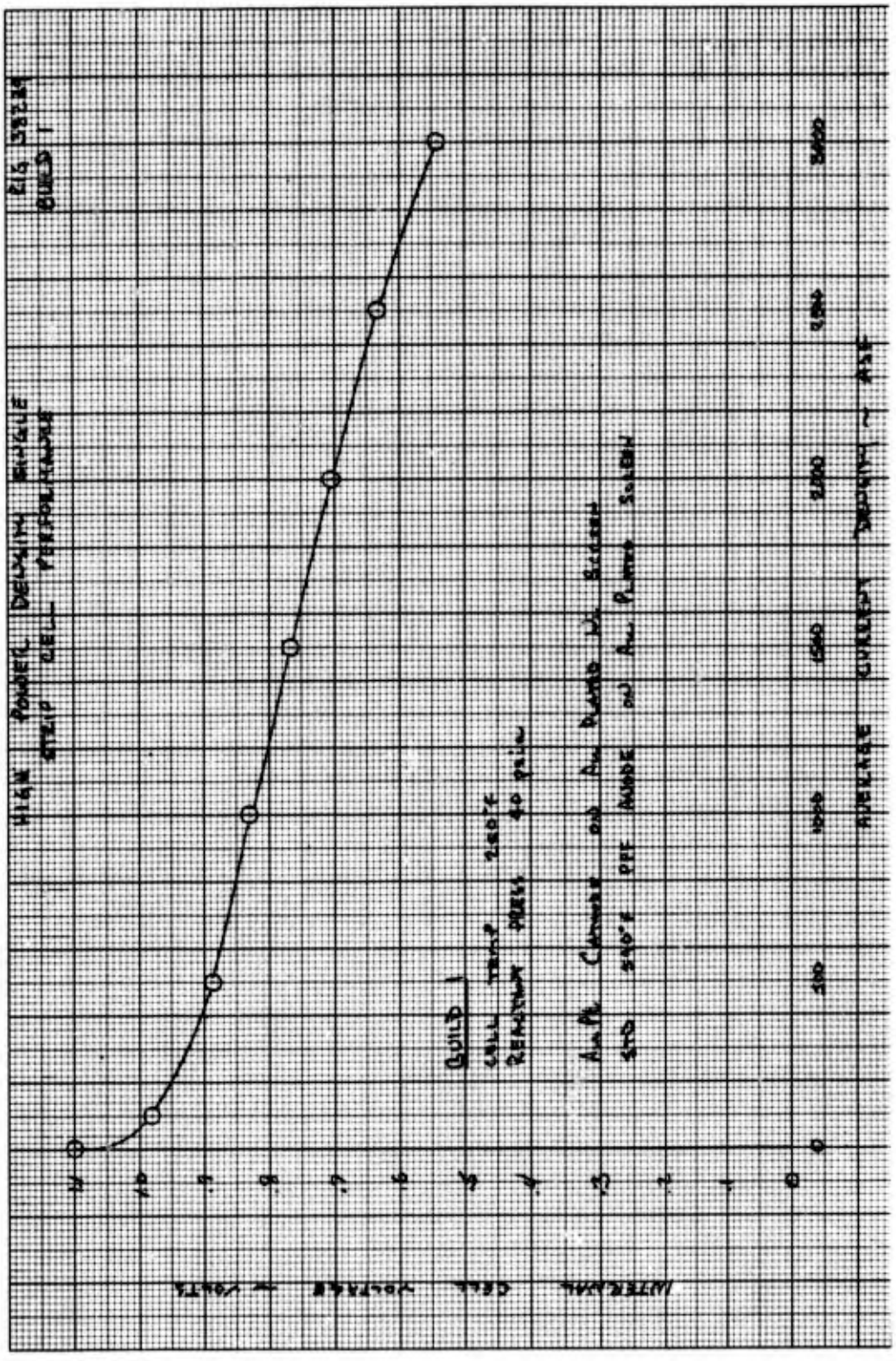

Figure 71 — Strip Cell 1, Initial Internal Performance

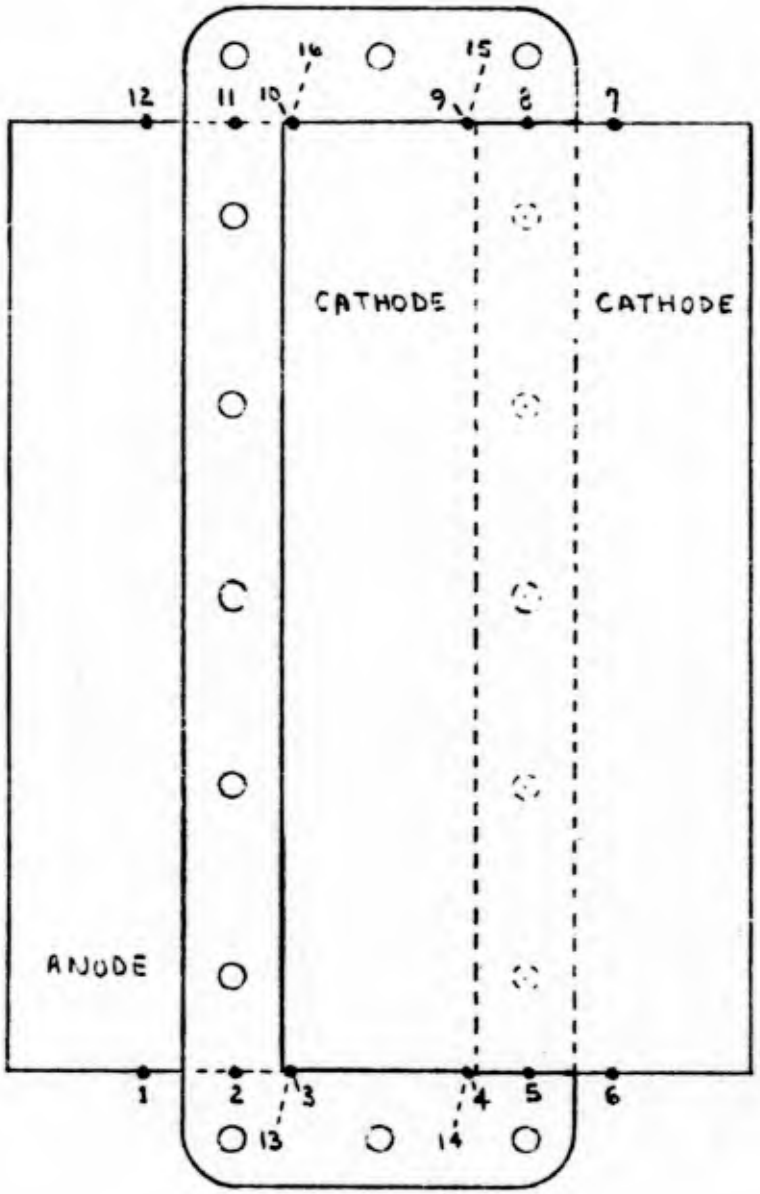

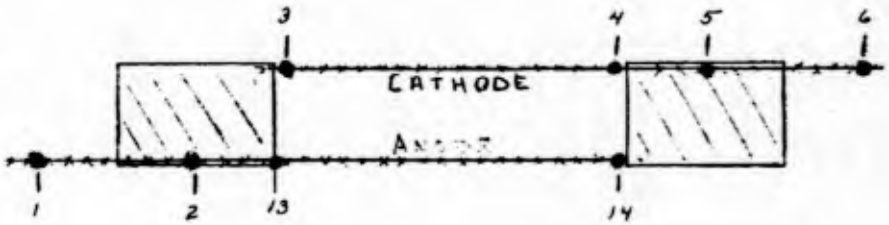

Voltage No.	Tap Locations	Voltage
1	4-13	0.579
2	4-14	0.607
3	3-14	0.631
4	4-9	0
5	6-1	0.464
6	—	-
7	5-2	0.506
8	9-16	0.570

Figure 72 — Strip Cell 2, Voltage Tap Locations

The cathode substrate loss of 24 mv (Voltage No. 3 minus Voltage No. 2) obtained on Strip Cell 2 was lower than that predicted based on analysis. This difference may have been due in part to a current density variation down the length of the strip cell and partial current flow through the oxygen field/coolant plate. Post test examination of the coolant plate showed metal corrosion indicating breakdown of the TFE dielectric coating, and therefore possible electrical contact between the cathode and cooler.

The cell was run for a total of 7.9 hours with 6 continuous hours at 3000 ASF. High current density decay (over 150 mv) was high, but was again attributed to the use of a low-sinter temperature anode. Single cell testing had by this time conclusively demonstrated the superior stability of high-sinter temperature anodes at high current density operation when compared to low-sinter temperature anodes.

The initial internal cell performance is shown in Figure 73. In comparison with Strip Cell 1, Strip Cell 2 gave higher performance reflecting the lower substrate losses. It also operated longer and more stably at 3000 ASF than did the first unit.

Strip Cell 3 – Strip Cell 3 was constructed with a high-sinter temperature (635°F) platinum anode that was fabricated using shop production procedures. It was fabricated on nickel screen anode having a nominal 0.3 mil silver plating.

Strip Cell 3, also had a gold/platinum cathode on nickel screen with two thicknesses of silver plating increased slightly over those of Strip Cell 2 for better conductivity (0.6 mil in the active area and 1.1 mil in the frame area). The other components of this assembly included a 10-mil reconstituted asbestos matrix and a 30-mil nickel ERP. The magnesium-plate cooler was coated with a 1.5-mil dielectric coating of Teflon on the oxygen field adjacent to the cathode. The Teflon coating thickness was increased by 50 percent to prevent the breakdown experienced in Strip Cell 12. The objectives of this test were to determine optimum running conditions and to evaluate substrate losses and current density variations in the cell.

Performance of this cell was considerably improved over that of the previous two cells. This improvement was attributed to a change in operating conditions. Previous cells were operated at coolant inlet temperature below 250°F to obtain electrode temperatures of 250°F when operating at 3000 ASF. A 250°F cell temperature may not have been high enough for proper water removal and could have resulted in partial flooding of the electrodes. In Strip Cell 3, a cell coolant inlet temperature of 250°F was maintained throughout the full load range, resulting in an electrode temperature of 260°F at 3000 ASF.

The cell's initial performance was 0.687 v at 3000 ASF but was unstable. It was shut down, refilled and returned to test. The performance after refill is shown in Figure 74. Post test examination revealed that the oxygen field dielectric Teflon coating had again broken down in several areas, and the oxygen field may have aided in current collection. Consequently, the performance curve was corrected to reflect a non-conductive oxygen field. This adjusted performance is shown as the lower curve in Figure 74. Despite this correction, the power density of this cell exceeded 1900 WSF.

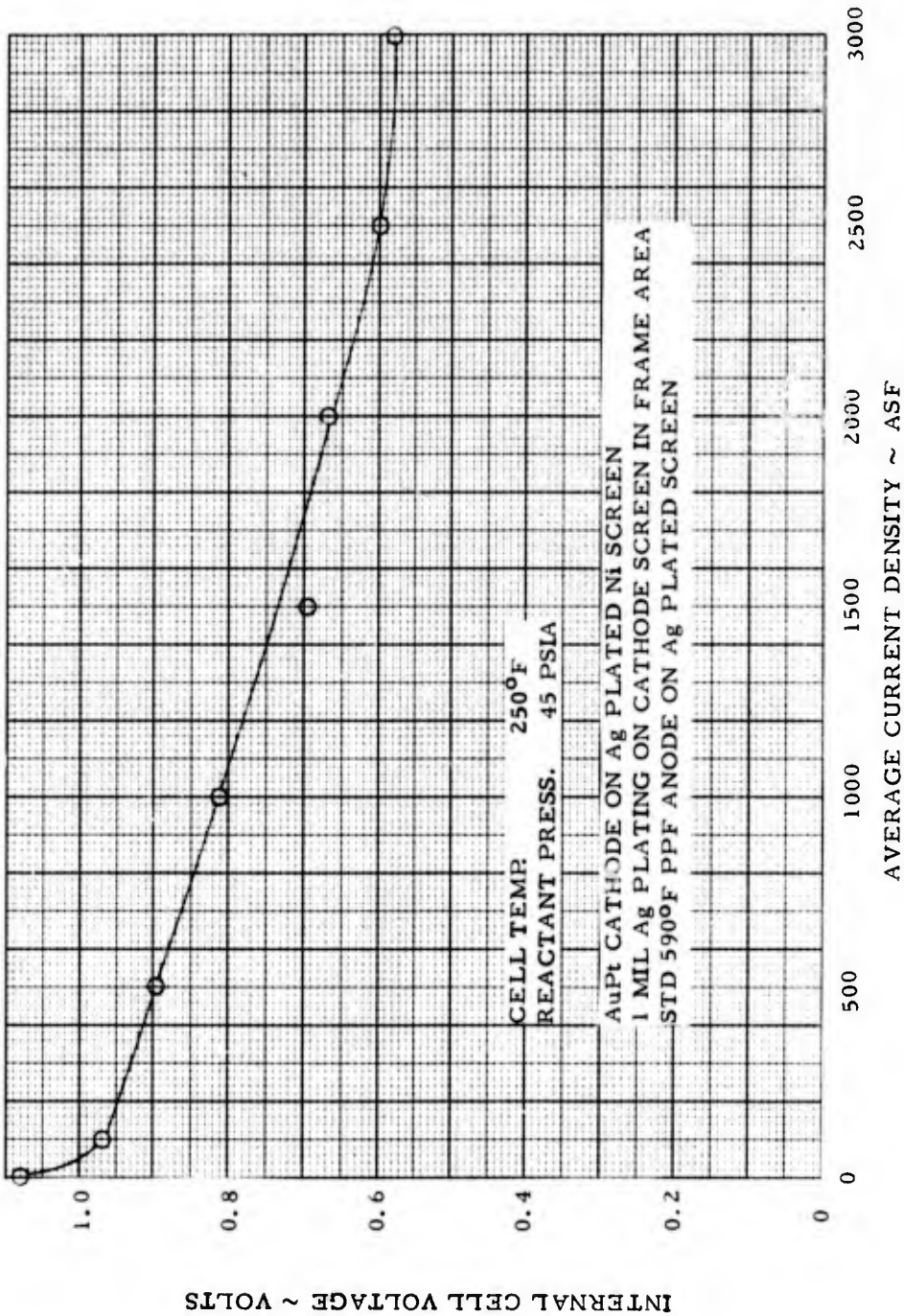

Figure 73 – Strip Cell 2, Initial Internal Performance

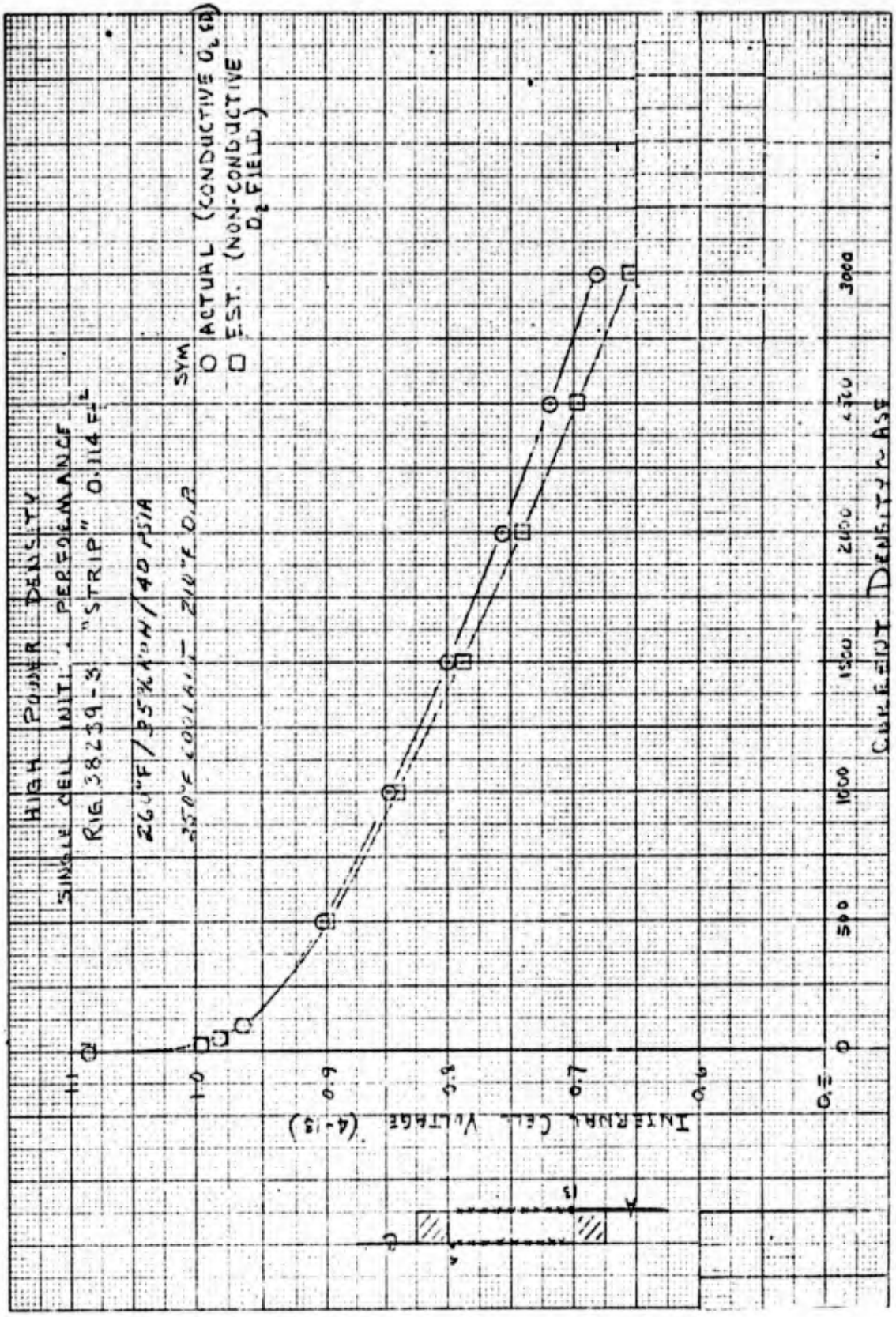

Figure 74 — Strip Cell 3, internal Performance

Strip Cell 4 – Strip Cell 4 featured a shop fabricated gold/platinum cathode instead of the laboratory gold/platinum cathodes of previous high power density cells. In addition, the cell included a 10-mil reconstituted asbestos matrix, a high-sinter temperature (635°F) anode, and a 30-mil nickel ERP. The substrate of both anode and cathode were plated with 0.6 mils of silver and represented a temporary compromise resulting from difficulties encountered in achieving good two-thickness plating of the substrate. A cooler similar to those in the first three builds was used. The test objectives of this cell were to evaluate the shop made cathode and operation of a new load controller capable of providing rapid load pulse transients.

The performance of the cell after refill (initial performance was low) is shown in Figure 75. However even after a refill its performance was considerably poorer than that of Strip Cell 3 in both the low current density, Tafel, and high current density regions. The cell was shut-down after exhibiting a high decay rate, note the change, at 500 ASF. However, prior to shut down, the load controller was operated successfully making the open circuit to 3000 ASF transients over a 50 percent duty cycle of 10-seconds on, 10-seconds off. A post-test examination and analysis indicated no particular problems with the various components of the cell and post-test electrode analyses indicated that both electrodes performed satisfactorily. No good explanation for the low performance was found.

Strip Cell 5 – In Strip Cells 1 through 4 the UEA and ERP's were essentially of the Configuration 1 design itemized in Table XXVII. With Strip Cell 5 the UEA and ERP were changed to a Configuration 2 design. The UEA was lightened by fabricating the electrodes on a 50 x 100 mesh screen and the ERP was reduced in thickness from 30 mils to 22 mils. The ERP pin pattern that contacts the anode was also changed, to increase coverage from 50 percent to 75 percent providing better anode support and greater contact for electrolyte transfer.

The 50 x 100 mesh screen was approximately three-fourths the weight of the 100 x 100 mesh screen. It is oriented with the 100 mesh pattern in the direction of current flow through the electrode, i.e. toward the frame. In this manner weight is reduced without sacrificing conductivity. The screens were plated with 0.5 mil of silver in the active area and 1.0 mil of silver in the frame area: An increase of cathode plating thickness of almost 100 percent in the active area and 200 percent in frame area relative to Strip Cell 3. With this set of screens, the first on which substrate plating was completely satisfactory, the development effort to achieve a good two thickness plate was completed.

Strip Cell 5's cathode was shop fabricated of gold/platinum catalyst. The anode, also shop fabricated, was a high-sinter temperature electrode and the cell incorporated a 10-mil reconstituted asbestos matrix.

The primary test objectives for this cell were to evaluate the new lightweight screen and ERP designs.

The performance on initial fill of Strip Cell 5 was comparable to that of Strip Cell 3, see Figure 76. Strip Cell 3 had demonstrated the best strip cell performance to date, 0.655 v at 3000 ASF (1960 WSF). After refill, Strip Cell 5's performance improved at high current densities, but was still slightly less than that of Strip Cell 3. Its performance was 0.625 v at 8000 ASF (1880 WSF), shown in Figure 76.

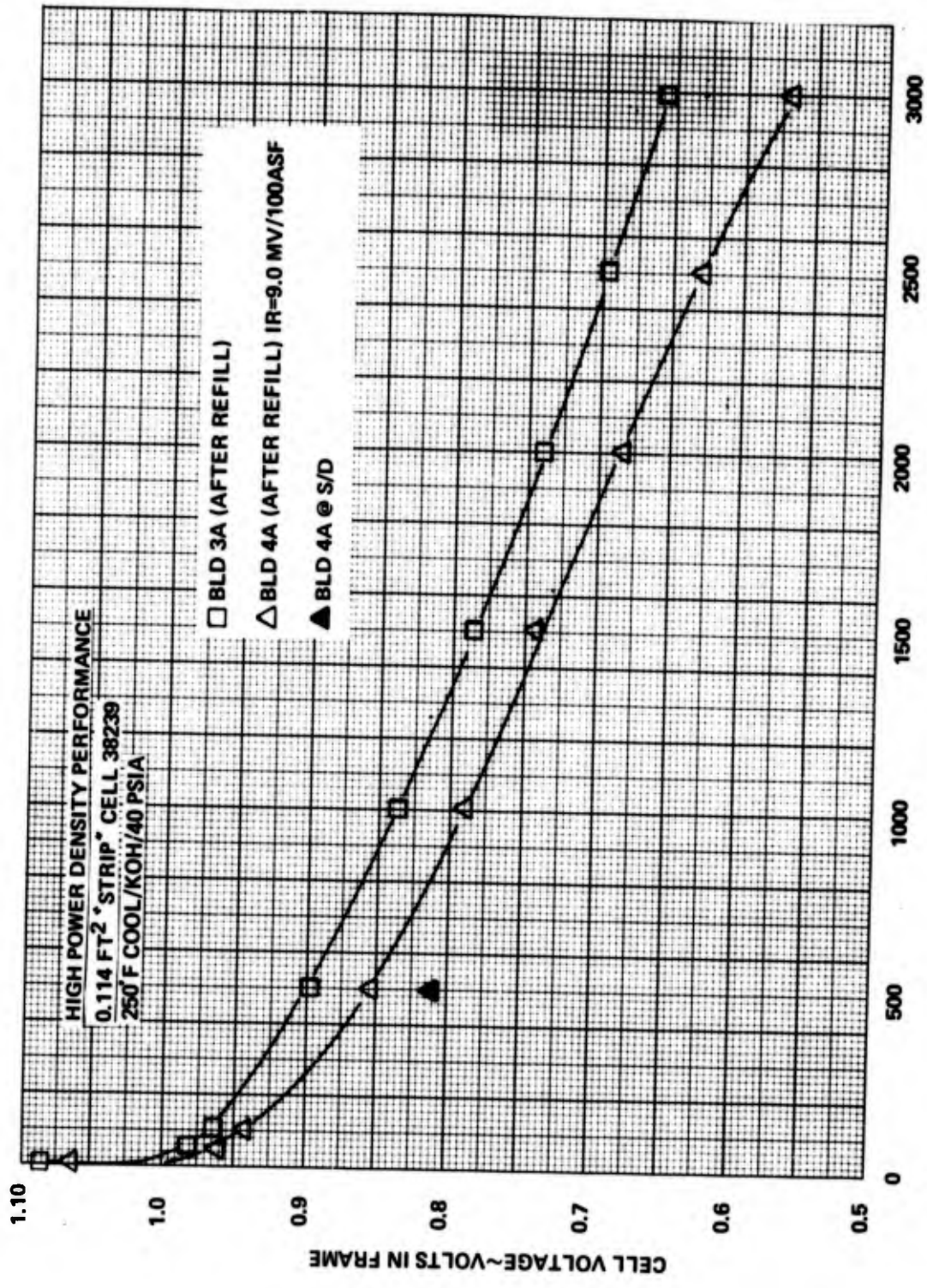

Figure 75 – Strip Cell 4, Performance

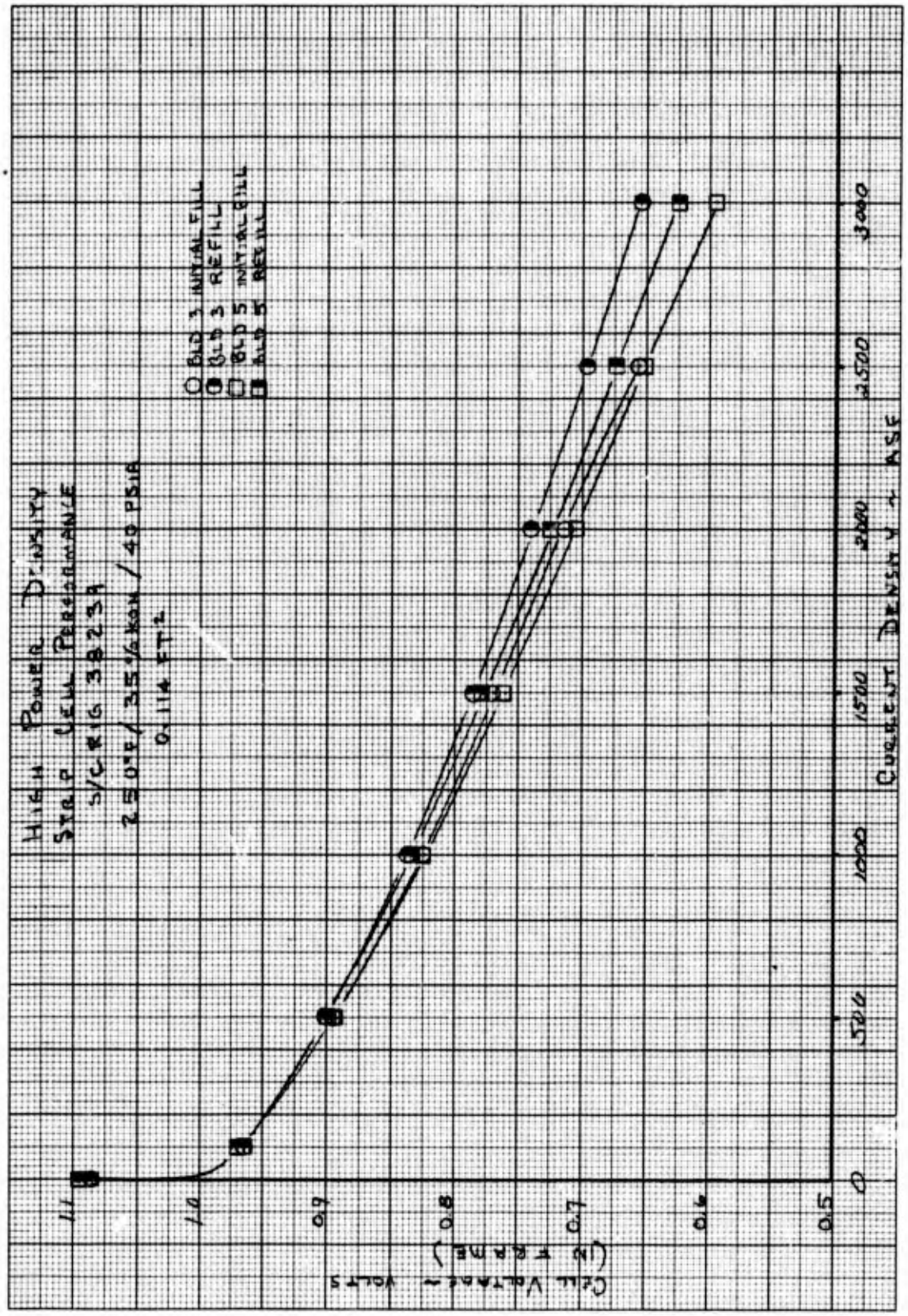

Figure 76 – Strip Cell Performance Comparison

An improvement in performance had been demonstrated after refill on all previous builds with high-sinter temperature anodes. The lower performance on intial fill was attributed to insufficient electrolyte fill. Therefore, tests were conducted to determine whether a special test procedure would have the effect of increasing the anode wetability. The procedure consisted of maintaining a voltage of 0.1v to 0.3v for 2.0 minutes while operating with nitrogen on the anode and oxygen on the cathode. A similar attempt was performed on the cathode by operating with nitrogen on the cathode and hydrogen on the anode. Both attempts were unsuccessful.

Diagnostics included cell IR and dilute oxygen. The IR results were 5.0 mv at 100 ASF; previous IR data ranged from 5.0 to 9.0 mv at 100 ASF. The results of the 20 percent oxygen test, shown in Figure 77, indicated a cathode diffusion loss of 5.0 mv at 100 ASF.

The cell was fully instrumented to determine the effect of the increased substrate plating thickness on performance. Figure 78 shows that although the voltage at the electrode edges (location 6-1) was lower in Strip Cell 5, the losses through the frame [location (5-2) minus location (6-1)] were substantially improved over Strip Cell 3. Based on these tests the reduced weight 50 x 100 mesh screen was judged suitable for use in future cells as was the reduced weight ERP which performed without problem.

Strip Cell 6 – Strip Cell 6, was the first cell of a Configuration 2 design, that incorporated a lightweight 3-mil electroformed nickel oxygen field for further weight improvement. The repeating unit specific weight of this design, at design power density, is 0.73 lb/kw. The cell also featured 50 x 100 mesh electrode substrates with two thicknesses of silver plating, (0.5 and 1.0 mil in active and frame areas repectively), a 22-mil nickel ERP and epoxy/fiberglass frames for both cooler and UEA. The new cell cooler assembly, shown in cross section in Figure 79, was fabricated in two steps: 1) the cell and cooler were separately unitized in epoxy/fiberglass frames and checked for cross leakage, and 2) the separate components were bonded together with a bond layer of epoxy/fiberglass at temperature and pressure.

The primary objective of this test was to evaluate the electroformed-nickel cooler/oxygen field assembly from a thermal and structural standpoint. Strip Cell 6 was tested at 3000 ASF under three conditions: 250°F-45 psi, 265°F-45 psi and 265°F- 54 psi. Performance curves obtained under these operating conditions are shown in Figure 80. The initial test was conducted at 250°F and 45 psi. The initial performance at 3000 ASF was 0.620 v. This was the highest performance to date after the initial electrolyte fill on a 635°F sintered anode. The cell was then refilled as previous experience had indicated the necessity of a refill to completely activate the anode, and the average response to refill has been about 45 mv at 3000 ASF on these cells. Upon restart, the cell showed a gain of only 10 mv to 0.630 v at 3000 ASF. The high initial performance level plus the small response to refill appears to indicate that the 635°F sintered anode was sufficiently wetted on the first fill to exhibit essentially normal performance.

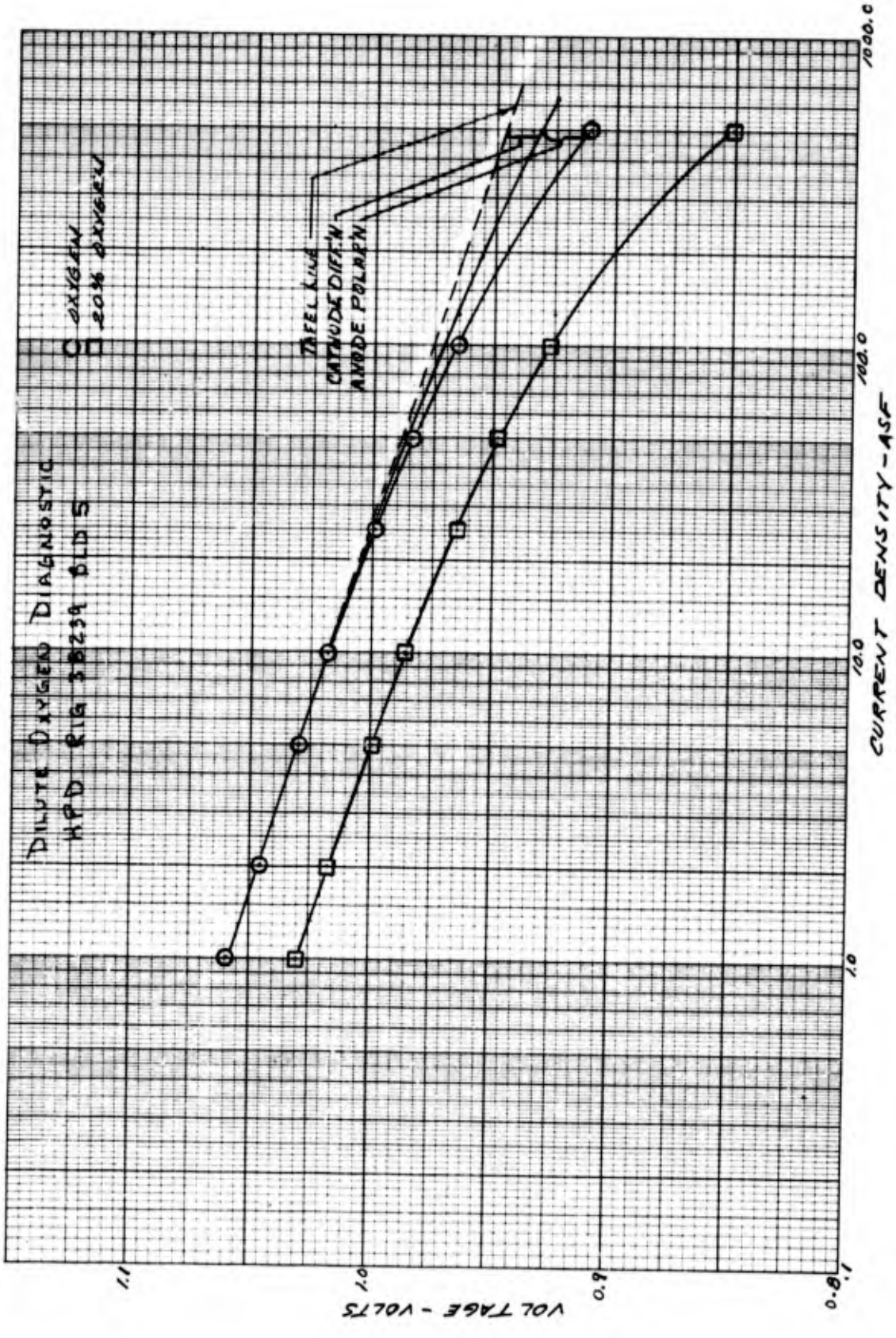

Figure 77 – Strip Cell 5, Dilute Oxygen Diagnostic Data

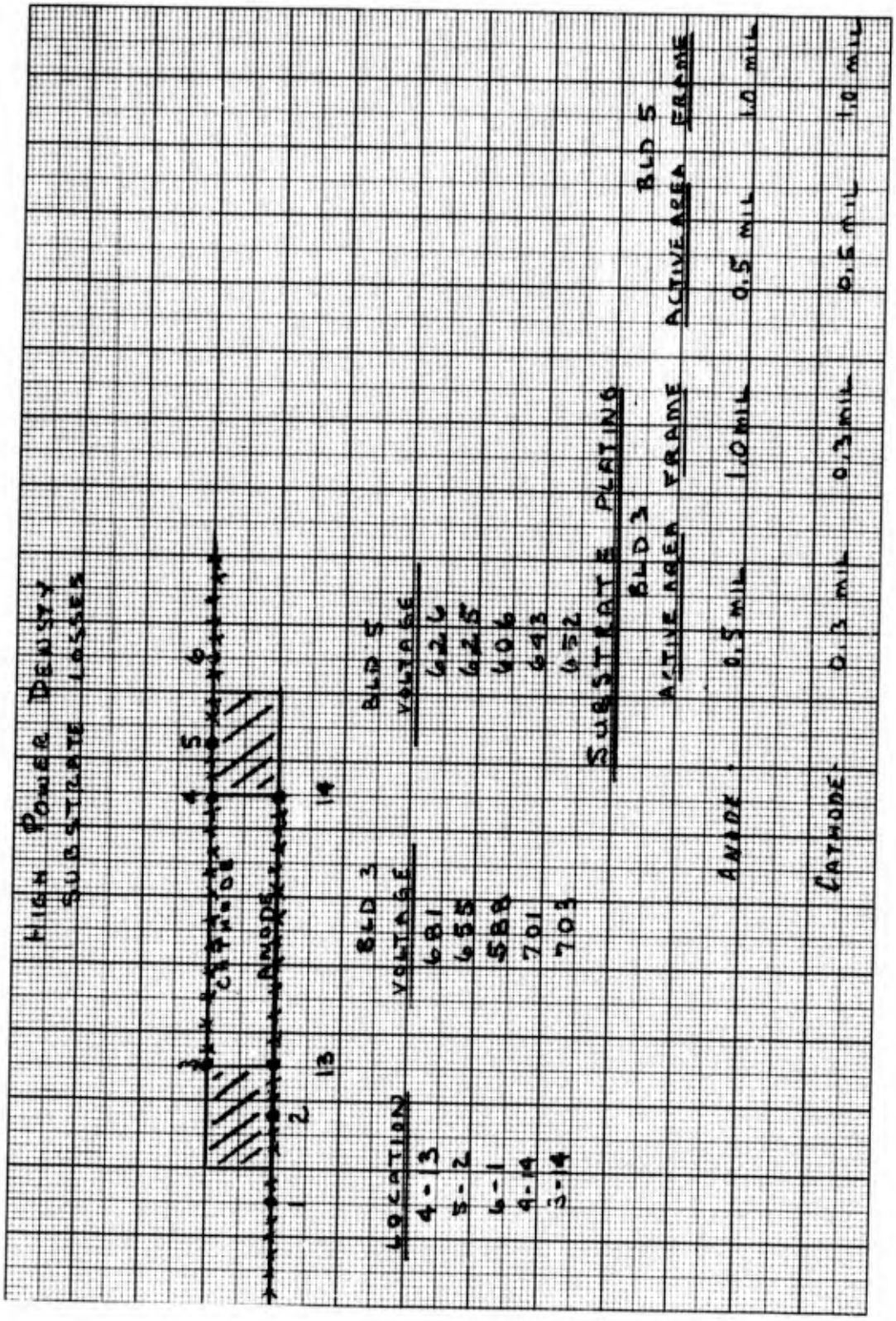

Figure 78 — Strip Cell Substrate Loss Comparison

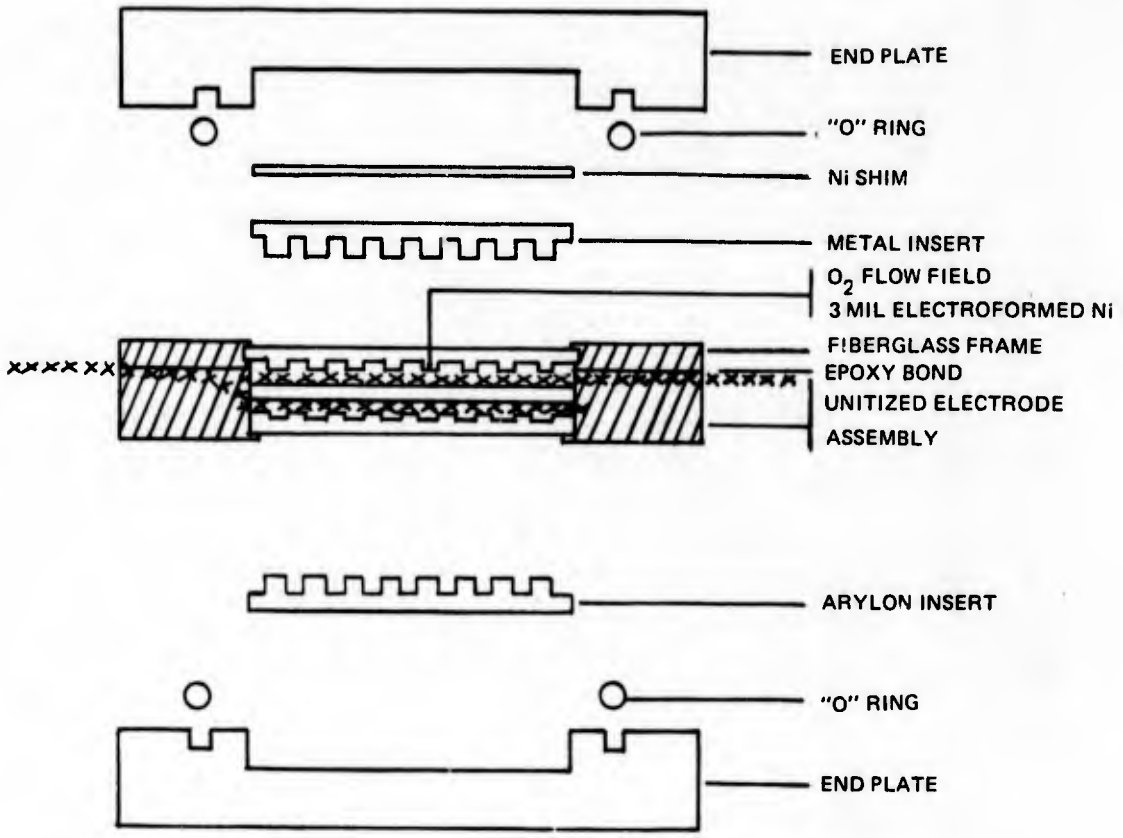

Figure 79 – Cross-Section of Single-Cell with Electroformed Nickel Cooler Plate

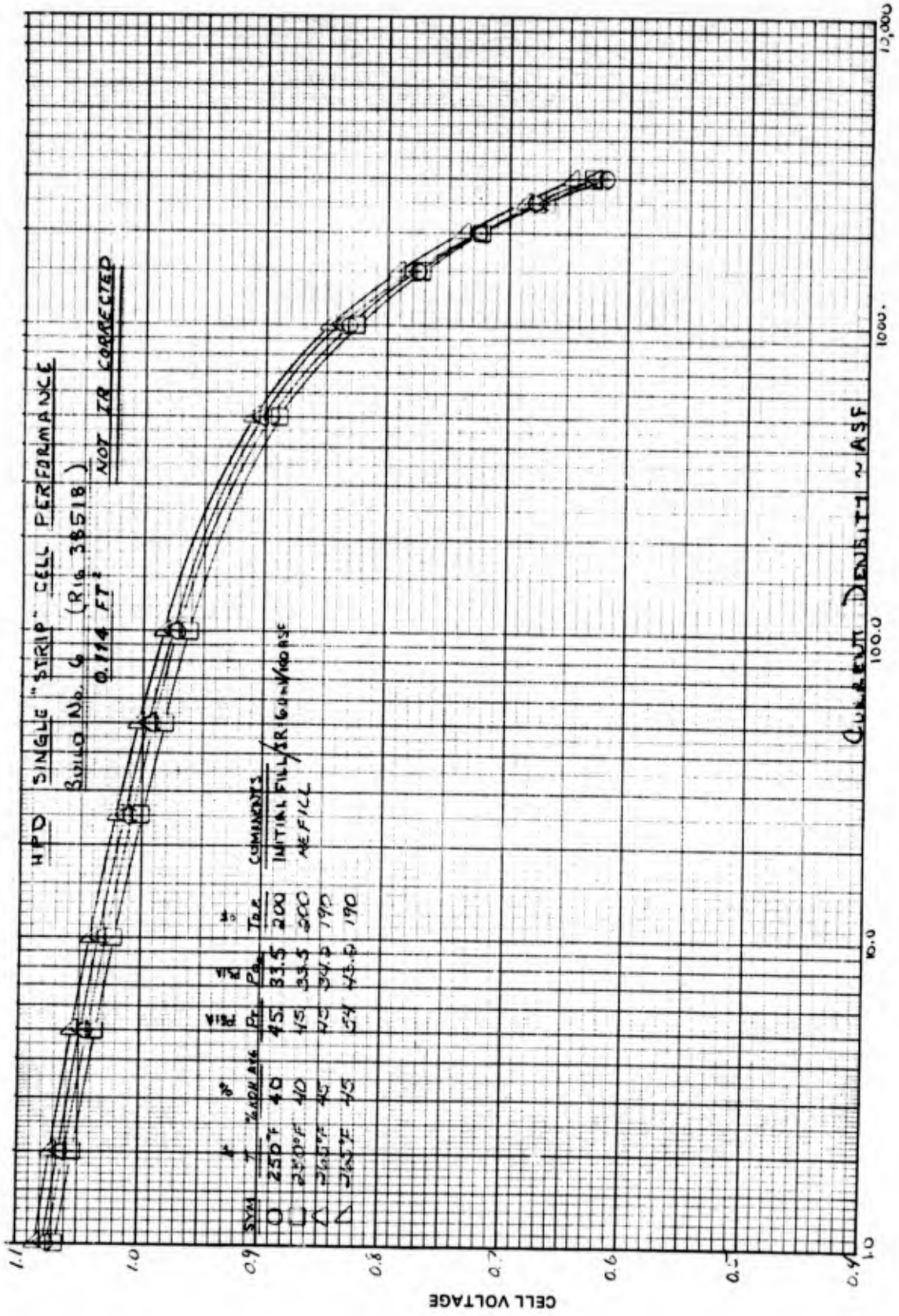

Figure 80 — Strip Cell 6, Performance Data

To evaluate the effects of higher temperature and pressure operation, the average cell temperature was raised to 265°F at 45 psi. As shown in Figure 80 the performance was increased slightly at lower current density, however, no increase was observed at 3000 ASF. Next, the pressure was raised to 54 psi, the cell voltage at 3000 ASF increased to 0.65 volts demonstrating a specific weight of 0.70 lb/kw. The cell was then shut down and removed from the test stand. Total time on this cell was 6.0 hours with 0.25 hours above 3000 ASF. Thermal performance of the cell was as expected. The electroformed-nickel cooler performed satisfactorily throughout the test. Thermocouples placed in the cooler and on the electrode showed a nominal temperature difference of 20°F from the electrode to the coolant at 3000 ASF. Data from the test are shown in Figure 81. This data was obtained at coolant flow rates consistent with those expected in the development unit testing. The cell was disassembled and inspected. Disassembly showed very little frame corrosion and no damage or deformation of the electroformed cooler. Consequently, the lightweight cooler design was judged ready for incorporation into future strip cells and development units.

HPD SINGLE CELL BLD. NO. 6
O_2 FIELD – COOLER EVALUATION

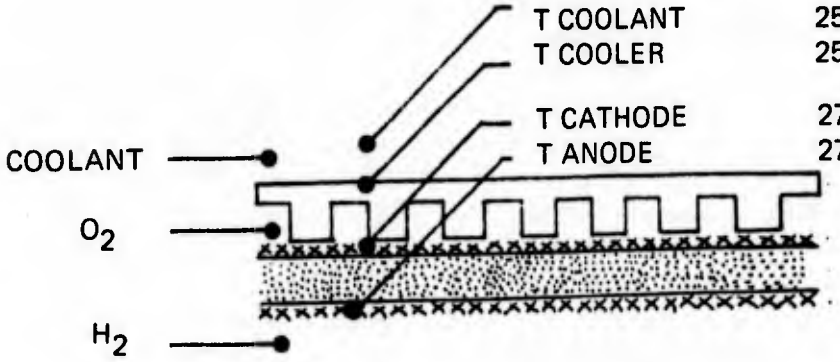

T/C LOCATION	RESULTS RUN 1	RUN 2
T COOLANT	252°F	264°F
T COOLER	253°F	267°F
T CATHODE	272°F	286°F
T ANODE	273°F	285°F

CONDITIONS: LOAD: 3000 ASF

COOLANT FLOW: 2.5 PPH

Figure 81 – Strip Cell 6, Oxygen Field/Cooler Temperature Data

Strip Cells 7, 8, and 9 – Strip Cells 7, 8, and 9 were the first units fabricated to Configuration 3. The cells differed from Configuration 2 in that the 22-mil nickel electrolyte reservoir plate was replaced with a 30-mil polysulfone ERP. The polysulfone was plated with nickel to render it wettable. The 3-mil electroformed nickel oxygen field was also changed. It was replaced with a 1.5-mil nickel oxygen field. The other features of Strip Cell 5 were retained, namely, 50 x 100 mesh electrode substrates with differential plating of 0.5 and 1.0 mils, 10-mil thick reconstituted asbestos matrices. Epoxy/fiberglass frames for both cooler and UEA, gold/platinum cathodes, and high-sinter temperature anodes. The primary objective of these tests was to evaluate the lightweight polysulfone electrolyte reservoir plate at high power density conditions.

Strip Cell 7 had a low initial performance and was unstable above 1500 ASF, see Figures 82. and 83. Dew point excursion tests indicated adequate ERP-anode electrolyte transfer although there was some hysteresis effect as shown in Figure 84. Because the cell exhibited poor performance, and had a high IR of 11.0 mv, it was refilled. During refill it developed reactant crossover and was disassembled. The exact nature of the crossover could not be determined, but it was suspected that a matrix imperfection may have caused the crossover.

As a result, Strip Cell 8, was built. It had the same features as Strip Cell 7 and had the same initial performance at 100 ASF as Strip Cell 7, see Figure 85. However, it was able to hold a higher stable performance. Again, the IR was high, 11 mv at 100 ASF, and the dew point excursion indicated a lack of dry-side tolerance, see Figure 86. The cell was then refilled and an additional 2 mils of pinch added to account for possible compression of the polysulfone ERP. After restart, the initial performance, as seen in Figure 85, was improved by 23 mv at 100 ASF and the IR was reduced to 9 mv. The dew point excursion, Figure 86 now indicated a normal response. A high current density performance calibration showed satisfactory performance until 2000 ASF was reached, see Figure 87. Above this point, the cell voltage began to drop. Following this, tests were conducted to measure the rapid electrolyte transfer capability of the anode-ERP combination. This was done by operating at high current densities for short periods of time with no water removal. Loads of 1000 ASF and 2000 ASF were operated for 90 seconds and 45 seconds respectively. These loads were operated both continuously and intermittently. Figures 88 through 90 show typical voltage traces of these tests. Initial results of these tests show the cell responded well at 1000 ASF with a marginal condition existing at 2000 ASF. Though electrolyte was being transferred from cell to ERP, indications were that the response required considerable improvement. The cell response deteriorated with continued testing and the unit was shut down.

The primary test objective of Strip Cell 9 was to explore further the operation of the polysulfone ERP under high power density conditions. The initial performance at 100 ASF compared favorably with the performance obtained on cells with nickel ERP's, see Figure 91. However, performance at current densities beyond 1500 ASF was poor. Dilute oxygen diagnostic tests showed the cathode performance to be good but the anode approached limiting current densities at between 1500 and 2000 ASF, as shown in Figure 92. A refill of the cell resulted in performance improvement at levels up to 2000 ASF but was still low when compared to previous cells with nickel ERP's. Dilute oxygen diagnostics showed the performance in the high current density region to be virtually unchanged.

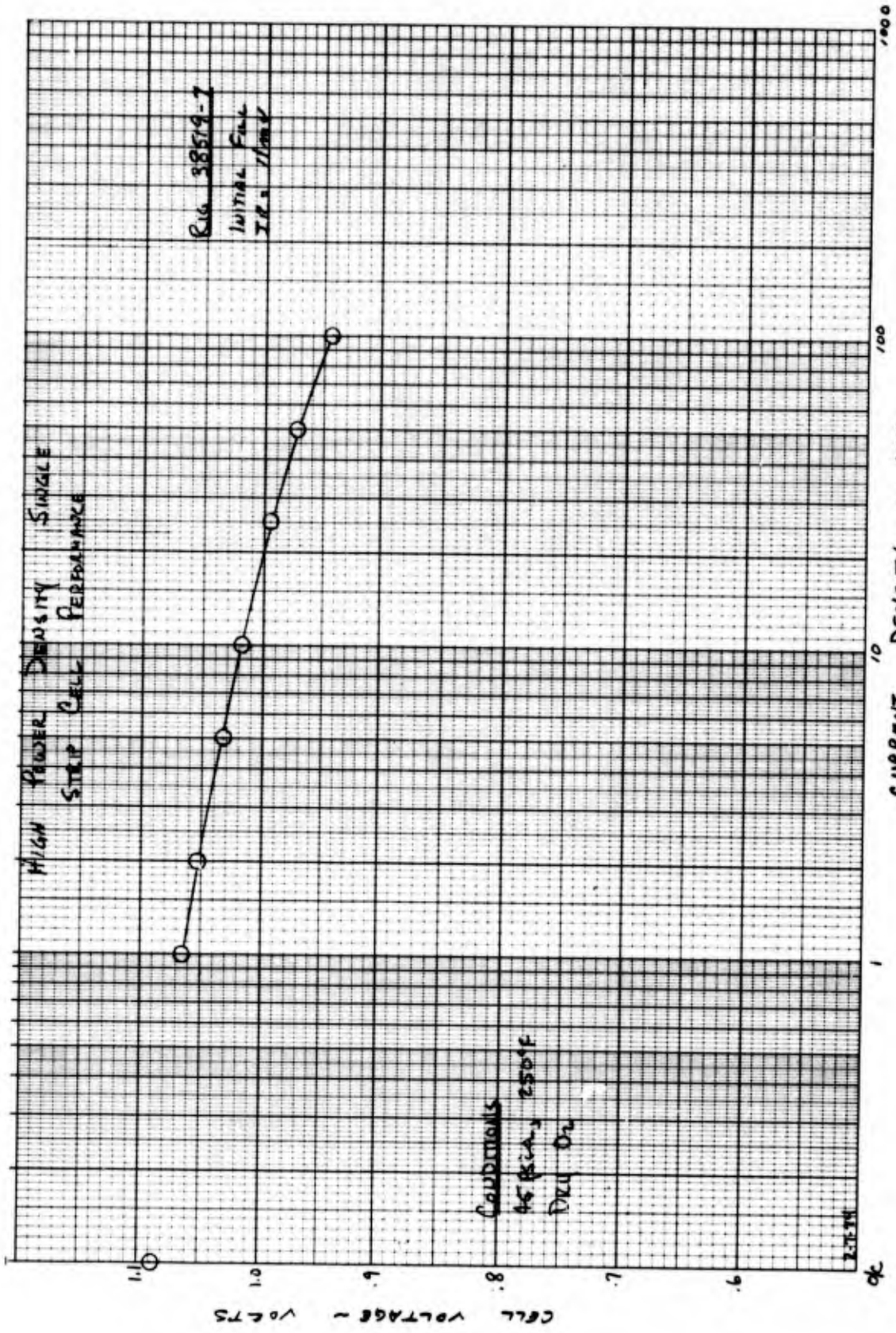

Figure 82 – Strip Cell 7, Performance at Low Current Density

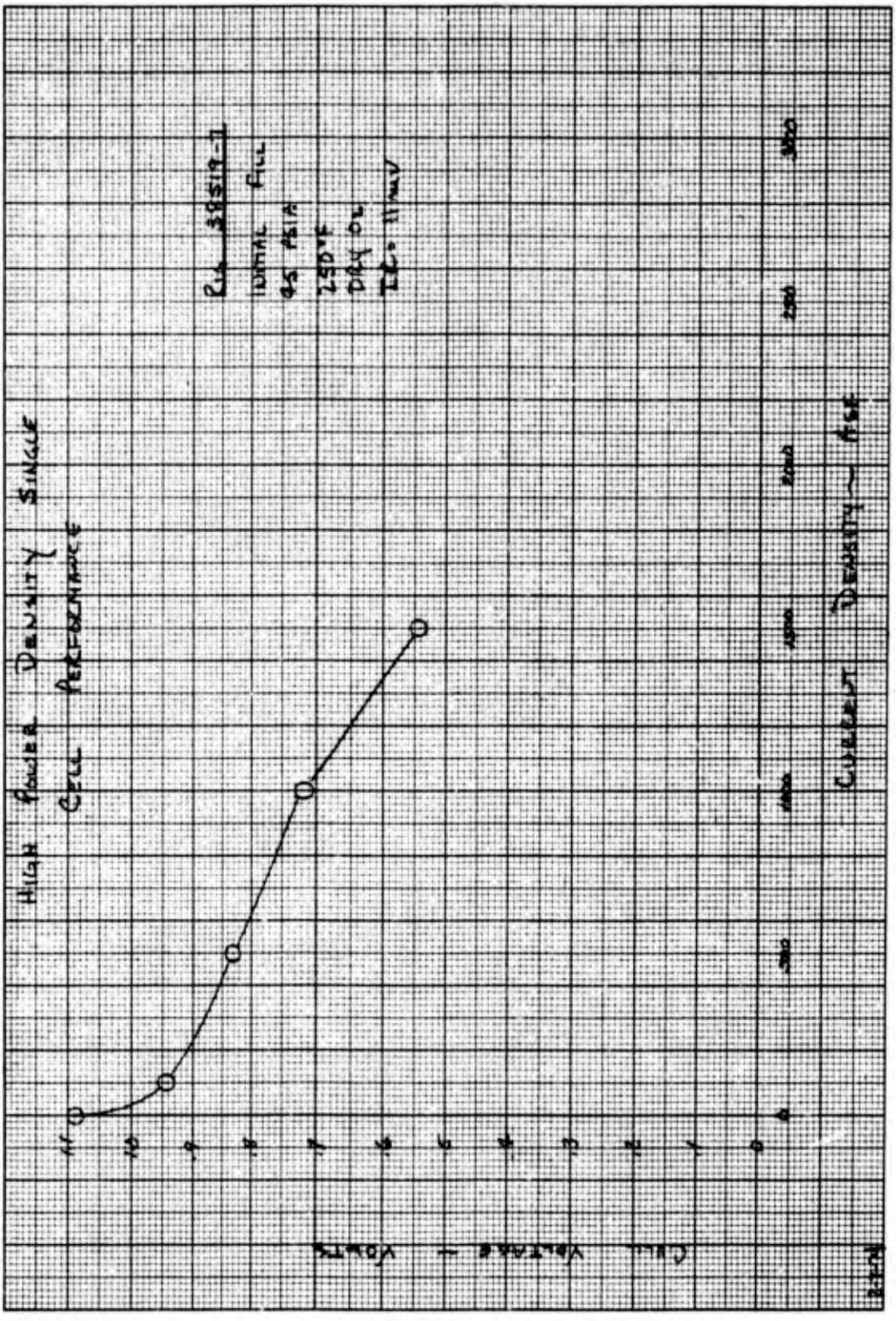

Figure 83 – Strip Cell 7, Performance at High Current Density

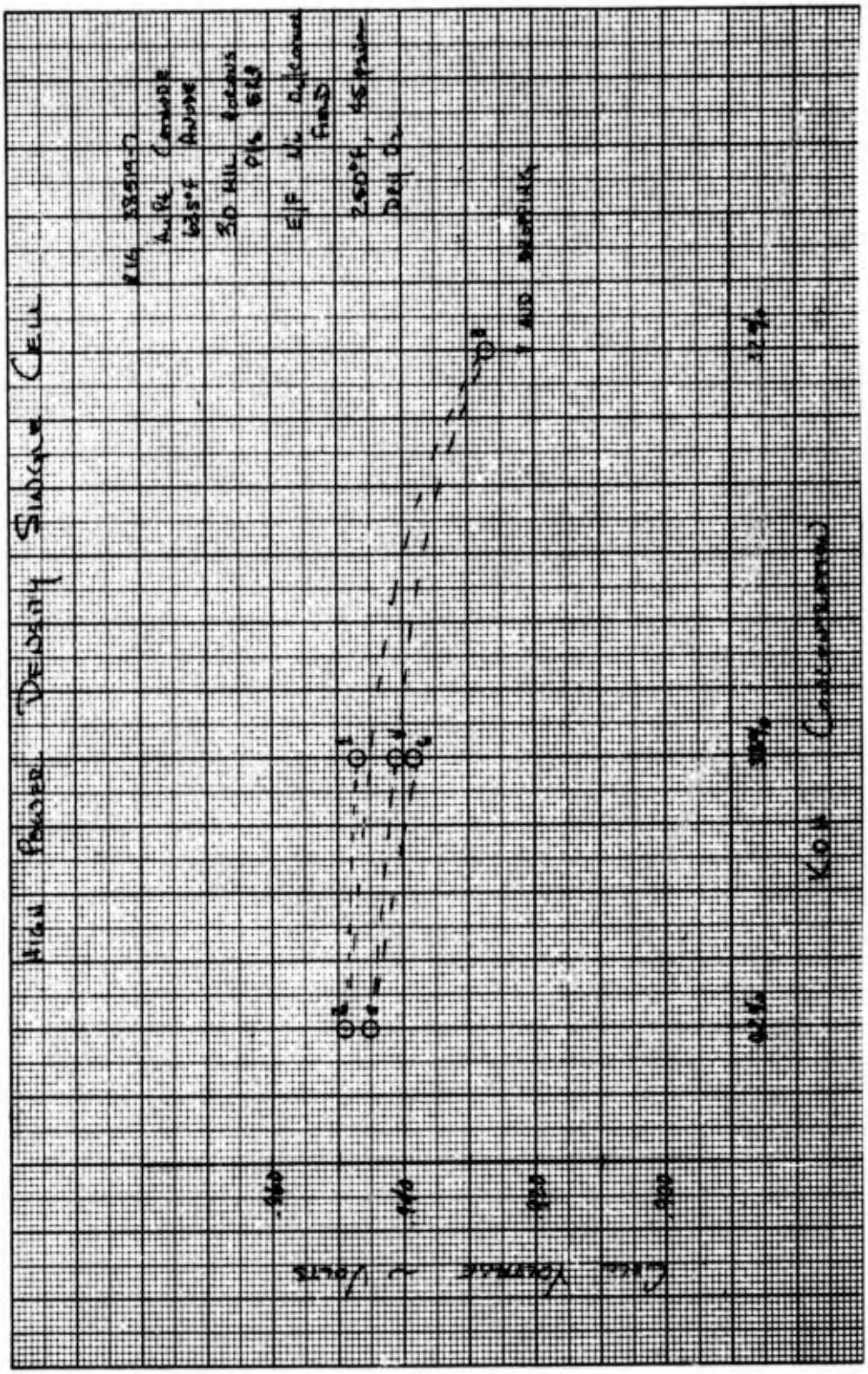

Figure 84 — Strip Cell 7, Dew Point Tolerance Test Results

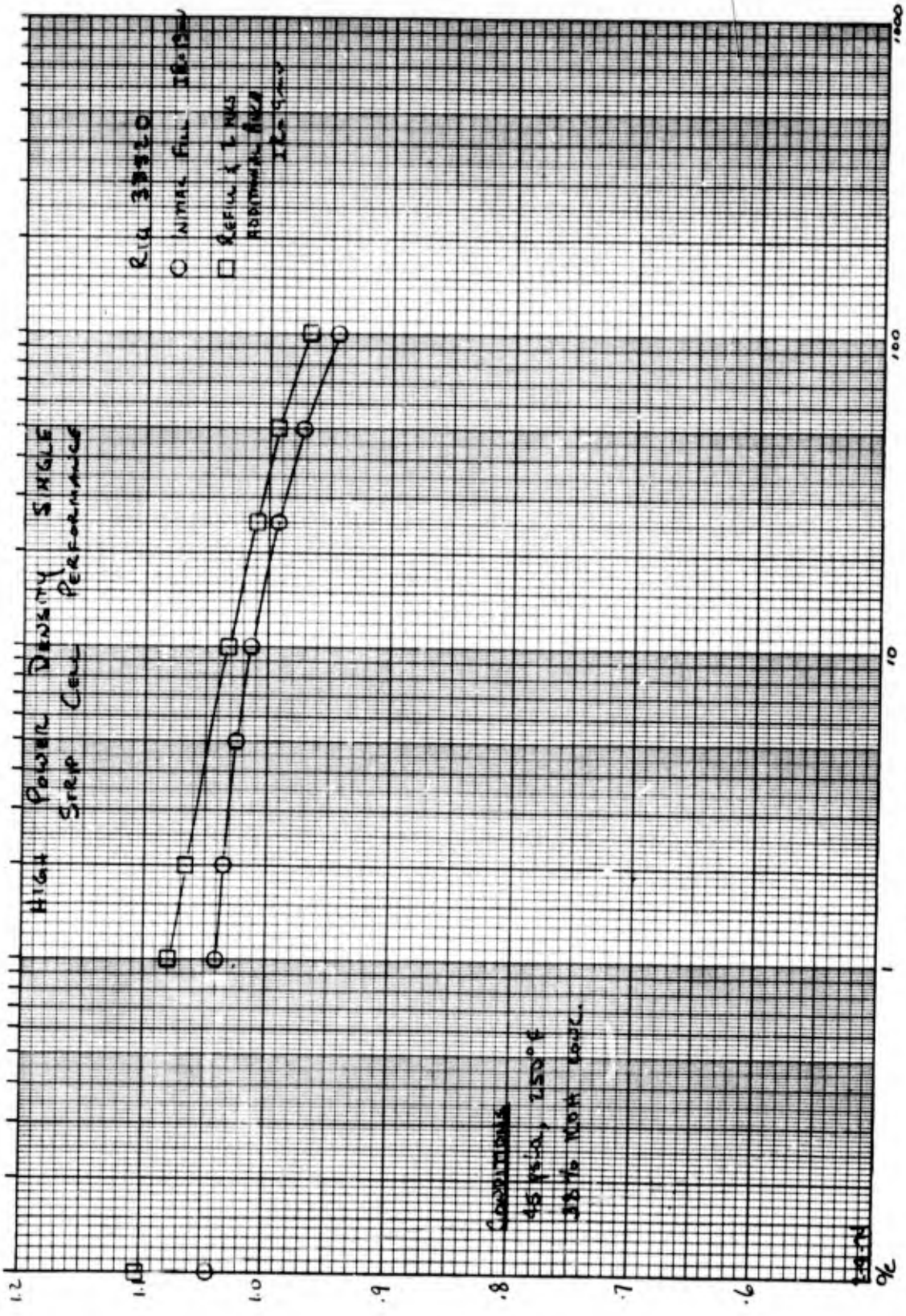

Figure 85 — Strip Cell 8, Performance at Low Current Density

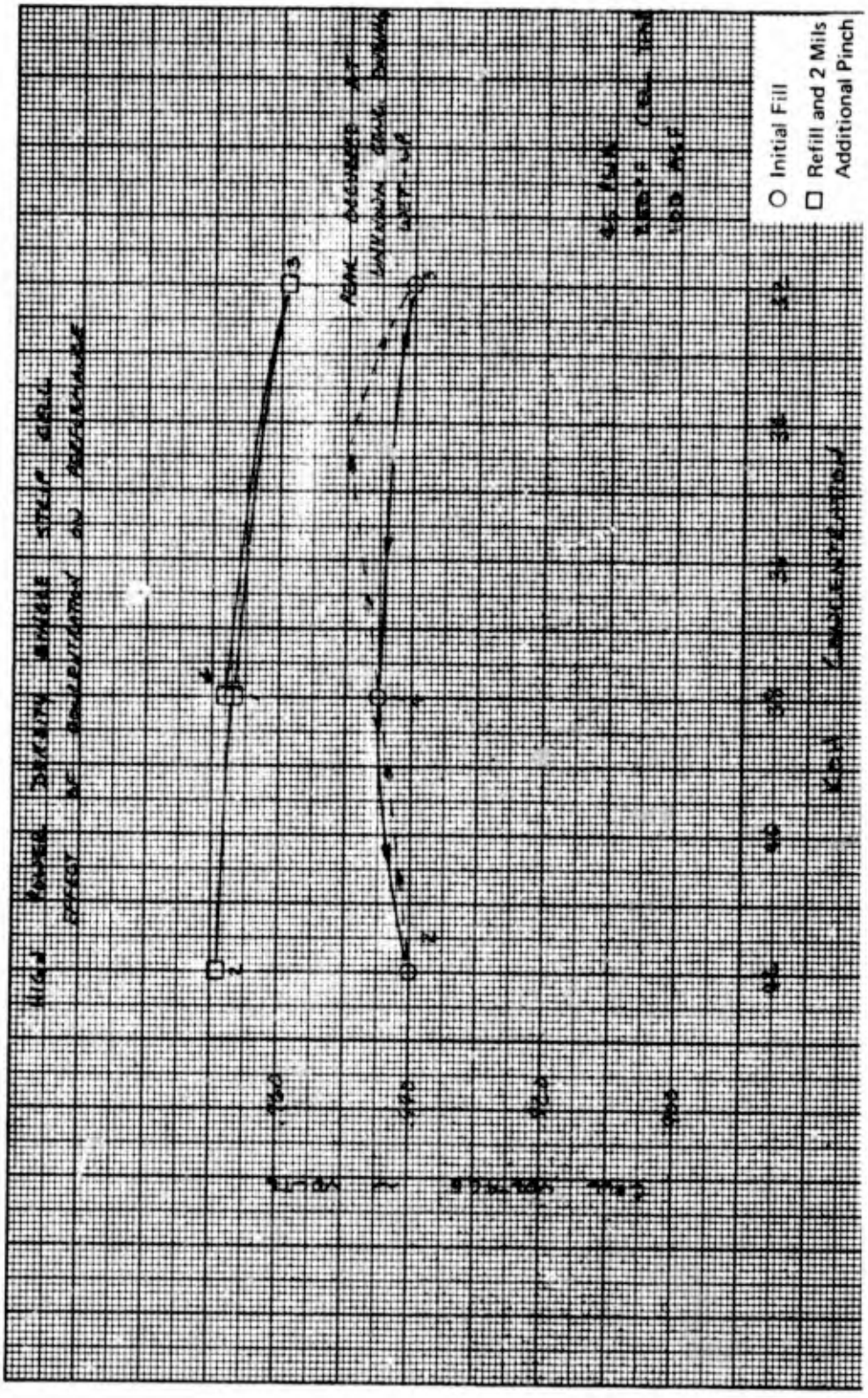

Figure 86 – Strip Cell 8, Dew Point Tolerance Test Data

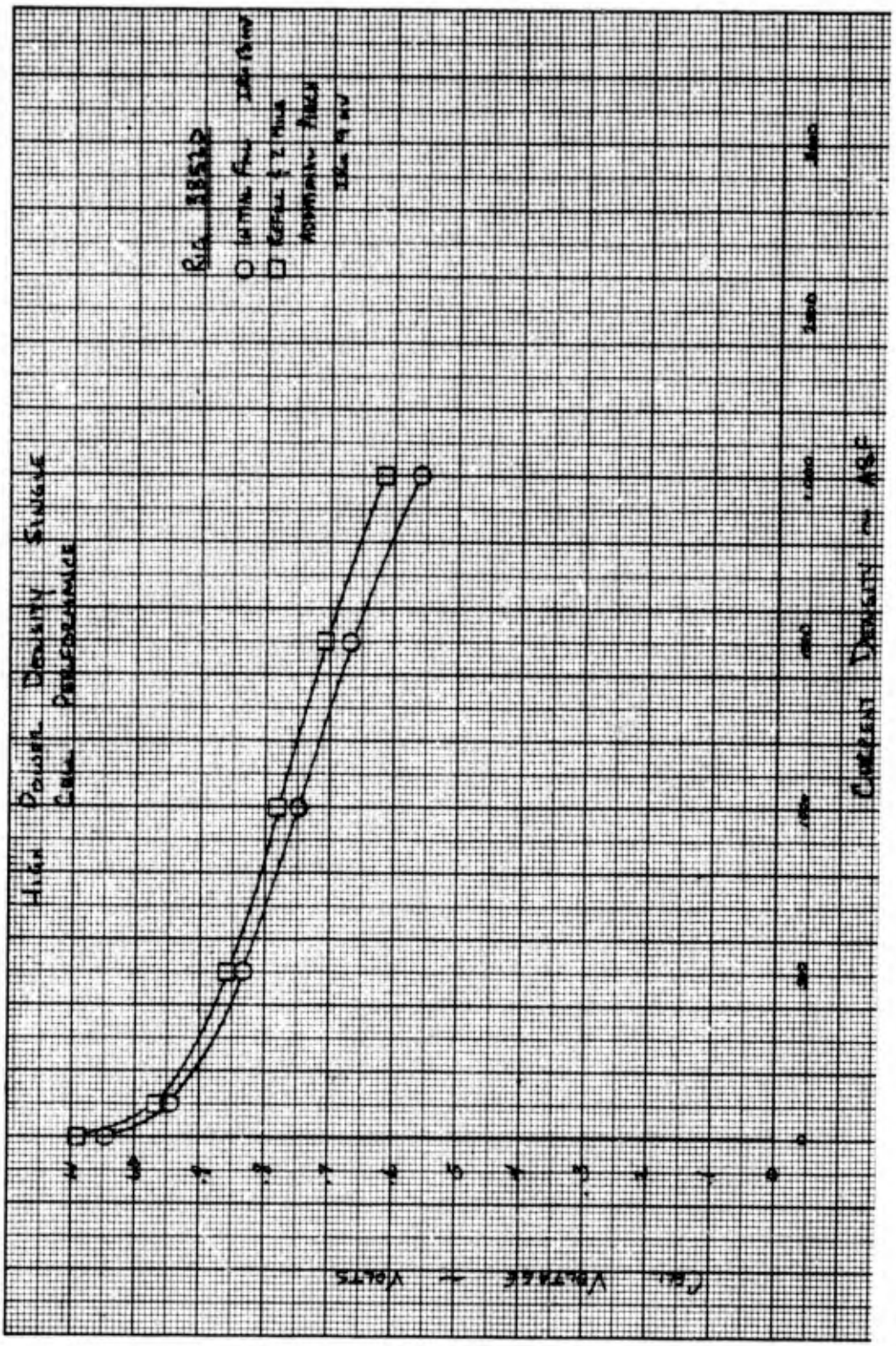

Figure 87 — Strip Cell 8, Performance at High Current Density

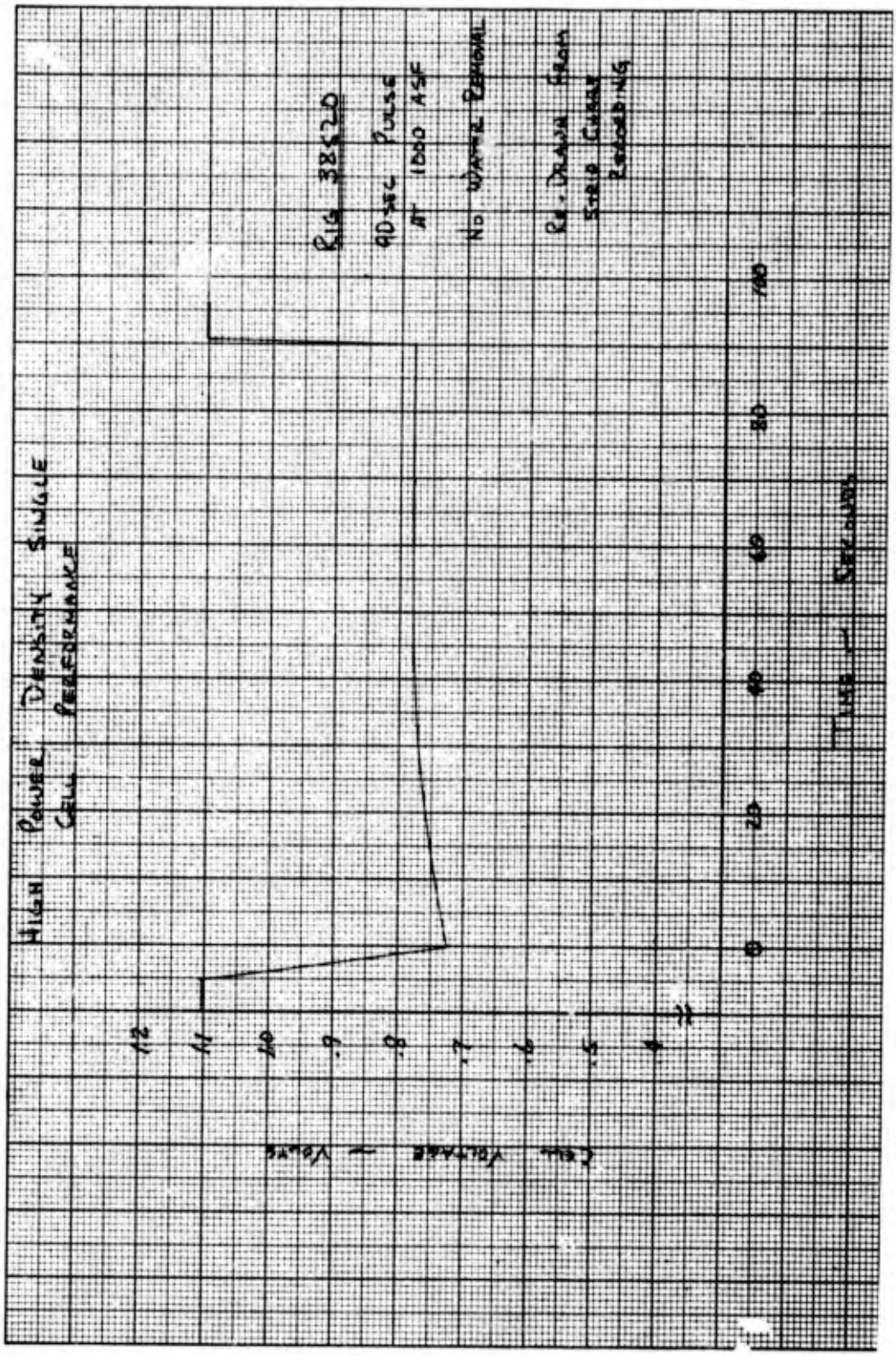

Figure 88 — Strip Cell 8, Cell Voltage During First 90-Second, 1000-ASF Test

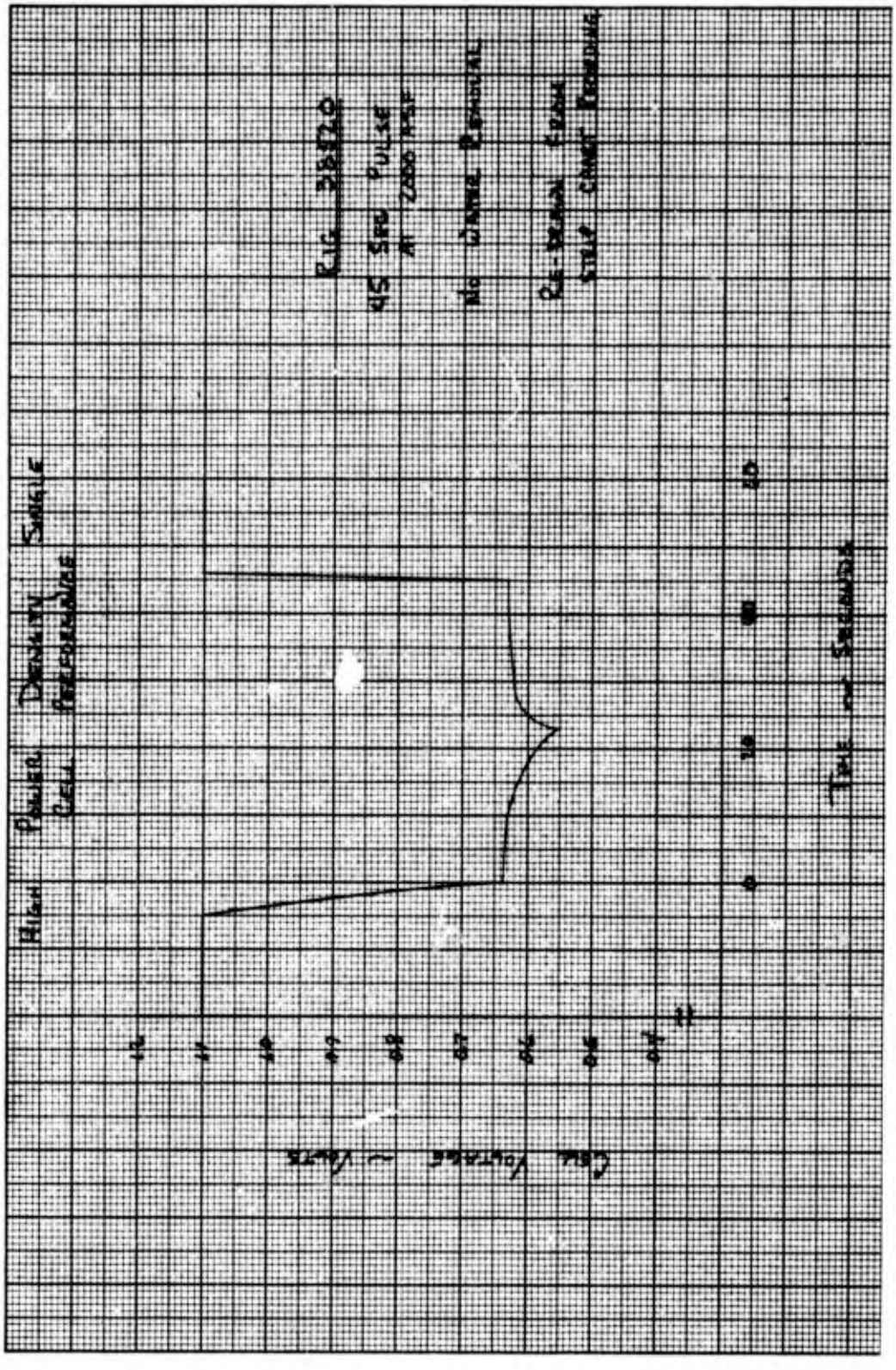

Figure 89 – Strip Cell 8, Cell Voltage During 45-Second, 2000-ASF Test

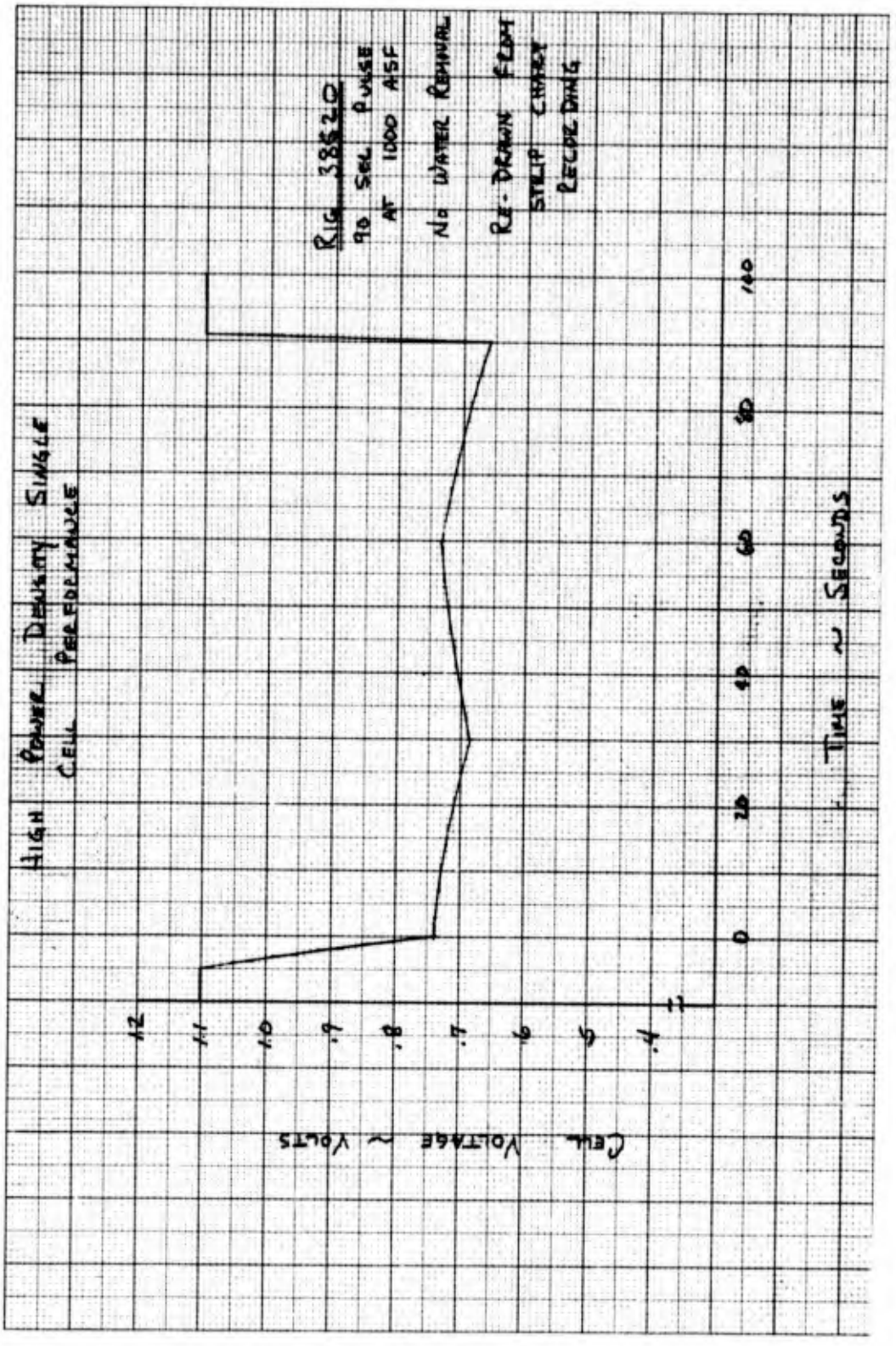

Figure 90 — Strip Cell 8, Cell Voltage During Second 90-Second, 1000-ASF Test

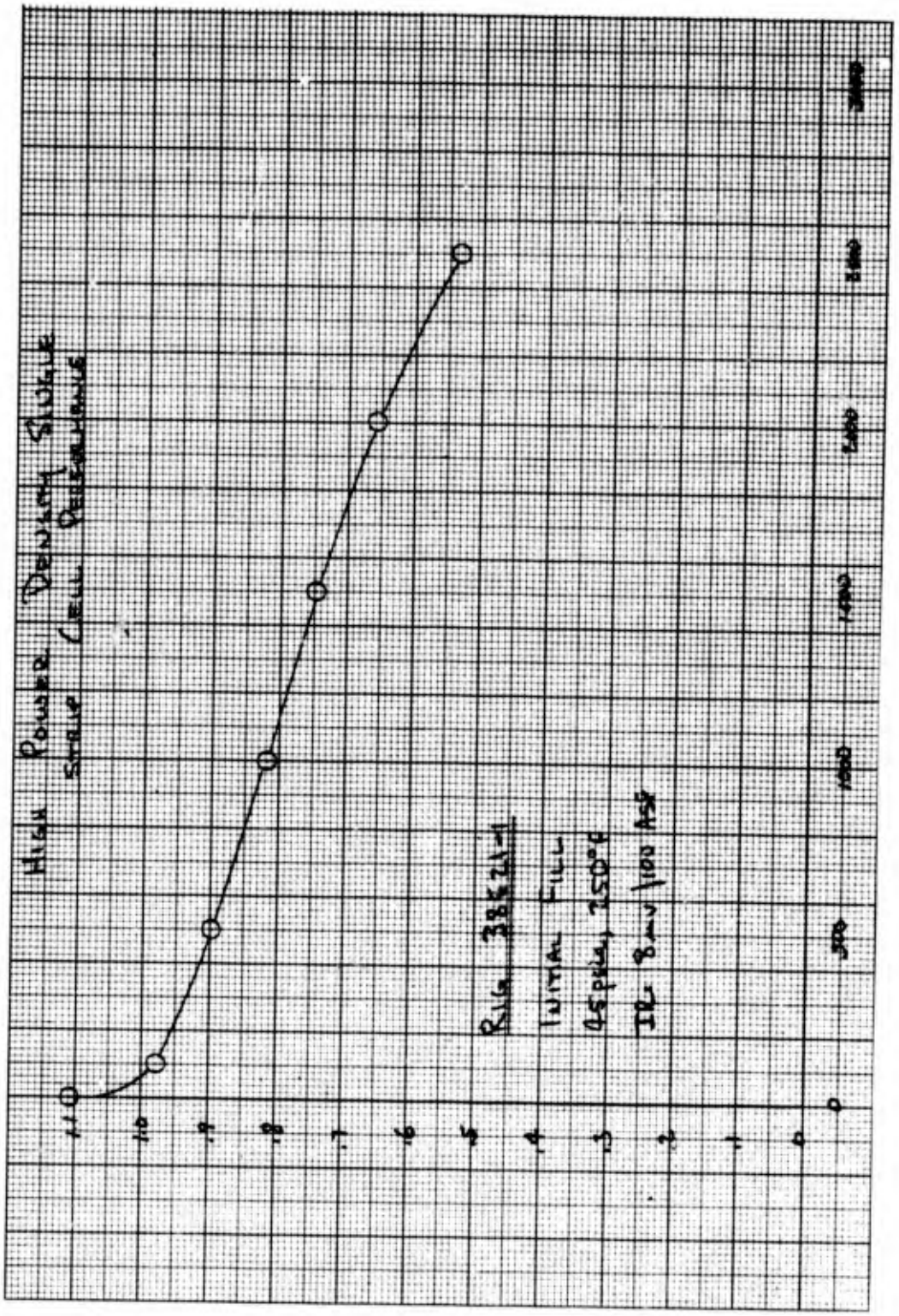

Figure 91 – Strip Cell 9, Initial Performance Data

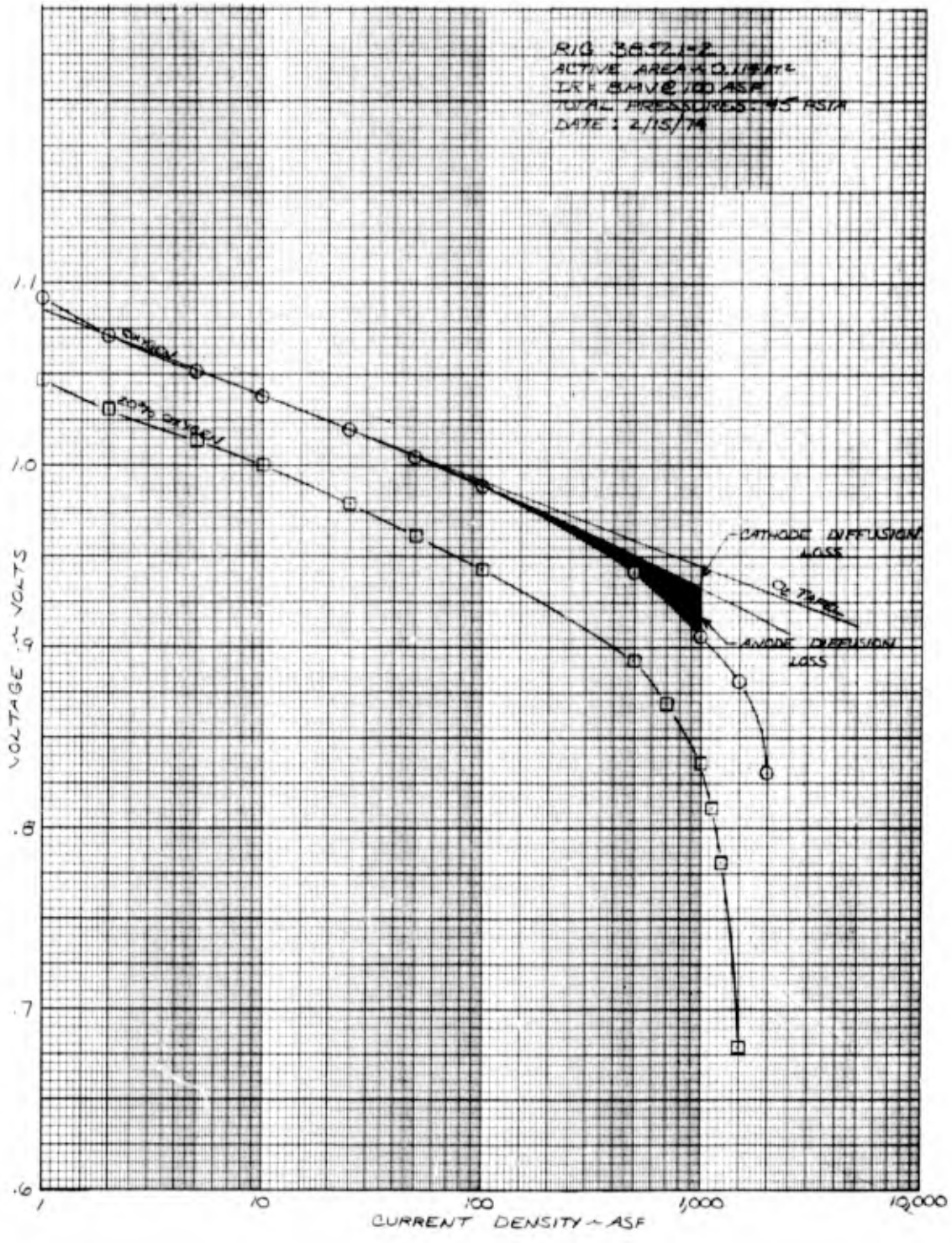

Figure 92 – Strip Cell 9, Individual Electrode Losses

An increase in cell pressure from 45 to 60 psia resulted in considerable improvement in high current density performance. Cell voltage gain in the activation region was normal, the anode limiting current was considerably improved, to beyond 3000 ASF, and the cell was able to operate stably 0.608 v at 3000 ASF, see Figure 93. The implications from this test were that the hydrogen was being restricted from reaching the anode reaction sites either by the ERP, the anode, or a combination of both. However, since the anodes in the cells with polysulfone ERP's (7, 8, and 9) were from the same manufacturing lot as that of Strip Cell 6, and since no limiting current phenomena had been noted on nickel ERP single cells, the problem was somewhat directed toward the polysulfone ERP. It was apparent that the polysulfone ERP either restricted hydrogen flow to the anode or did not transfer electrolyte properly, resulting in a poor gas/electrolyte interface in the anode. The first improvement was to increase the number of hydrogen access holes in the polysulfone ERP for the next single cell test.

Strip Cell 10 – Strip Cell 10 featured a polysulfone ERP with an increased number of hydrogen access holes. These holes are perpendicular to the plane of the ERP and allow the flow of hydrogen from behind the ERP to the anode surface. The number of holes in the ERP was increased from 194 to 388 and the diameter of each hole was increased from 38 to 42 mils. Except for this change, the cell was identical to the previous Configuration 3 cells.

The initial performance after refill is shown in Figure 94 and for the first time a cell with a polysulfone ERP operated stably at 3000 ASF at 45 psia.

Dilute gas diagnostics were conducted and showed no unusual anode diffusion loss and a higher than normal cathode diffusion loss. At 1000 ASF, a typical cathode diffusion loss is about 10 mv. The cathode diffusion loss on this cell was 22 mv as shown in Figure 95. The higher cathode loss was not unexpected because manufacturing quality tests showed this cathode to be marginal at high current densities in contrast to the three previous cells. No unusual anode diffusional losses were seen. This seemed to indicate that no basic problem existed with polysulfone ERP's at high current densities.

After completing the diagnostics, two tests were conducted with no water removal. A load of 2000 ASF was held for 45 seconds with a stable voltage of 0.729 v. A load of 3000 ASF was sustained for 30 seconds with a stable voltage of 0.618 v. These voltages were slightly higher than those obtained during steady-state operation.

Next, the total pressure was raised to 60 psia and a calibration was performed. As shown in Figures 95 and 96, performance at 100 ASF increased by 10 mv to 0.979 v, and at 3000 ASF, performance increased by 40 mv to 0.657 v.

The 3000-ASF load point was held for one hour. Performance decayed 13 mv from the initial 0.657 v during this time period, see Figure 97. During the one hour continuous operation, the voltage oscillated 20 to 30 mv. The reason for these oscillations is not understood; however, it may be caused by either a load system instability or a cell electrolyte interface phenomenon. Upon completion of this 3000 ASF endurance, the test unit was shut down overnight.

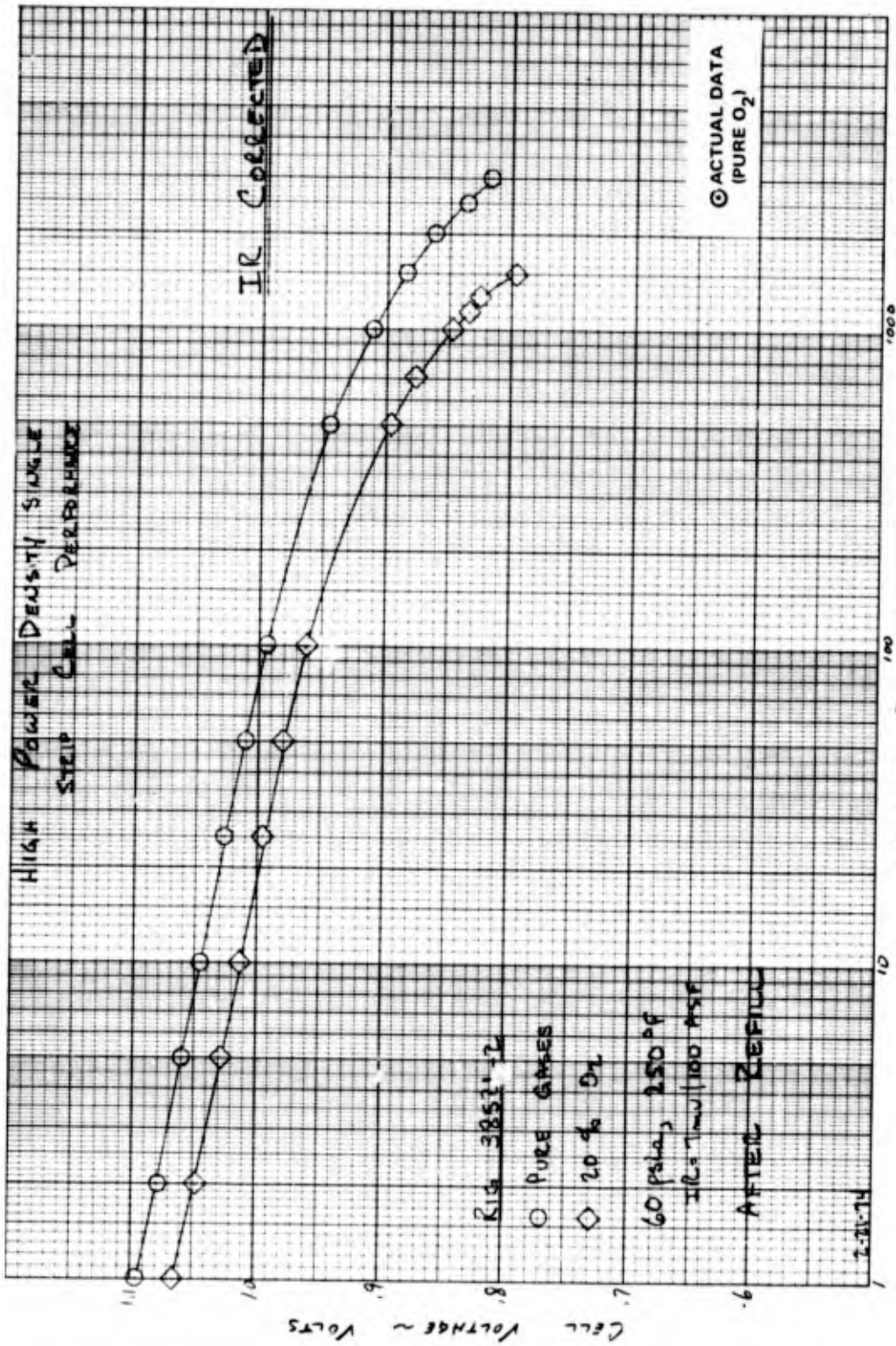

Figure 93 – Strip Cell 9, Dilute Oxygen Diagnostic Data

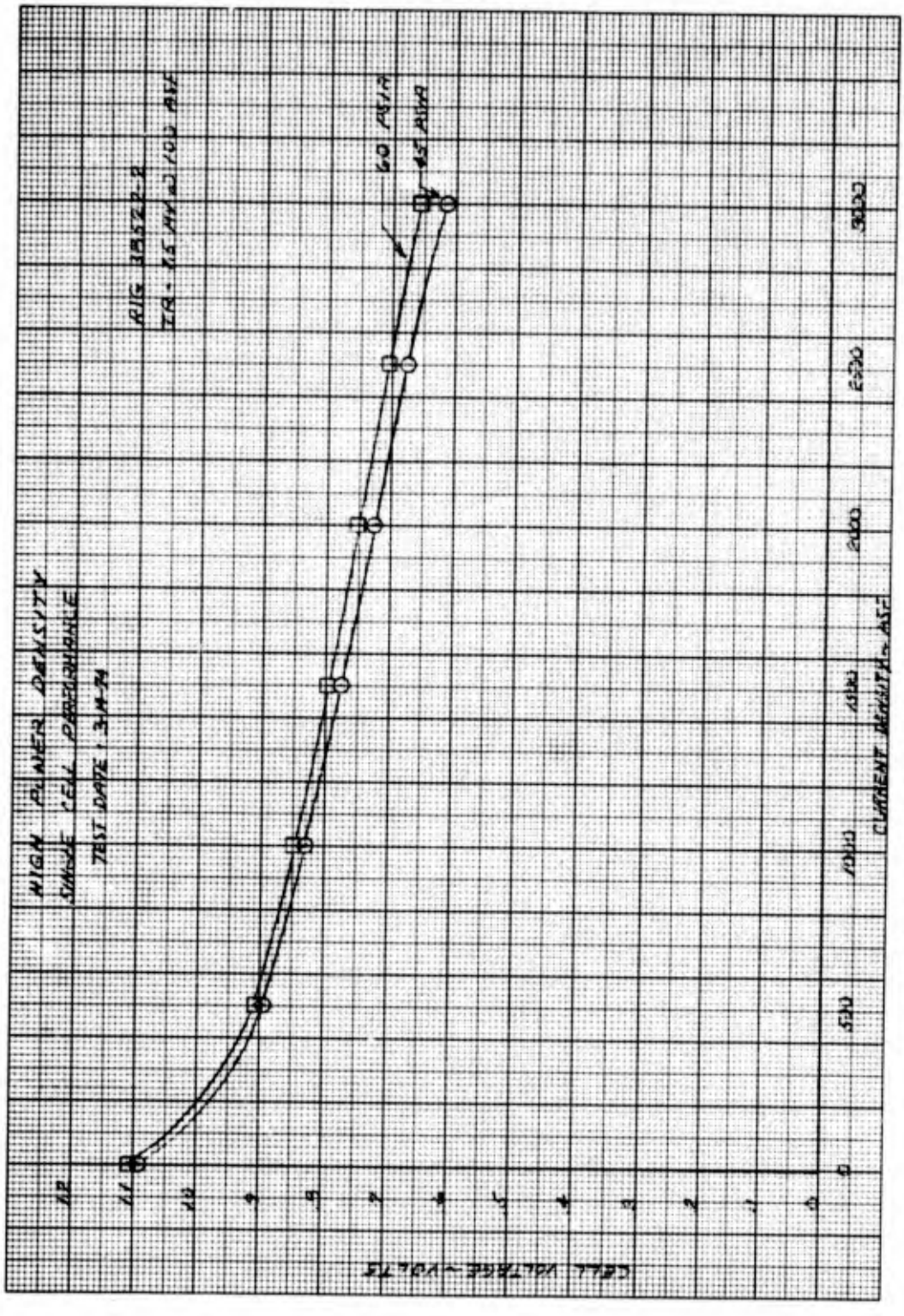

Figure 94 — Strip Cell 10, Performance Calibration to 3000 ASF

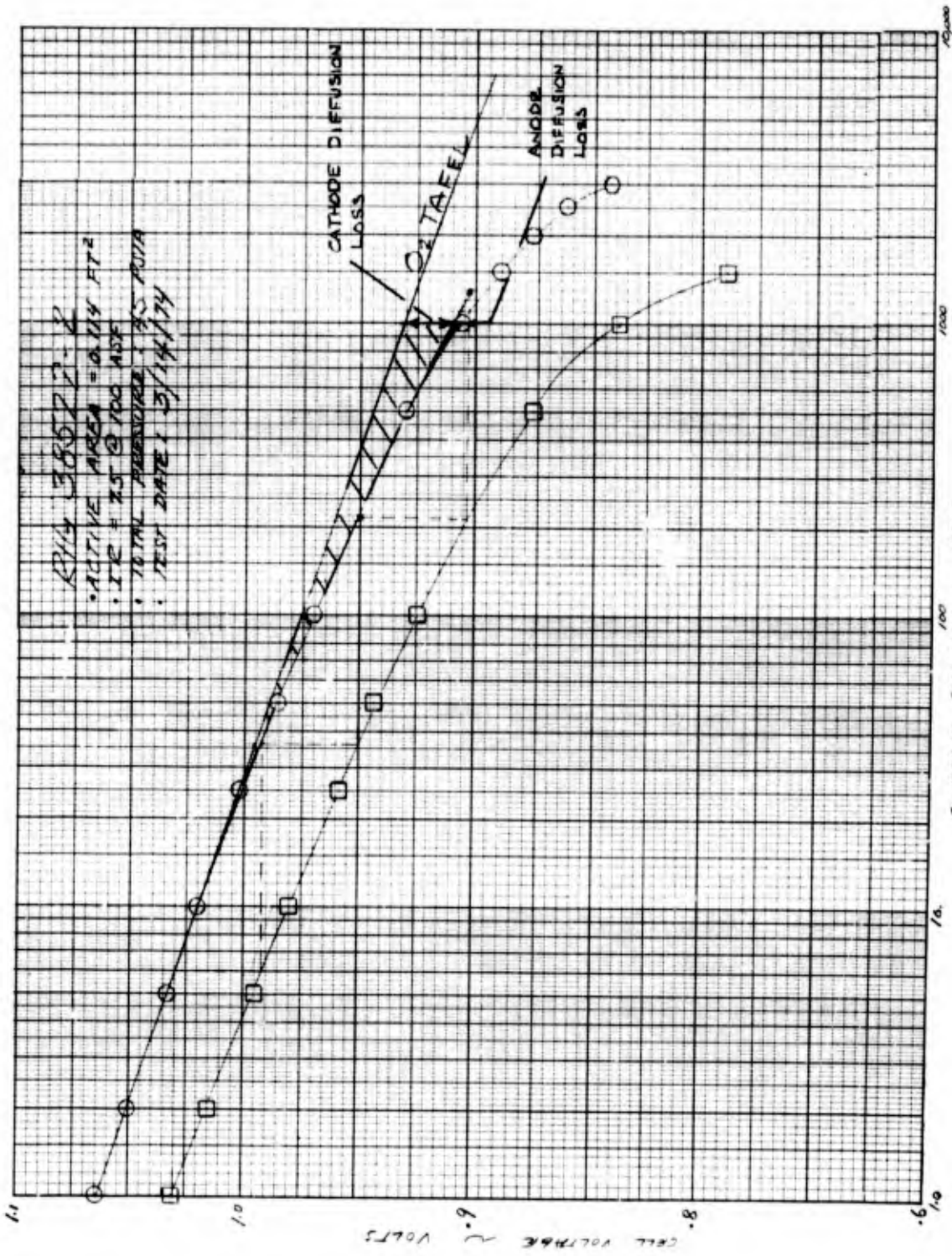

Figure 95 – Strip Cell 10, Dilute Oxygen Diagnostic Data

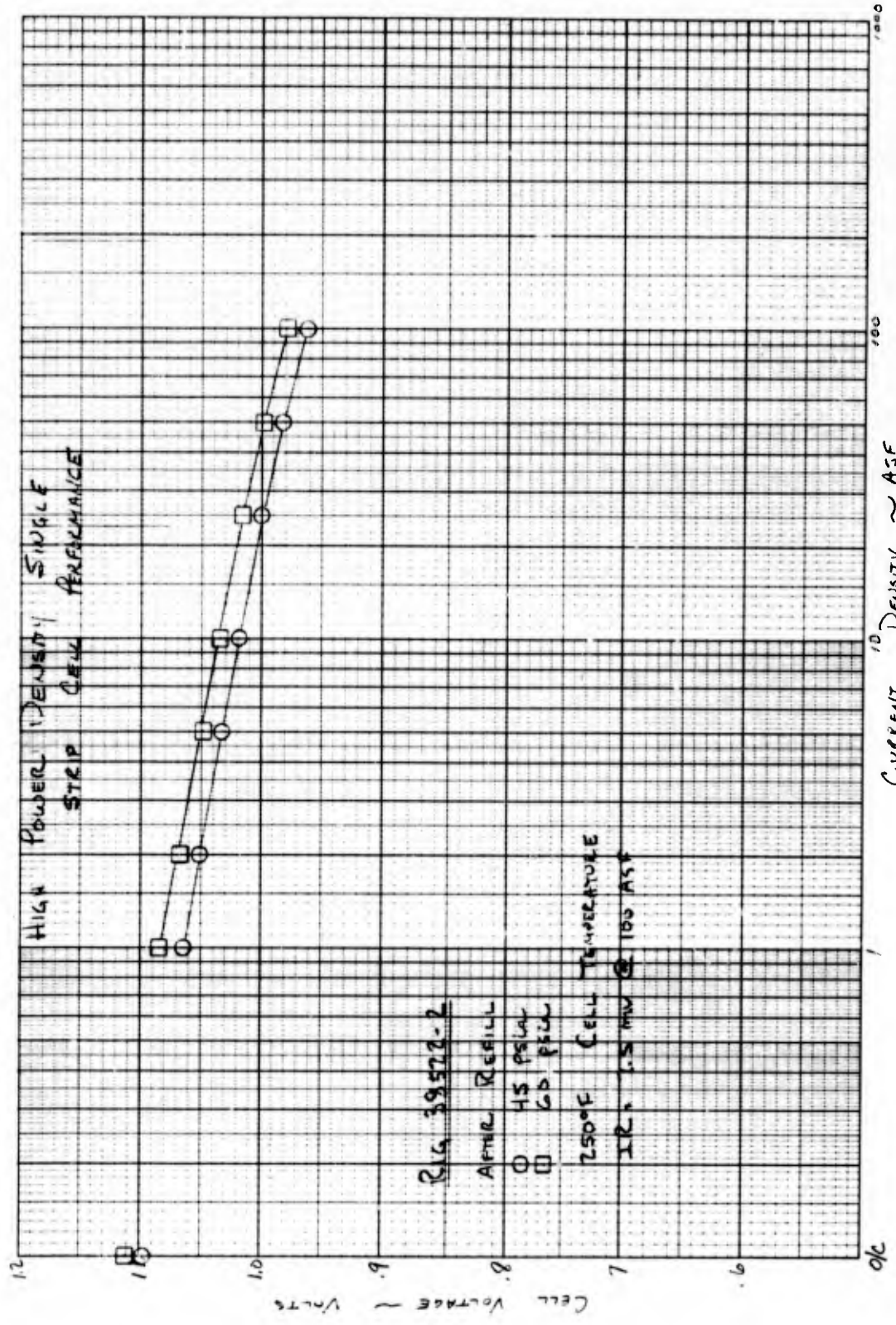

Figure 96 – Strip Cell 10, Performance at Low Current Density

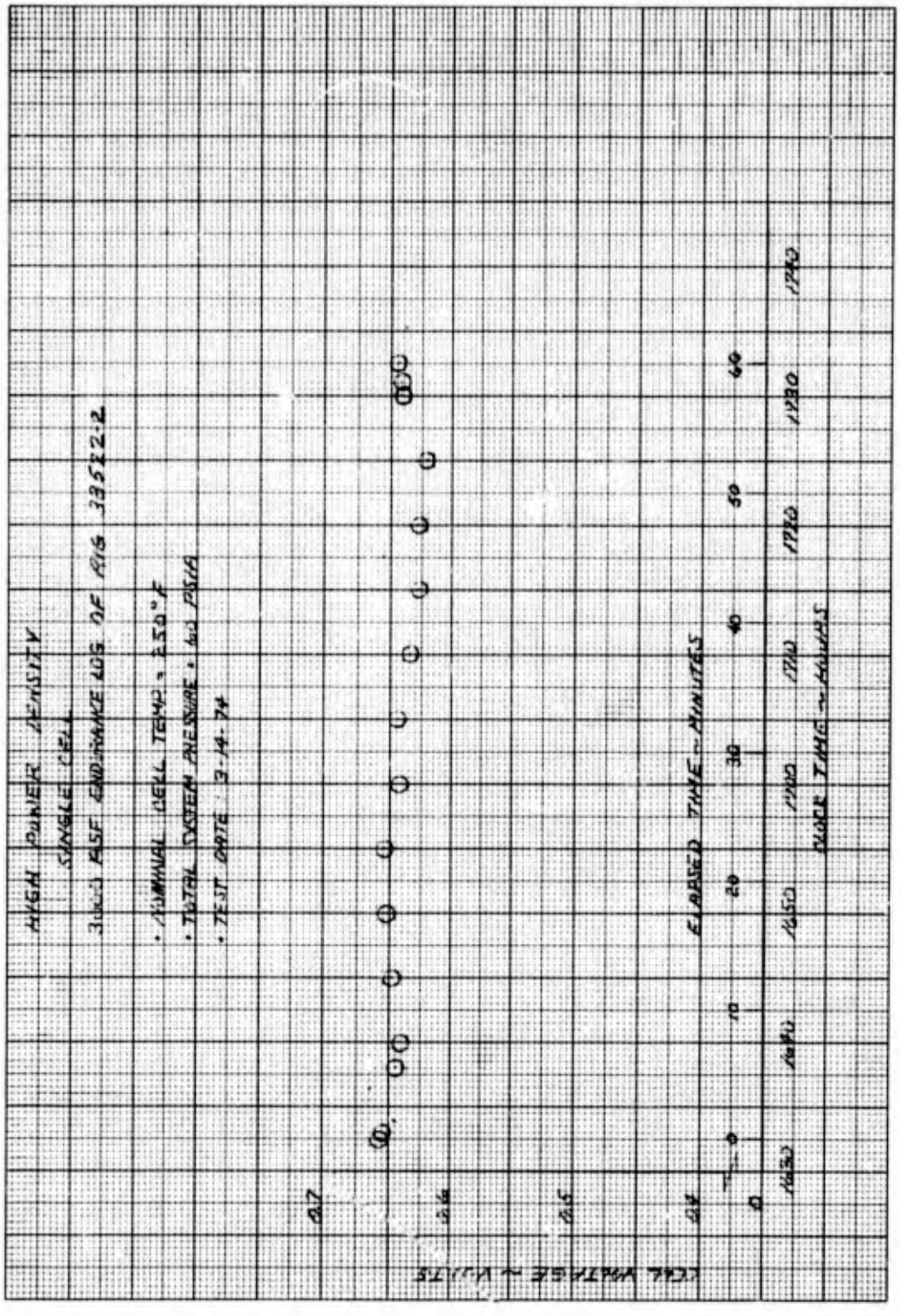

Figure 97 – Strip Cell 10, 3000 ASF Endurance

Upon restart the next day, the 100 ASF performance had dropped approximately 25 mv. Diagnostics revealed a change in the cell's IR, which increased from 7.5 mv to 15 mv. The cell was then removed for teardown and inspection. As inspection revealed no mechanical changes, the cell was reassembled and refilled.

The cell was restarted and a performance calibration to 3000 ASF was conducted. The performance loss was almost completely recovered as it was within 8 mv from the previous operation, see Figure 98. It is believed that the loss of performance and corrresponding increase in IR was because of a loss of electrolyte during either the shutdown cycle or the one hour 3000-ASF test.

Following calibration, a series of twelve 50 percent duty cycles were conducted. Each cycle was operated from open circuit to 3000 ASF, "two seconds on, two seconds off" as shown in Figure 99 for one minute duration. A 30-minute conditioning occurred between each cycle. No degradation in power output occurred from the first to the twelfth series, as shown in Figure 100. During this operation, the maximum demonstrated power density was 2030 WSF. This completed the test on this cell and on single cells of Configuration 3.

Strip Cell 11 – Strip Cell 11 was built to design Configuration 4 except that it had a 10-mil thick matrix rather than a 5-mil matrix. Configuration 4 features a combined ERP/hydrogen flow field for additional weight improvement. The combined ERP/hydrogen flow field for this cell was manufactured by heat bonding strips of nickel-plated porous polysulfone to a 5-mil polysulfone film. The strips were 62.5 mils wide, 20 mils thick and were spaced 80 mils apart as shown in Figure 101. Total void volume of the ERP strips was 1 cubic centimeter, equivalent to a 7 mil thick conventional ERP.

The UEA from Strip Cell 10 was used in this cell. This UEA had accumulated 24.1 hours, including 1.1 hours at 3000 ASF. The initial performance of Strip Cell 11 at 100 ASF, as shown in Figure 102, was 0.954 v at 60 psia reactant pressure. This voltage was 11 mv below the performance of Strip Cell 10 at shutdown. A performance calibration to 2000 ASF produced a stable cell voltage of 0.655 v, as shown in Figure 103. Cell performance was unstable above 2000 ASF, however.

Dilute gas diagnostics were performed to attempt to determine whether the electrodes or the combined ERP hydrogen flow field was the cause of the instability in cell performance at high loads. The results of the test were that there was no change in cathode diffusional losses, and only a 9 mv increase in anode diffusional loss at 500 ASF between the operation in Strip Cell 10 and this initial operation of Strip Cell 11. The increase in anode diffusion was not unexpected because of the change in the ERP configuration. However, the magnitude was not large enough to explain the inability to operate above 2000 ASF.

Following the dilute gas diagnostics, a 45 second, no-water-removal load point was operated at 1000 ASF. This was conducted to determine whether the ERP was taking up the water produced. The cell produced a steady voltage of 0.761 v during the 45 seconds, indicating that the ERP strips were taking up water as expected.

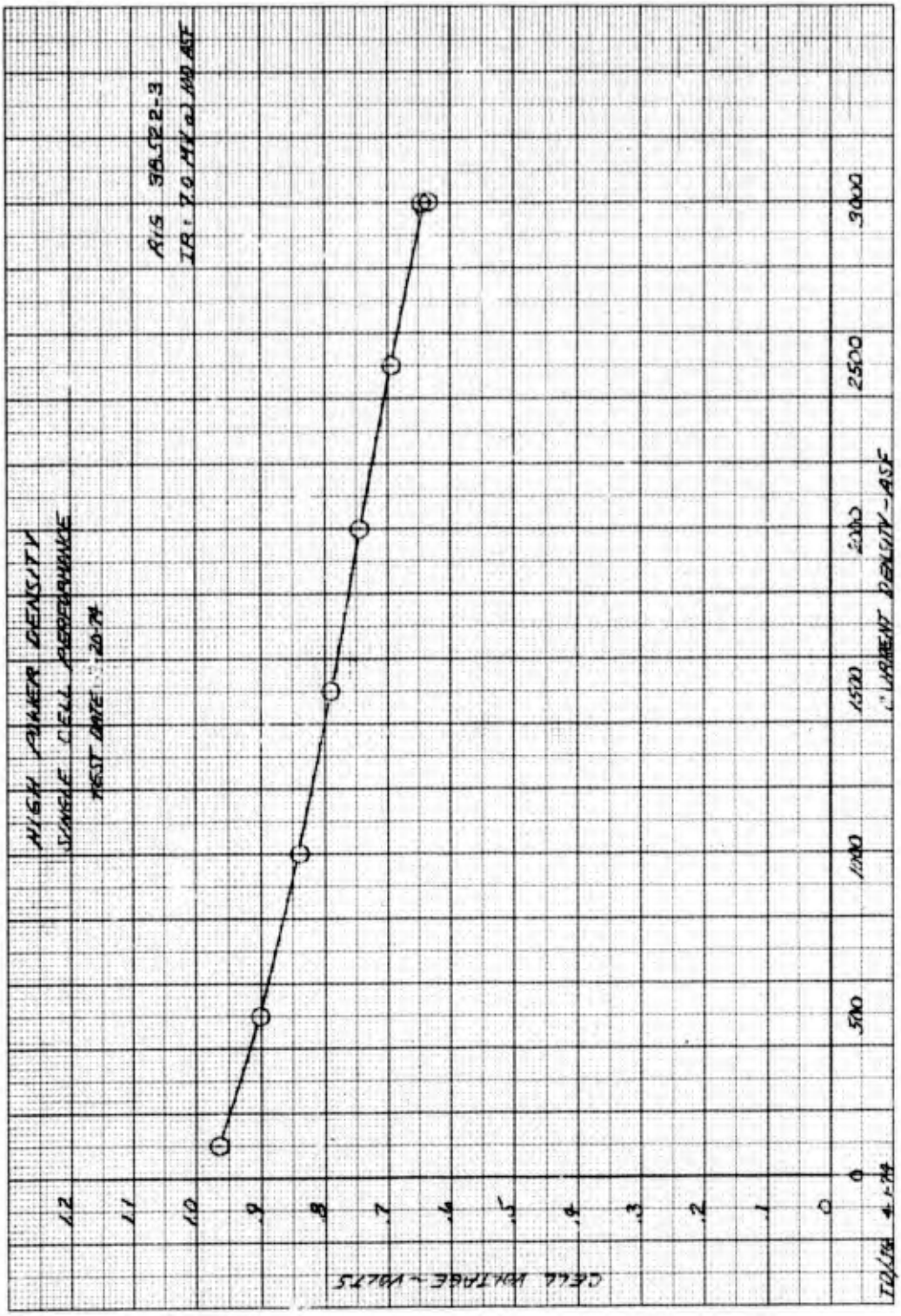

Figure 98 – Strip Cell 10, Performance Calibration to 3000 ASF

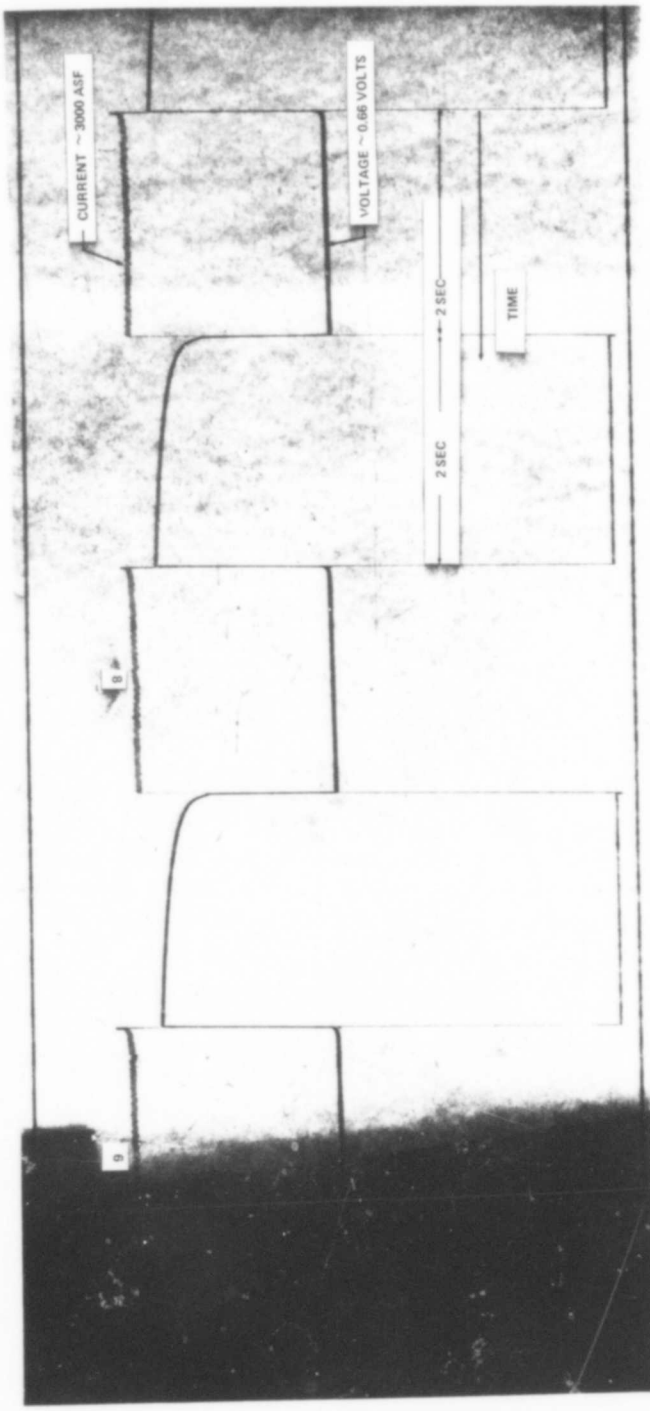

Figure 99 — Strip Cell 10, Visicorder Trace of 12th Cycle-Pulses - 7 through 9
2 Seconds On - 2 Seconds Off Cycle at 3000 ASF

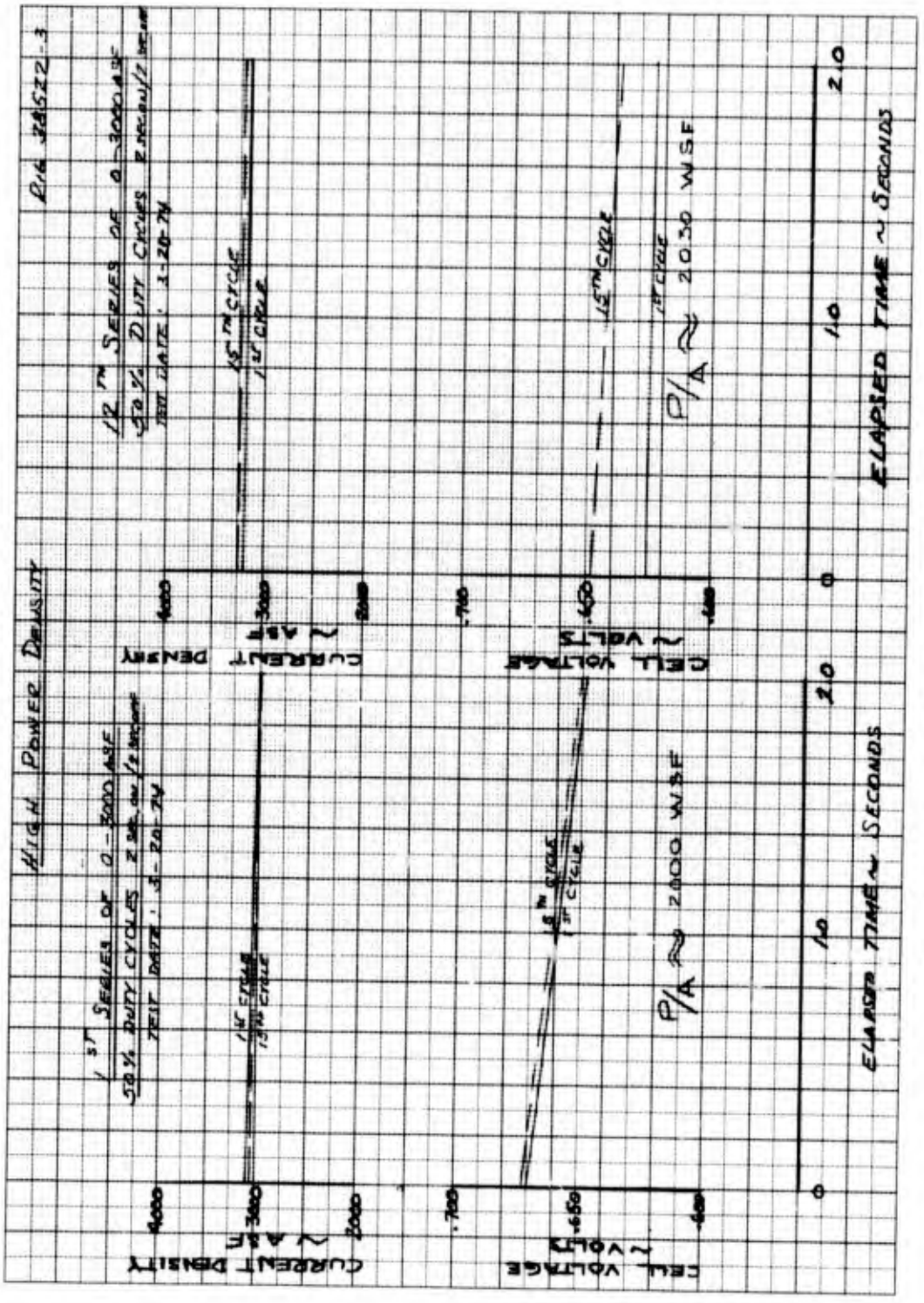

Figure 100 – Strip Cell 10, Summary of Cycle Testing

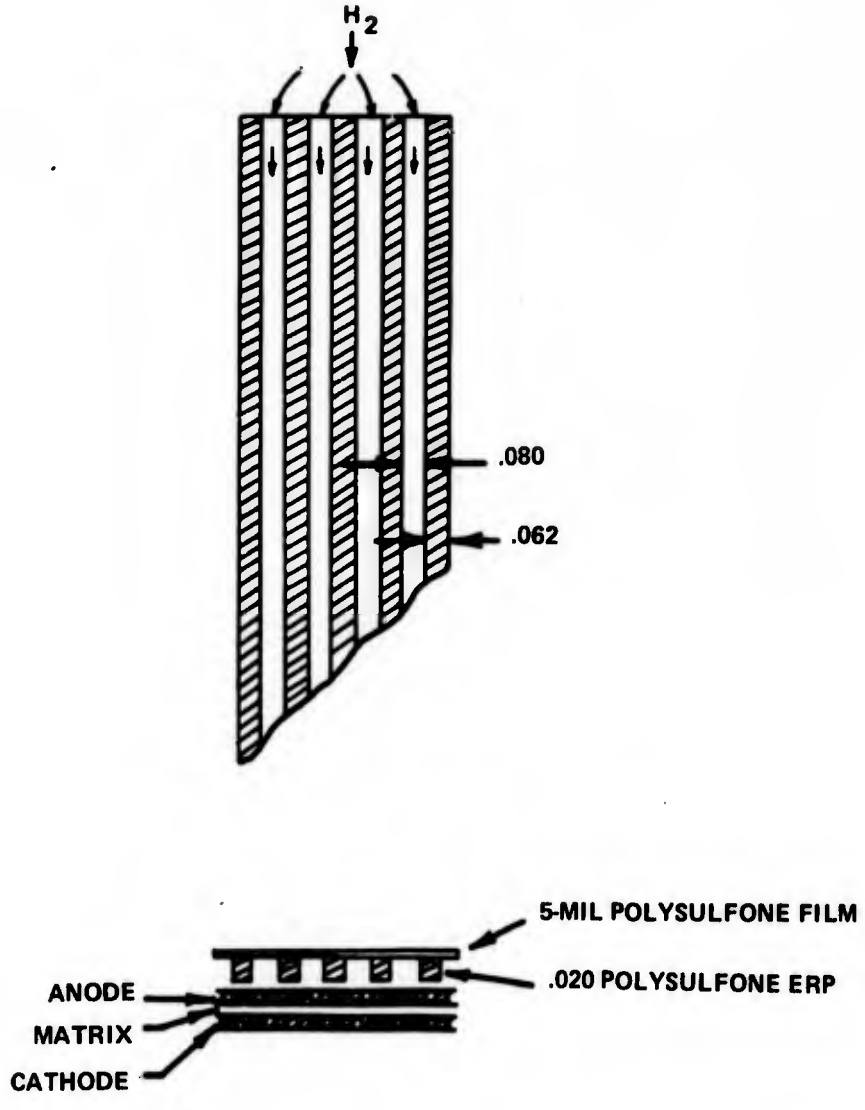

Figure 101 – Schematic of Combined ERP/Hydorgen Flow Field

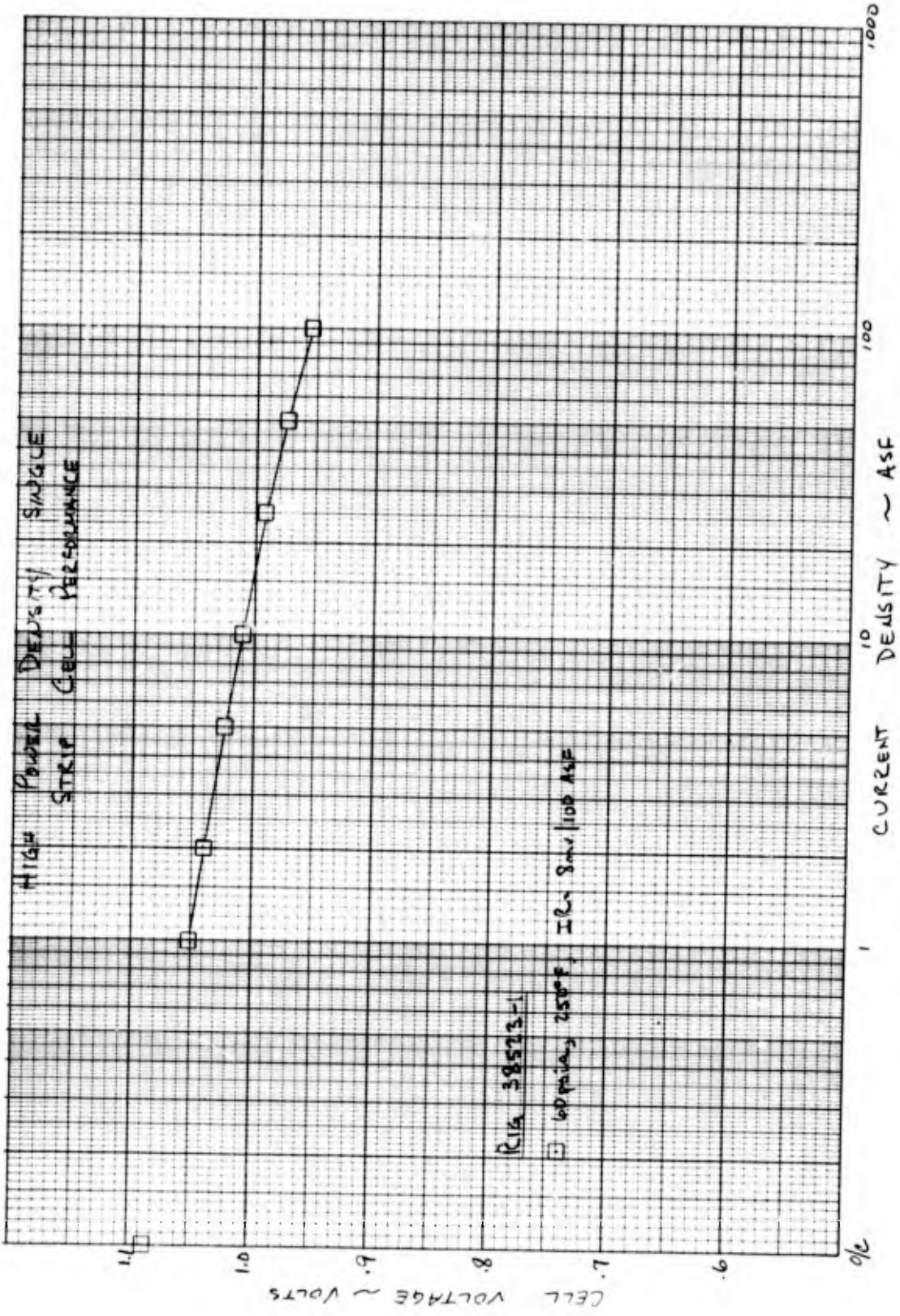

Figure 102 – Strip Cell 11, Performance Calibration to 100 ASF

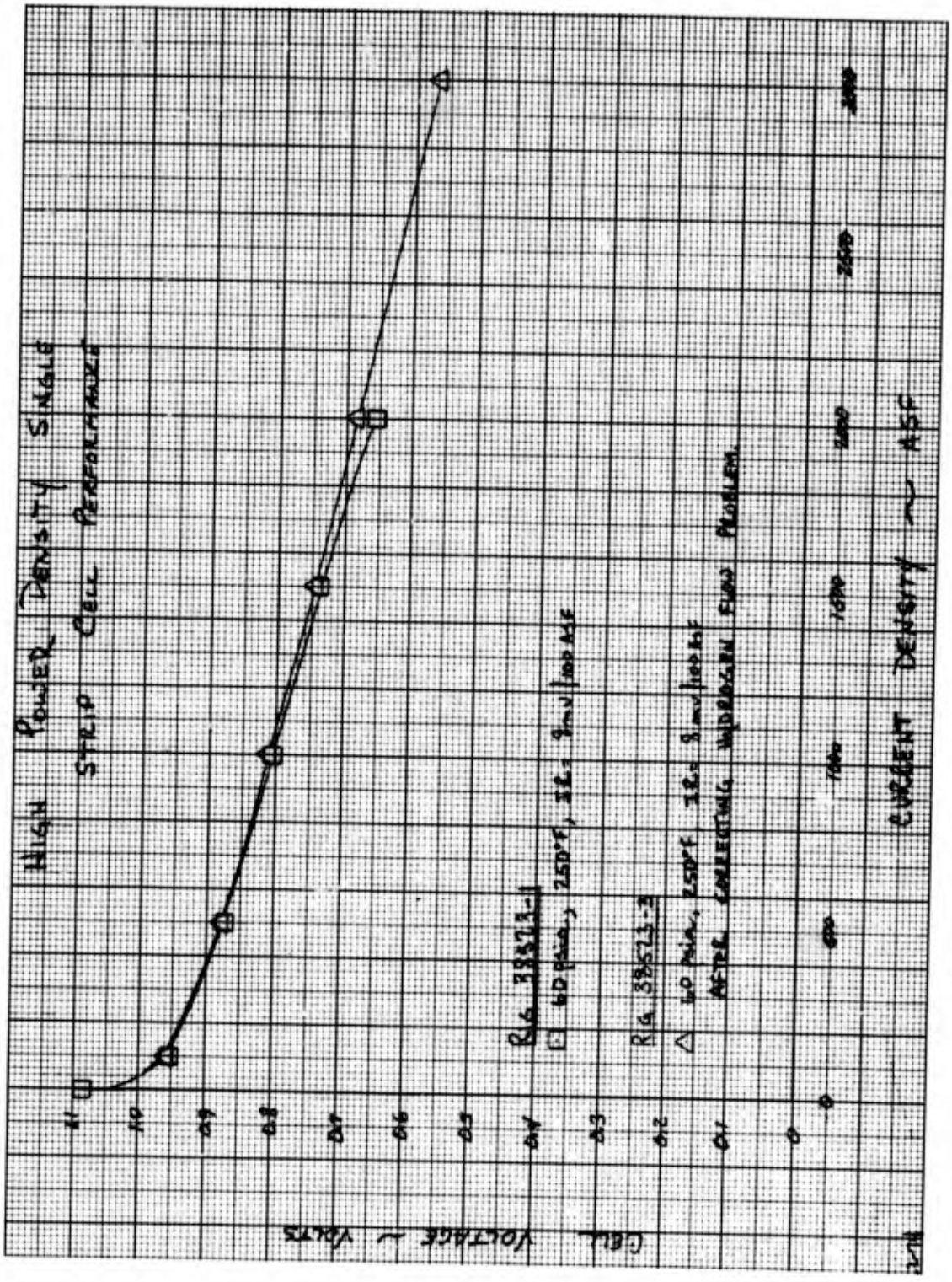

Figure 103 — Strip Cell 11, Performance Calibration to 3000 ASF

The cell was shut down and refilled. Upon restart, the voltage of 100 ASF was 0.958 v. A high current density calibration produced unchanged cell performance. At 2000 ASF, the voltage was 0.651 v and the cell's performance again was unstable above this load.

No-water-removal operation was conducted at 1000, 1500, and 2000 ASF points. Performance was essentially the same as that obtained during the dynamic water-removal calibration. Following this, 50 percent duty cycles at 2000 ASF were operated for a total of 20 seconds on load.

Inspection of the cell after teardown revealed the possibility that all the hydrogen flow did not go through the combined ERP/hydrogen flow field. Because of the particular design of the endplates, some of the hydrogen flow could have bypassed the anode. This would have resulted in insufficient water removal from the cell, and a probable flooding condition at loads above 1000 ASF. The flow problem, corrected by inserting a solid shim between the endplate and hydrogen flow field, ensured all the flow had to pass across the face of the electrode.

With the flow problem corrected, the cell was reassembled and restarted. Initial 100 ASF performance was 0.958 v. A calibration to 2000 ASF produced a stable voltage of 0.685 v, which is an increase of 30 mv over the previous two calibrations. In addition, 50 percent duty cycles with no water removal were operated at 2000 ASF and 3000 ASF. The cycles were the standard "two-seconds on – two-seconds off" with 40 seconds total time at 2000 ASF and 20 seconds total time at 3000 ASF, see Figure 104. Maximum cell voltage was 0.685 v at 2000 ASF and 0.565 v at 3000 ASF. However, performance was still lower than expected and it was concluded that this was primarily the result of insufficient electrode support and high resistance to hydrogen flow through the combined hydrogen field/ERP. To improve the design it was decided to modify the dimensions of the ERP strip arrangement on the next single cell. Power density at 3000 ASF was 1695 WSF.

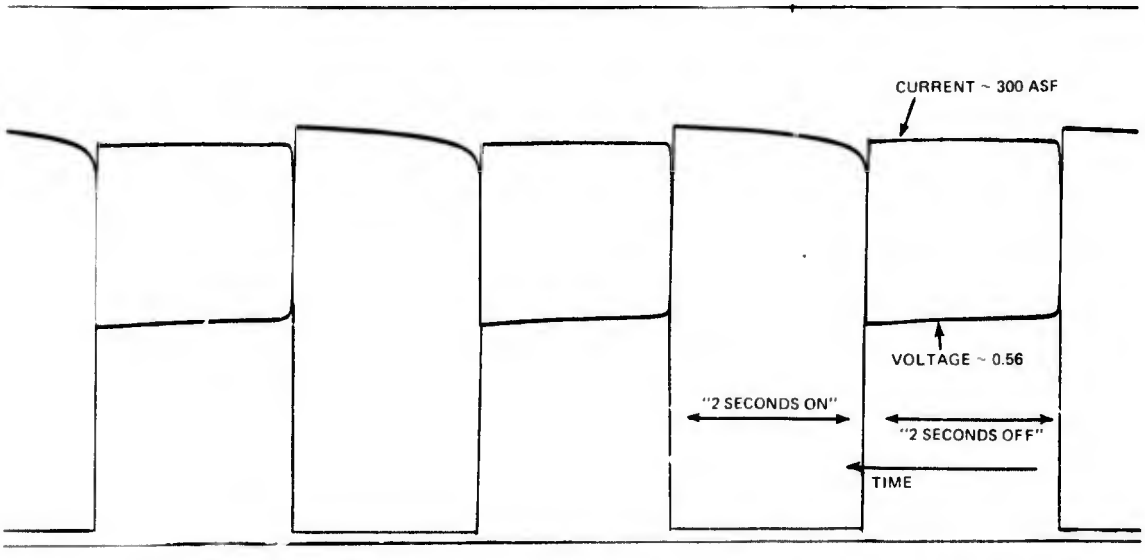

Figure 104 – Strip Cell 11, Visicorder Trace of Pulsed Operation to 3000 ASF

Strip Cell 12 – Strip Cell 12 was built to Configuration 4, which features a combined ERP/H_2 flow field and a 5-mil matrix. The combined field was modified slightly from that used on Strip Cell 11 in order to improve anode support, to decrease resistance to hydrogen flow, and to provide more electrolyte volume. The strips used in Strip Cell 12 were 62.5 mils wide, 30 mils thick and were spaced 62.5 mils apart. Total void volume of the ERP strips increased to 1.7 cc from 1.0 cc.

The initial performance of Strip Cell 12 at 100 ASF, as shown in Figure 105, was 0.974 v at 45 psia reactant pressure. A performance calibration to 2000 ASF produced a stable cell voltage of 0.703 v, as shown in Figure 106. This compares to a value of 0.655 at 60 psia obtained in Strip Cell 11 and is within 20 mv of that obtained on Strip Cell 10. Cell performance, however, was unstable at above 2000 ASF.

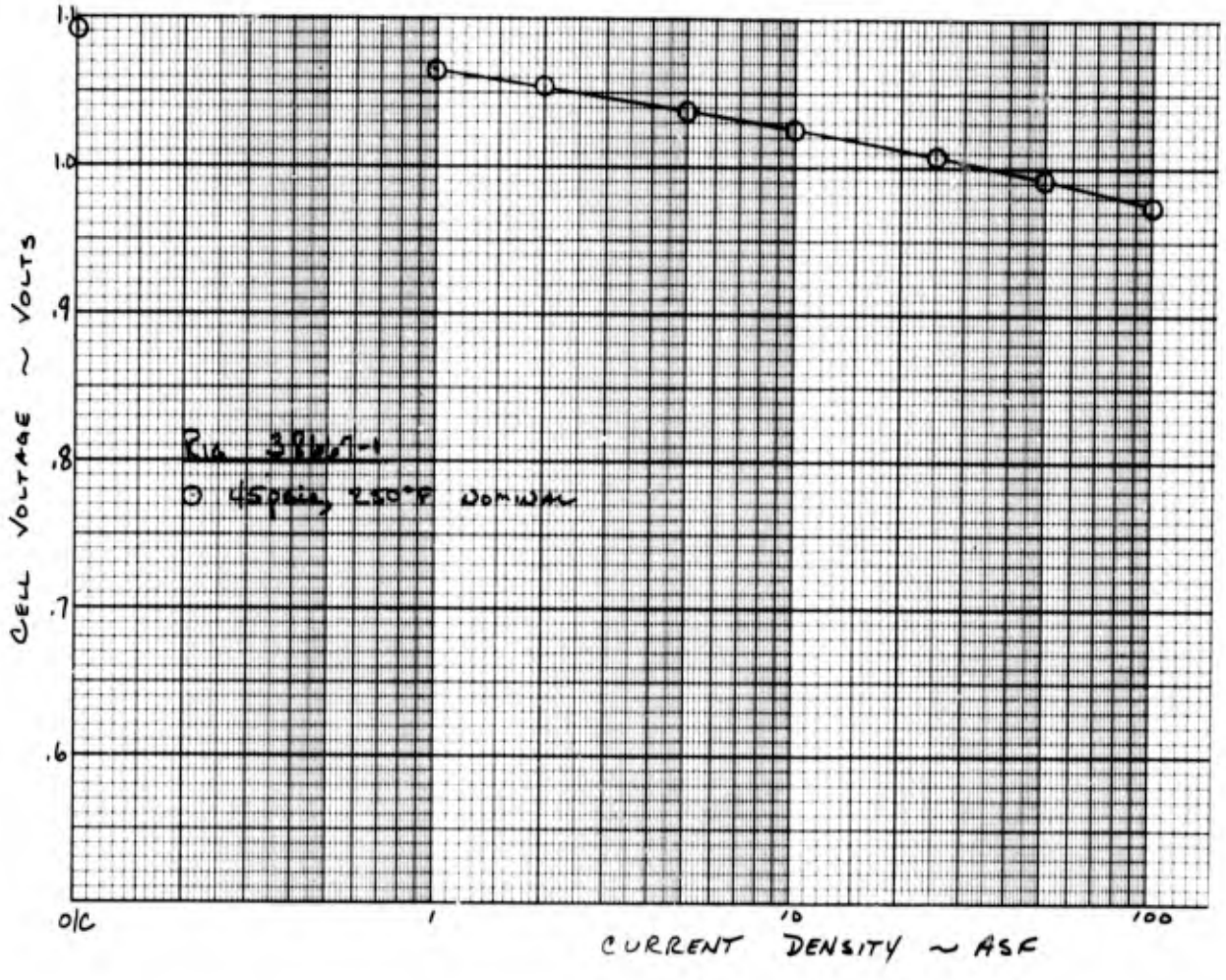

Figure 105 – Strip Cell 12, Performance Calibration to 100 ASF

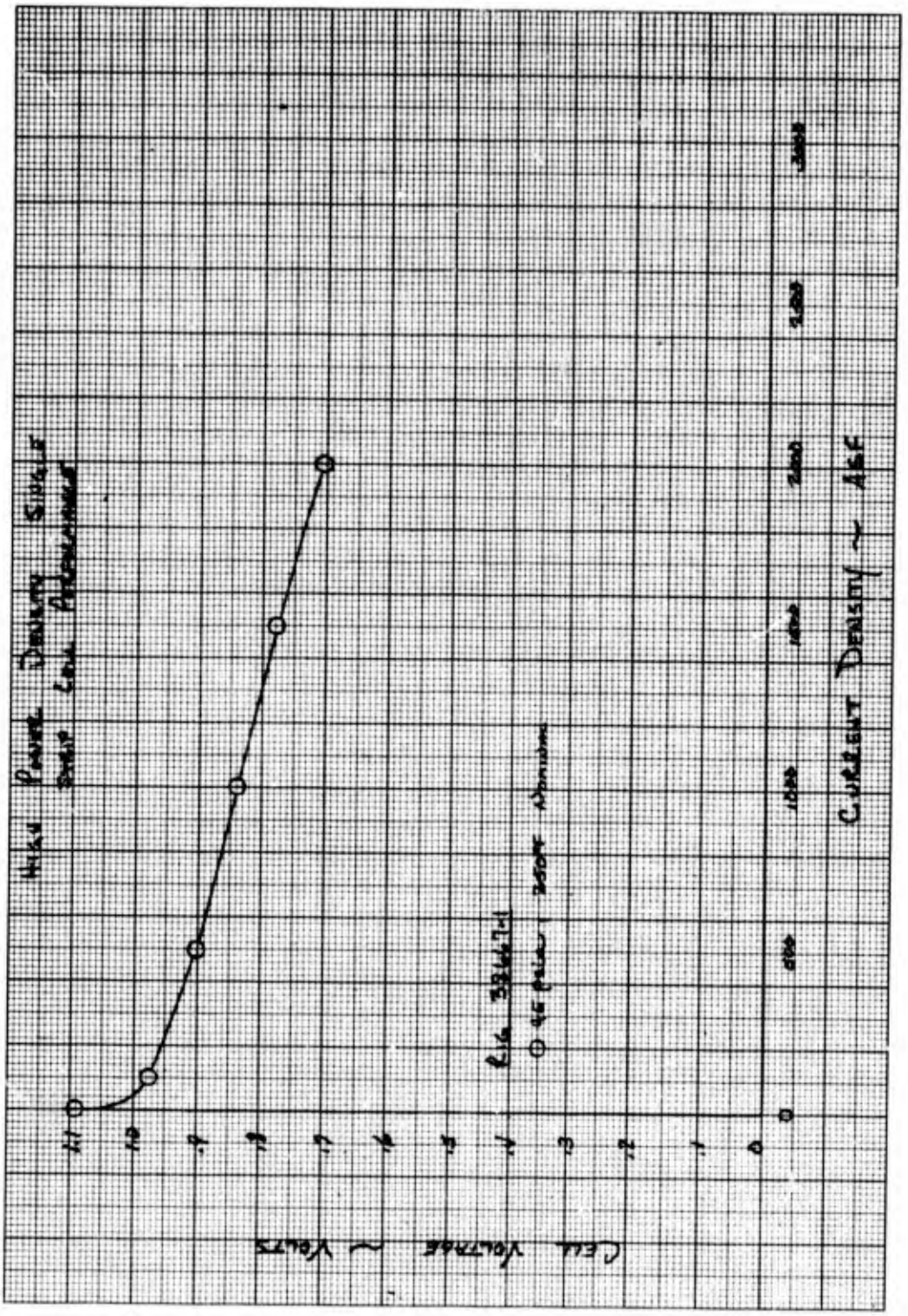

Figure 106 – Strip Cell 12, Performance Calibration to 2000 ASF

After completing the high current density calibration, the cell was returned to a 100 ASF load in preparation for IR and dilute gas diagnostics. Approximately 45 minutes after setting 100 ASF, the cell performance decayed rapidly with a simultaneous increase in coolant pressure drop. The cell was shut down and pulled for teardown and inspection. Disassembly revealed that reactant crossover had occurred and the subsequent heat caused deformation of the plastic coolant field which resulted in the increase in coolant pressure drop.

Although the cause of the reactant crossover was not directly resolved, the problem area was found to be between the ends of two segmented strips. The distance between the ends of strips is larger than the lateral distance between them and this may have resulted in an excessive unsupported area. This situation was corrected in the next single cell. In addition, a structural analysis of the cell layup with a 5-mil matrix was undertaken. No errors in pinch, operating conditions, or stand malfunctions were found.

The premature failure of the cell prevented diagnostics which would have provided information on individual electrode polarizations and thereby indicate the results of the improved ERP/H_2 field. The improved cell performance, however, indicated that the redesign was in the right direction. The next cell incorporated essentially the same ERP design with the ERP strip ends brought closer together.

Strip Cell 13 – Strip Cell 13 was built with a Configuration 4 combined ERP/H_2 field and a 10-mil thick matrix. The combined field was modified slightly from that used in Strip Cell 12; the end-to-end gap of ERP strip segments was reduced , as shown in Figure 107. This change was made because structural analysis of Strip Cell 12 indicated: 1) improper support of the anode by the ERP may have been the cause of crossover; and 2) reduction of the relatively large gap (125 mils) between the ends of the ERP strips to 60 mils would properly support the anode.

The cell assembly as it was ready to go to test is shown in Figure 108. Testing began with steady operation at 45 psia and 100 ASF to bring the electrolyte to a known concentration. Initial performance at 100 ASF was 0.986 v, as shown in Figure 109. A 45-psia performance calibration to 3000 ASF produced a stable cell voltage of 0.612 v, see Figure 110. The electrolyte was dried out to 60 percent KOH, and a continuous no-water-removal test was run at 3000 ASF for 20 seconds. During this period the cell voltage dropped from 0.615 v to 0.510 v. After re-conditioning the electrolyte to 60 percent another no-water-removal test was run. This time the test was in the 50-percent-duty-cycle mode(two-seconds on – two-seconds off) at 3000 ASF for a total power delivery time of 16 seconds. Performance was 0.640 ± 5 mv throughout this test. The cell was then shut down and removed for refill.

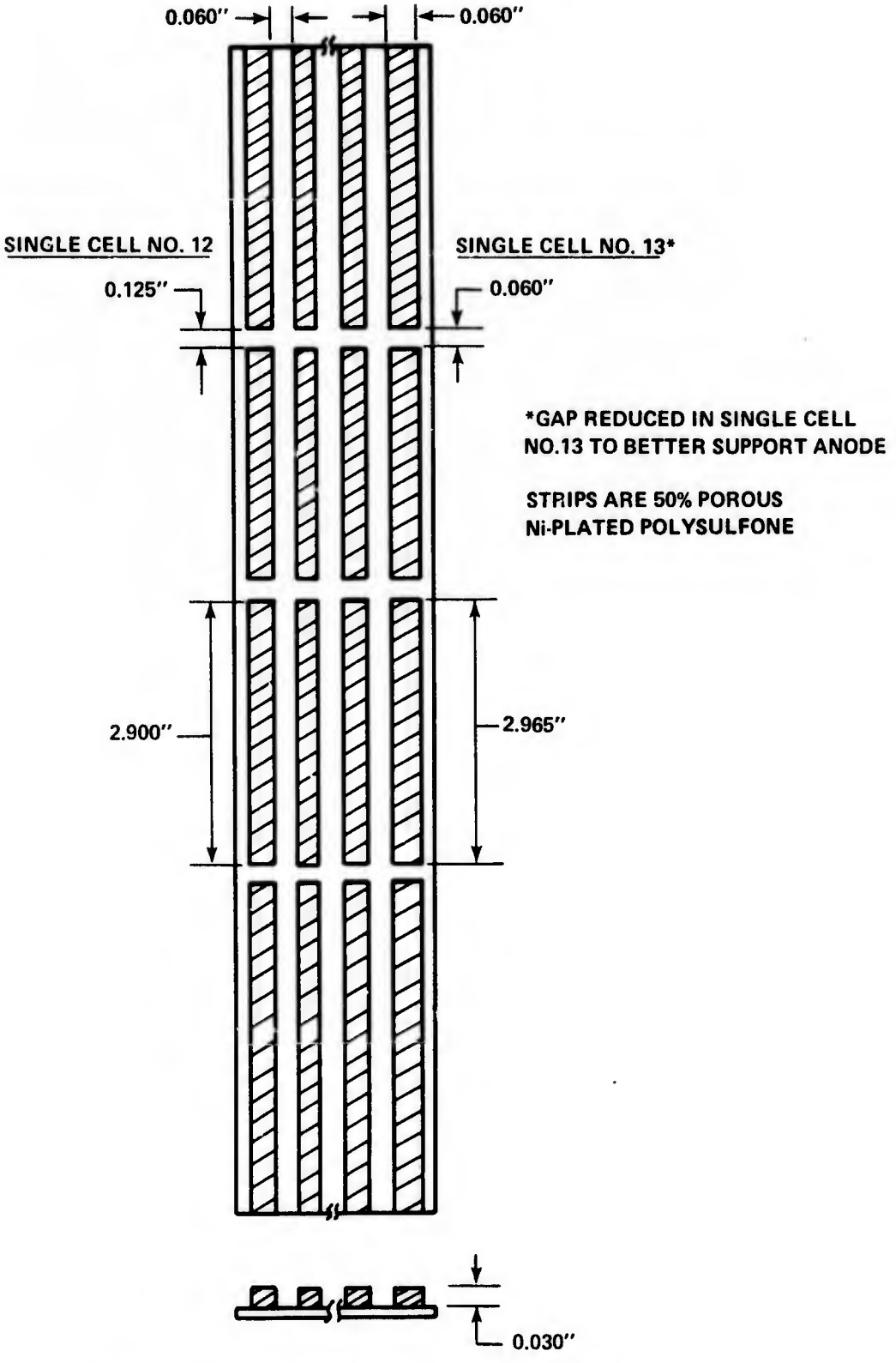

Figure 107 – Combined ERP/H_2 Flow Field Modifications

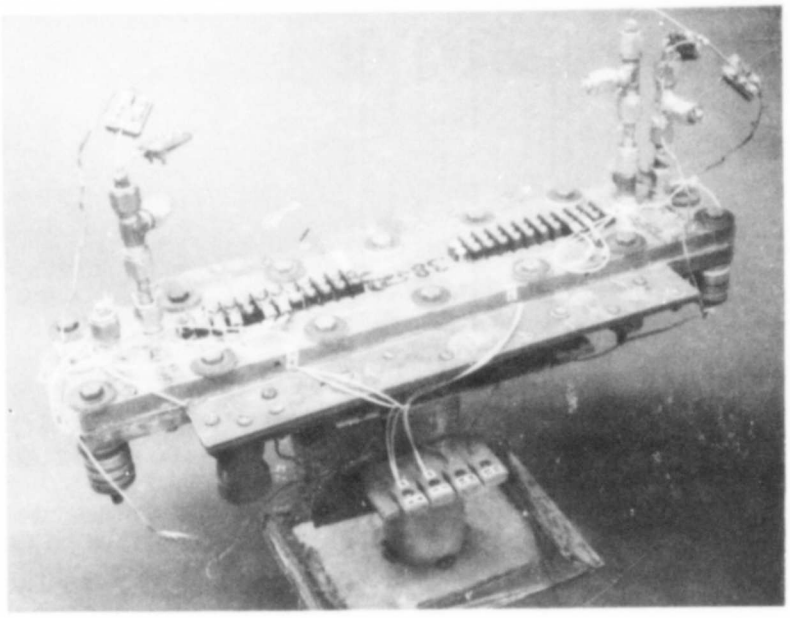

Figure 108 – Strip Cell 13

After refill, the 100-ASF performance at 45 psia was unchanged at 0.985 v. The performance calibration to 3000 ASF produced a stable cell voltage of 0.630 v, 18 mv higher than the initial fill performance; see Figure 110. Performance calibration at 3500 ASF produced a voltage of 0.599 v.

Following this test, the total reactant pressure was increased to 60 psia. Performance calibrations produced: 0.994 v at 100 ASF, 0.662 v at 3000 ASF, and 0.613 v at 3500 ASF, as shown in Figures 109 and 110. Next a 3-minute continuous load point at 3000 ASF with water removal was run. This test produced a performance of 0.660 v initially and 0.635 v at the end of 3 minutes. A return to the 50 percent duty cycle (two-seconds on – two-seconds off) at 3000 ASF produced a cell voltage of 0.660 ± 5 mv from the first to the last pulse, over a period of 60 seconds.

Following the 30-second, 50-percent duty cycle mission, the cell was shut down for an overnight hold at room temperature on inert gases. After restart, the cell was operated continuously for 15 minutes at 3000 ASF. The initial voltage was 0.669 v and the final voltage was 0.634 v. The cell was then returned to room temperature for the weekend.

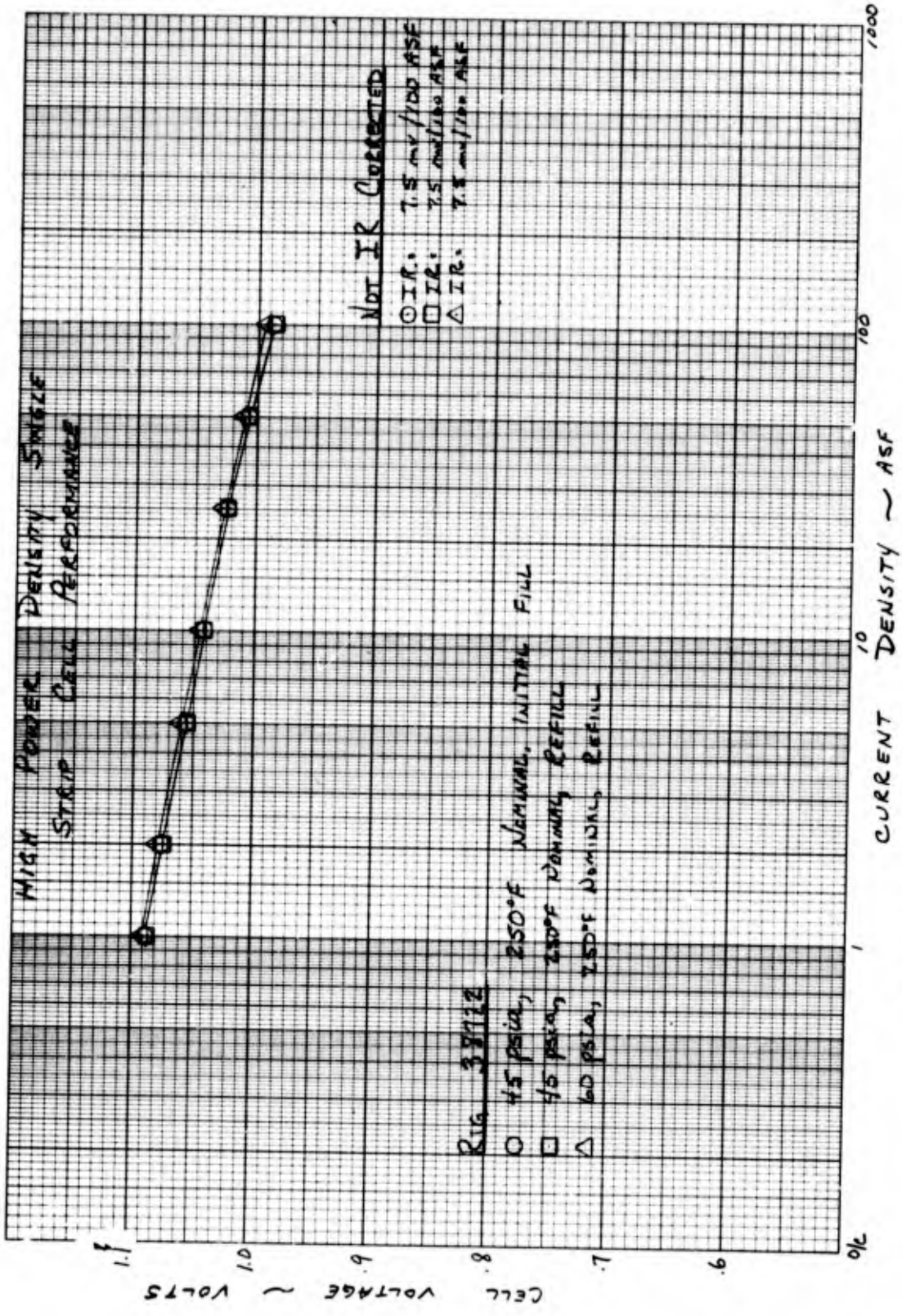

Figure 109 – Strip Cell 13, Performance Calibration to 100 ASF

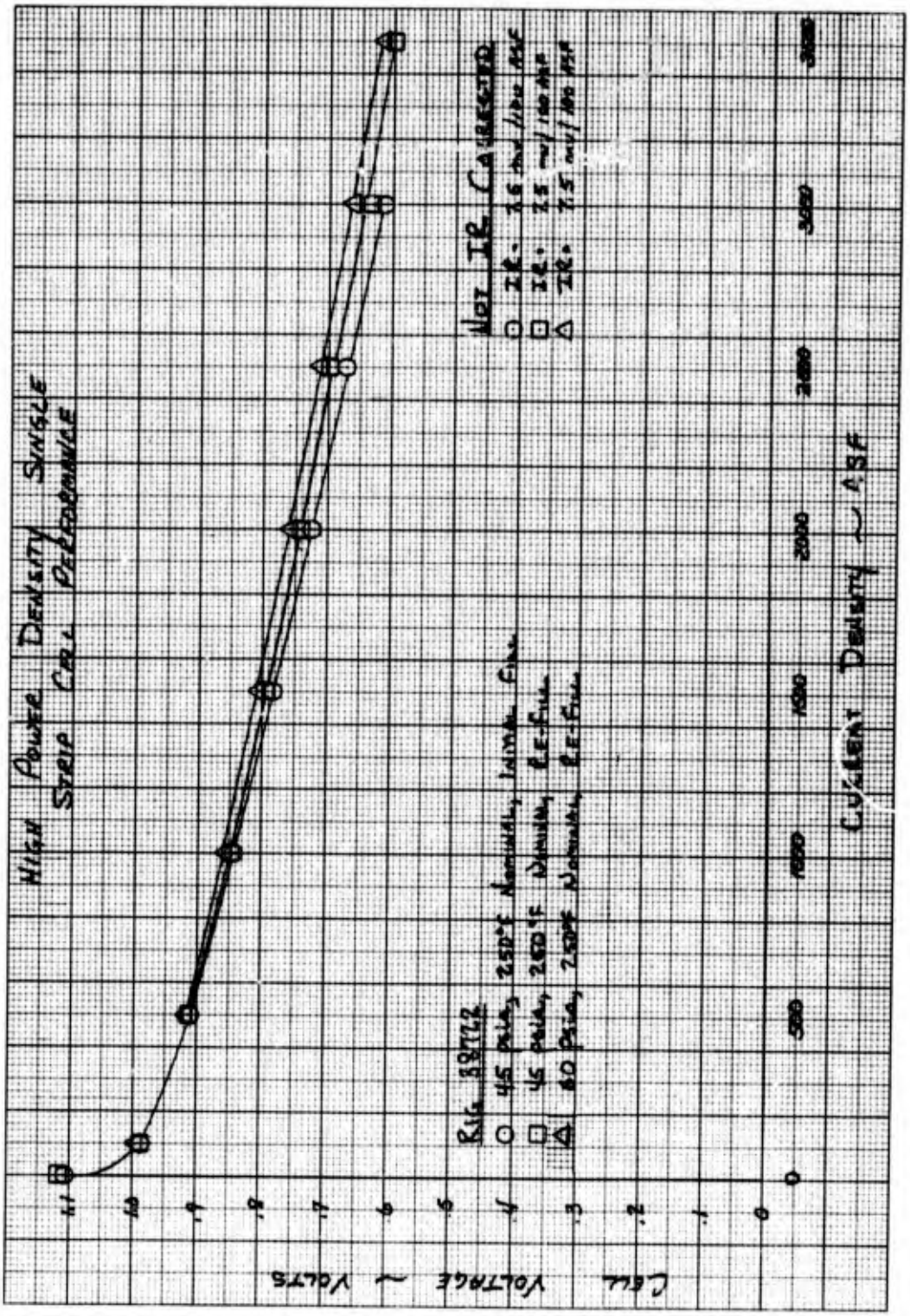

Figure 110 — Strip Cell 13, Performance Calibration to 3500 ASF

Upon restart, the initial cell voltage was 0.971 v at 100 ASF. Following restart, the cell was operated continuously for 132 minutes at 3000 ASF with dynamic water removal. The cell voltage was initially 0.502 v, rose to 0.578 v as the cell temperature stabilized, and then decayed to a final voltage of 0.234 v. The cell was then refilled and recalibrated at 60 psia. 52 percent KOH and 250°F. The cell performance recovered to 0.653 v at 3000 ASF.

Three 50-percent duty cycles, two-seconds on – two-seconds off, were then conducted; the first two at 3000 ASF and the last at 3500 ASF. In the first test, the cell was operated for 84 cycles (5.6 minutes) using dynamic water removal. The voltage loss during this test was 7 mv, as shown in Table XXX, Event 5. After conditioning the electrolyte to 60 percent, the cell was subjected to 15 cycles of two seconds at 3000 ASF and two seconds at open circuit with water storage in the ERP. Initial voltage was 0.617 v and rose to a final level of 0.663 v. Table XXXI presents the voltage during each pulse of the test. The electrolyte was then again dried to 60 percent and 10 cycles were operated at 3500 ASF. Again, the cell voltage rose throughout the test, see Table XXXI, Test B.

The cell was next cycled in the two-seconds on – two-seconds off mode at 60 psia, 32 percent KOH, 250°F, 3000 ASF for five hours with dynamic water removal. More than 4500 operating cycles were completed during this test. The voltage as a function of time for this test is presented in Figure 111. During the entire period, the cell voltage remained within 10 mv of 0.640 v. Diagnostics following this operation indicated the cell to be in good condition and capable of further testing.

Total load time accumulated on this cell was 23.0 hours with 308 minutes at 3000 ASF and 2.5 minutes at 3500 ASF. Approximately 154 minutes of the time was obtained in the cycling mode at 3000 ASF, and more than 4600 cycles were completed. A chronology of events is presented in Table XXX.

Strip Cell 14 – Strip Cell 14 was constructed with the Configuration 4 combined H_2/ERP field and a 5-mil thick matrix.

Initial performance of the cell was excellent, as shown in Figures 112 and 113. Figure 113 shows the performance of this cell with a 5-mil matrix is significantly better than that of a previous Configuration 4A cell having a 10-mil matrix. At 60 psia reactant pressure a cell voltage of 0.650 v at 3500 ASF was obtained which resulted in a power density level of 2280 WSF. Following diagnostics, a 150-minute endurance program was begun. The program consisted of 3000 continuous cycles of 3 seconds on load followed by 2 seconds at open circuit. Product water was removed by a flowing hydrogen stream. For the first half of the test the load was approximately 3200 ASF. After 1500 bursts the power density was 2130 WSF at 3170 ASF. In the last half of the test, the load level was increased to approximately 3600 ASF. Power density in this half ranged from 2240 WSF, initially to 2190 WSF at cycle 3000 with a peak of 2320 WSF at 3650 ASF near Cycle No. 2400. A log of this test is presented in Figure 114. No problems were encountered. The peak power density of 2320 WSF was consistent with a powerplant specific weight of 0.52 lb/kw and represents another step toward the goal of 0.5 lb/kw. The final calibration, after the endurance program, showed a change from initial performance of only 33 mv at 3500 ASF. About 60 percent of this variation was due to an increase in ohmic polarization (IR), with most of the balance due to a decrease in electrode activation level.

TABLE XXX

STRIP CELL 13 TEST SUMMARY

Event	Mode	Water Removal	Current Density ASF	Initial Voltage	Peak Voltage	Final Voltage	Load Time
1	Continuous	Dynamic	3000	0.660	0.660	0.635	3 Minutes
2	Cyclical†	ERPS*	3000	0.660	0.660	0.660	30 Seconds
3	Continuous	Dynamic	3000	0.669	0.669	0.634	15 Minutes
4	Continuous	Dynamic	3000	0.502	0.578	0.234	132 Minutes
5	Cyclical†	Dynamic	3000	0.651	0.651	0.644	2.8 Minutes
6	Cyclical†	ERPS*	3000	0.617	0.663	0.663	30 Seconds
7	Cyclical†	ERPS*	3500	0.527	0.619	0.610	20 Seconds
8	Cyclical†	Dynamic	3000	0.633	0.646	0.640	151 Minutes

Note: Calibrations and diagnostics not included in this table.

†Cyclical operational mode is 2 seconds of load followed by 2 seconds without load.
*ERPS - Water storage in ERP

TABLE XXXI

MISSION SIMULATION TESTS

(60 psia, 2-seconds On - 2-seconds Off, water storage in ERP)

	TEST A 3000 ASF		TEST B 3500 ASF	
Cycle	Voltage (Volts)	Power Density (WSF)	Voltage (Volts)	Power Density (WSF)
1	0.617	1850	0.527	1850
2	0.604	1810	0.542	1900
3	0.628	1880	0.561	1960
4	0.635	1900	0.596	2080
5	0.633	1900	0.609	2130
6	0.642	1930	0.619	2160
7	0.652	1950	0.615	2150
8	0.653	1960	0.611	2140
9	0.665	2000	0.607	2120
10	0.663	1990	0.610	2140
11	0.661	1980		
12	0.663	1990		
13	0.654	1960		
14	0.657	1970		
15	0.663	1990		

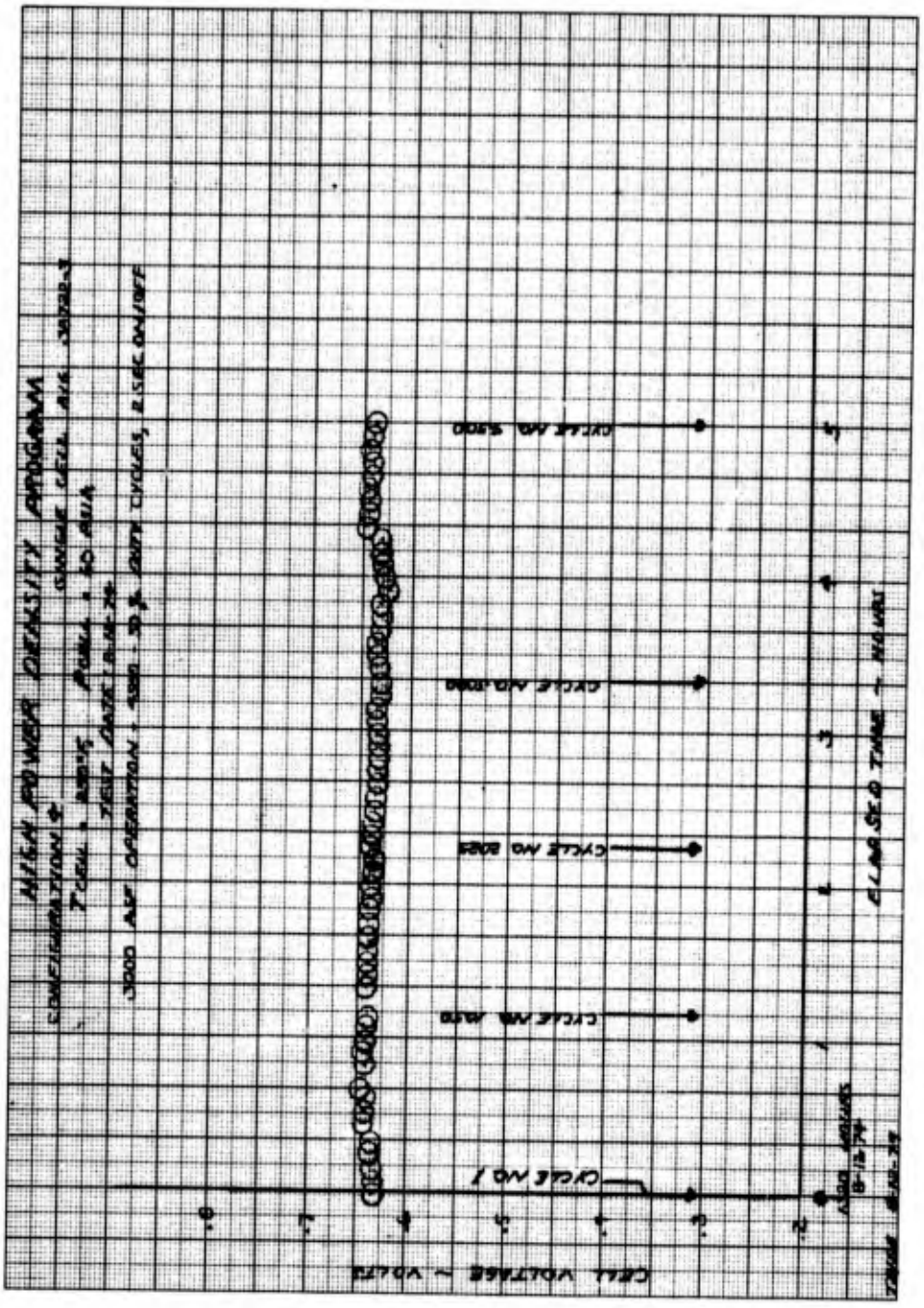

Figure 111 – Strip Cell 13, Cyclical Operation Endurance Test

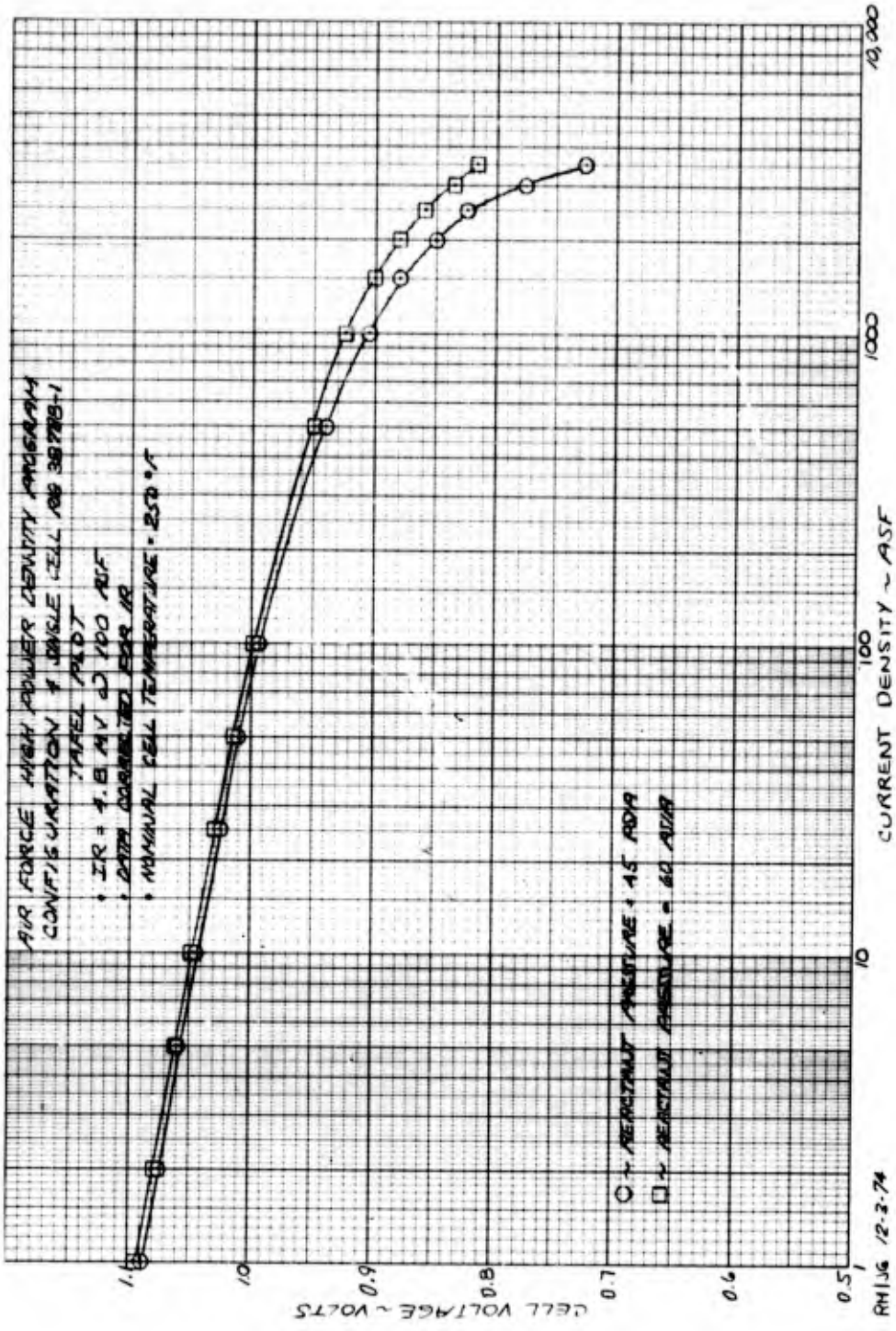

Figure 112 – Strip Cell 14, Tafel Data

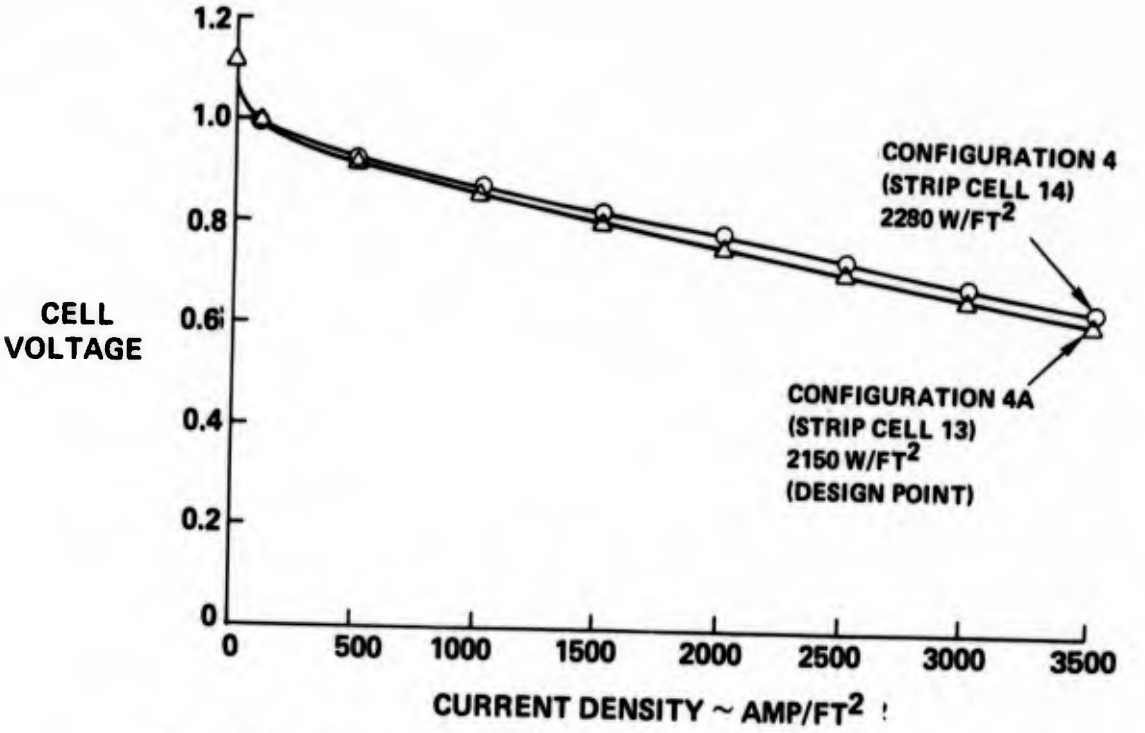

Figure 113 – Performance Comparison: Strip Cell 14 vs. Strip Cell 13

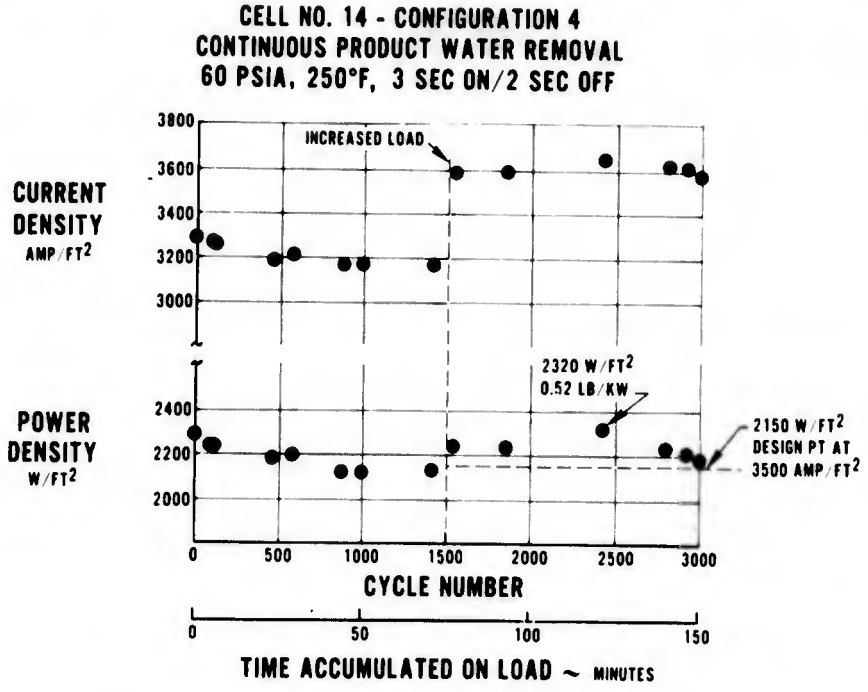

Figure 114 – Strip Cell 14, Cyclical Endurance Test

Following an electrolyte refill the cell was returned to test. Performance after the refill was down from the final calibration of the previous test, mostly as a result of higher anode diffusion losses. In order to determine if the test stand is suitable for conducting higher operating pressure tests in the future, the cell was calibrated at 45, 60, 75, and 90 psia. No problems were encountered and the test stand and cell behaved normally.

Total load time on Strip Cell 14 was 8.5 hours, with over 150 minutes in the 3100-3700 ASF range in the cycling mode.

Strip Cell 15 – Strip Cell 15 was constructed to the Configuration 4 design with a combined ERP/H_2 field and a 5-mil thick matrix. The objective of this test was to obtain performance data at reactant pressure up to 90 psia.

The performance of this cell is shown in Figure 115. It was good at all levels of pressure. At 60 psia a cell voltage of 0.680 v at 3500 ASF was obtained resulting in a power density of 2380 WSF. Power density demonstrated at 75 psia was 2810 WSF and at 90 psia 3000 WSF at a current density of 5000 ASF. Some apparent effects of temperature were noted at the higher current densities resulting in higher than predicted performance gains. The structural integrity of the cooler was demonstrated in this test. Operation at a cell pressure of 90 psia results in a pressure differential of 60 psia across the cooler at normal operating temperatures. No problems were noted with the cooler because of these conditions.

C. DEVELOPMENT OF LIGHTWEIGHT STACK COMPONENTS

1. Introduction

The first high power density cell, plaque, and repeating stack section designs conceived under this program were based on the experience of earlier development efforts sponsored by the Air Force Aero Propulsion Laboratory, to develop a "dual-mode" power system, and by the NASA Lewis Research Center, to develop lightweight fuel cell technology. Review and evaluation of these designs showed, however, that they would require development and improvement to meet the unique requirements of this program. Specifically, additional weight reduction was required and methods by which to fabricate these lighter designs would also require development. For example, the two heaviest components of the stack repeating unit, see Table XXVII, Configuration 1, are the electrode substrate screens and the metallic ERP. They represent almost 40 percent of the total weight. A successful development effort was conducted to reduce the weight of both of these items. Another area requiring special development was fabrication of thin lightweight plaque and cooler structures. Although plaques and other assemblies had been fabricated under the NASA-Lewis Program with thin-lightweight sections, these had been operated at only one quarter to one third the pressures required by this program, 45-60 psia. Similarly, evaporative coolers had been used in other power system designs, but none with weight goals as low as necessary for this program had been developed before. The work that led to the successful fabrication of each of these items is described below. Their successful operation is described with the specific cells and plaques in which they were tested.

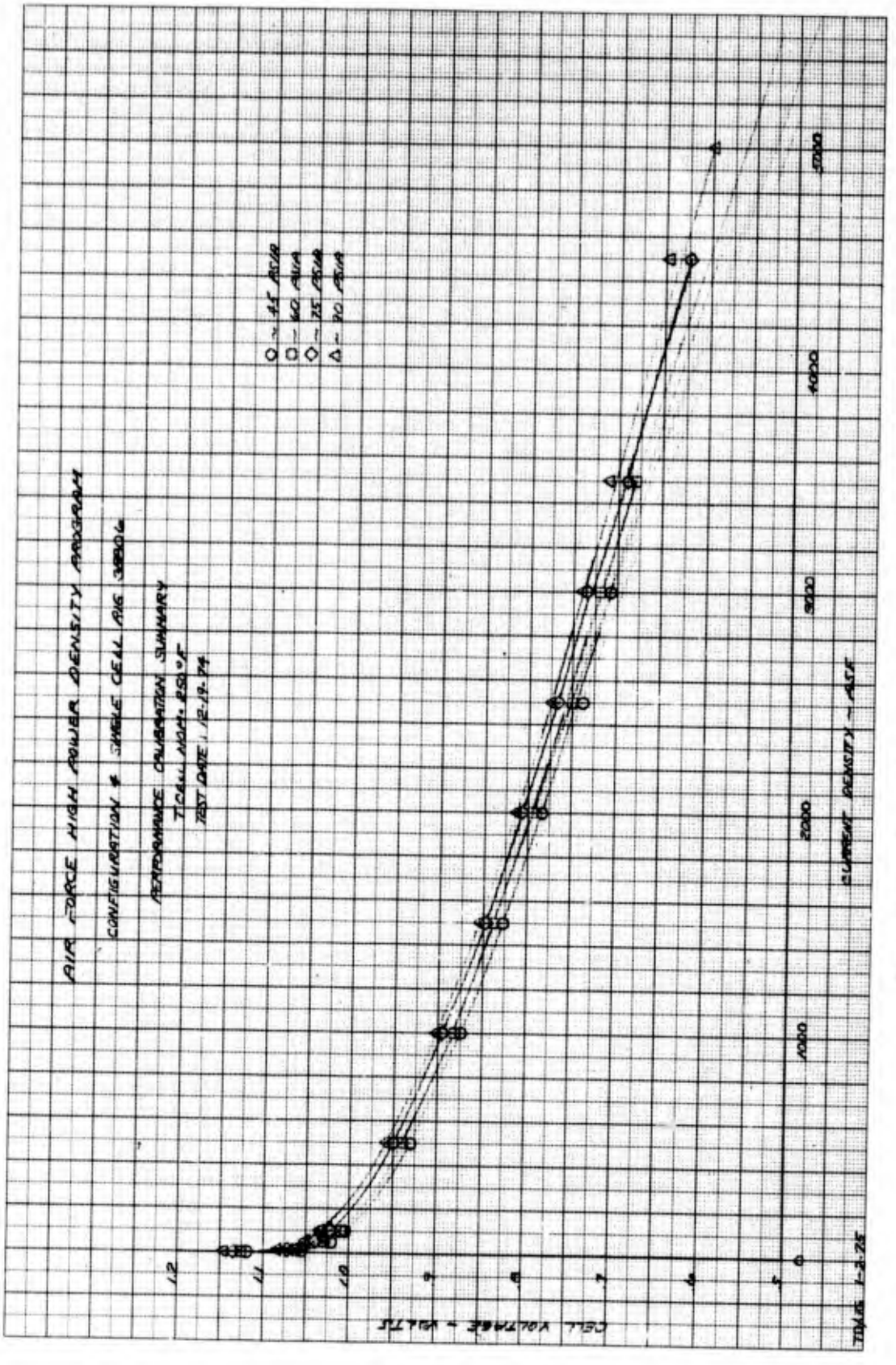

Figure 115 – Strip Cell 15, Performance Calibration to 5000 ASF

2. Electrode Substrate

The requirements the screen substrate of a high power density cell must satisfy are:

(1) Weight - minimum

(2) Structural - provide adequate and uniform compression and support of matrix

(3) Thermal - Limit I^2R heating in edge frame and intercell seal to 45°F above maximum cell temperature

(4) Electrical - IR loss limited to 70 mv/cell average at 3000 ASF

Analysis indicated a lighter 50 x 50 mesh substrate screen could satisfy structural requirements. Analysis also indicated electrical and thermal requirements would require a 100 x 100 mesh screen with a two-thickness silver plate (0.5 mil in the active area and 1.0 mil in the frame area). However, the thermal and electrical properties requirements are determined by the high current flow which is primarily unidirectional, i.e., toward the long edge of the strip cell. As a result a lighter 50 x 100 mesh assymmetrical screen of 2-mil nickel wire with a two-thickness nickel plate was selected for development.

The asymmetrical 50 x 100 mesh of 2-mil nickel wire screen was available commercially, but achieving the desired two-thickness nickel plate required development.

Early attempts at the two-thickness silver plating, on symmetrical 100 x 100 mesh 2-mil nickel wire screen, produced substrates which were unsatisfactory because of wrinkling and a tendency to "oil-can". This phenomenon had also occurred in plating trails of the asymmetrical 50 x 100 mesh nickel screen.

Investigation of the problem by the plating vendor isolated the most probable cause of the problem to be the technique used to obtain the two levels of plating. First a 0.5-mil plate was applied to the entire screen. Then, the screen was masked with wax in the areas that were not to receive additional plating. After plating to 1 mil in the appropriate areas, the wax was removed.

The vendor felt that the handling of the unsupported screen, in addition to the thermal stresses on the screen during the application and removal of the masking wax, promoted the formation of wrinkles and the "oil-can" effect.

Satisfactory substrates without any wrinkles or "oil-can" effect were obtained when a stretching frame was used during the plating process. The frame or holding fixture was used to stretch the screen before and during plating. Once the initial 0.5 mil of silver was deposited on the screen, the wire overlaps became locked together forming a rigid structure. Masking, additional plating and wax-mask removal were completed in the frame. The resultant substrates were wrinkle free and had no tendency to "oil-can".

3. Nonmetallic Electrolyte Reservoir Plate

Development of a lightweight non-metallic Electrolyte Reservoir Plate (ERP) was begun under the NASA-Lewis Advanced Fuel Cell Program (NAS3-15339). This program selected two primary candidates for study: (1) self-bonded fibrillar carbon and (2) sintered polysulfone resin. Porous samples of each material were prepared in the laboratory: The fibrillar carbon material was self-wetting and the porous polysulfone was given a thin electroless plate to make it wettable. These samples were evaluated against the requirements shown in TABLE XXXII.

TABLE XXXII

LIGHTWEIGHT ERP REQUIREMENTS

Weight	Minimum
Pore Size	3 to 8 Microns
Porosity	As high as practical
Electrolyte Flow	Readily wet by electrolyte - minimum hysteresis P vs V
Compressive Strength	200 psi minimum
Environment	200-300°F 25 to 45 weight percent aqueous KOH and hydrogen
Configuration	Flat plate, 10 to 30 mils thick, reactant flow passages in one face

Both materials were found to be satisfactory. The polysulfone ERP however was significantly lighter than the carbon and was selected for further development.

Consequently, two separate but complimentary efforts were begun under this program and the NASA-Lewis Program to evaluate alternate procedures suitable for shop production of porous polysulfone ERP's in development program quantities. Success was achieved under this program.

Fabrication of the porous-polysulfone ERP's is a four step process: (1) Preparation of the powder, (2) Sintering of the powder into a porous sheet, (3) Formation of a flow field in one face of the ERP and, (4) Nickel plating the porous polysulfone plates to make the plates wettable.

Initial efforts concentrated on making a powder of the required particle size distribution from the pellets supplied by the manufacturer. An initial procedure was attempted to grind the particles in a ball mill from pellets, however, particles of the required size could not be obtained. The diameter was an order of magnitude larger than desired.

Following construction of a spray booth, powder samples were prepared by a solvent flash-off method similar to that which had been used on a much smaller scale in the laboratory. A solution of polysulfone resin pellets in methylene chloride (dichloromethane) is sprayed into a large container and is allowed to settle on a liquid surface. The spray booth and liquid surface are maintained at room temperature. The resulting powder is separated by decanting and drying. Final separation and grading is effected by sieving. Both the powder shape and size can be altered by changing the percent of polysulfone dissolved in the solvent and by varying the air pressure used in the spray gun. Particles were produced of the correct size range, 6×10^{-5} to 9×10^{-5} in.

This powder was then used to fabricate trial ERP's. Again a process different from that used in the laboratory had to be developed. The method finally developed for sintering the powder into a sheet was based on a dry powder casting process, rather than slip casting with a liquid slurry used in laboratory. This manufactucturing change proved to be the single-most significant improvement in transferring the laboratory process to a shop porcess. It resulted in more rugged parts than had been previously fabricated, with improved thickness control (±1.5 mil vs. ±4.5 mils for parts fabricated under NAS3-15329) and improved surface finish. The pore size of one of these parts was measured by mercury intrusion and found to be in the 1.5 to 6.7 micron range as shown in Figure 116.

Previously, the hydrogen flow fields were pressed into the ERPs following casting and sintering. With the change to the dry casting process, a procedure for molding the flow fields into the part during the casting process was developed, combining the second and third steps of the process.

The final step in the manufacture of the porous polysulfone ERP's is nickel plating the ERP to improve its wettability. The laboratory electroless plating process was transferred into the shop. This replacement plating procedure uniformly coats the polysulfone particles of the sintered ERP with nickel making it wettable. The plating is done in four stages; cleaning, sensitizing, activation, and nickel plating. Upon completion of the plating trials, water takeup tests were conducted to determine the effectiveness of the plating. The average porosity of twenty ERP's was found to be 42 percent. One sample, which showed a calculated porosity of 43 percent based on water takeup measurements, was determined by mercury intrusion to have a porosity of 47 percent. This result indicates a high degree of plating effectiveness.

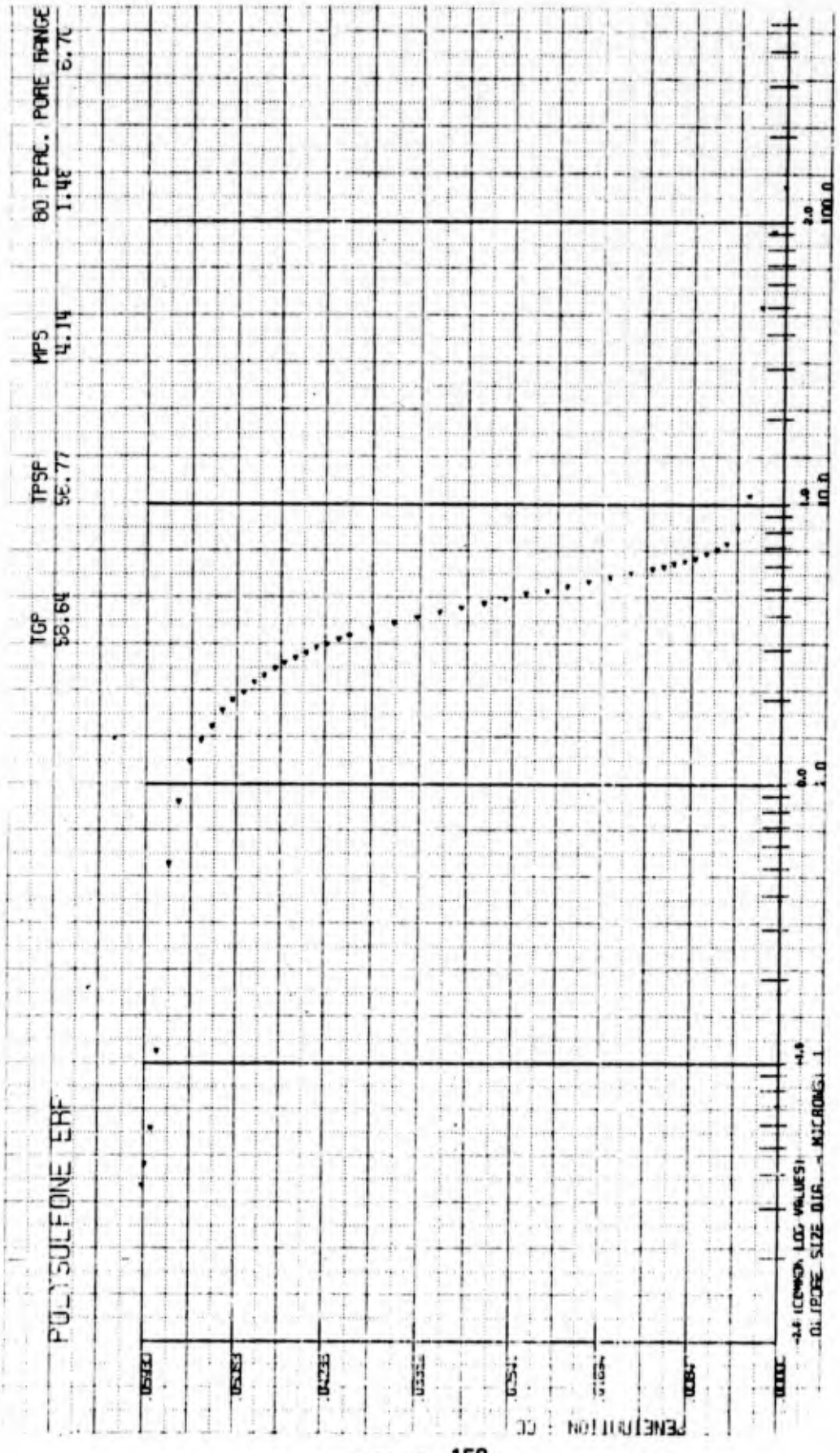

Figure 116 — Polysulfone ERP Pore Size Data

Structural tests were conducted on samples of 30-mil thick plated and unplated porous polysulfone to determine their mechanical properties. The results are presented in Table XXXIII.

TABLE XXXIII

ERP COMPRSSIVE STRENGTH

Sample	Proportional Limit - psi	Modulus - psi
Unplated PWA 56-4	210	2.5×10^5
Unplated PWA 56-5	230	2.0×10^6
Ni Plated PWA 57-9	1500	8.8×10^5

The results indicate the compressive strength of the ERP's is adequate since the compressive load they experience in a cell or stack assembly is approximately 100 psi (68.9 n/cm^2).

Following the successful development of shop procedures for the manufacture of 30-mil parts, development of 20-mil parts was completed for use in still lighter cells.

4. Six-Cell Plaque Unitization

The method for fabricating the six-cell plaque tested in this program was based on the laminated unitization method P&WA uses for fabricating the unitized electrode assemblies for convential space and undersea powerplants. This is a method of building up a cell frame by heat and pressure bonding precut layers of epoxy impregnated glass fiber cloth into a rigid one-piece assembly. The method as applied to six-cell plaques is as follows: Epoxy/fiberglass prepreg sheets are cut to the planform shown in Figure 117. Two 2-mil thick prepreg planforms are next bonded to six asbestos matrices, one for each strip cell. The prepregs overlap the edge of the asbestos matrix by 0.010 in. and are heat sealed to the matrix. Additional layers of prepreg are added to build up the intercell strip thickness. A slot is then cut into the intercell strip to permit threading the electrodes into place. This is done from the anode to the cathode side of the cell. Successive layers of prepreg are added, together with the ERP's, to complete the assembly. As additional layers of prepreg are added they are heat-tacked together to insure alignment until final bonding occurs. In the outer layers the intercell strips are not slotted. The lay-up is then press cured between heated platens which causes the epoxy to flow into the slots and screen voids, sealing the entire assembly. The pressed unit is then final cured in an oven.

Initial plaque assemblies were fabricated with electrodes and electrolyte reservoir plates bonded into a single plaque as shown in Figure 118. An intercell seal width of 0.375 in. was used in all plaques. The principal requirements of the intercell seal are to: 1) provide a positive gas seal for the electrode screen and for the cell's matrix; and 2) electrically insulate electrodes lying in a common plane. Some problems were encountered with leakage through the intercell

seal areas and electrical shorting. Shorting problems were overcome by using extreme care during the layup and insuring that no extraneous strands of wire mesh from the electrode substrate remained after trimming electrodes to size. The integrity of the intercell seal is a function of a) the resin flow in the epoxy/fiberglass prepregs, b) pressure applied to the part in molding and, c) temperature of the part while subjected to pressure. Early difficulties were traced to epoxy fiberglass prepreg with a low resin content and flow properties. The use of this material resulted in insufficient flow of resin and, consequently, failure to fill void areas in the screen. At the other extreme, other prepregs which had adequate or above average flow allowed to much resin flow and resulted in resin "flash" in undesirable areas such as ports and electrode active areas. Flow of resin is also a function of the pressure applied to the part while at temperature. Unless the proper pressure is applied, too little or too much flow of resin may result. Lamination pressure was controlled by establishing a correct uncompressed height of the lay-up and then pressing it to "stops" or "shims" of the proper thickness placed on the outside of the part being fabricated. With proper control of the epoxy/fiberglass prepreg material characteristics and laminating temperature and pressure, plaques with leak tight intercell seals were attained. Figure 119 shows a completed 6-cell plaque. Initially, the thicker the plaque, the better the chances of obtaining a good part. Thus, Configuration 1 plaques containing 30 mil ERP's and frame thickness of about 0.050 in. were more easily fabricated than the Configuration 2 plaques with 20 mil ERP's and 0.040 inch frames.

The 3-mil thick nickel foil strips, on the right-hand end of the plaque, are individual cell voltage leads. These were imbedded in the frame and extended between the anode and ERP's. Anode and cathode thermocouples, at the top and bottom of the figure, were also included in the assembly. Configuration 3 plaques, however, differed from Configuration 1 and 2 plaques and required a change in fabrication method. In Configuration 3 plaques the nickel ERP's used earlier and were replaced with polysulfone ERP's. The polysulfone ERP's cracked during fabrication. This cracking was associated with the thermal expansion differences between epoxy/fiberglass and polysulfone. When it cracked, pieces of the polysulfone ERP could become lodged between the ERP and electrode and result in matrix damage at assembly. To overcome this, Configuration 3 plaques were made in two steps. First a plaque assembly utilizing the electrodes and matrix and measuring about 20 mils in thickness was fabricated. Then, a frame to house the six individual ERP's was made separately and bonded to the anode side of the plaque with a thin fiberglass-epoxy layger glue line, see Figure 120. ERP's were then placed in the resulting cavities at the time of assembly of the development unit. This was the method used to fabricate the last 6-cell plaques tested in this program.

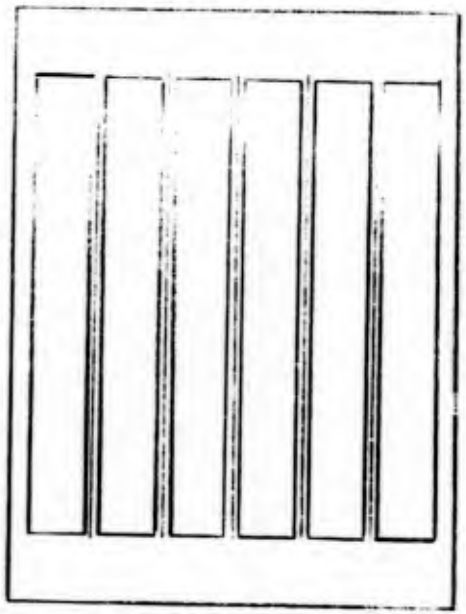

PRECUT EPOXY/FIBERGLASS PREPREG WITH INTERCELL SLOTS

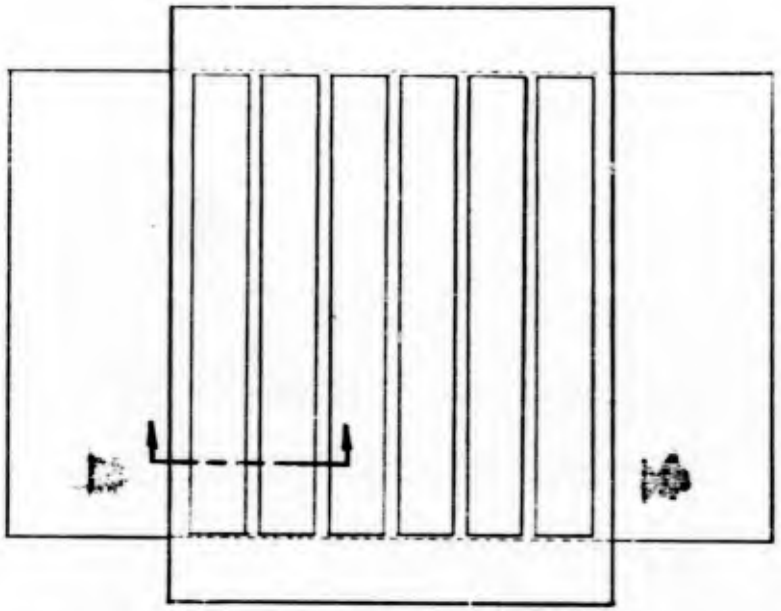

EPOXY/FIBERGLASS PREPREG WITH MATRICES AND ELECTRODES INSTALLED

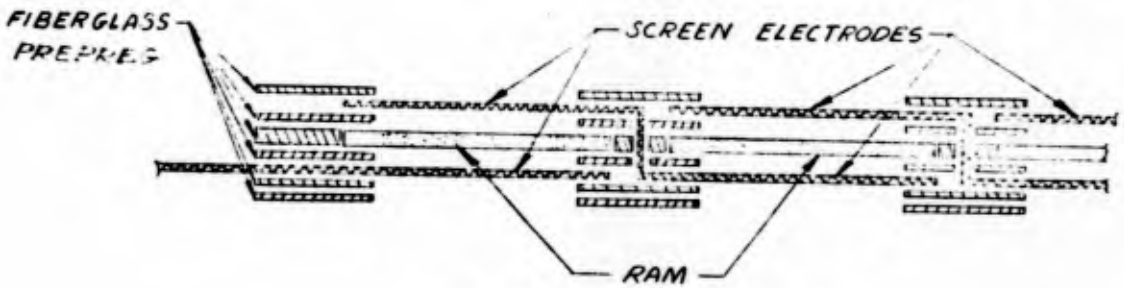

PLAQUE UEA LAYUP

Figure 117 – Laminated Unitization Technique

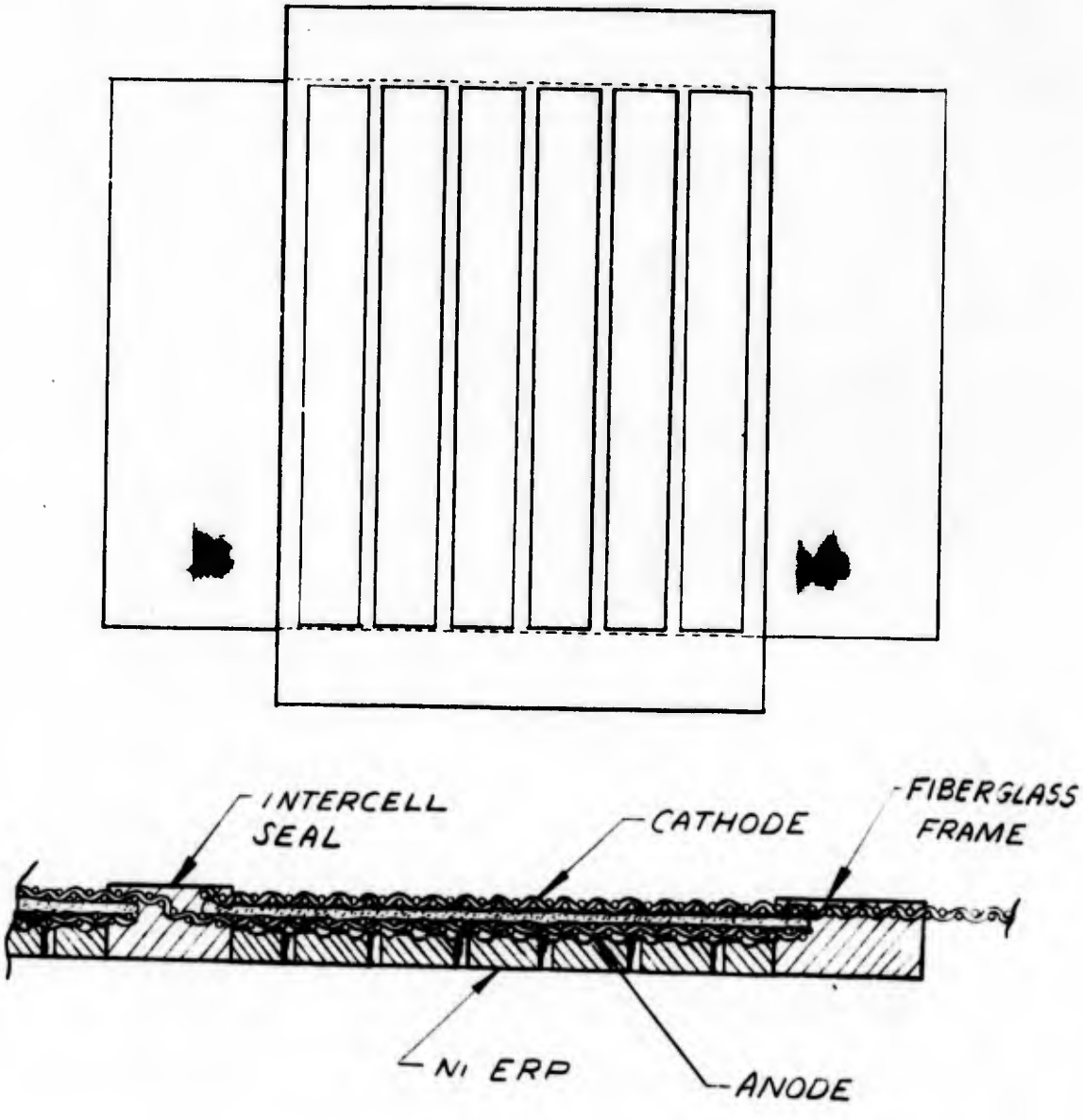

Figure 118 – Single Frame Six-Cell Plaque Design

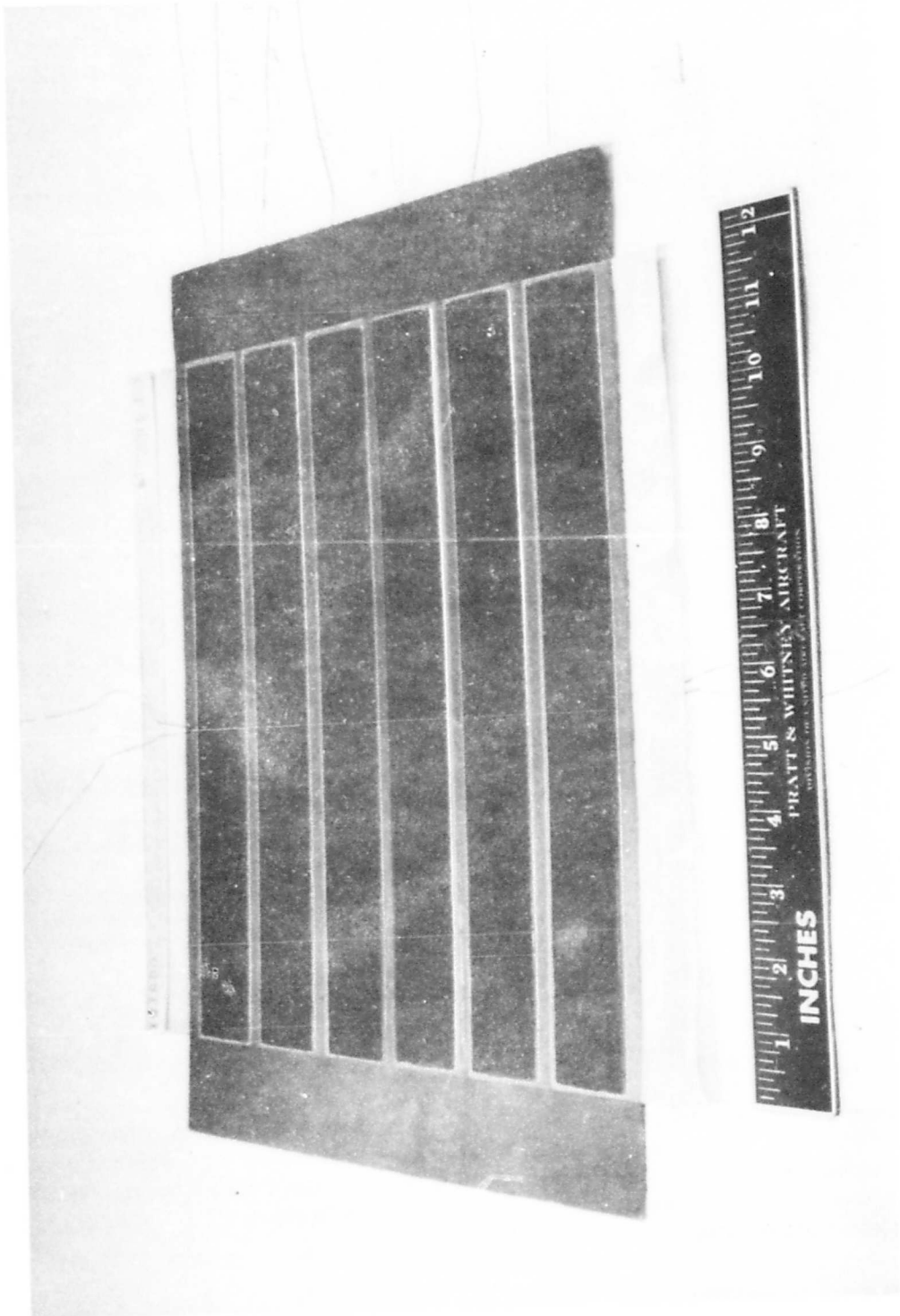

Figure 119 – Six-Cell High Power Density Plaque

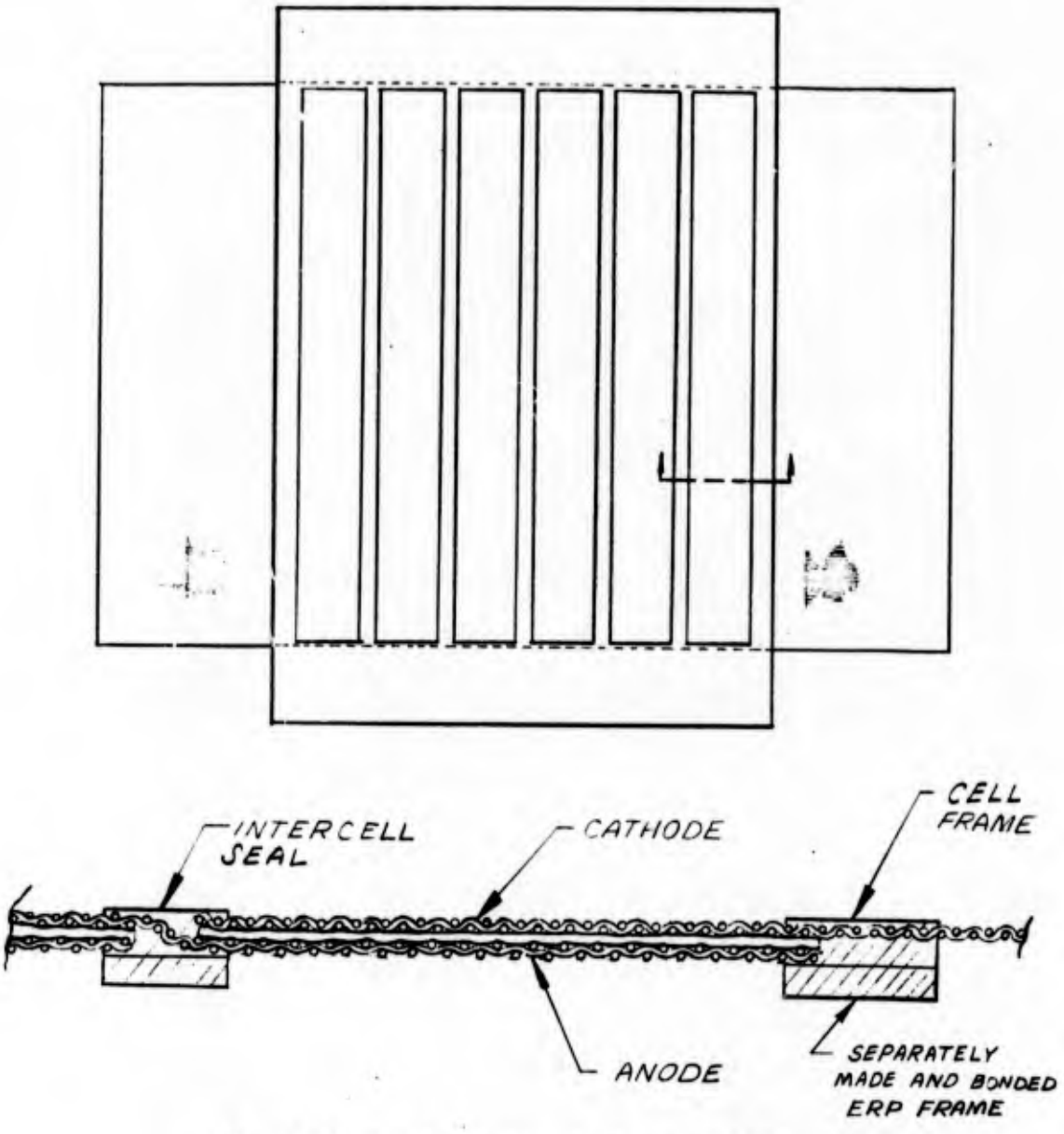

Figure 120 – Six-Cell Plaque with Separate ERP Frame

5. Cooler Development

The System Definition Studies, reported in Section III, resulted in the selection of an evaporative cooling system for the high power density powerplant. This system is predicated on a lightweight oxygen field/evaporative cooler assembly that is located between the cathodes of adjacent plaques. This arrangement is shown schematically in Figure 121. The functions of the cooler assembly are:

- Separate the oxygen and coolant
- Provide oxygen and coolant flow fields
- Electrically isolate cells within a plaque
- Electrically isolate cells from coolant
- Conduct heat from cells to coolant

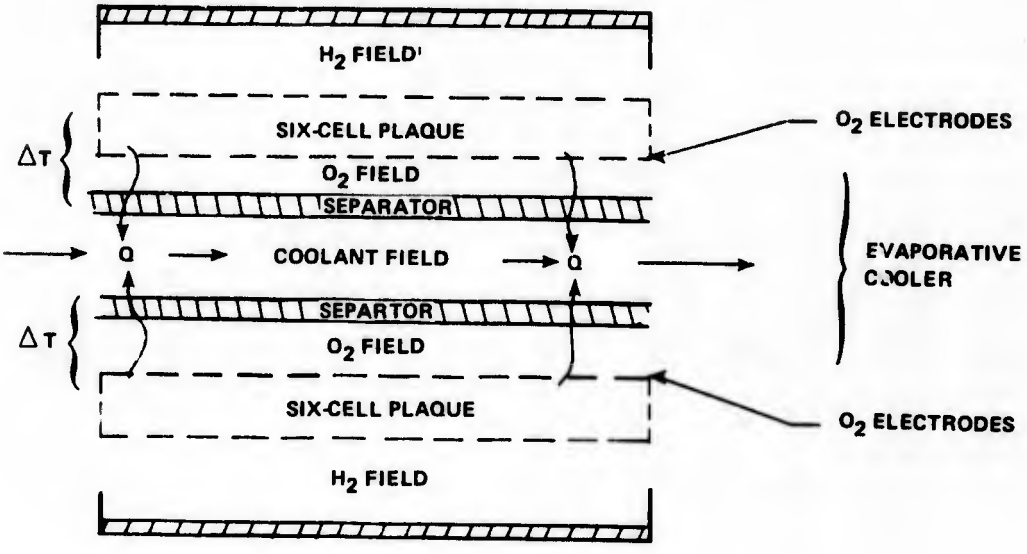

Figure 121 – Evaporative Cooler Schematic

Two cooler design concepts were considered for this application. They are shown in Figure 122. Both designs satisfy all the itemized functional requirements. Candidate 1 was judged to be the easier of the two to fabricate but was not as light as Candidate 2. Candidate 1 consists of separate metallic inserts which form flow fields and transfer heat toward the cooler. The dielectric electrically insulates the inserts from the structural separator which is a metal foil. This foil separates the oxygen and coolant and withstands the pressure differential between these fluids. As an alternative the foil-dielectric composite could be replaced by a dielectric sheet if it had sufficient structural strength and integrity to prevent leakage. The cooler field in this design can be fabricated from either a metallic or dielectric material.

In the Candidate 2 design electroformed-nickel inserts are bonded into a frame similar to the six-position frame into which individual cells are bonded to form a plaque. One insert is aligned with each cell. In this arrangement the inserts are electrically isolated from each other by the frames and the cooler field, which is fabricated of a dielectric. If the cooler field is fabricated of a conducting material then an insulating material must be used to separate the inserts and the field.

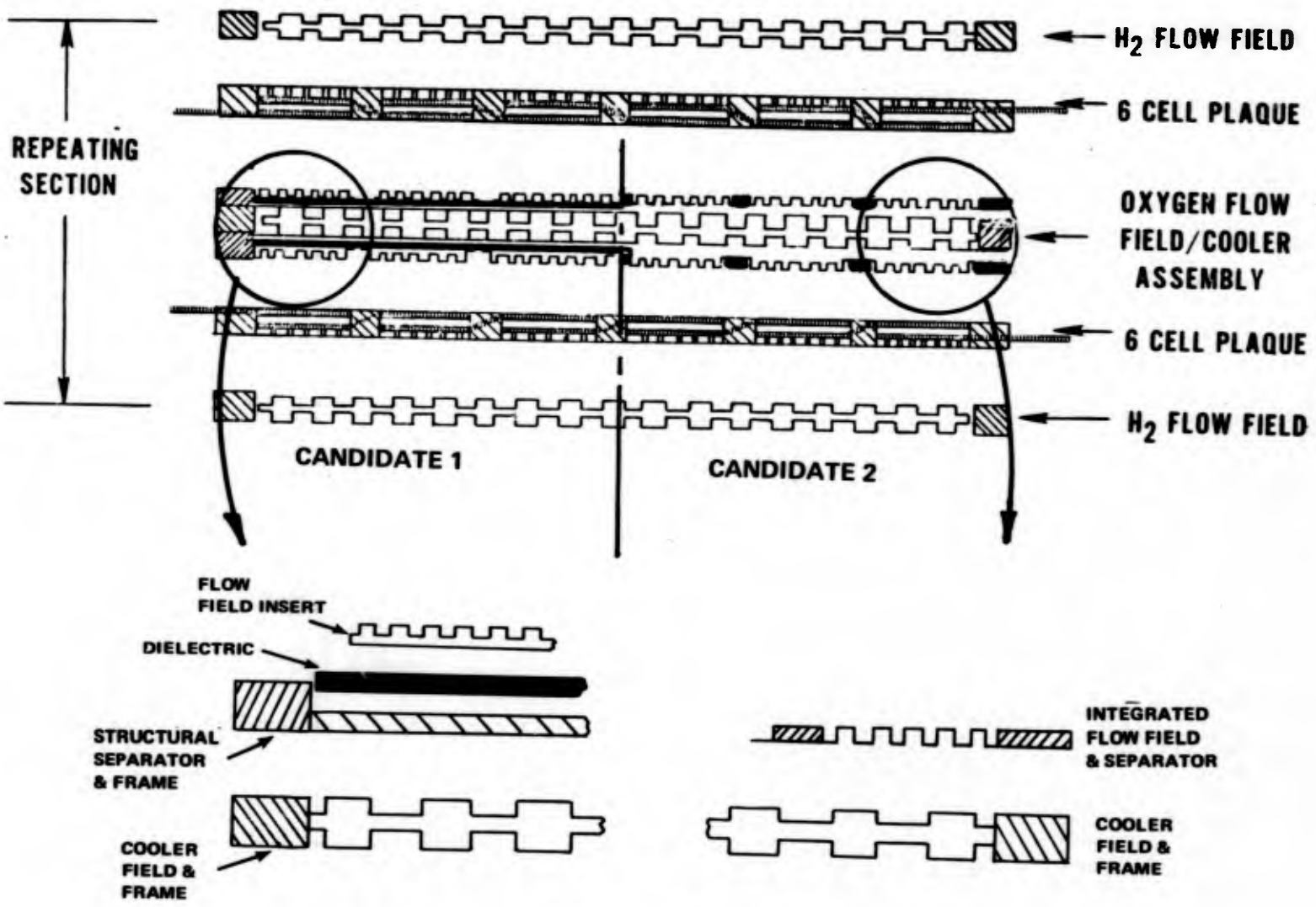

Figure 122 — Candidate Evaporative Cooler Designs

Development of both approaches was begun. A unit based on the Candidate 1 design was eventually selected as a baseline cooler assembly. Although Candidate 2 design cooler assemblies were fabricated and tested, fabricating problems and leakage through both the frames and electroformed inserts prevented their successful use. This design can be significantly lighter than Candidate 1 and is worthy of additional development in the future.

Development of the Candidate 1 design began with fabrication of the oxygen flow field inserts. Two approaches were evaluated. In the first, pin fields were chemically etched into a magnesium plate, bonded to a nickel sheet with a dielectric, and the pins were then coated with epoxy or were nickel plated for corrosion protection. This approach could be used to fabricate inserts or eventually pin fields bonded directly to the nickel separator foil. The screen printed pattern used to chemically etch the pins into the magnesium plate is shown in Figure 123. The dimensions of the field produced with this pattern are: depth - 15 mils, pin diameter - 50 mils, pin pitch - 65 mils. A field etched with this pattern into a magnesium-nickel composite is shown in Figure 124. The composite is 18 mils of magnesium bonded to a 1-mil nickel foil with a 1-mil thick cross linked phenoxy bonding layer. Pin pattern definition was good and only occasional and acceptable irregularities were found. The oxygen flow fields for Development Unit 1 were fabricated using this method and were nickel plated for corrosion resistance. They were bonded to a 3-mil nickel foil with a FEP film.

The second approach to pin-field fabrication was electroforming the field of nickel. The nickel field had the advantage of being inherently corrosion resistant and the lighter of the two designs because the pins were hollow. The first electroformed strips were made with a material thickness of 3 to 3.5 mils. Structural tests of the fields showed they had more than adequate strength in compression to withstand the maximum plaque compressive load of 150 psi, see Figure 125. A set of fields was also tested in which the hollow pins were filled with an epoxy/silver compound for improved thermal conductivity, these fields were even stiffer than the unfilled ones. However, analysis and subsequent testing showed the unfilled pins had adequate thermal conductivity without the addition of the epoxy/silver compound.

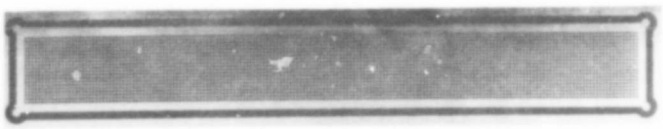

Figure 123 – Silkscreen Pin Pattern on Magnesium Plate

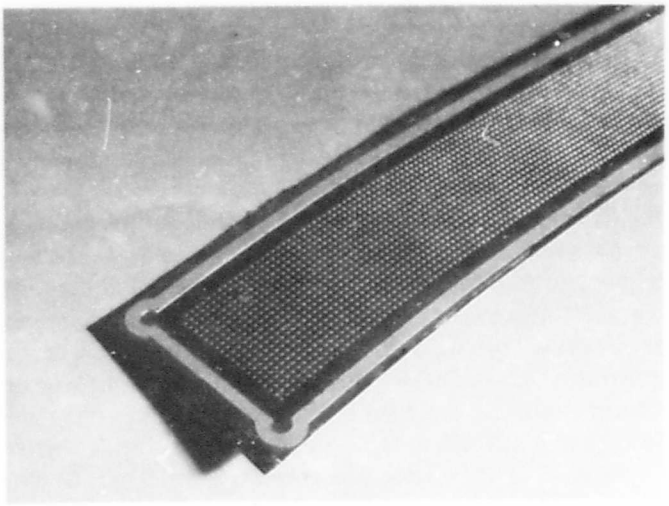

Figure 124 – Chemically-Etched Magnesium Pins on Nickel Strip

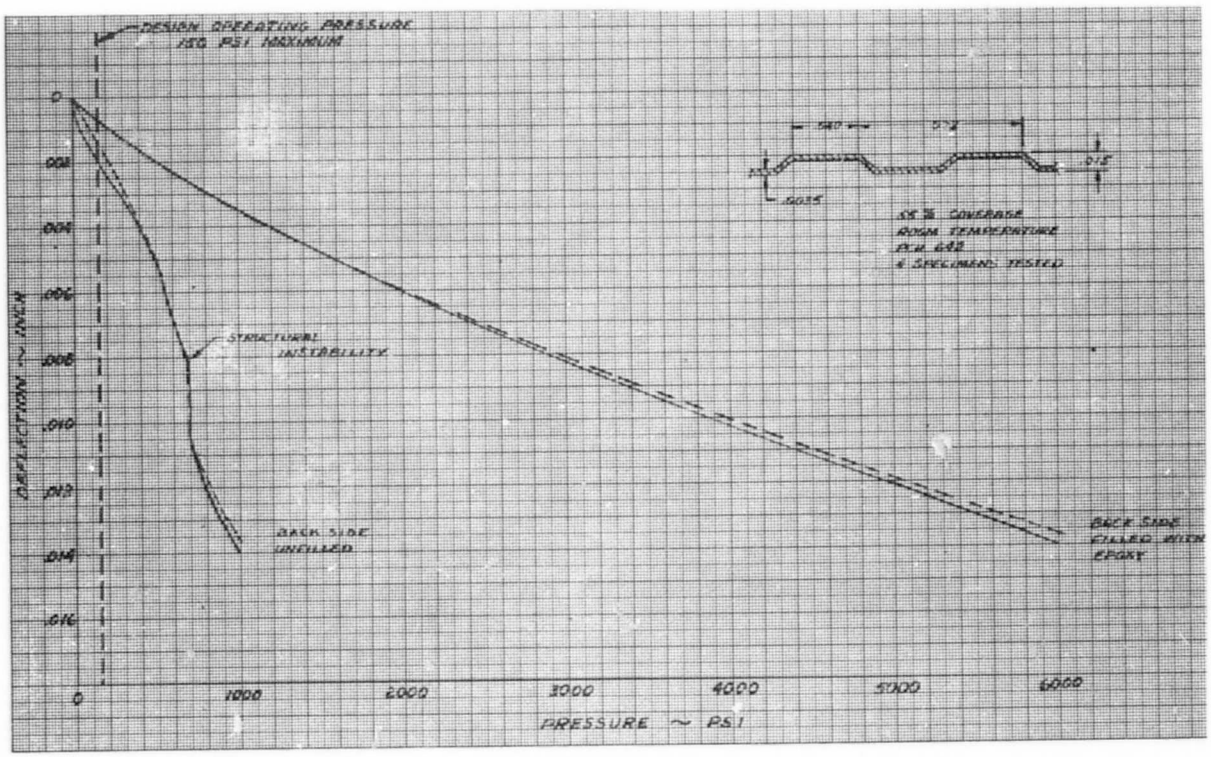

Figure 125 – Compression Test of Electroformed Flow Fields

To achieve the full weight potential of the Candiate 2 design, thinner fields, with a thickness of only 1.5 mils, were fabricated, see Figure 126.

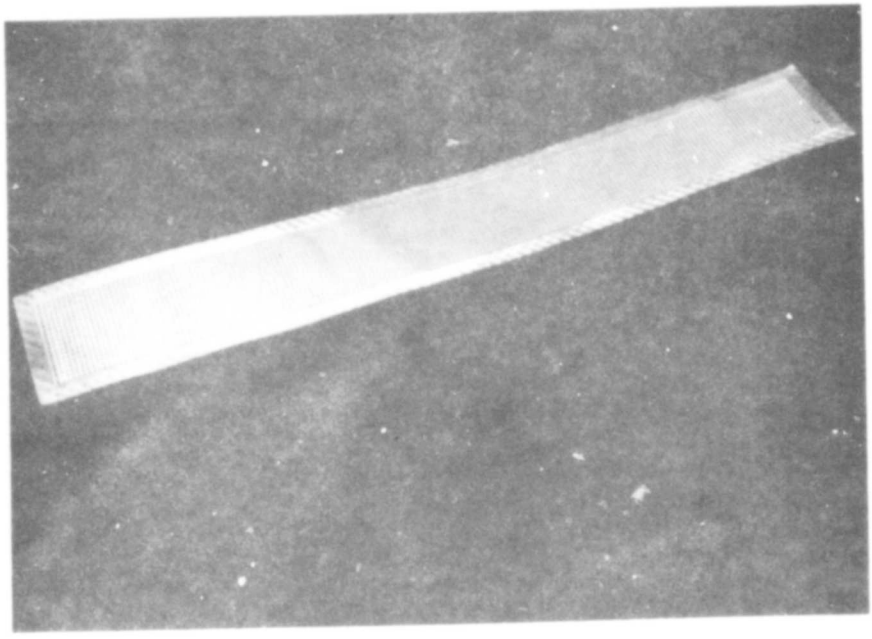

Figure 126 – Electroformed-Nickel Flow Field

These fields were incorporated into a Candidate 2 design cooler assembly and it was tested in Development Unit 2. It was fabricated using the epoxy/fiberglass lamination method described earlier for plaques.

The nickel fields were prepared for bonding by roughening the surfaces of the edges to be bonded into the laminate. Trial cooler assemblies made in this manner leaked in the intercell port areas, see Figure 127. The intercell strips are reduced in thickness at each end, see Section A-A of Figure 127, to allow oxygen to flow freely from the inlet port across the intercell strips to the adjacent cells. The first attempt to eliminate this problem was to increase the strip thickness in this area and to increase the slot length to maintain the same flow area. This reduced leakage, but leakage was not completely eliminated. The second approach, which did effectively eliminate leakage, was to bond a 2-mil-thick film of etched FEP to the intercell strips on the oxygen side of the cooler.

The cooler assembly for Development Unit 2 was built to this design with the additional FEP strips. Pressure checks of the assembly showed the 1.5-mil electroforms had pinhole imperfections, and were leaking. To eliminate this cross leakage, from reactant to coolant, the electroforms were back filled with an epoxy/silver compound.

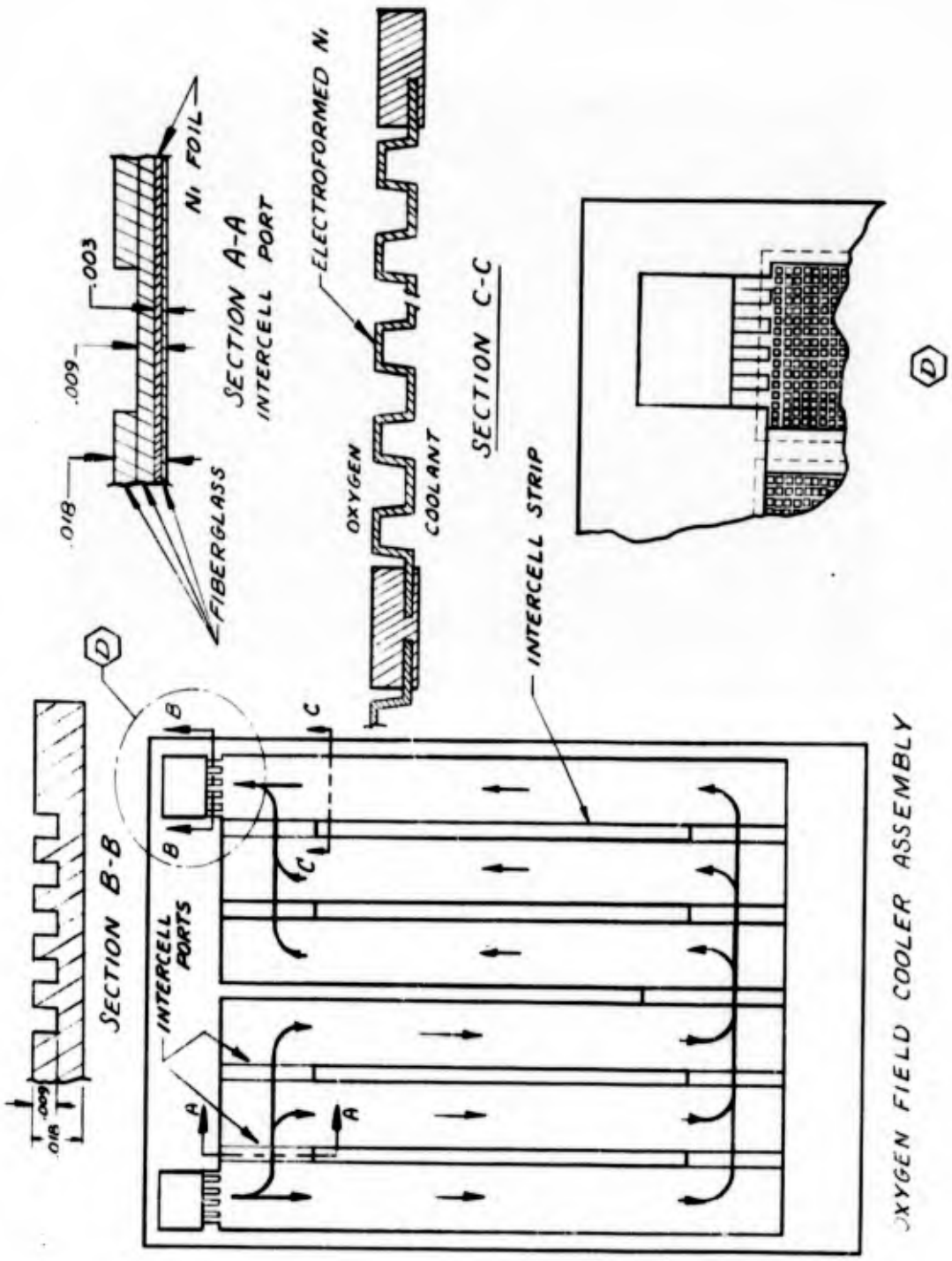

Figure 127 – Oxygen Field/Cooler Assembly

With the pin fields filled, the leakage was eliminated and the cooler was incorporated into Development Unit 2. Post-test examination of the cooler showed the epoxy/fiberglass had delaminated from the nickel electroforms. In light of the results, alternate designs were needed. The alternatives considered are shown in Figure 128. Alternative A incorporated 3-mil nickel electroforms which had been fabricated without pinhole leakage, but retained the thin fiberglass frame for oxygen distribution. To eliminate delamination, additional development would be required. Alternative B, retained the 1.5-mil electroform but incorporated an insulated backup nickel foil to prevent leakage. This configuration increased the stack temperature rise and the weight factor to some extent. With this configuration, however, both pinhole leakage and frame porosity problems were of no concern. Alternative C added high thermal conductivity filler to the pin field of Alternative B to minimize the thermal gradient through the cooler.

Thermal analyses of each alternative, see Table XXXIV, showed that the temperature gradient through "B" was highest, but still acceptable. As a result, Alternative B was selected for fabrication and incorporation in Development Unit 3.

The procedure to make this assembly was as follows: a composite laminate of a 2-mil nickel foil and a 2-mil epoxy/fiberglass prepreg sheet was made first. The composite was then unitized into a laminated fiberglass/epoxy frame. Next, the individual electroformed-nickel fields were bonded in their proper positions with a small amount of epoxy. A single rib was bonded to the foil in the center for oxygen flow direction. Oxygen flow parts were formed by extending the electroformed nickel foil into the oxygen manifold.

This arrangement was successfully tested in Devleopment Units 3, 4, and 5 and was accepted as a baseline cooler assembly design.

Cooler fields of two designs were investigated, one formed of a serrated aluminum foil, see Figur. 129, and the other machined from plastic sheet stock. The advantage of the serrated aluminum foil was that it provided a maximum frontal area for flow and had excellent thermal conductivity. A trial cooler field was fabricated and tested for pressure drop and flow distribution. The flow pattern tested is shown in Figure 130.

Flow distribution tests showed no evidence of stagnation or maldistribution. The test was run with water flow rates of 6 pph to over 100 pph. Pressure drop tests using dry nitrogen indicated a very low pressure drop through this configuration. The results of these tests are presented in Figure 131. During the testing program the manufacturer of the serrated foil indicated that the material was not available in desired height of 30 to 40 mils. The minimum height available was approximately 75 mils which would raise cooler weight prohibitively. As a result this approach to a cooler field was dropped.

Polysulfone was selected as the plastic material from which to machine dielectric cooler fields. This material was selected for its low density and environmental compatibility. It was also used for fabrication of the hydrogen flow fields. It was first evaluated in Development Unit 1. Post-test examination showed it was prone to stress-cracking and shrinkage.

CONFIGURATION 1
BASELINE

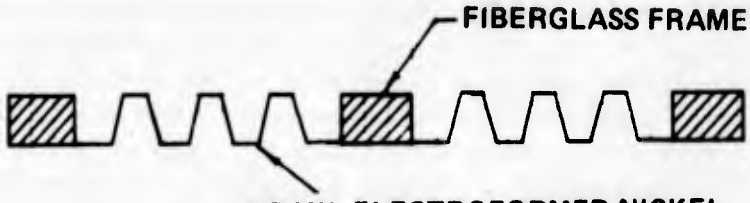

ALTERNATIVE A — SAME AS BASELINE EXCEPT FOR 3 MIL ELECTROFORMED NICKEL

ALTERNATIVE B

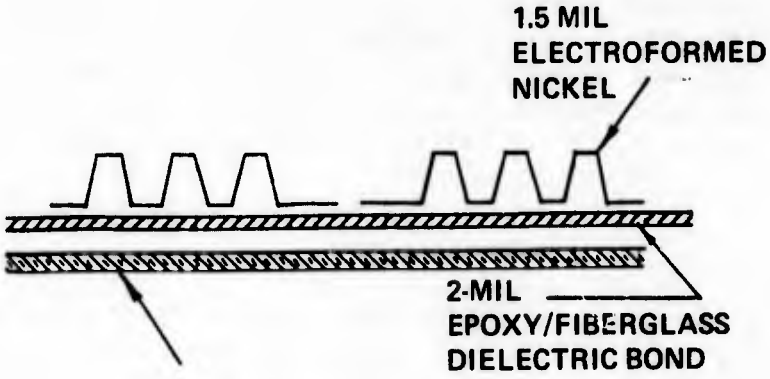

ALTERNATIVE C — SAME AS ALTERNATIVE B EXCEPT THAT ELECTROFORMED NICKEL BACKFILLED WITH HIGH THERMAL CONDUCTIVITY MATERIAL

Figure 128 – Alternative Cooler Configurations

TABLE XXXIV

COOLER THERMAL ANALYSES SUMMARY

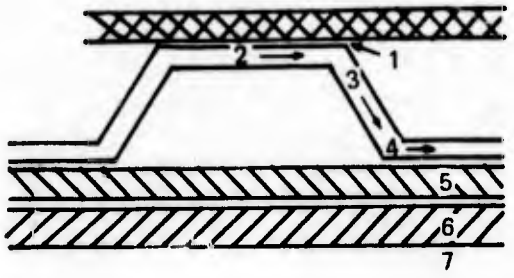

1. ELECTRODE TO PIN
2. PIN TO SIDE
3. ALONG PIN SIDES
4. SIDE TO PIN BOTTOM
5. THRU 2-MIL FIBERGLASS LAMINATE
6. THRU 3-MIL Ni FOIL
7. FOIL TO 212°F BOILING WATER

		ALTERNATIVES		
LOCATION	BASELINE	A	B	C
1	9.9°F	9.9°F	9.9°F	9.9°F
2	--	--	3.3	--
3	4.7	3.1	5.5	4.7
4	1.3	0.8	2.5	1.3
5	--	--	10.3	5.0
6	--	--	0.2	0.2
7	14.1	14.1	14.1	14.1
TOTAL ΔT	30.0°F	27.9°F	45.8°F	35.2°F

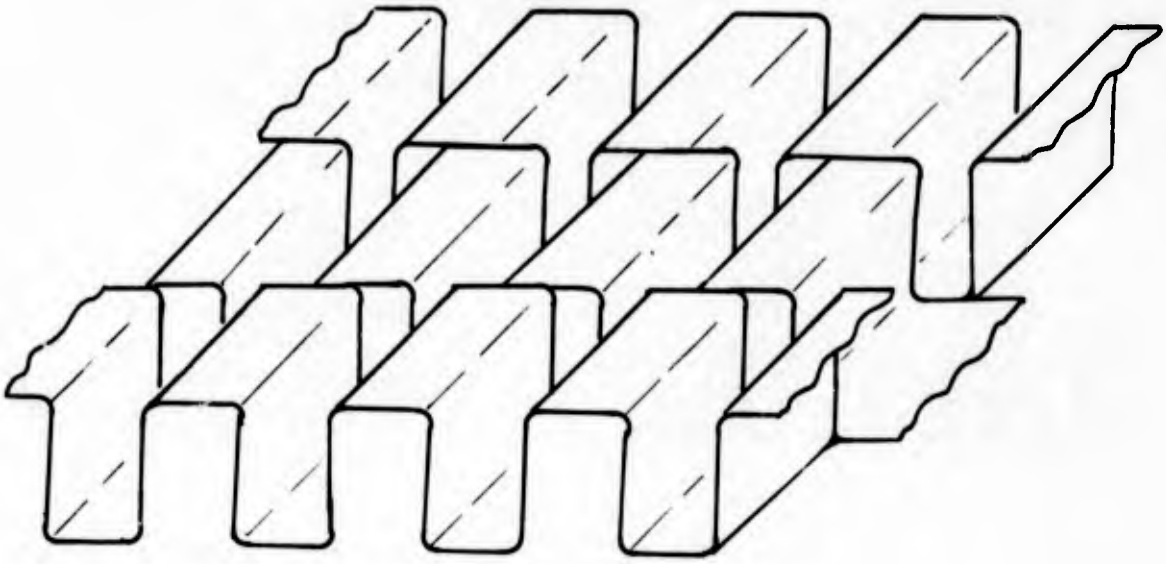

Figure 129 – Serrated Foil

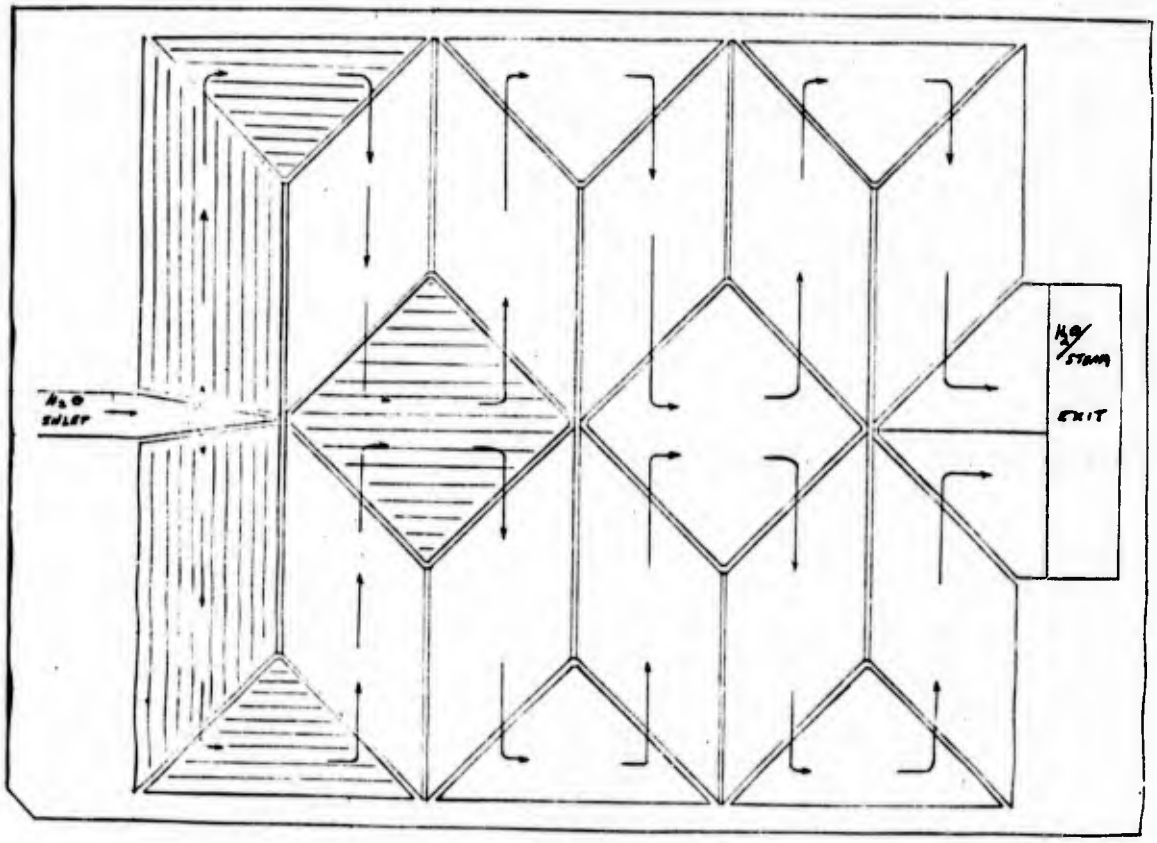

Figure 130 – Serrated Metal Foil Cooler Flow Pattern

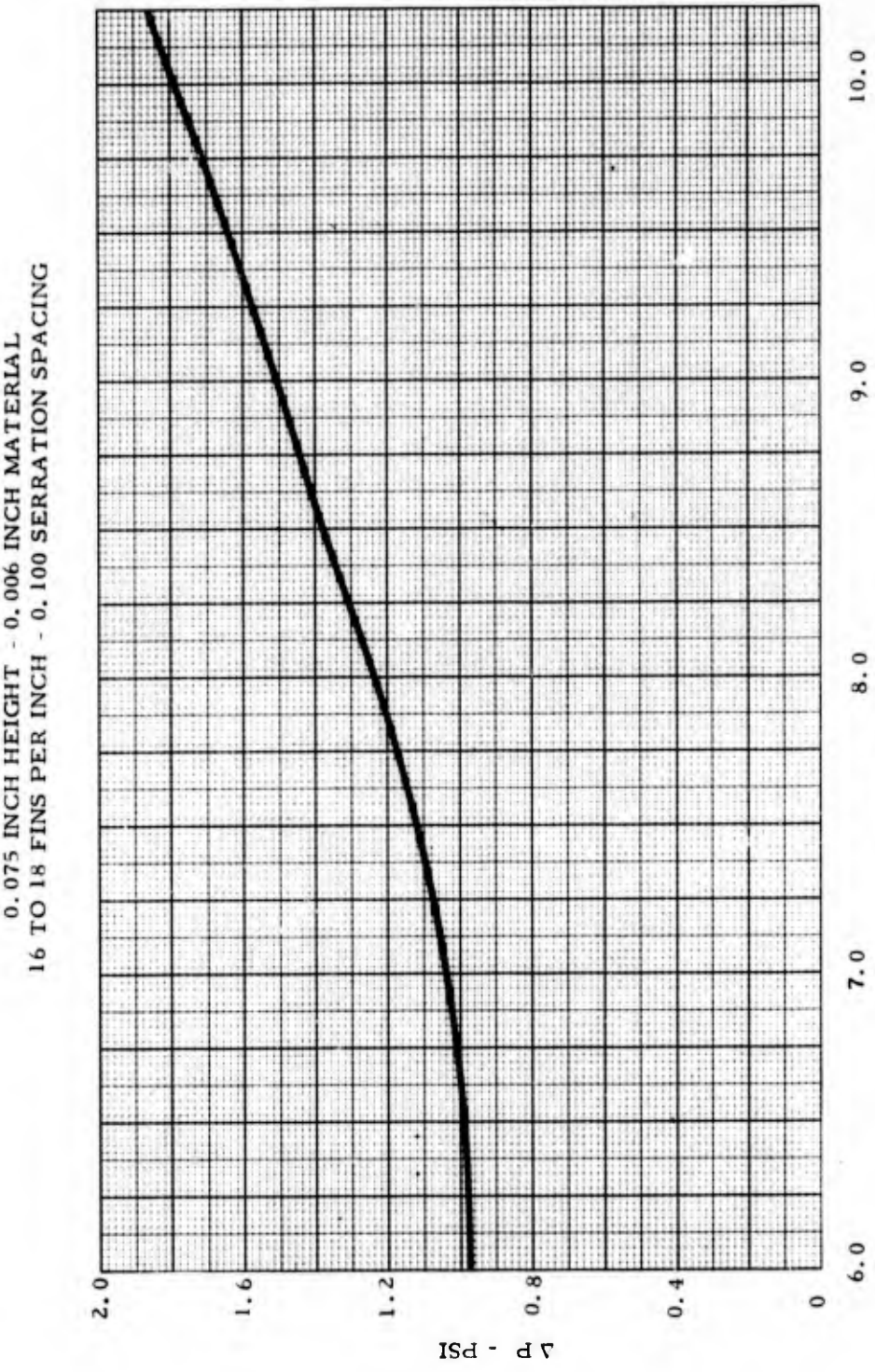

Figure 131 — Serrated Foil Field Pressure Drop

Astrel was selected for subsequent development units because even though it is slightly more dense than polysulfone, it has a higher temperature capability (500°F for Astrel vs. 340°F for polysulfone) and is much less susceptible to stress cracking. However because of difficulty in obtaining sheet stock, Astrel cooler and hydrogen fields were not incorporated into Development Units 2 and 3 which continued to use polysulfone fields.

When Astrel sheet stock was received it was machined to the same field patterns as the polysulfone and tested in Development Units 4 and 5. In these tests the Astrel was less prone to stress-cracking and no shrinkage or heat distortion was encountered. The Astrel fields incorporated into Development Unit 4 are shown in Figures 132 and 133.

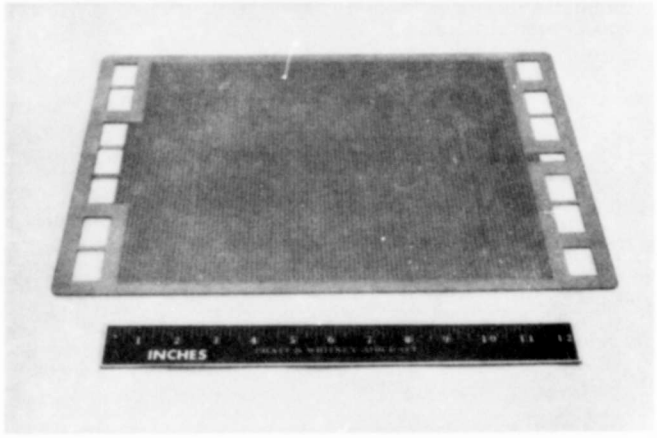

Figure 132 – Astrel Cooler Flow Field

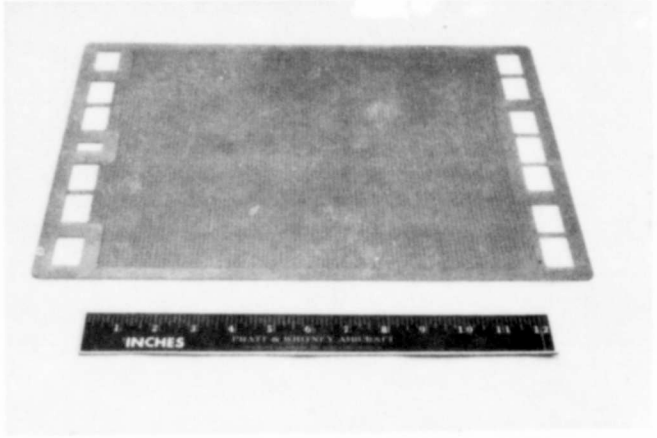

Figure 133 – Astrel Hydrogen Flow Field

6. Development Unit Assembly Methods

The stackup for Development Unit 1 is shown in Figure 134. Fiberglass frames were used to house machined polysulfone coolant and hydrogen flow fields. It was sealed with butyl rubber gaskets between mating component frames. Hypon, a low temperature curing epoxy adhesive, was used to mount the butyl gaskets and to keep them from slipping or blowing out under pressure. However, gasket displacement was a problem during the tests of Development Unit 1 and was attributed to breakdown of the Hypon at the operating temperature. An improved high temperature adhesive was obtained. This adhesive, a P&WA formulation of Novalac epoxy cured polybutadiene nitrile rubber, was successfully tested in bench trails with 4 1/2 x 4 1/2 in. single cell end plates. A dummy stack containing the butyl gaskets, nickel foil, and fiberglass sealing surfaces of the test unit was fabricated. The bench test was sealed with an 88 psi seal load. A pressure test was conducted at 45 psia and 200°F and the rig was then held at 45 psig and 270°F for two hours without leaks. This new adhesive was used to rebuild Development Unit 1 for additional testing.

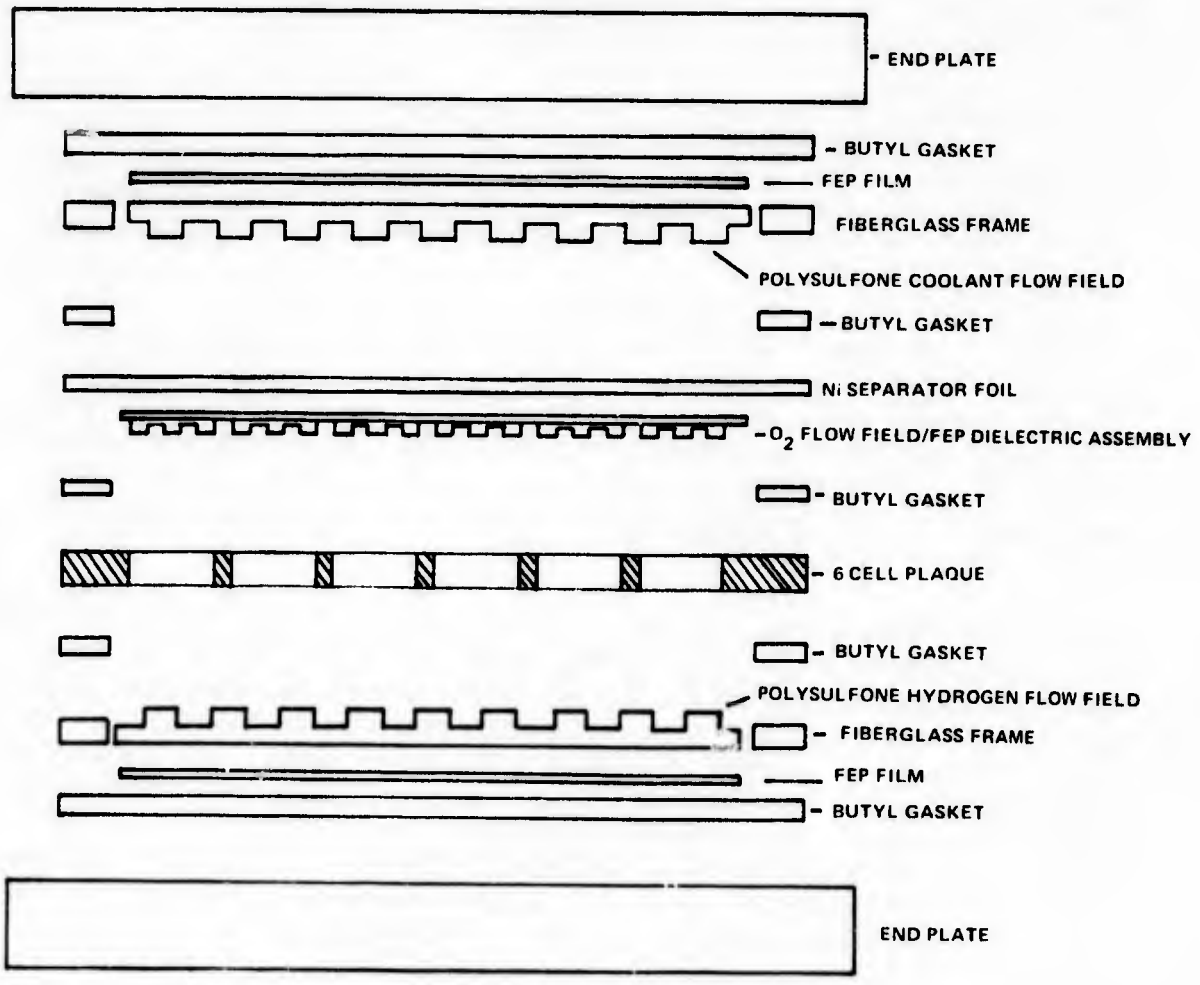

Figure 134 -- Development Unit Assembly Stackup

The test was completed at design temperature and pressure with no external leakage. Post test analysis however, showed that poor end-cell performance in the development unit was due to poisoning of the electrode by the combination of butyl rubber gaskets and the polybutadiene rubber sealing material. Independent bench tests indicated that neither the butyl rubber gasket nor the polybutadiene rubber sealing material exposed to the electrode separately were sufficient to poison the electrodes.

To overcome the electrode poisoning problem a revised gasket formulation of ethylene propylene was laboratory tested together with the polybutadiene rubber sealing material to determine any electrode poisoning effects. It was found that his combination had little poisoning effect. A new curing process was also defined which included a nitrogen purge during cure to further reduce any deleterious effects of the gasket adhesive interaction. This combination of sealing materials was incorporated into Development Unit 2. No significant external leakage was experienced but post-test examination revealed partial plugging of the oxygen ports with adhesive and partial coverage of the end cells with adhesive. With the problem of potential electrode poisoning and the flow of adhesive into ports and onto electrodes, it was decided to eliminate all rubber and adhesive combinations from the assembly. This required a change to a one piece laminated plaque and cooler assembly.

Development Unit 3 was assembled with all laminated construction. It consisted of a single six-cell plaque, an oxygen field/cooler assembly, two end caps, and steam and hydrogen field frames. Each of these component parts was fabricated separately of epoxy/fiberglass laminations and cured at standardized conditions. The five bonds required to assemble the unit were made with 2-mil epoxy/fiberglass bonding layers cured at temperature and under pressure. A sketch of the layup appears in Figure 135. To develop and verify bonding procedures a set of trial parts was assembled and pressure tested. They successfully underwent thermal cycling and pressure testing to 40 psig. The Configuration 2 six-cell plaque development unit was bonded in the same manner. It was pressure and heat cycled to 275°F for 24 hours while mounted between end plates with "O" ring seals. No leakage was noted either before or after filling with electrolyte. Upon heatup to 250°F, for an operating test, it developed two external oxygen leaks. Examination and inspection of the unit showed that the leakage had occurred in the bonding joint between the plaque and cooler assemblies and was due to delamination of the bond.

At this point, a reevaluation of the bonding technique, including surface preparation, methods, and curing temperature and pressure was made. At the same time, analytical study was undertaken to determine the theoretical stresses induced in the assembly by temperature and pressure cycling and the tolerance buildup between mating parts. The results indicated that the sum of the stresses due to pressure, temperature, and tolerance buildup did not exceed 100 psi. A series of test samples, using various surface preparations, and curing temperatures and pressures, were prepared and subjected to structural tests to evaluate bond strength. The shear strength test results on the various samples showed that most of these bonds exceeded the strength of the laminates themselves giving a useable value of over 1000 psi for the system. Since the design analysis indicated that induced stresses were less than 100 psi, it was concluded that inadequate surface preparation was responsible for the delaminations experienced in earlier trials. To correct this problem, a detailed surface preparation procedure which stressed cleanliness in all steps was prepared. This procedure was followed to for all subsequent development unit bonds.

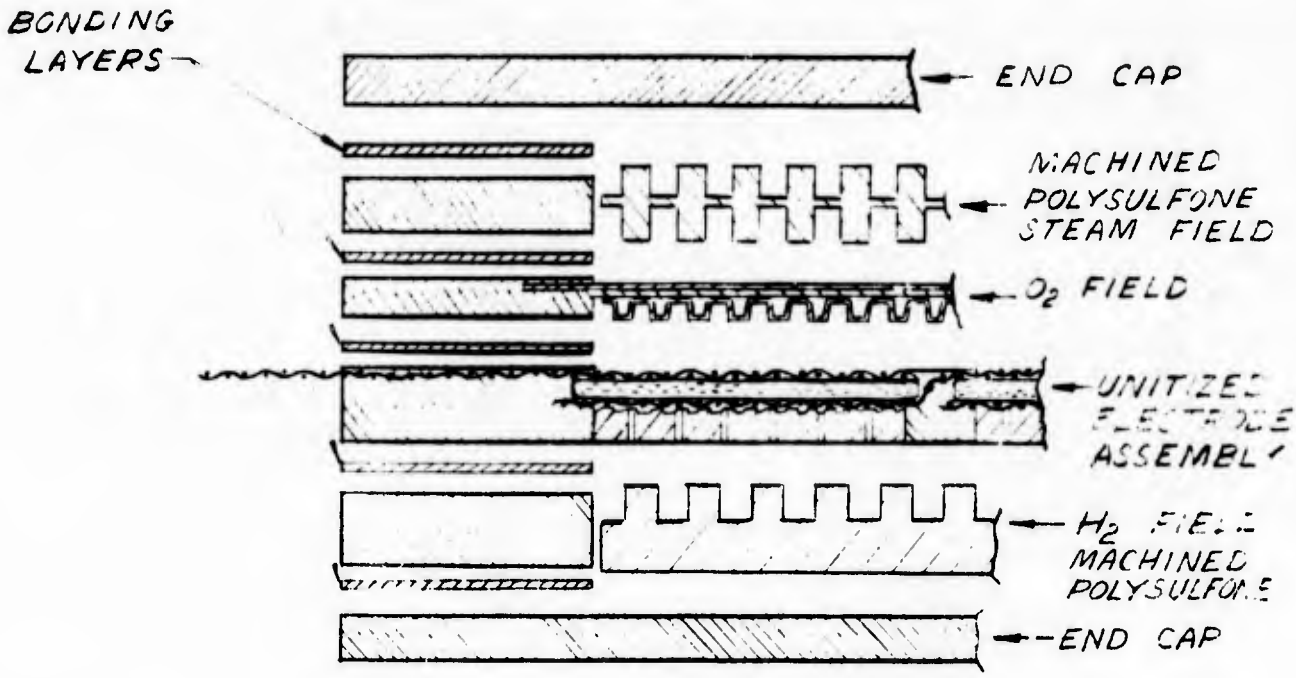

Figure 135 – Bonded Development Unit Assembly

A simulated plaque was then assembled using 2-mil bonding layers together with a film of Hypon epoxy on each side to provide additional wetting and adherence. In addition, to insure more uniform loading of the bonded joints, rubber gaskets were placed between the endplates and the simulated plaque to spread compressive load evenly. The unit was heat and pressure cycled several times with no leakage or evidence of delamination.

Development Unit 3 was bonded with the improved bonding procedures. During heatup it developed a leak, however, the leakage was not due to bond delamination. It was caused by displacement of the gasket between the endcap and the top end plate.

To remedy this situation, the rubber gasket material was changed to a more temperature-compatible material (silicon rubber) and the surfaces of the endcaps were roughened. No further leakage was noted after making these modifications. All subsequent development units were assembled in this way and were tested for extended periods with no leakage. Post test examination of the development units showed the bonds were good and there was no evidence of leakage or delamination.

D. DEVELOPMENT UNIT TESTING

1. Introduction

The objective of the Development Unit Testing activity was to demonstrate operation of the repeating section of a full-size stack at Reference System design power densities. A complete repeating section development unit consisting of two 6-cell plaques and an evaporative cooler

was operated at a power density of 2265 WSF, 5 percent higher than the goal power density. In all, five development units were tested, see Table XXXV. More than 60 simulated missions were demonstrated, with 50 simulated missions accumulated on one unit.

TABLE XXXV

HIGH POWER DENSITY DEVELOPMENT UNIT TEST SUMMARY

Development Unit No.	Rig No.	Features	Cell Stack Design Specific Weight (lbs/kw) @ 2150 WSF	Max. Demon. Power Density (watts/ft^2)	No. Starts	Total Load Time (hrs)	3000 ASF Load Time (min)
1	38410	Single Plaque Configuration 1	0.95	1030	4	16.7	0
2	38465	Single Plaque Configuration 2	0.76	1200	3	5.1	0
3	38622	Single Plaque Configuration 2	0.73	2040	2	6.7	1
4	38668	Single Plaque Configuration 3	0.69	2050	6	29	25
5	38781	Dual Plaque Configuration 3	0.67	2265	10	10.7	5

The first three cell configurations developed through Strip Cell testing, see Section IVB, were incorporated into development units and tested. The last unit had cells of Configuration 3 and achieved an equivalent cell stack specific weight of 0.67 lb/kw. The lightest cell design, Configuration 4, remains to be tested at the development unit level. The weights of each of these cell configurations is itemized in Table XXXVI. Incorporation of the Configuration 4 Cell, demonstrated in the strip cell tests, into a development unit would reduce repeating unit weight to 0.45 lb/kw at the Reference System design power density. This is the next step in the development of the stack repeating section.

2. Development Unit Test Equipment

To permit testing of development units a facility with rapid high current switching and rapid data acquisition capability was required. The equipment used consisted of an especially constructed test stand and a data link to Power Utility's Automatic Data Acquisition and Recording computer system.

A high current solid-state switch was built expressly for this testing and had the capability to switch up to 500 amperes. It was used to switch between open circuit and preselected loads. The on-load and off-load times were individually programable for time durations of 1 second minimum to 15 seconds maximum. The stand also contained instrumentation for control of pressures, temperatures, and flows and monitoring individual cell voltages and loads.

TABLE XXXVI

DEVELOPMENT UNIT CONFIGURATIONS

Item	Configuration 1	Configuration 2	Configuration 3	Configuration 4
2 - 6 Cell Plaques				
Substrates	†0.30 lbs (100x100 Mesh)	†0.23 lbs (50x100 Mesh)	†0.23 lbs	†0.23 lbs
Catalyst	†0.12	†0.11	†0.11	†0.11
Matrix	†0.06 (10-Mil RAM)	†0.06	†0.06	0.03
Electrolyte	0.10	0.10	0.10	C.06
Frame	0.11 (Epoxy/Fiberglass 5-Mils Pinch)	0.11	0.11	0.09
	0.69 lbs	0.61 lbs	0.61 lbs	0.52 lbs
H_2 Flow Field/ERP				
Field Insert	0.14 (Polysulfone)	†0.18 (Astrel)	†0.18	0.09 (Plated Porous Polysulfone ERP/H_2 Flow Fields 0.025 Field Depth)
Field Frame	0.16 (Epoxy/Fiberglass)	†0.16	†0.16	
ERP	†0.67 (30-Mil Ni)	†0.47 (20-Mil Ni)	†0.17 (20-Mil Polysulfone)	0.11 (Epoxy/Fiberglass Frame)
Electrolyte	0.084	0.05	0.01	0.01
ERP Frame	0.21 (Epoxy/Fiberglass)	0.14	0.14	
	1.26 lbs	1.00 lbs	0.66 lbs	0.21 lbs
Coolant Flow Field				
Field Insert	0.09 (Polysulfone)	†0.11 (Astrel)	†0.11	0.07 (Unplated Porous Polysulfone 20-Mil Flow Field)
Frame	0.09 (Epoxy/Fiberlass)	†0.09	†0.09	0.09 (Epoxy/Fiberglass Frame)
	0.18 lbs	0.20 lbs	0.20 lbs	0.16 lbs
O_2 Flow Field/Cooler Assembly				
Field Insert	†0.27 (Ni-plated Magnesium)	†0.16 (Electroformed Ni Without Backfill)	†0.16	†0.16
Separator	0.23 (3-Mil Ni)	0.08 (1-Mil Ni)	0.08	0.08
Frame	0.11 (Epoxy/Fiberglass)	†0.15	†0.15	†0.15
Dielectric	0.08 (FEP)	0.04 (Epoxy/Fiberglass)	0.04	0.04
	0.69 lbs	0.43 lbs	0.43 lbs	0.43 lbs
Repeating Unit Weight	2.82 lbs	2.14 lbs	1.89 lbs	1.32 lbs
Lbs/kw at 2.15 kw/ft^2	0.95	0.73	0.64	0.45

†Actual Weights

The test stand constructed and used for development unit testing is shown in Figures 136 and 137. A schematic of the stand is shown in Figure 138.

It provides:

1) Reactant and coolant capability for closed loop testing up to 13.5 kw, equivalent to a 5 repeating unit stack.

2) Reactant conditioning capability to run at open cycle conditions to 2.7 kw.

3) Rapid solenoid switching from saturated to dry gases and to various bypass modes.

4) Two levels of load: Open circuit to 25 amp loads set by a Tafel-IR diagnostic resistive load system and open circuit to 500 amp loads set with an external power supply. Relay switching between the two systems permit diagnostics to be performed at anytime during a test.

Coupled to the stand was an Automatic Data Acquisition and Recording (ADAR) computer link. The ADAR capability was initially installed on the test stand to meet two objectives:

1) Provide for periodic data acquistion during continuous endurance tests, and

2) Provide for continuous data acquisition during short-term high power density operation.

The data was acquired and recorded on a Hewlett-Packard 2100 series computer incorporating an HP 2402 data acquisition subsystem, see Figure 139. This system had the capability of recording at 14 channels/second with an accuracy of ± 0.02 percent of full scale. A total of 45 parameters was selected for automatic recording: 24 temperatures, 4 pressures, 16 voltages, and current. The computer was also programmed to calculate load and to sum and average cell voltages.

A typical data printout and key are shown in Figure 140. This data display was automatically printed out each time a data recording was made. The frequency of readings was programmable and typically 15 minute intervals were used for the lower power continuous testing. This format was also the output from any unscheduled data acquisition.

In addition to the scheduled data acquisitions with complete printouts, a fast scan program was established. When this program was used, the computer scanned the data every ten seconds until the load dropped below 50 amps or until 89 readings had been taken. Fast scan data was stored on a magnetic disc. The program provided for a paper tape and two printout options. Figure 141 shows a typical fast scan printout.

As the program evolved to pulsed high power operation, the fast scan program became unsuitable because it provided for data scanning only once every 10 seconds while the program missions for pulsed operation included on-load times as short as two seconds.

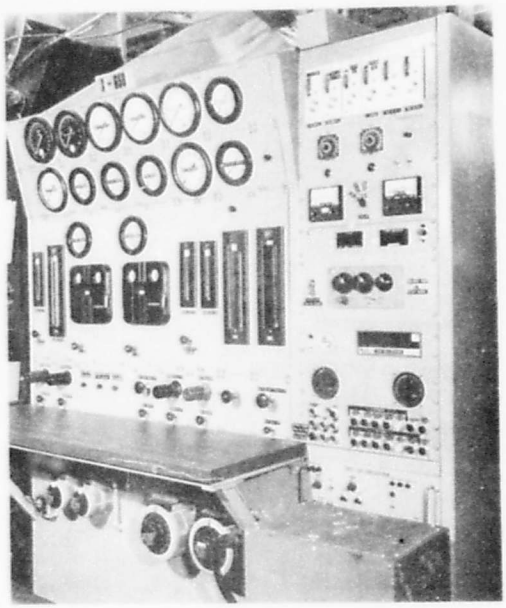

Figure 136 – Development Unit Test Stand (Front)

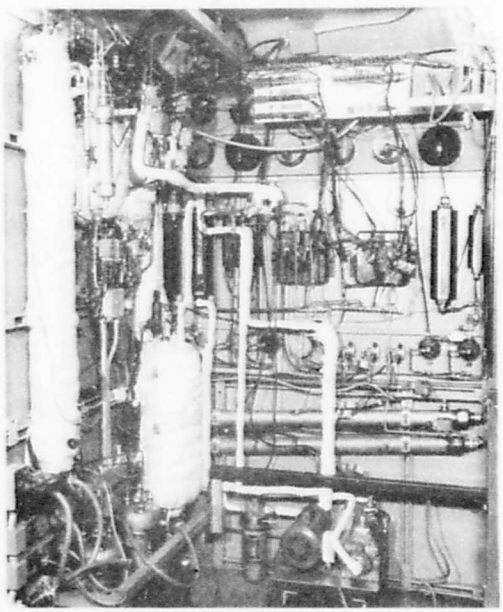

Figure 137 – Development Unit Test Stand (Back)

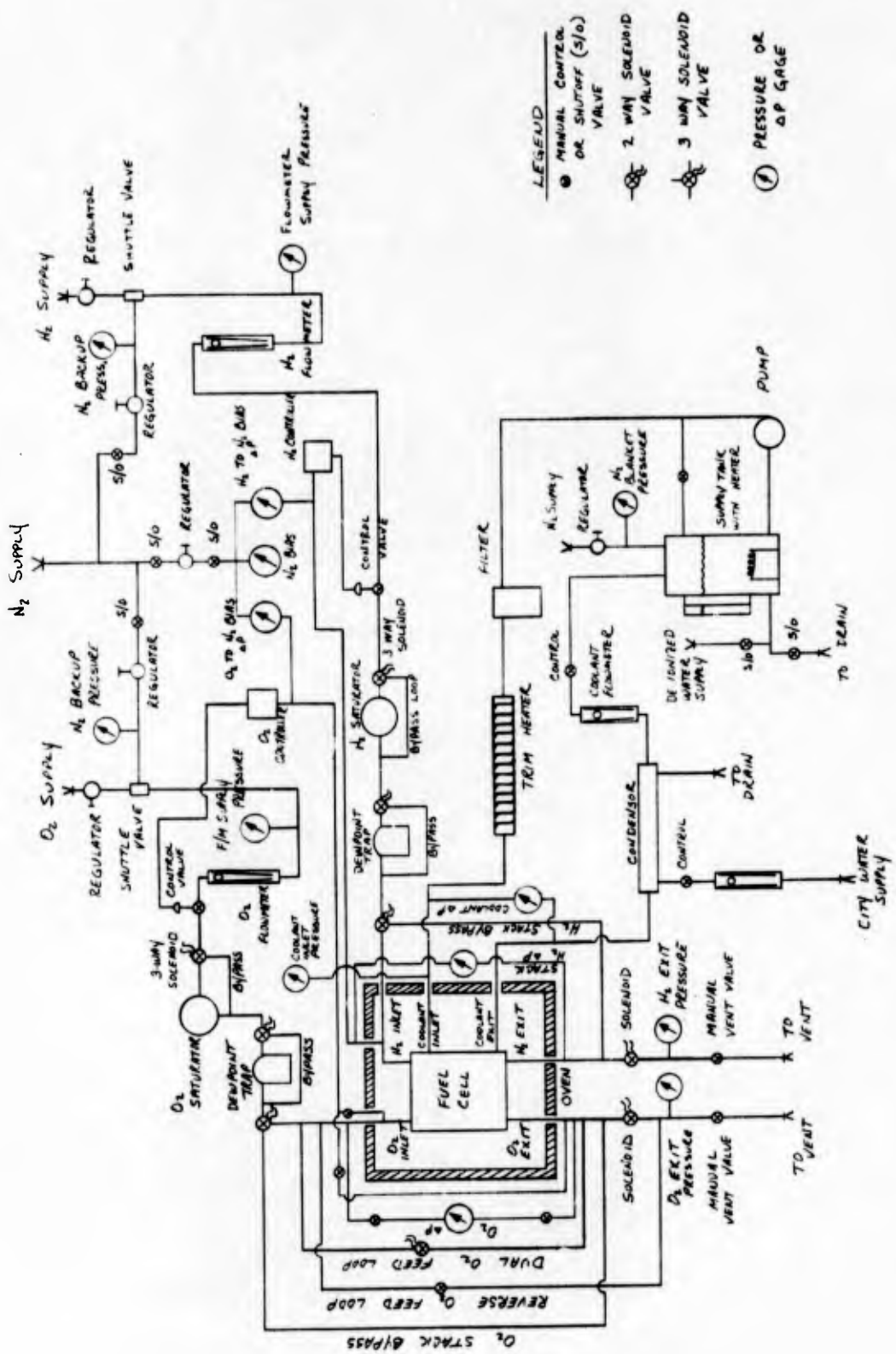

Figure 138 – Development Unit Test Stand Schematic

Figure 139 – Data Acquisition Computer System

*** HPD PLAQUES ***

RIG 38668-4 STAND X-658 DATE 10/23/74 TIME 12 9

AMPS	ASF	T-VLT	T-PWR	B-VLT	B-PWR	S-VLT	AVE	P1-VLT	P2-VLT
169.70	1488.6	4.703	798.1	4.668	792.1	4.703	.784	4.705	.000

CELL VOLTAGES:

1	2	3	4	5	6
.772	.786	.782	.792	.788	.782

PRESSURES:

OP-3	HP-3	CP-1	CP-3
.000	.000	.000	.000

TEMPERATURES: (DEG.F)

HT-5	HT-6	HT-4	OT-5	OT-6	OT-4	CT-1	CT-2	ST-1	ST-2	ST-3	ST-4
214.	255.	162.	254.	258.	160.	246.	608.	262.	259.	261.	259.

HT-3	HT-2	HT-1	OT-3	OT-2	OT-1	CT-4	CT-5	CT-6	ST-5	ST-6	ST-7
172.	180.	91.	175.	191.	96.	219.	243.	112.	261.	240.	252.

The abbreviations used for X-658 High Power Density printouts are shown below.

H. P. D. PRINTOUT ABBREVIATIONS

AMPS	ASF	T-VLT	T-PWR	B-VLT	B-PWR	S-VLT	AVE	P1-VLT	P2-VLT
LOAD CURRENT	AMPS PER SQUARE FOOT	TOTAL PLAQUE VOLTAGE	TOTAL PLAQUE POWER	BUS VOLTAGE	BUS POWER	SUM OF CELL VOLTAGE	AVERAGE CELL VOLTAGE	PLAQUE 1 VOLTAGE	PLAQUE 2 VOLTAGE

CELL VOLTAGES:

PRESSURES:

OP-3	HP-3	CP-1	CP-3
OXYGEN CELL ΔP	HYDROGEN CELL ΔP	COOLANT CELL EXIT	COOLANT CELL ΔP

TEMPERATURES: (DEG. F)

HT-5	HT-6	HT-4	OT-5	OT-6	OT-4	CT-1	CT-2	ST-1	ST-2	ST-3	ST-4
H_2 STACK INLET	H_2 STACK EXIT	H_2 TRAP DEW POINT	O_2 STACK INLET	O_2 STACK EXIT	O_2 TRAP DEW POINT	COOLANT INLET	COOLANT EXIT	STACK	STACK	STACK	STACK

HT-3	HT-2	HT-1	OT-3	OT-2	OT-1	CT-4	CT-5	CT-6	ST-5	ST-6	ST-7
H_2 SATURATOR GAS	H_2 SATURATOR WATER	H_2 FLOW METER	O_2 SATURATOR GAS	O_2 SATURATOR WATER	O_2 FLOW METER	COOLANT SUPPLY TANK	COOLANT TRIM HEATER	COOLANT CONDENSER EXIT	STACK	STACK	STACK

Figure 140 – High Power Density Data Printout

*

** STAND **

658,1

** OK **

TO DUMP H.P.D.(X-658) STORED READINGS:

1 : AREA TTY
2 : PUNCH AT CENTRAL (CALL A.D.A.R. PERSONEL FIRST)
3 : CONSOLE AT CENTRAL (CALL A.D.A.R. PERSONEL FIRST)
4 : EXIT

INPUT OPTION:

1

*** HPD PLAQUES ***

RIG CHECKOUT STAND X-658 DATE 4/30/73 TIME 1511

					CELL VOLTAGES:					
AMPS	T-VLT	T-PWR	B-VLT	B-PWR	1	2	3	4	5	6
342.00	3.600	1231.2	3.400	1162.8	.601	.603	.600	.598	.601	.599
342.00	3.600	1231.2	3.400	1162.8	.601	.603	.600	.598	.601	.599
342.00	3.600	1231.2	3.400	1162.8	.601	.603	.600	.598	.601	.599
342.00	3.600	1231.2	3.400	1162.8	.601	.603	.600	.598	.601	.599
342.00	3.600	1231.2	3.400	1162.8	.601	.603	.600	.598	.601	.599
342.00	3.600	1231.2	3.400	1162.8	.601	.603	.600	.598	.601	.599
342.00	3.600	1231.2	3.400	1162.8	.601	.603	.600	.598	.601	.599
342.00	3.600	1231.2	3.400	1162.8	.601	.603	.600	.598	.601	.599
342.00	3.600	1231.2	3.400	1162.8	.601	.603	.600	.598	.601	.599
342.00	3.600	1231.2	3.400	1162.8	.601	.603	.600	.598	.601	.599

*** HPD PLAQUES ***

RIG CHECKOUT STAND X-658 DATE 4/30/73 TIME 1511

						PRESSURES:			
7	8	9	10	11	12	OP-3	HP-3	CP-1	CP-3
.000	.000	.000	.000	.000	.000	.000	.000	.000	.000
.000	.000	.000	.000	.000	.000	.000	.000	.000	.000
.000	.000	.000	.000	.000	.000	.000	.000	.000	.000
.000	.000	.000	.000	.000	.000	.000	.000	.000	.000
.000	.000	.000	.000	.000	.000	.000	.000	.000	.000
.000	.000	.000	.000	.000	.000	.000	.000	.000	.000
.000	.000	.000	.000	.000	.000	.000	.000	.000	.000
.000	.000	.000	.000	.000	.000	.000	.000	.000	.000
.000	.000	.000	.000	.000	.000	.000	.000	.000	.000
.000	.000	.000	.000	.000	.000	.000	.000	.000	.000

*** HPD PLAQUES ***

RIG CHECKOUT STAND X-658 DATE 4/30/73 TIME 1511
TEMPERATURES:

HT-5	HT-6	HT-4	OT-5	OT-6	OT-4	CT-1	CT-2	ST-1	ST-2	ST-3	ST-4
288.	293.	298.	304.	309.	314.	319.	324.	329.	334.	339.	344.
288.	293.	298.	304.	309.	314.	319.	324.	329.	334.	339.	344.
288.	293.	298.	304.	309.	314.	319.	324.	329.	334.	339.	344.
288.	293.	298.	304.	309.	314.	319.	324.	329.	334.	339.	344.
288.	293.	298.	304.	309.	314.	319.	324.	329.	334.	339.	344.
288.	293.	298.	304.	309.	314.	319.	324.	329.	334.	339.	344.
288.	293.	298.	304.	309.	314.	319.	324.	329.	334.	339.	344.
288.	293.	298.	304.	309.	314.	319.	324.	329.	334.	339.	344.
288.	293.	298.	304.	309.	314.	319.	324.	329.	334.	339.	344.
288.	293.	298.	304.	309.	314.	319.	324.	329.	334.	339.	344.

Figure 141 – Fast Scan Printout

A faster scan program was written to provide for continuous reading of selected parameters for 90 seconds. The parameters scanned were 12 cell voltages, 2 plaque voltages, 1 total voltage, and 1 current. The calculations the program made were: 1) the current density in ASF, 2) the sum of plaque voltages, and 3) the total power based on the sum of plaque voltages. Figure 142 shows a typical printout for this program. For shorter pulses this data was augmented with a 12-channel strip chart recorder.

3. Test Program

Development Unit 1

The first single plaque development unit to be tested was of the Configuration 1 design as itemized in Table XXXVI. The specific weight of repeating units of this design is 0.95 lb/kw when operated at the Reference System design power density of 2150 WSF. The unit consisted of one 6-cell plaque, as shown in Figure 143, a cooler assembly as shown in Figure 144, and machined polysulfone hydrogen and cooler fields as shown in Figures 145 and 146. The assembly order of these parts with gaskets, end plates, and spacers is shown in Figure 147. Figure 148 shows the assembled and instrumented test unit prior to installation in the test stand. Each cell consisted of a 30-mil thick reconstituted asbestos matrix, a 635°F sintered PPF anode, and a gold-platinum catalyzed cathode. The electrode substrates were 100 x 100 mesh 2-mil thick nickel wire screens plated with 0.5 mil of silver in the active area and 1.0 mil in the frame and intercell seal areas. The cooler assembly consisted of chemically milled magnesium oxygen fields, plated with nickel for corrosion protection, and bonded with an FEP film to a 3-mil thick nickel-foil backup sheet. Crazing problems were encountered with the polysulfone flow fields where they were in contact with the butyl rubber gaskets. Consequently the edges were machined from the fields and epoxy/fiberglass frames were installed around the fields isolating them from contact with the butyl gaskets.

The initial testing of the unit was limited to 200°F and 100 ASF as a precaution since this was the first development unit tested in the program. Following heatup and electrolyte conditioning on saturated gases, the initial voltage at 100 ASF was 5.81 v. The individual cell voltages were as follows:

Cell	1	2	3	4	5	6
Voltage	0.965	0.963	0.961	0.975	0.975	0.974

After approximately two hours on load at 100 ASF, standard Tafel data and IR diagnostics were taken. The resulting low current density calibration is shown in Figure 149. A graphic log of the entire test is shown in Figures 150 and 151.

RIG 387#1=1 START 1=658 DATE 12/ 4/74 TIME 1124

M	S	ARMS	ASP	T=VLT	P=SUM	T=PWR	PL=1	PL=2	C=1	C=2	C=3	C=4	C=5	C=6	C=7	C=8	C=9	C=10	C=11	C=12	M	M
111221	3	.00	5.0	13,436	13,435	6.9	6,750	6,685	1.128	1.125	1.124	1.125	1.126	1.124	1.071	1.122	1.115	1.121	1.125	1.130	111221	3
111221	5	.02	.2	13,436	13,436	.3	6,750	6,685	1.128	1.125	1.125	1.125	1.126	1.125	1.070	1.122	1.115	1.121	1.125	1.130	111221	5
111221	6	.03	.3	13,436	13,438	.4	6,751	6,686	1.128	1.125	1.125	1.126	1.126	1.125	1.071	1.122	1.115	1.121	1.125	1.130	111221	6
111221	8	.15	1.1	13,438	5,912	.7	2,105	2,028	1.128	1.125	1.125	1.126	1.126	1.125	1.071	1.122	1.115	1.121	1.125	1.130	111221	8
111221	9	366.62	3217.7	4,991	5,012	2458.4	2,546	3,065	.494	.489	.364	.374	.417	.542	.514	.484	.491	.489	.497	.548	111221	9
11122110		366.25	3335.5	5,038	5,071	2278.3	2,763	3,207	.491	.453	.441	.432	.404	.394	.543	.514	.517	.519	.521	.569	11122110	
11122112		366.88	3393.4	5,951	6,217	2485.8	2,993	3,314	.514	.481	.493	.483	.469	.424	.566	.533	.538	.539	.535	.578	11122112	
11122113		391.44	3433.7	6,189	6,378	2496.8	2,994	3,385	.529	.504	.480	.486	.446	.443	.588	.558	.553	.552	.545	.586	11122113	
11122114		393.73	3453.8	6,338	6,476	2549.8	3,041	3,435	.535	.519	.501	.499	.514	.453	.586	.561	.564	.560	.554	.596	11122114	
11122115		395.28	3467.4	6,419	12,743	5937.1	6,387	6,356	.535	.989	1.016	1.026	1.035	1.036	1.029	1.053	1.046	1.051	1.056	1.060	11122115	
11122116		.07	.6	12,826	12,989	.6	6,521	6,468	1.073	1.074	1.076	1.077	1.082	1.076	1.056	1.081	1.074	1.076	1.080	1.085	11122116	
11122117		.05	.4	13,024	13,112	.7	6,588	6,525	1.091	1.090	1.092	1.093	1.096	1.092	1.057	1.093	1.086	1.088	1.092	1.096	11122117	
11122118		.01	.1	13,134	13,169	.1	6,629	6,564	1.101	1.099	1.101	1.102	1.104	1.101	1.061	1.103	1.093	1.095	1.100	1.104	11122118	
11122119		.13	1.1	13,282	13,236	1.7	6,655	6,582	1.107	1.105	1.106	1.107	1.110	1.106	1.063	1.104	1.097	1.100	1.104	1.108	11122119	
11122121		392.40	3446.1	5,892	6,259	2458.8	2,984	3,355	.475	.496	.430	.471	.465	.415	.562	.542	.554	.544	.540	.587	11122121	
11122122		392.43	3449.4	6,281	6,456	2533.4	3,032	3,424	.517	.522	.479	.504	.506	.452	.579	.560	.567	.558	.552	.594	11122122	
11122123		394.84	3463.5	6,417	6,554	2587.7	3,092	3,462	.528	.534	.494	.517	.521	.469	.586	.574	.576	.565	.557	.596	11122123	
11122124		395.23	3475.7	6,498	6,596	2613.4	3,114	3,482	.531	.541	.502	.524	.528	.476	.589	.576	.582	.571	.561	.599	11122124	
11122125		396.57	3487.7	6,527	6,609	2620.9	3,117	3,492	.534	.546	.505	.528	.530	.475	.588	.579	.586	.572	.563	.601	11122125	
11122126		396.85	3491.4	6,538	12,717	5947.4	6,373	6,343	.527	.552	1.003	1.018	1.034	1.028	1.025	1.049	1.045	1.048	1.053	1.057	11122126	
11122127		.01	.1	12,799	12,975	.1	6,515	6,468	1.071	1.072	1.074	1.076	1.081	1.077	1.049	1.080	1.073	1.078	1.079	1.082	11122127	
11122129		.14	1.2	13,014	13,142	1.5	6,584	6,518	1.098	1.089	1.092	1.092	1.095	1.092	1.057	1.092	1.086	1.087	1.091	1.094	11122129	
11122130		.01	.1	13,122	13,175	.1	6,624	6,552	1.104	1.098	1.101	1.101	1.104	1.101	1.061	1.098	1.092	1.094	1.098	1.101	11122130	
11122131		.11	1.0	13,189	13,224	1.5	6,659	6,574	1.106	1.104	1.106	1.106	1.106	1.105	1.062	1.103	1.097	1.098	1.103	1.106	11122131	
11122132		388.90	3411.9	6,281	6,478	2519.4	3,043	3,435	.497	.530	.457	.513	.488	.450	.575	.563	.576	.559	.550	.593	11122132	
11122133		394.97	3456.8	6,458	6,595	2599.4	3,122	3,473	.522	.546	.485	.541	.520	.479	.585	.573	.583	.568	.558	.598	11122133	
11122134		395.61	3472.0	6,552	6,644	2629.8	3,151	3,493	.526	.553	.496	.544	.537	.488	.587	.580	.589	.573	.562	.599	11122134	
11122135		397.27	3484.6	6,582	6,644	2639.5	3,146	3,498	.525	.550	.499	.540	.541	.489	.586	.583	.592	.575	.564	.601	11122135	
11122137		397.15	3482.9	6,580	6,628	2631.6	3,132	3,496	.521	.550	.499	.538	.542	.485	.583	.584	.594	.575	.564	.600	11122137	
11122138		396.51	3478.2	6,562	12,706	5938.4	6,369	6,337	.516	.550	.494	1.014	1.031	1.025	1.023	1.047	1.044	1.048	1.052	1.055	11122138	
11122140		.06	.5	12,793	12,972	.8	6,516	6,457	1.071	1.073	1.076	1.075	1.081	1.076	1.048	1.079	1.074	1.079	1.082	1.085	11122140	
11122141		.01	.1	13,008	13,097	.1	6,584	6,514	1.098	1.089	1.092	1.092	1.095	1.092	1.055	1.091	1.086	1.086	1.091	1.093	11122141	
11122142		.01	.1	13,118	13,172	.1	6,624	6,548	1.108	1.098	1.101	1.101	1.103	1.100	1.059	1.098	1.092	1.093	1.098	1.100	11122142	
11122143		.07	.6	13,186	13,221	.9	6,650	6,578	1.106	1.104	1.107	1.106	1.105	1.105	1.061	1.102	1.097	1.098	1.102	1.105	11122143	
11122144		391.56	3434.7	6,382	6,544	2582.2	3,085	3,458	.494	.542	.481	.526	.511	.474	.577	.566	.585	.565	.554	.596	11122144	
11122145		394.66	3461.9	6,507	6,638	2616.8	3,145	3,485	.516	.556	.486	.545	.534	.489	.582	.577	.594	.572	.561	.599	11122145	
11122146		396.53	3478.3	6,577	6,651	2637.3	3,155	3,496	.519	.561	.489	.547	.544	.493	.583	.581	.594	.575	.563	.600	11122146	
11122147		396.83	3479.2	6,589	6,644	2635.4	3,148	3,498	.516	.563	.491	.548	.546	.498	.581	.583	.596	.575	.563	.599	11122147	
11122148		396.98	3474.5	6,577	6,623	2623.2	3,128	3,494	.511	.563	.490	.546	.548	.484	.578	.583	.597	.575	.563	.600	11122148	
11122149		395.27	3467.3	6,558	12,742	5936.4	6,394	6,351	.915	1.007	1.024	1.029	1.041	1.034	1.027	1.052	1.048	1.050	1.055	1.059	11122149	
11122150		.15	1.3	12,829	12,988	1.9	6,527	6,462	1.074	1.075	1.079	1.078	1.083	1.078	1.048	1.080	1.078	1.078	1.080	1.083	11122150	
11122151		.14	1.2	13,022	13,107	1.8	6,591	6,516	1.092	1.091	1.094	1.095	1.097	1.093	1.055	1.092	1.086	1.087	1.092	1.094	11122151	
11122152		.14	1.2	13,128	13,179	1.8	6,631	6,548	1.101	1.100	1.103	1.102	1.105	1.101	1.059	1.098	1.092	1.093	1.098	1.101	11122152	
11122153		.15	1.3	13,191	6,416	1.9	2,984	3,433	1.107	1.105	1.108	1.107	1.109	1.105	1.060	1.102	1.096	1.098	1.103	.688	11122153	
11122155		392.25	3448.8	6,411	6,596	2587.1	3,116	3,479	.498	.554	.457	.543	.525	.484	.584	.573	.592	.571	.559	.599	11122155	
11122156		394.92	3464.2	6,555	6,654	2627.9	3,156	3,498	.512	.563	.476	.553	.543	.494	.582	.579	.596	.575	.563	.601	11122156	
11122157		395.73	3471.3	6,597	6,662	2636.2	3,158	3,504	.512	.567	.485	.555	.546	.495	.582	.582	.598	.577	.564	.601	11122157	
11122158		395.41	3468.5	6,581	6,641	2625.9	3,140	3,501	.508	.566	.485	.553	.550	.489	.579	.584	.598	.577	.564	.601	11122158	
11122159		394.34	3459.1	6,526	8,598	3398.5	3,128	5,478	.501	.566	.482	.550	.549	.482	.574	.583	.599	.576	.564	.600	11122159	
111231	0	.00	.0	12,348	12,823	1.2	6,437	6,386	1.037	1.046	1.051	1.051	1.059	1.051	1.036	1.063	1.057	1.059	1.064	1.067	111231	0
111231	1	.17	1.5	12,884	13,025	2.2	6,549	6,476	1.088	1.081	1.085	1.083	1.087	1.082	1.059	1.084	1.078	1.078	1.083	1.086	111231	1
111231	3	.05	.4	13,056	13,134	.7	6,606	6,524	1.095	1.094	1.096	1.096	1.099	1.095	1.056	1.093	1.088	1.088	1.093	1.096	111231	3
111231	4	.07	.6	13,147	13,192	.9	6,640	6,552	1.103	1.102	1.105	1.103	1.106	1.102	1.059	1.099	1.093	1.094	1.099	1.102	111231	4
111231	5	.02	.2	13,203	13,233	.3	6,662	6,571	1.109	1.107	1.110	1.108	1.111	1.106	1.060	1.102	1.097	1.098	1.103	1.106	111231	5
111231	6	.02	.2	13,242	13,262	.3	6,678	6,584	1.112	1.110	1.113	1.111	1.114	1.109	1.062	1.105	1.099	1.100	1.105	1.108	111231	6
111231	7	.08	.7	13,267	13,282	1.1	6,689	6,593	1.115	1.112												

Figure 142 — Fast Scan Continuous Reading Printout

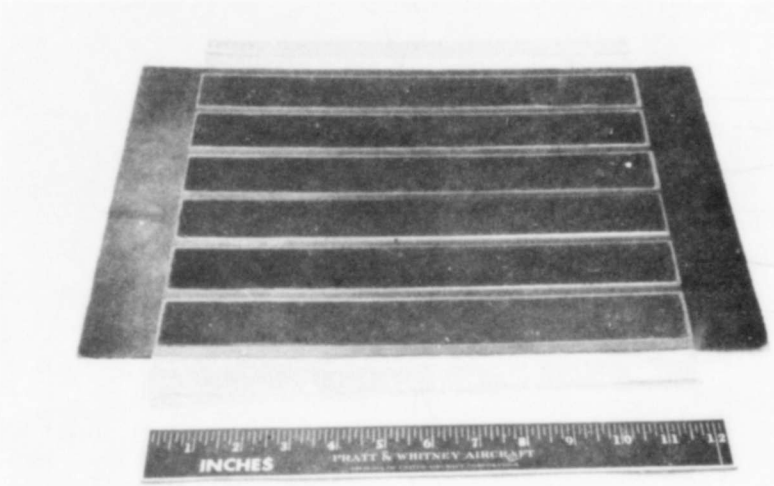

Figure 143 – Configuration 1 Six-Cell Plaque

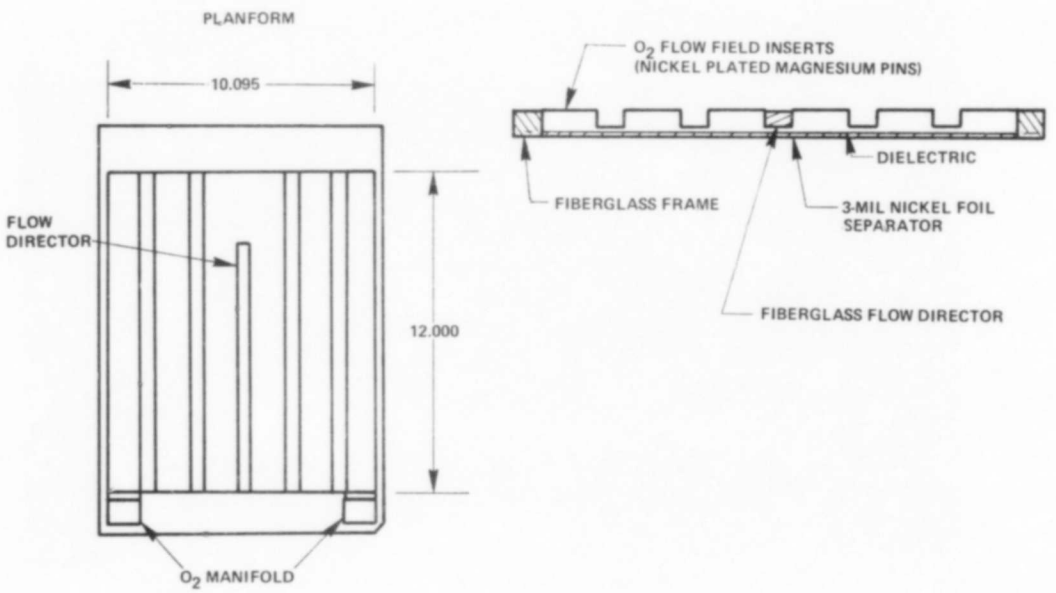

Figure 144 – Configuration 1 Cooler Assembly

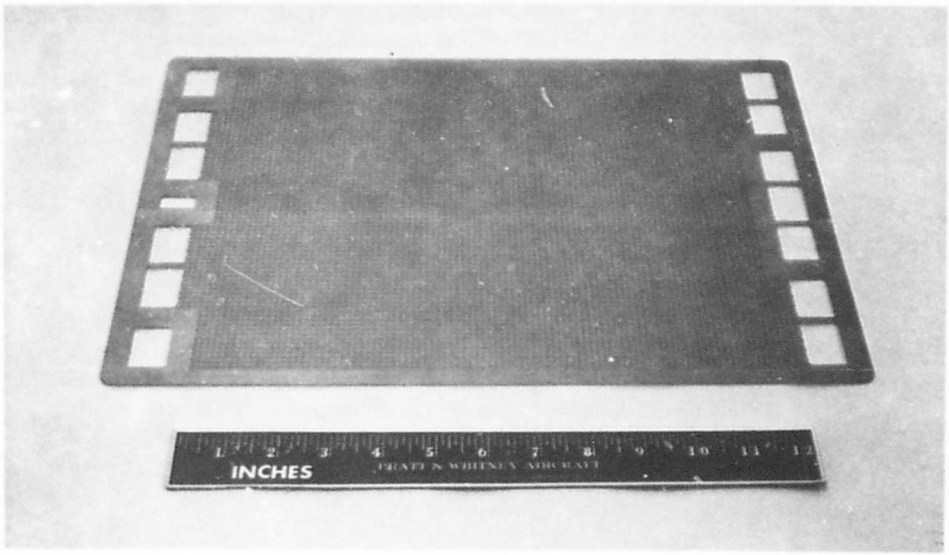

Figure 145 – Configuration 1 Hydrogen Field

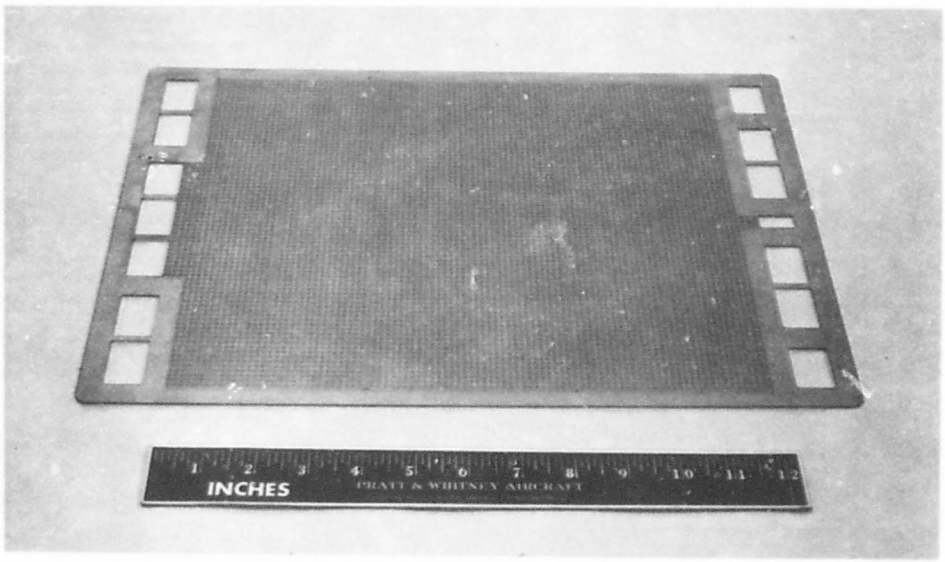

Figure 146 – Configuration 1 Cooler Field

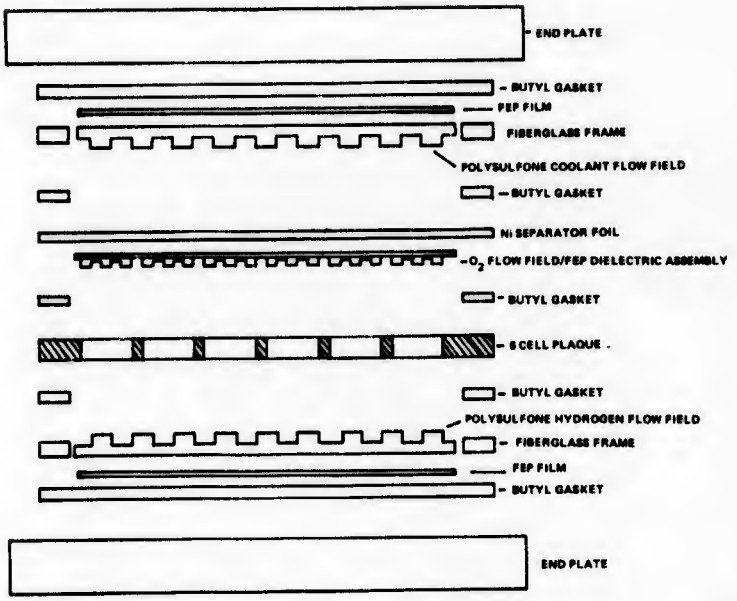

Figure 147 – Cross Section of Configuration 1 Development Unit

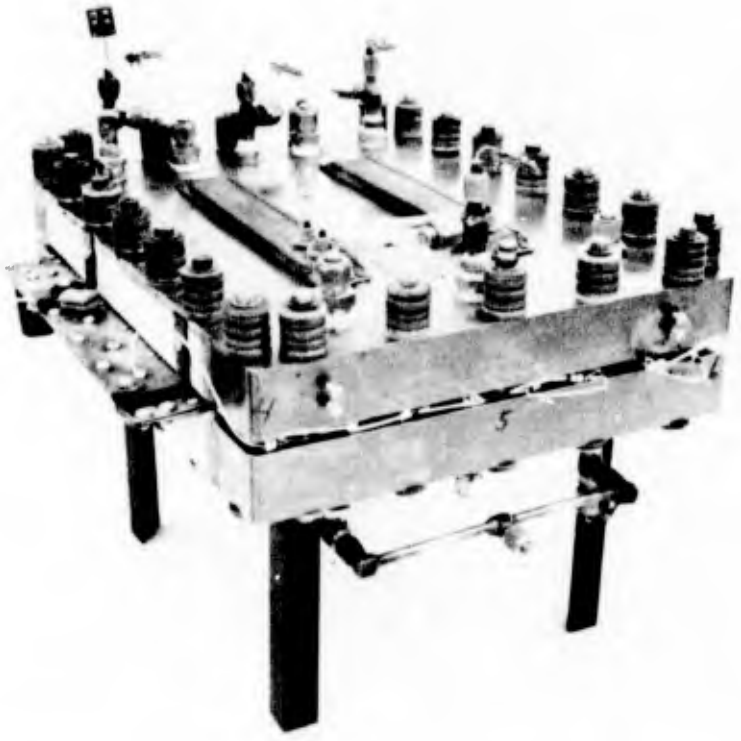

Figure 148 – Configuration 1 Development Unit - Assembled and Instrumented

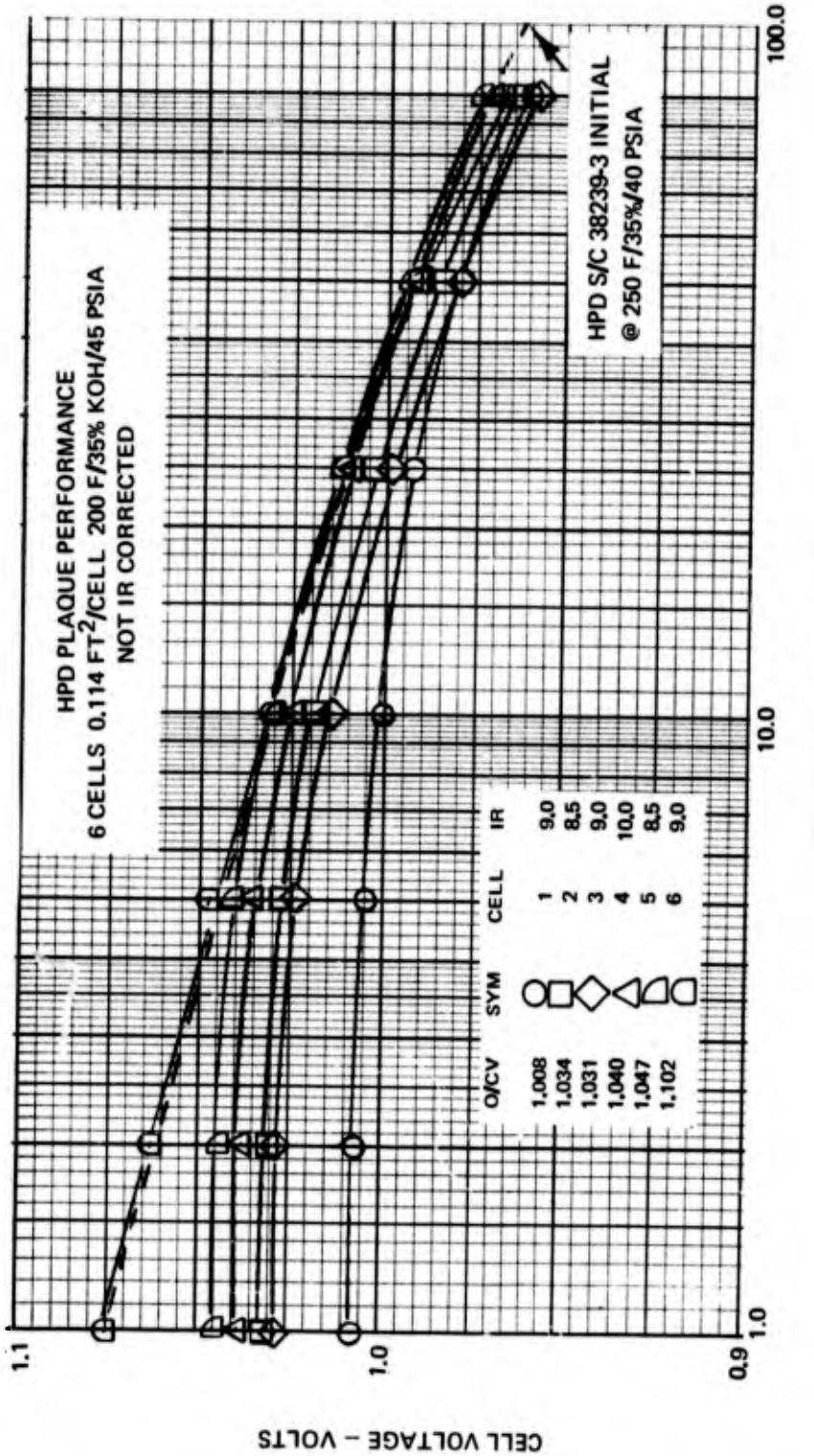

Figure 149 – Development Unit 1 - Individual Cell Tafel Data

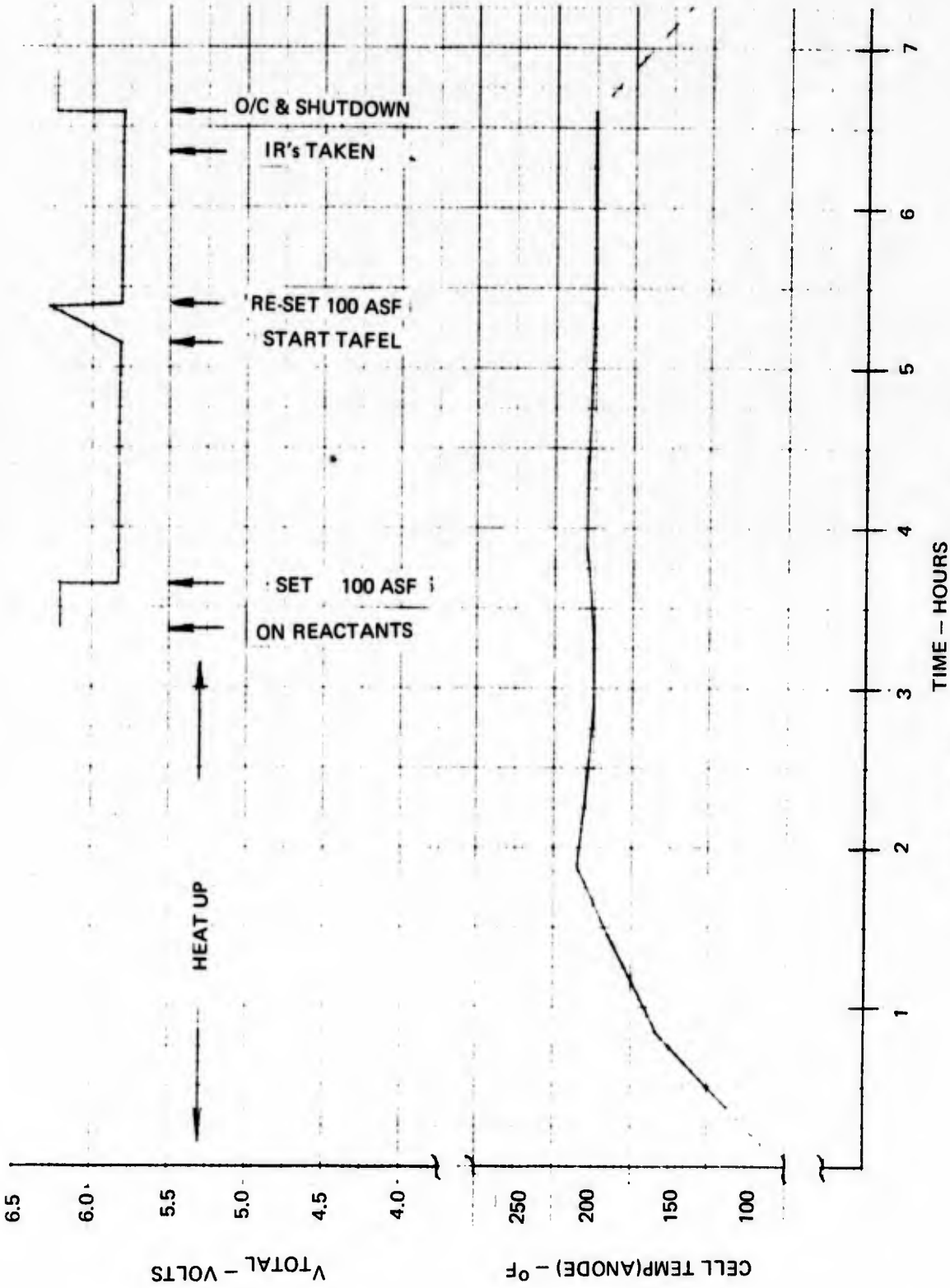

Figure 150 — Development Unit 1 - Graphic Log

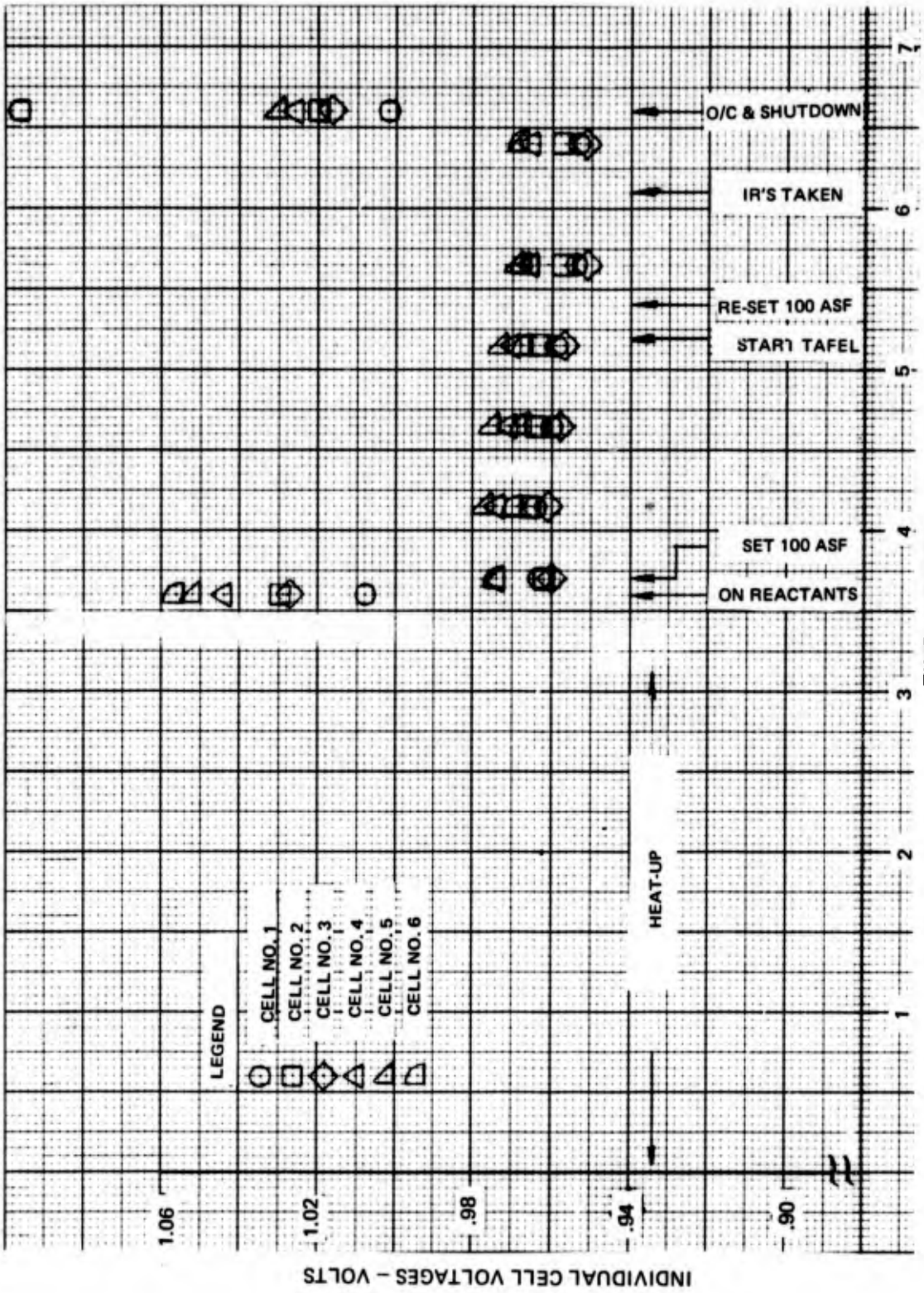

Figure 151 — Development Unit 1 - Single Cell Voltages

Cell performance was normal and the data indicated that the plaque's single cells were of comparable performance to Strip Cell 3. However, the flattening of the curves at very low current density is an indication of cell shorting. The amount of shorting can be estimated by extrapolating the straight portion of the curve between 50 and 100 ASF. For example, the short on Cell 1 is estimated to be about 20 ASF. IR's were taken by the standard current interrupter method. The IR's for the individual cells were:

Cell		1	2	3	4	5	6
IR	mv @ 100 ASF	9.0	8.5	9.0	10.0	8.5	9.0

These IR's were slightly higher than the 7 to 8 mv experienced on previous single cell tests. The reason for the high IR's was probably insufficient pinch as evidenced in the lack of field indentation on the electrodes observed when the unit was later disassembled.

Since the diagnostics indicated higher than desired cell IR and also shorting of the individual cells, the unit was shut down. Midway into the shutdown, leakage from the oxygen cavity to the coolant cavity was observed. The unit was disassembled to determine the source of the leakage and shorting. Inspection of the components revealed that the 5-mil FEP dielectric between the oxygen fields and the nickel foil had shrunk allowing the magnesium oxygen fields to contact the nickel separator foil and short out the individual cells. Inspection also indicated that the short at Cell 1 caused several small holes in the nickel foil allowing the leakage from the oxygen cavity into the coolant cavity.

Prior to the replacement of the nickel foil and the reassembly of the unit, bench tests of the FEP film were conducted to determine if the film could be dimensionally stabilized. Heat cycles at 270°F resulted in shrinkage of 0.25 inches in a 15.5-inch length. Shrinkage did not occur after the second half-hour cycle.

Two rebuilds of this test unit were made. Both rebuilds resulted in premature test termination due to oxygen reactant leakage by the seal between the unitized electrode assembly and the nickel foil of the cooler.

The first rebuild of the unit incorporated a preshrunk FEP dielectric between the oxygen field and nickel foil. The FEP film was also extended over the entire planform (into the seal area) to minimize the possibility of any shorting. Supports were also added to the oxygen manifold ports since inspection during the teardown showed that the FEP film had extruded into the port area. The unit was pressure tested to 45 psig with no leaks from either reactant or coolant cavities. The unit was then mounted in the test stand and prepared for startup. During the heatup to operating temperature, at normal reactant pressure, the gasket between the UEA and cooler was displaced allowing a significant oxygen leak. The unit was removed from the test stand and returned to the assembly floor for disassembly.

The unit was rebuilt with the FEP dielectric cut back from the sealing area and pressure checked to 45 psig with no problems. The unit was then reinstalled in the test stand and heatup was initiated. After holding at 200°F for one and half hours at ambient pressure, the tie bolts were retorqued to 55 inch-pounds from an initial 45 inch-pounds in an effort to achieve higher sealing loads. The unit was then pressurized and heatup to 265°F was begun. The gasket was displaced again after approximately one hour at normal reactant pressure and operating temperature. The unit was torn down and the failure attributed to a lack of high temperature capability of the Hypon adhesive used to hold the gaskets in place. An improved high temperature adhesive was obtained. This adhesive, a Pratt & Whitney formulation of Novalac epoxy cured polybutadiene nitrile rubber, was tested in bench trials using the 4 in. x 4 in. cell end plates. A dummy stack containing the butyl gasket, nickel foil, and fiberglass sealing surfaces of the test unit was fabricated. The bench test was sealed with an 88 psi seal load. A pressure test was conducted at 45 psig and 200°F and, in addition, the unit was held at 45 psig and 270°F for two hours with no leaks. Rebuild of the test unit with the new adhesive was then initiated.

Upon restart, the initial 100 ASF performance was 5.68 v. Peak performance was 5.73 v at 100 ASF. This performance compares favorably with the single cell experience. Tafel and IR diagnostics were conducted and are shown in Figure 152. The IR's at 6.0 to 9.0 mv at 100 ASF were 1 to 2 mv higher than expected, indicating that the stack was slightly underpinched. The Tafel data shows a loss in activation of 20 mv at 10 ASF from the first test, which corresponds to an active area loss of about 50 percent. At 100 ASF, Cell 1 was 30 to 40 mv lower than Cells 2 through 5 and Cell 6 was 15 to 20 mv lower. Throughout the test, Cells 1 and 6 were low in performance, with Cell 1 being the poorest performer of the plaques. The voltage readouts were erratic because the leads had broken during rebuild. Consequently, some individual cell voltages could not be recorded accurately. Valid total voltage and individual cell performance trends were documented, however.

After completing the diagnostics, a calibration to high power densities was started. The maximum current density set was 500 ASF. At this level, Cells 1 and 6 had difficulty holding load. At the 500 ASF conditions, a 5-psig-oxygen field differential pressure was encountered which led to oxygen control problems. The problem was diagnosed as probable oxygen manifold or porting problems and the unit was shut down for inspection.

The oxygen fittings were removed from the end plate for inspection of the manifolds. The 5-mil ERP dielectric film had extended over the Exmet port insert at the inlet of the oxygen field, causing a high pressure drop across the port. The excess was cut away and the inlet and exit to the unit were reversed to insure that this problem would not recur. Cell 1 was now positioned at the oxygen inlet.

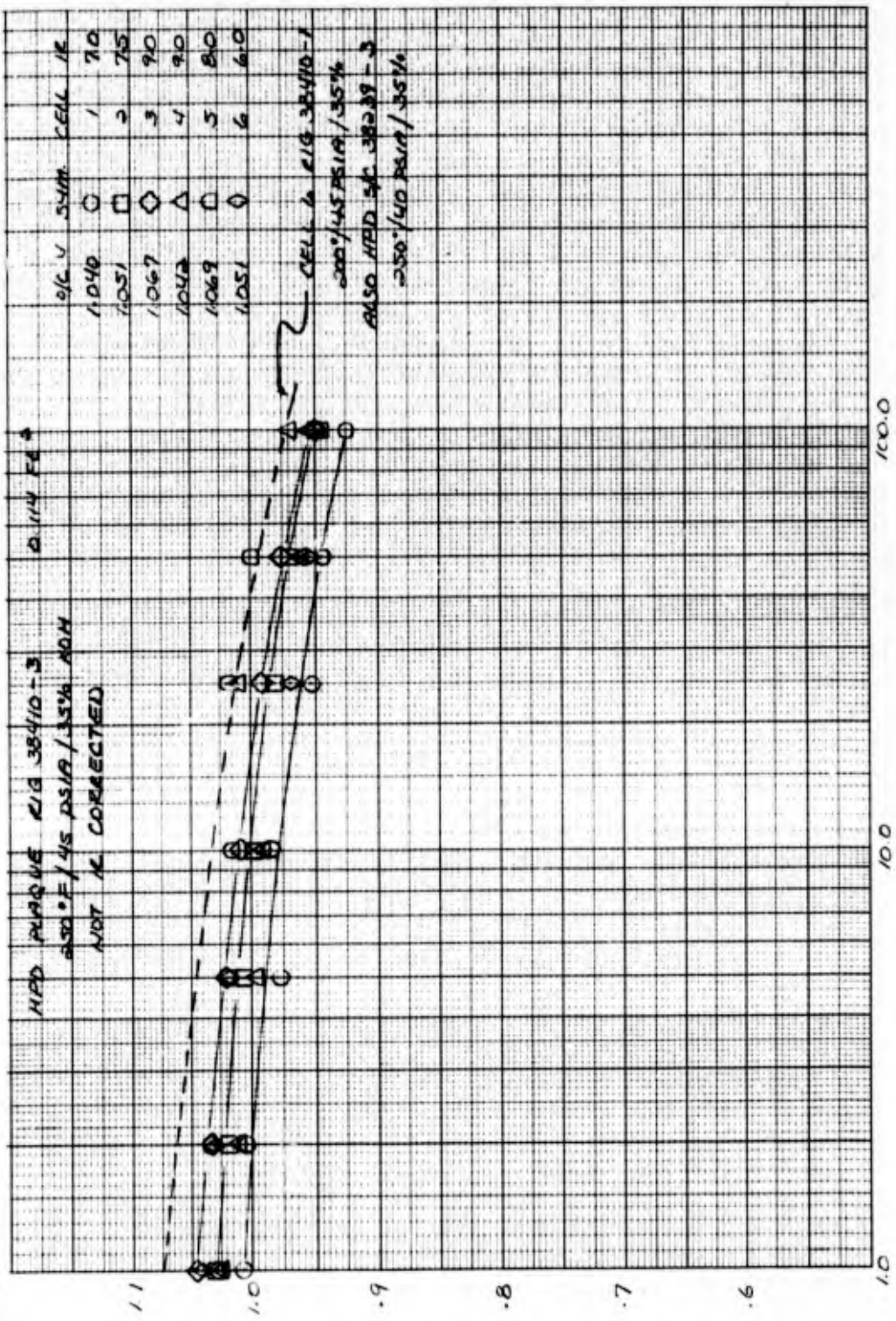

Figure 152 – Development Unit 1 - Individual Cell Tafel and IR Data

The unit was restarted for a performance calibration to high power density. Performance at 100 ASF was the same as that of the previous test. A calibration to 1500 ASF was conducted. This is shown in Figure 153. At 1500 ASF, the stack had no oxygen flow control problems, indicating that cutting back the excess film was an effective solution to the pressure drop problem. The performance of Cells 1 and 6, however, was much lower than the other four, thus it was necessary to operate at an oxygen overpressure in order to establish steady state conditions at 1500 ASF. Following the calibration, two spikes to 2000 ASF were conducted. A power level of 705 watts at the busbars was obtained. This corresponds to approximately 1030 WSF or 1.98 lb/kw for this configuration. The individual cell performances at 2000 ASF were: 0.533, 0.649, 0.645, 0.642, 0.629 and 0.215 v for Cells 1 through 6 respectively. The average performance of Cells 2 through 5, was 0.640 v at 2000 ASF, corresponding to 1280 WSF or 1.60 lb/kw for this test configuration. This performance, although better than that of Cells 1 and 6, was still somewhat low with respect to single cell experience and indicated an electrode problem. The fact that Cells 1 and 6 were end cells suggested a poisoning phenomenon, perhaps associated with the gasket or adhesive adjacent to these cells. This phenomenon would also affect the middle cells, but to a lesser extent.

Next, a dew point tolerance at 500 ASF was conducted to determine if the electrolyte volumes in each cell were satisfactory. Data points were taken at 210, 215, 220 and 250°F. The tolerance data, shown in Figure 154 indicates that Cells 1 and 4 were relatively wet and Cell 6 was relatively dry.

Following this, a pulse-load program was conducted from 0 to 1000 ASF. These pulses were set for five seconds "on load" and 12 seconds "off" for approximately three minutes duration, see Figure 155. This type of loading simulates the HPD fuel cell mission. No significant stand pressure fluctuations resulted during the pulsed-load program and the electronic pulsing switch performed satisfactorily. This completed the test program on the unit.

Post-test teardown and inspection revealed the following:

1) No signs of shorting.

2) An area on Cell 6 cathode of approximately 1 in^2 was covered by seal adhesive.

3) The coolant inlet port was partially blocked by gasket instrusion.

4) The physical appearance of the UEA was good. The cathodes in Cells 1 and 6 were a different color from the cathodes of Cells 2 through 5. The nickel-plated-magnesium oxygen field inserts from Cells 1 and 6 were also more discolored than those from Cells 2 through 5.

5) The dielectric and 3-mil nickel separator foil dimpled down into the oxygen field in intercell areas and this, apparently, was part of the cause of the large (6 psig at 1500 ASF flow) oxygen field pressure drop.

6) The epoxy/fiberglass frame showed signs of corrosion of the epoxy at the oxygen inlets and exits.

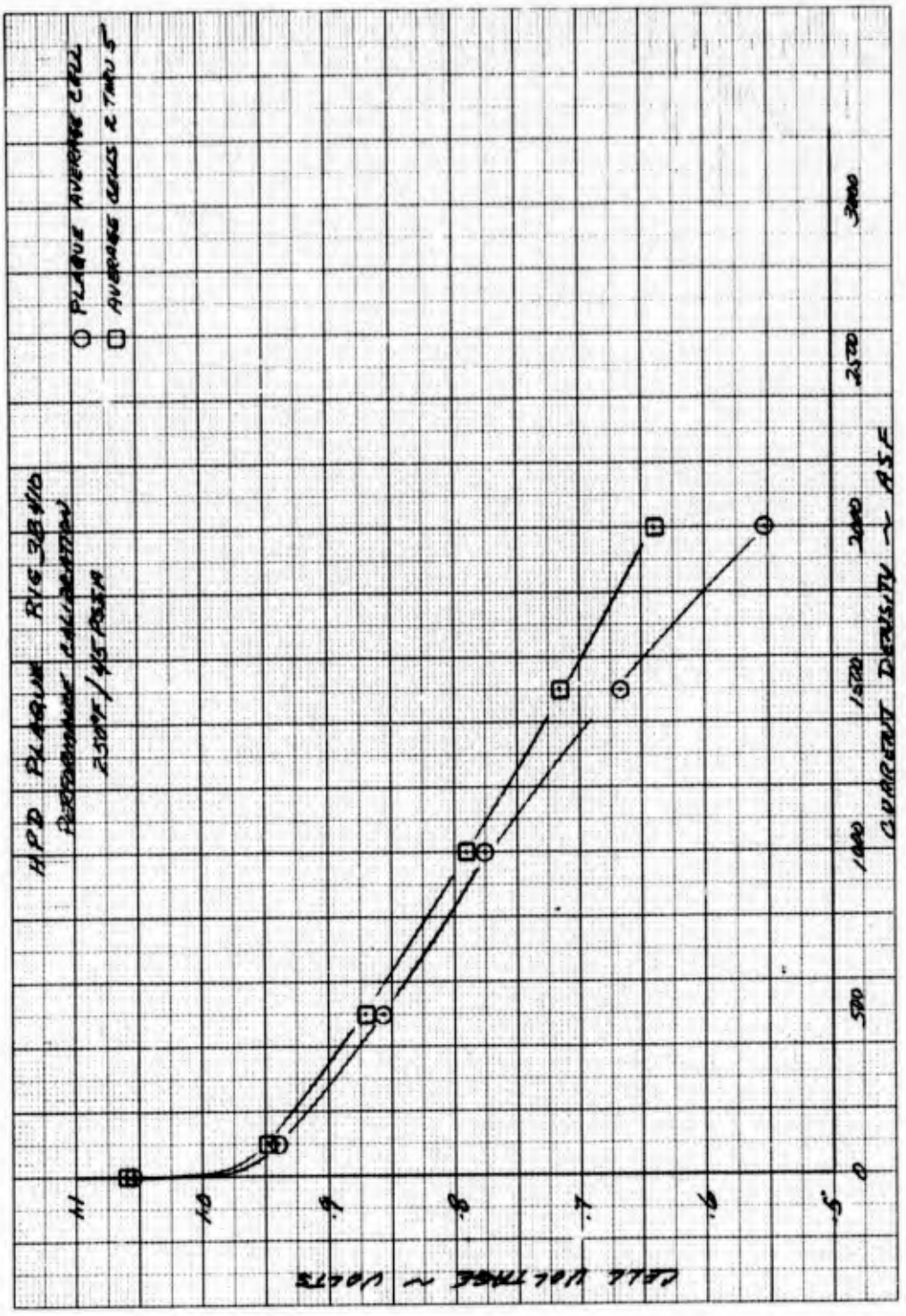

Figure 153 — Development Unit 1 - Performance Calibration

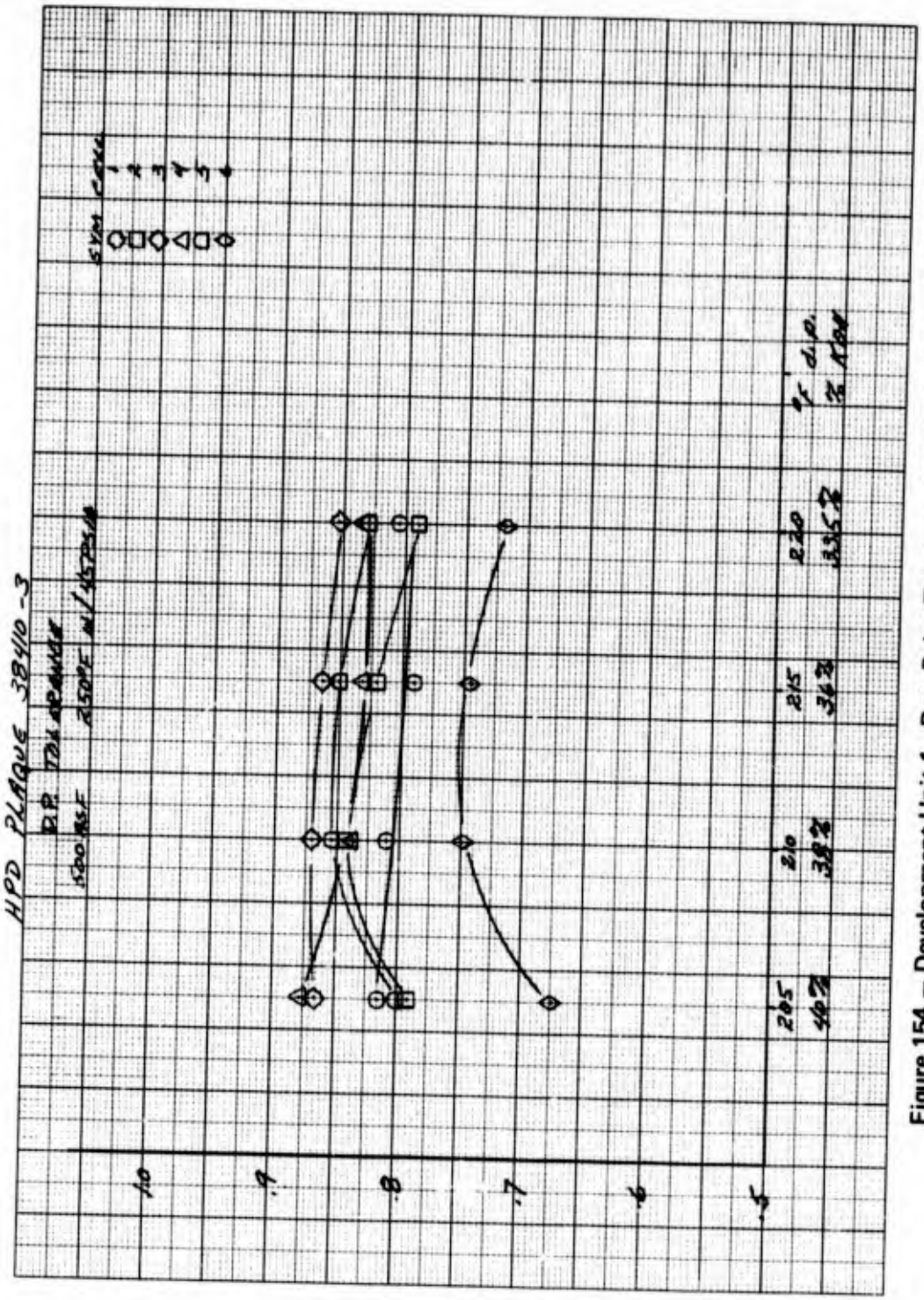

Figure 154 – Development Unit 1 - Dew Point Tolerance Data for Individual Cells

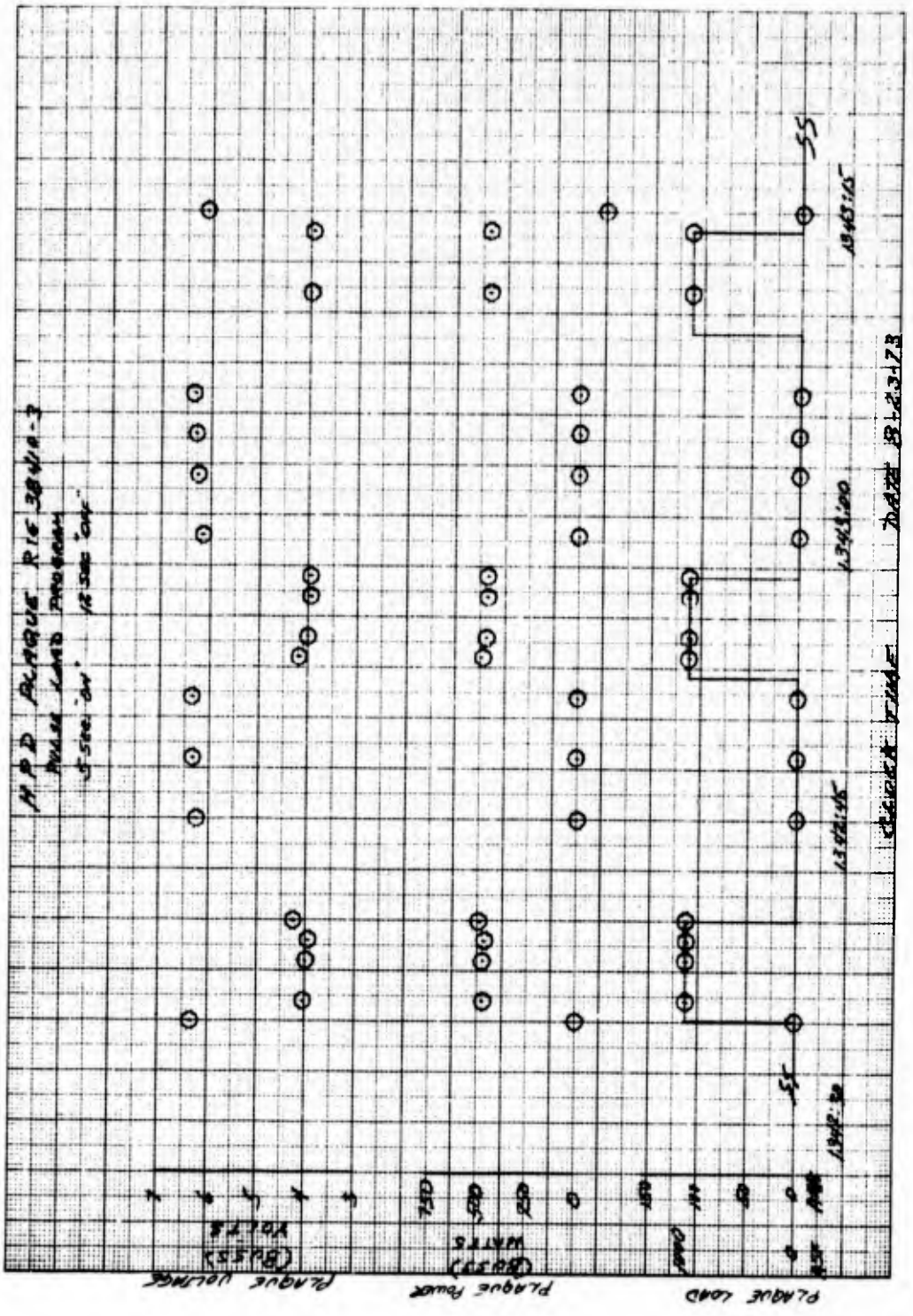

Figure 155 – Development Unit 1 - Pulse-Load Tests

Upon completion of the teardown, the 6-cell plaque was sent to the laboratory for post-test analysis of the electrodes in an effort to determine the cause of the low performance.

Laboratory half-cell testing showed high activation losses on all cells. Cell 6's cathode had a loss of over 60 mv of activation. An activation loss of 45 mv would represent a 90 percent loss of catalyst surface area. Anode losses for all cells averaged 54 mv, with Cell 1 the highest at 75 mv.

Next, X-ray diffraction tests were conducted on cathodes from Cells 1, 4, and 6 to determine the amount of cathode catalyst recrystallization. These tests indicated that all the cells were approximately equal and that catalyst recrystallization could account for only 10 mv of activation loss. Physical surface area measurements confirmed this conclusion and also indicated that catalyst corrosion was not a major problem since corrosion itself would lead to a reduction in surface area.

A special half-cell test was then conducted on a cell cathode to determine whether or not oxidation of the screen substrate was a contributing factor to the low performance. For this test, the electrode was wrapped in gold-plated screen to give an additional current path for the reaction. No change in the activation level was noted as a result of this configuration.

To investigate the possibility of poisoning, a series of potentiometer sweeps were conducted on the electrodes from the plaques. Under normal circumstances, this test discloses the presence of poisons since the oxidation cycle of the sweeps tends to "burn off" the poisons, thereby exposing a more active area and causing a change in the shape of successive sweeps. As can be seen in Figure 156, this was not the case.

Since the butyl-rubber gaskets and the polybutadiene rubber sealing material were under suspicion, half-cell tests were conducted in an attempt to artificially poison electrodes with effluents from these materials. The results of the tests indicated that neither the glue nor the gasket material above were sufficient to poison the electrodes. The combination of the two, however, produced a poisoning effect that not only caused a 60 percent loss of activation, but also was immune to both oxidation and reduction.

As a result of the tests, it was concluded that electrode poisoning due to adhesives and gaskets was responsible for a large part of the performance loss experienced in the development unit test. Gaskets with a different formulation were ordered for assembly of the second development unit.

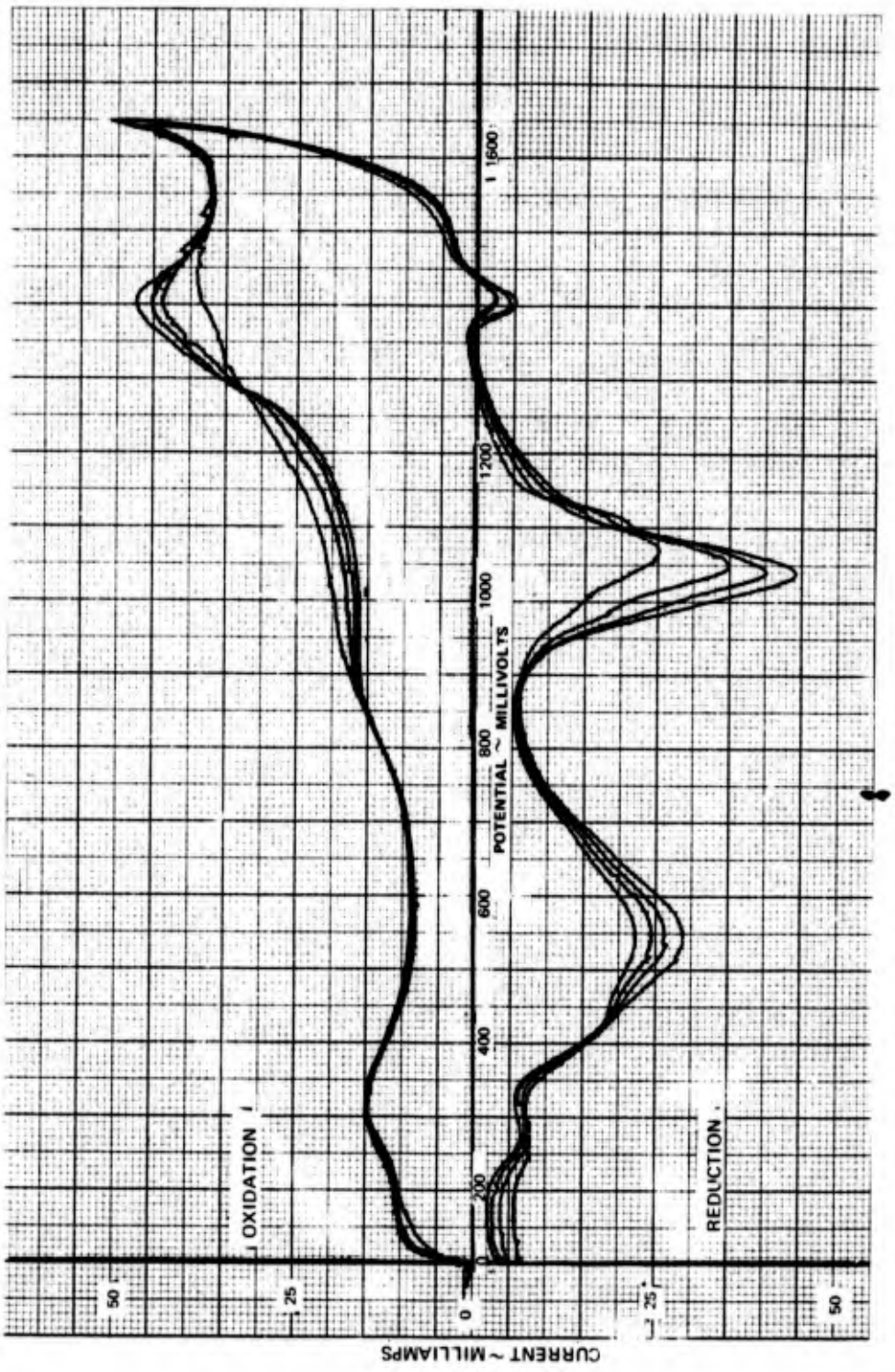

Figure 156 – Four Successive Sweeps of Gold-Platinum Cathode

Development Unit 2

The seond development unit to be tested was of the Configuration 2 design. This unit differed from the Configuration 1 development unit as follows:

- The electrode substrates were changed from 100 x 100 mesh screen to 50 x 100 mesh screen.
- The ERP thickness was reduced from 30 mils to 20 mils.
- The oxygen flow field/cooler assembly was of the Candidate 2 design, see Figure 157. It was fabricated with 1.5-mil thick electroformed nickel flow fields, back-filled with a silver epoxy compound, laminated into an epoxy/fiberglass frame. The completed assembly is shown in Figure 157.
- A revised gasket formulation (ethylene propylene) was used in an attempt to minimize electrode poisoning effects.

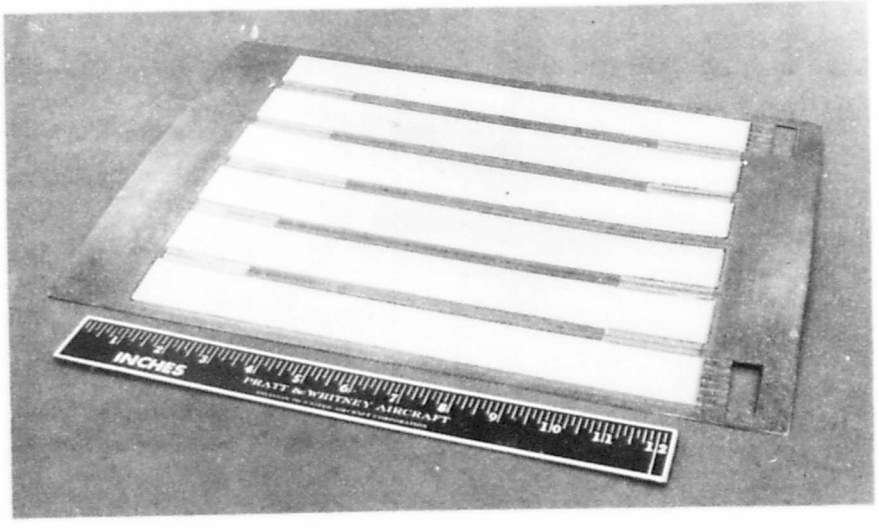

Figure 157 – Development Unit 2 - Cooler Assembly

The repeating unit specific weight of this unit was 0.76 lb/kw at the design operating power density of 2150 WSF. This is slightly higher than the 0.73 lb/kw cited in Table XXXVI for this configuration. The reason for the difference is that the cooler assembly itemized in Table XXXVI for Configurations 2, 3, and 4 is a Candidate 1 design and this development unit incorporated a Candidate 2 design cooler with epoxy filled flow fields. Had the flow fields not been backfilled this cooler would have been lighter than the Candidate 1 design

and the weight of the unit would have been less than 0.73 lb/kw. Section IVC discusses the two cooler designs and their development.

The initial part of the test program for this development unit was an operational checkout at 200°F and a current density of 100 ASF. During this part of the program a small oxygen-to-coolant cavity leak developed but did not interfere with the test program. Included in this portion of the testing were Tafel and IR diagnostics. Following heatup and conditioning on saturated gases, the initial six-cell 100-ASF voltage was 5.82 v. The individual voltages were as follows:

Cell	1	2	3	4	5	6
Voltage	0.948	0.971	0.979	0.979	0.977	0.969

Shortly after going on load, standard Tafel data and IR diagnostics were measured. The resulting low current density calibration is shown in Figure 158. The cell performance at 200°F was the highest level obtained in a 6-cell plaque and compared favorably with single cell data also shown in Figure 158. Cell 1 did have an apparent short as shown by the flattening of its curve in the low current density region. The IR's for the individual cells were:

Cell	1	2	3	4	5	6
IR $(\frac{mv}{100\ ASF})$	9.6	7.5	9.0	8.4	9.5	10.6

Following the completion of the diagnostics, the stack was put on dry oxygen to determine the effect this would have on performance. The reason for this change to dry oxygen was that bench tests on Configuration 2 trial oxygen field/cooler assemblies indicated that the oxygen inlet-to-exit differential pressure could approach 6 psi at high current density flows. This same differential pressure could be reduced to 2 psi by operating on dry gas. In the plaque, however, the oxygen differential pressure was about 9 psi, indicating an additional problem. No change in individual cell voltage was recorded after switching to dry oxygen.

Next, the unit was put on inerts and heated to 250°F cell inlet temperature. Following heatup and conditioning, the initial 250°F, 100 ASF six-cell performance was 5.73 v. The individual cell voltages shown in Figure 159, were as follows:

Cell	1	2	3	4	5	6
Voltage	0.928	0.958	0.964	0.963	0.962	0.958

This decrease in performance was not expected. However, one possible explanation is the lower oxygen partial pressure resulting from the heatup from 200°F to 250°F at a constant 35 percent KOH. Because the oxygen to coolant leakage was increasing, it was decided that a high power density calibration would be obtained and that the loss in performance at 250°F would be investigated later.

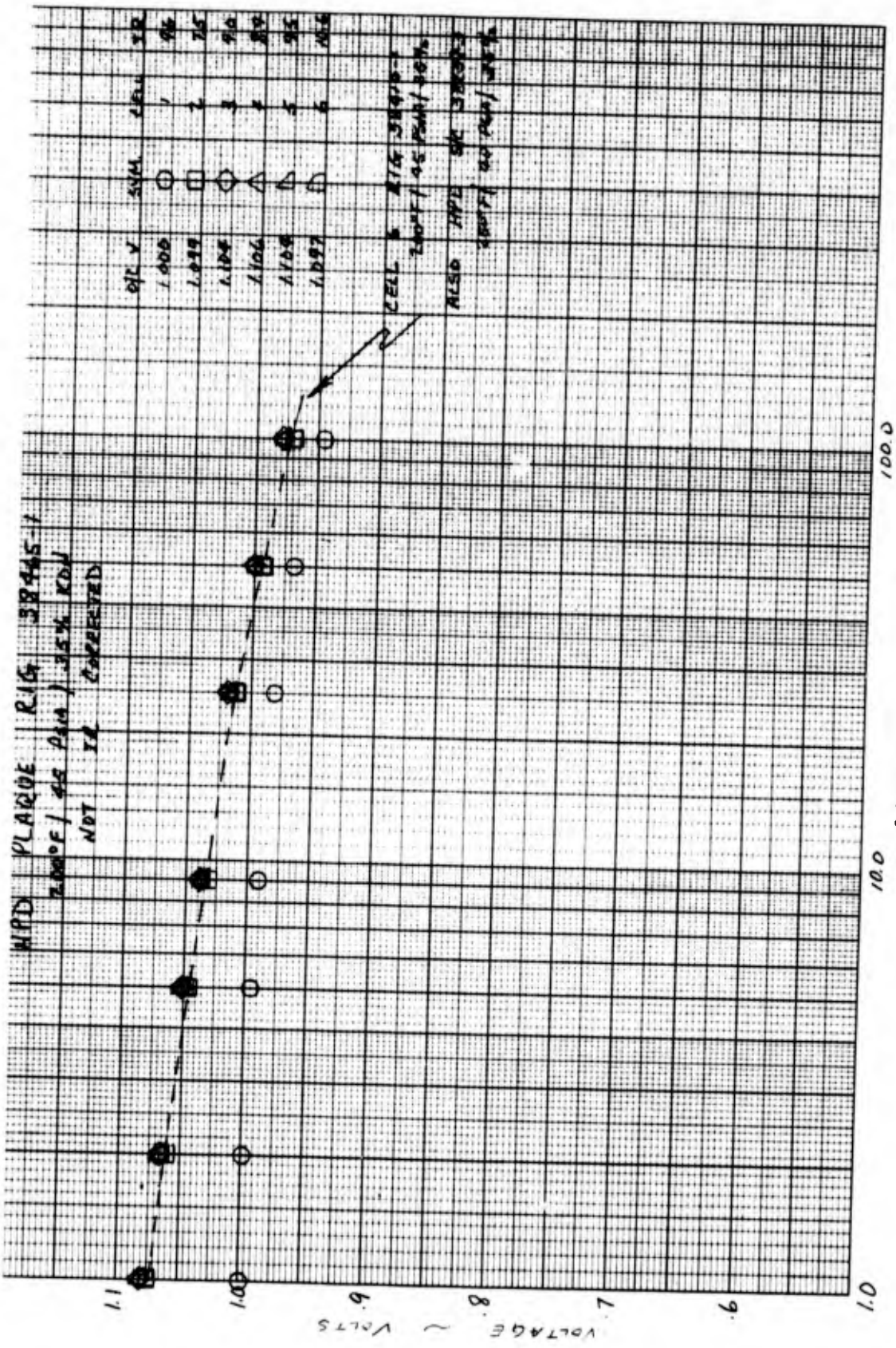

Figure 158 – Development Unit 2 - Tafel and IR Data

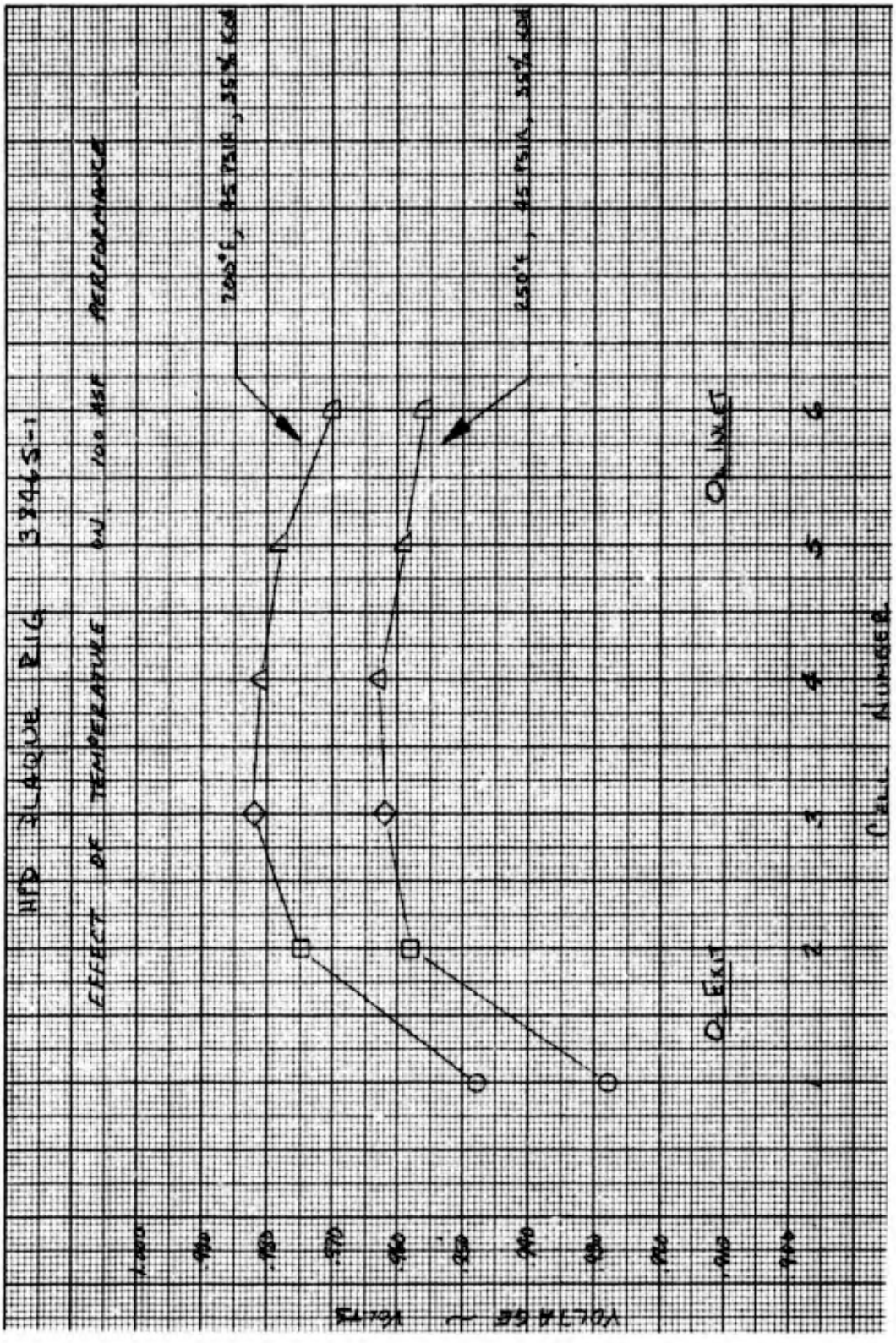

Figure 159 – Effect of Temperature on Individual Cell Voltage

The results of the high current density calibration were that stable performance could not be held above 1000 ASF because of the instability of Cell 1. Individual cell voltages at 1000 ASF were as follows:

Cell	1	2	3	4	5	6
Voltage	0.637	0.710	0.745	0.808	0.806	0.786

Upon completion of the high power density calibration, the effect of an inlet oxygen over-pressure up to 5 psi was determined. It was surmised that the performance of Cell 1, which was at the oxygen exit, might be improved if the oxygen inlet pressure were increased to compensate for the oxygen field pressure drop. However, no change in individual cell voltages occurred at 100 ASF.

Following this portion of the program, a pulsed-load program was conducted from 0 to 3300 ASF maximum. A composite performance curve is shown in Figure 160. These pulses were set for two seconds "on load" and 12 seconds "off" for approximately two minutes. The highest recorded spike produced 0.82 kw, which is 60 percent of design performance. The unit was shut down upon completion of the pulsed-load program.

The unit was restarted after having reversed the inlet and exit lines on the stack. The purpose was to determine if the low performance of Cell 1 could be attributed to an oxygen flow-differential pressure problem rather than a poisoning or electrochemical problem. By reversing the lines and thereby putting Cell 1 at the oxygen inlet, any performance increase in Cell 1 and subsequent performance decrease in Cell 6 could be directly attributed to an oxygen flow-differential pressure problem. In restarting the unit, Cell 6 (oxygen exit) took unusually long to reach a stable open circuit. Shortly thereafter, it was determined that the stack had reactant crossover and it was shut down for refill.

The stack was refilled and returned to test. Oxygen flow through the stack could only be obtained with Cell 6 at the oxygen exit. The cell was restarted at 100 ASF, 200°F cell temperature. The objective was to determine the effect of increasing the total pressure on cell performance. The total pressure was increased by 6 psi with essentially no change in cell performance. Attempts at increasing performance by operating at 38 percent average KOH vs. 35 percent also resulted in no change in individual cell performance.

Throughout the test, several attempts were made to operate the stack with the dual-feed oxygen system dead-ended to alleviate the pressure-drop problem. Each time, a rapid performance decay was noted, particularly on the cell nearest the oxygen exit port. This problem was eventually traced to a build-up of inerts in the stand's oxygen saturator. It is felt that this phenomenon was at least partially responsible for the low performance of the exit side cell and possibly contributed to the lower performance seen in other cells throughout the test. The unit was then shut down and returned to assembly for teardown and inspection.

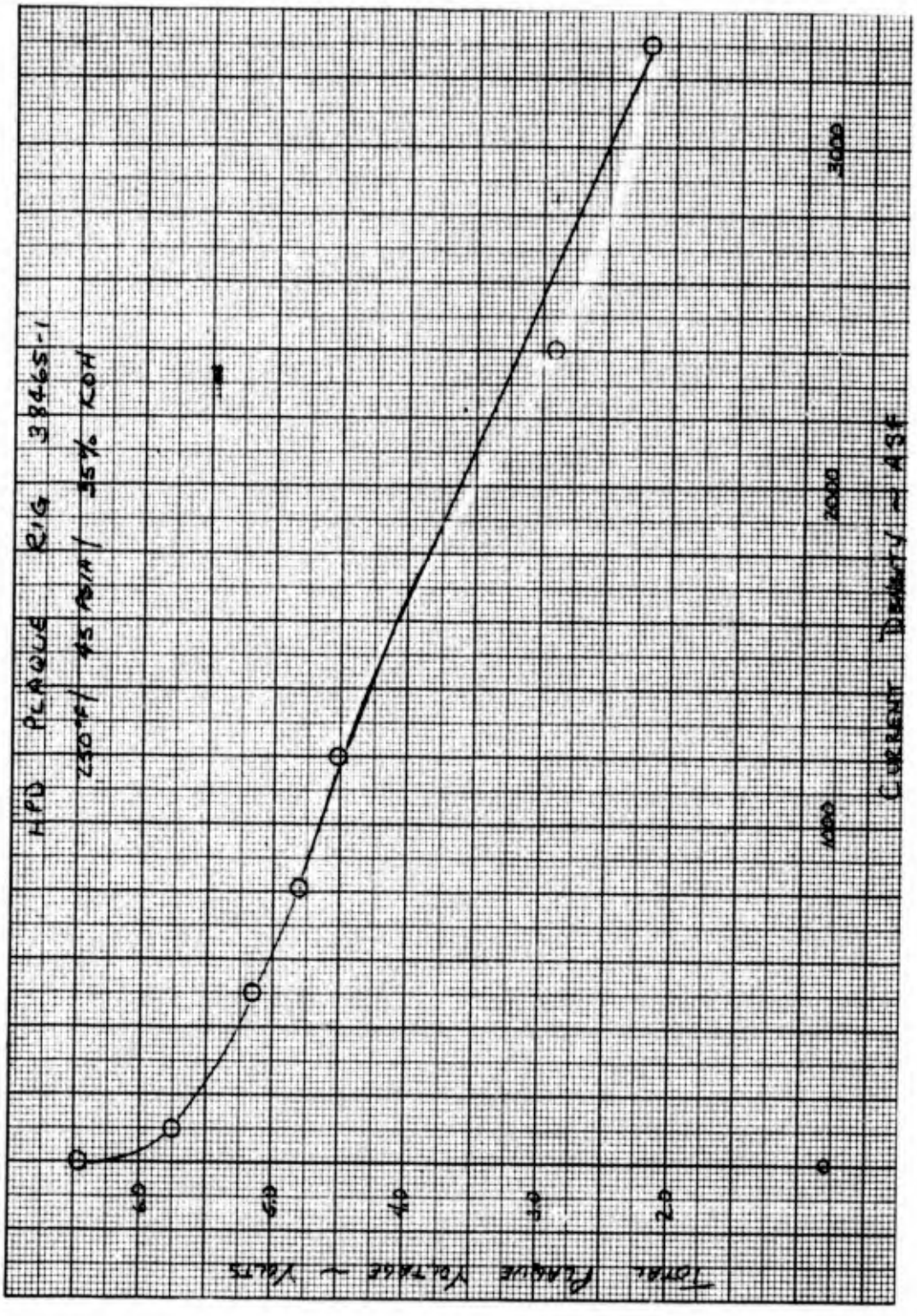

Figure 160 — Development Unit 2-Performance Calibration Based on Pulse Load Data

Inspection of Development Unit 2 disclosed the following:

- The oxygen port at Cell 6 was almost completely blocked with adhesive. This was the major cause of the high oxygen pressure drop.

- Approximately 10 percent of the active area of the cathodes of Cells 1 and 6 was covered with adhesive.

- Some delamination of the epoxy/fiberglass from the nickel cooler strips was noted. In addition, some of the silver-epoxy filler had come out of the back of the cooler strips. Because of the damage caused by teardown, it was not known which of these phenomena caused the oxygen-to-coolant leakage.

- Laboratory analysis of the electrodes disclosed that all cells had some loss of catalytic activity. X-ray diffraction analysis of the catalyst revealed no large loss in surface area due to structural changes. This led to the conclusion that the loss of activity was probably due to poisoning caused by the gasket material. Even though the poisoning effect was less than experienced in the first test it was judged necessary to eliminate the rubber gaskets entirely from proximity to the electrodes.

Development Unit 3

The third development unit was again a Configuration 2 design with a repeating unit specific weight of 0.73 lb/kw. This was the second Configuration 2 development unit to be tested. Two major changes were instituted as a result of testing of the first Configuration 2 development unit.

- Seals between individual components were made using epoxy/fiberglass laminates instead of gaskets. This was done to eliminate catalyst poisoning, gasket slippage, and to provide closer dimensional control of the development units.

- The oxygen field/cooler assembly was changed to Candidate 1 design with a 1-mil nickel separator foil coated with a 2-mil thick fiberglass-epoxy dielectric layer.

The cross-section of this unit is shown in Figure 161. Achieving satisfactory leak-free inter-component bonds required development of improved bonding techniques. This work is described in Section IIIC4.

Following the completion of the bonding investigation, this unit was assembled and was readied for test. Initially leakage occurred near the oxygen inlet, between the endplate and endcap. This was remedied by changing the endgasket material to more temperature compatible material, using a thicker gasket in the oxygen manifold areas and roughening the surfaces of the endplates.

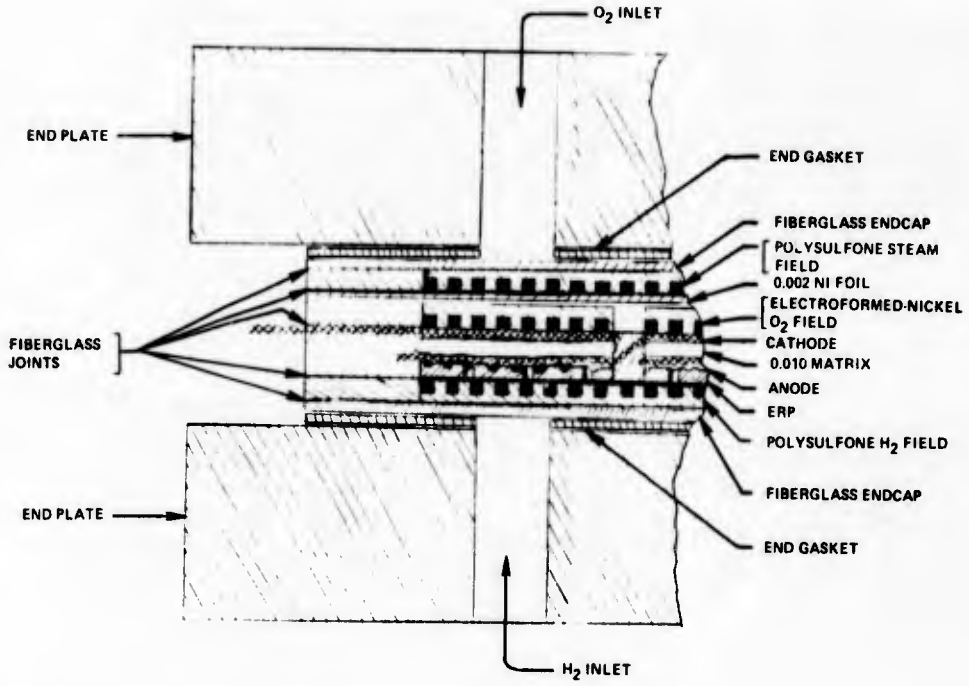

Figure 161 – Cross-Section of Development Unit 3

The rig was heated at 30 psia reactant pressure. Upon reaching 250°F a performance point was taken at 100 ASF. The average cell performance was 0.951 v. Following this, the pressure was raised to 45 psia. Diagnostics taken included an IR measurement (5.8 mv/cell at 100 ASF), a Tafel slope measurement, see Figure 162, and a calibration to 2500 ASF, see Figure 163.

The performance of the plaque out to 1500 ASF was very good and comparable to single cell data. Above this level Cell 6 voltage was unstable, apparently due to an oxygen flow restriction. Points were run at 1000 and 2500 ASF in the no-water-removal mode. In each case Cell 6 fell off rapidly. In an effort to improve the performance of this cell, the reactant pressure was raised to 60 psia. Before the rig could be stabilized at this pressure, the end-gasket slipped near the coolant inlet manifold, and the rig was shut down.

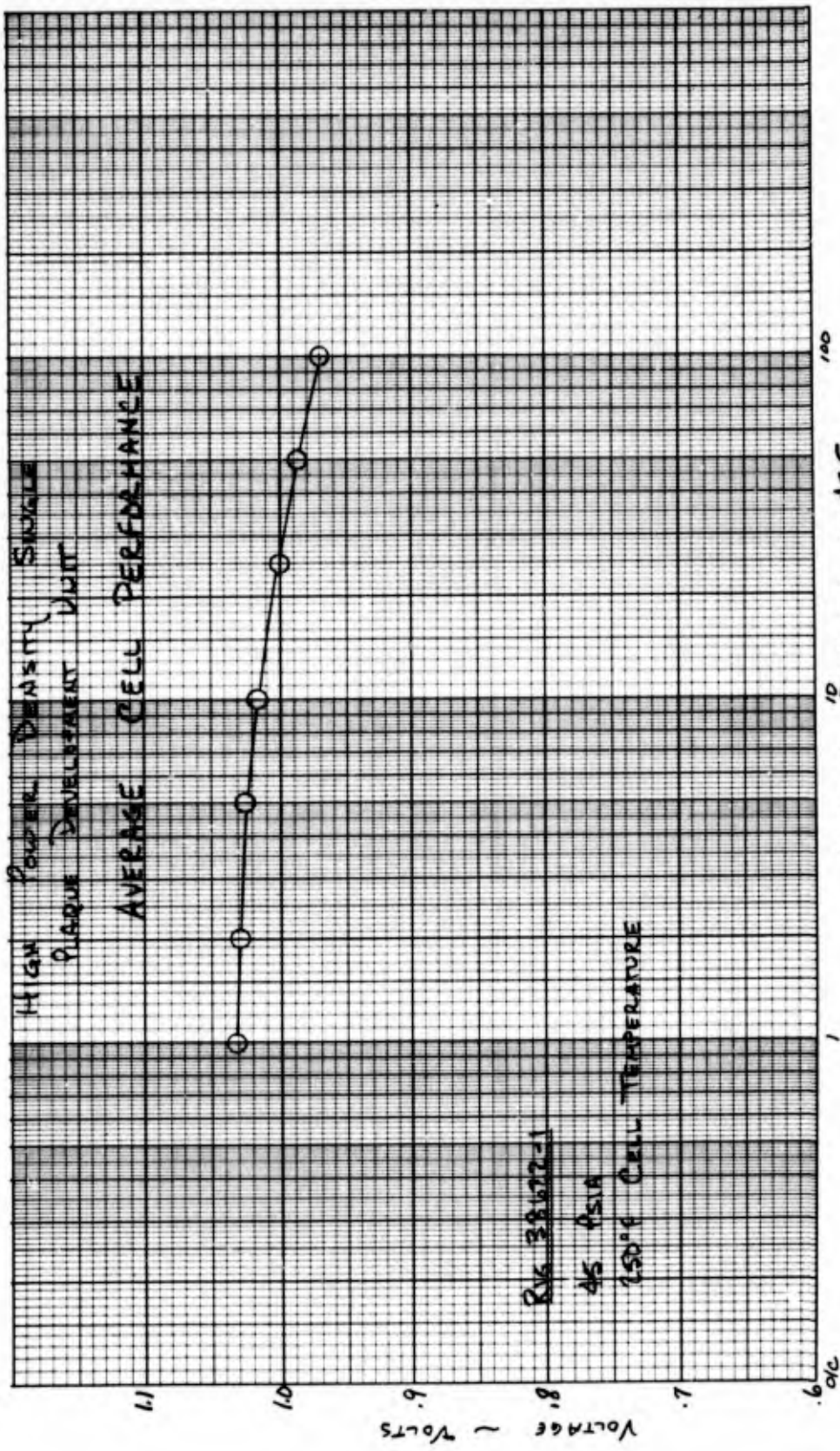

Figure 162 – Development Unit 3 - Tafel Data

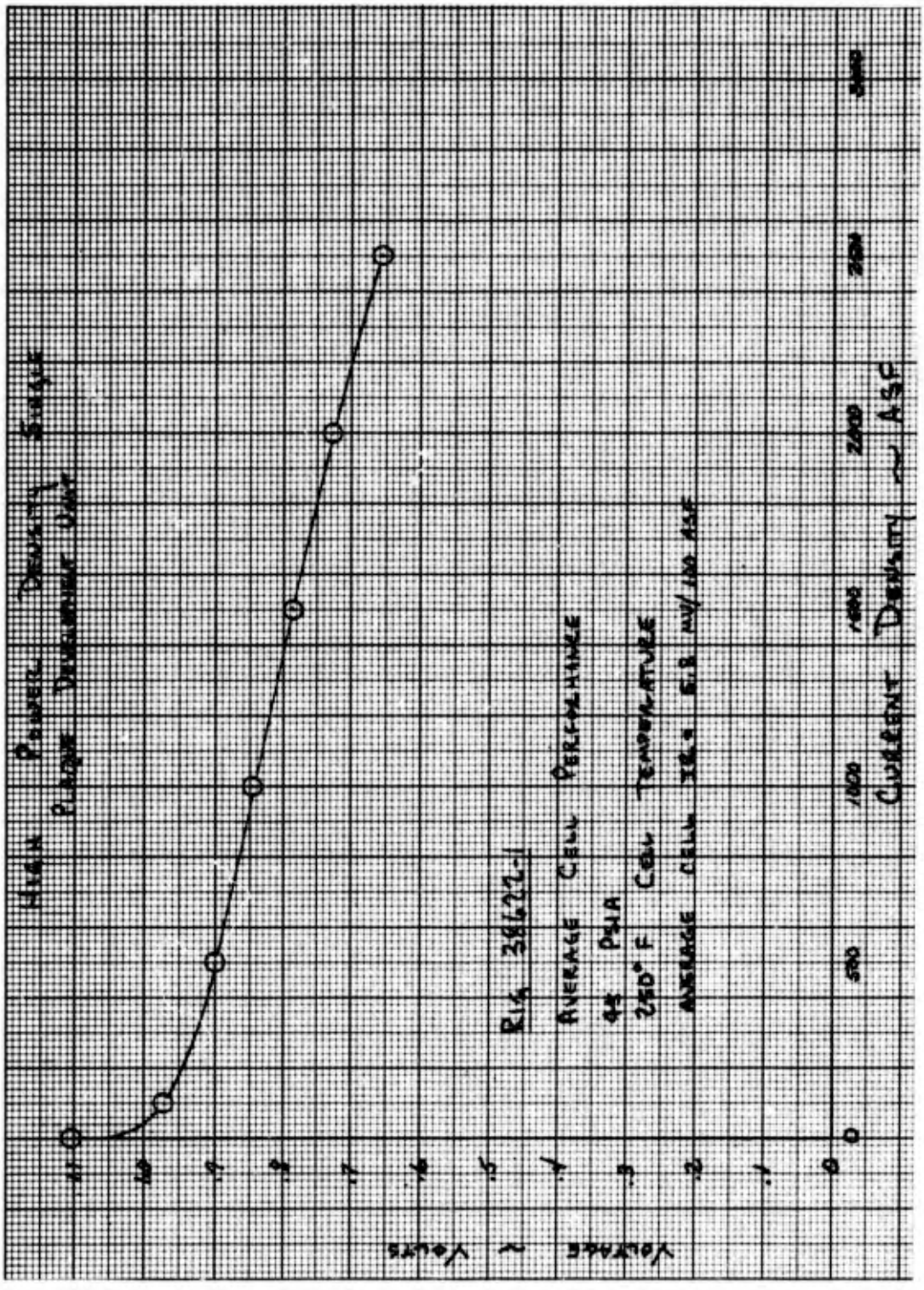

Figure 163 – Development Unit 3 - Performance Calibration

The rig was returned to test after a refill with the end gaskets cemented to the epoxy/fiberglass endcaps. Initial performance at 45 psia, 100 ASF was 0.963 v with Cell 6 low at 0.939 v. The lower performance probably reflected the fact that the oxygen restriction had increased since the first run. Low power calibrations were run out to 550 ASF with normal oxygen flow, reversed oxygen flow, and dual feed. As can be seen in Table XXXVII, the performance of Cell 6 was improved in either the reversed or dual-feed modes. The dual-feed mode (oxygen fed to both inlet and exit ports of the plaque) was selected for subsequent high current density operation of this unit to avoid starving Cell 1. After raising the reactant pressure to 60 psia, a performance calibration utilizing dual oxygen feed was run to 3200 ASF, see Figure 164. At 3200 ASF the initial power density was 2040 WSF. Above 2000 ASF Cells 4 and 5 were unstable, and the 3200 ASF point was held for only 10 seconds. After this test, the rig was shut down. As no loss of pressure or leakage was experienced during this run the epoxy/fiberglass and end gasket bonding techniques were judged workable for future development unit testing.

Teardown of the Development Unit 3 disclosed that excessive pinch at the ends of the cell active areas had caused indentations in the electrodes averaging 5 mils. This lowered the effective field depth by one-third, from 15 to 10 mils, in the areas shown in Figure 165. In addition, a small ridge of epoxy flash at the edge of the active area near both the oxygen ports further reduced the flow area. With the existing oxygen flow configuration, all oxygen was forced to flow through the restricted areas, causing a high pressure drop. This was probably a major contribution to the end-cell instability seen during high current density testing. To alleviate this problem, an effort was made to bypass some of the flow past the end-cell active areas into the intercell spacers between the end-cells and the next inboard cells on succeeding development units. Attention was also given to eliminating the ridges at the port/active area interface and obtaining a more uniform pinch.

An additional problem was oxygen leakage into the cooler which rendered the cooler inoperable. The cause of the leakage was two 1/8 inch cracks in the 1-mil nickel foil. Since these cracks occurred in the region of high pinch it was felt that more uniform pinch would avoid this problem in subsequent development units.

TABLE XXXVII
DEVELOPMENT UNIT 4

LOW POWER CALIBRATION AT 45 PSIA, 250 F WITH VARIOUS O_2 FLOW PATTERNS

CURRENT DENSITY AMP/FT^2	6-CELL AVERAGE VOLTAGE			CELL NO. 6 VOLTAGE		
	O_2 NORMAL	O_2 REVERSED	DUAL FEED	O_2 NORMAL	O_2 REVERSED	DUAL FEED
100	.963	.962	.960	.939	.958	.942
200	.938	.938	.936	.906	.925	.911
550	.879	—	.883	.811	—	.856

CONCLUSION – EITHER REVERSED O_2 FEED OR DUAL FEED IMPROVES PERFORMANCE OF LOW CELL (NO. 6). DUAL FEED SELECTED FOR HIGH-I/A OPERATION TO AVOID STARVING CELL NO. 1.

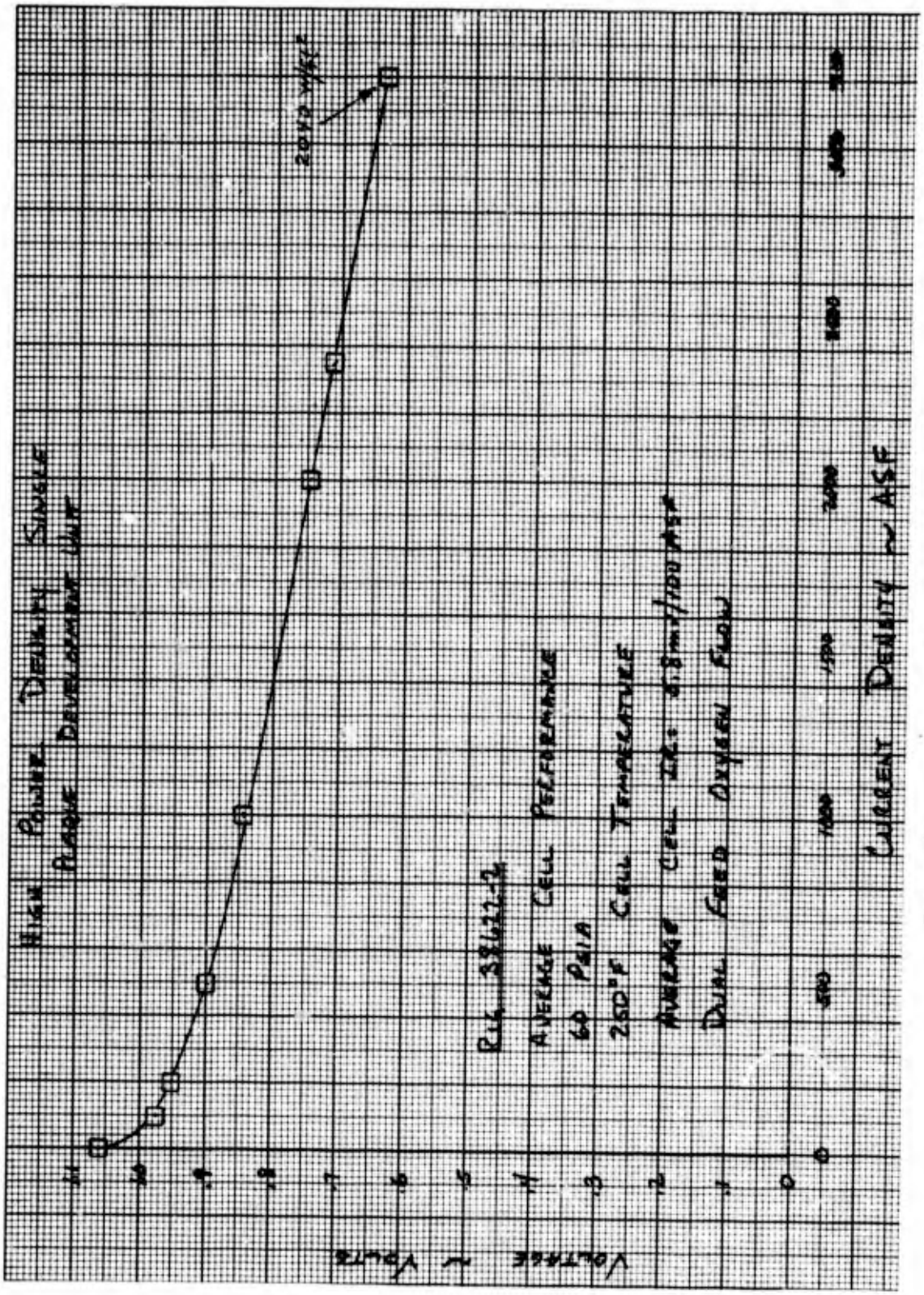

Figure 164 — Development Unit 3 - Performance Calibration

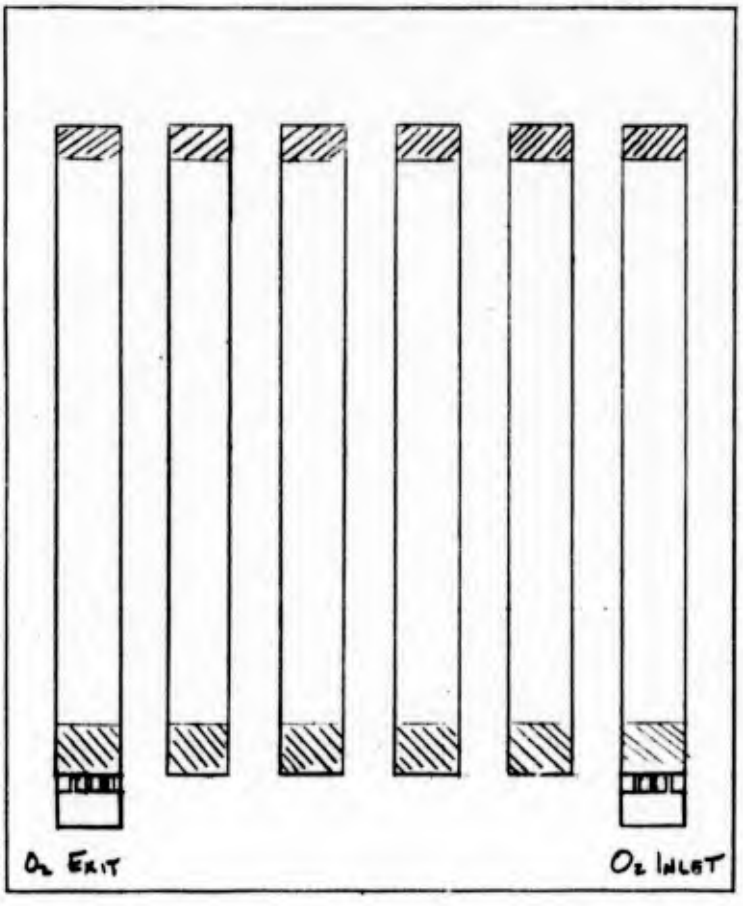

Figure 165 – Schematic of Cathode Side of Development Unit 3 Plaque

Development Unit 4

The next development unit to be tested was single plaque development unit of Configuration 3 design. This design has a repeating unit specific weight of 0.69 lb/kw at 2150 WSF. The unit featured nickel plated porous polysulfone electrolyte reservoir plates, machined Astrel coolant and hydrogen flow fields, and electroformed nickel oxygen fields. This was the first development unit to employ Astrel flow fields. The oxygen field/cooler assembly was laminated of a 3-mil thick electroformed nickel sheet and a 2-mil thick sheet of dielectric material. The use of a 3-mil thick nickel sheet in the cooler assembly caused this unit specific weight to be 0.69 lb/kw rather than the 0.64 lb/kw of Table XXXVI.

The initial heatup disclosed the need for additional matrix compression (pinch). This was accomplished by the addition of shims and the rig was refilled and returned to test. The performance was very good throughout the entire performance range and compared favorably to that observed in single cells. See Figure 166.

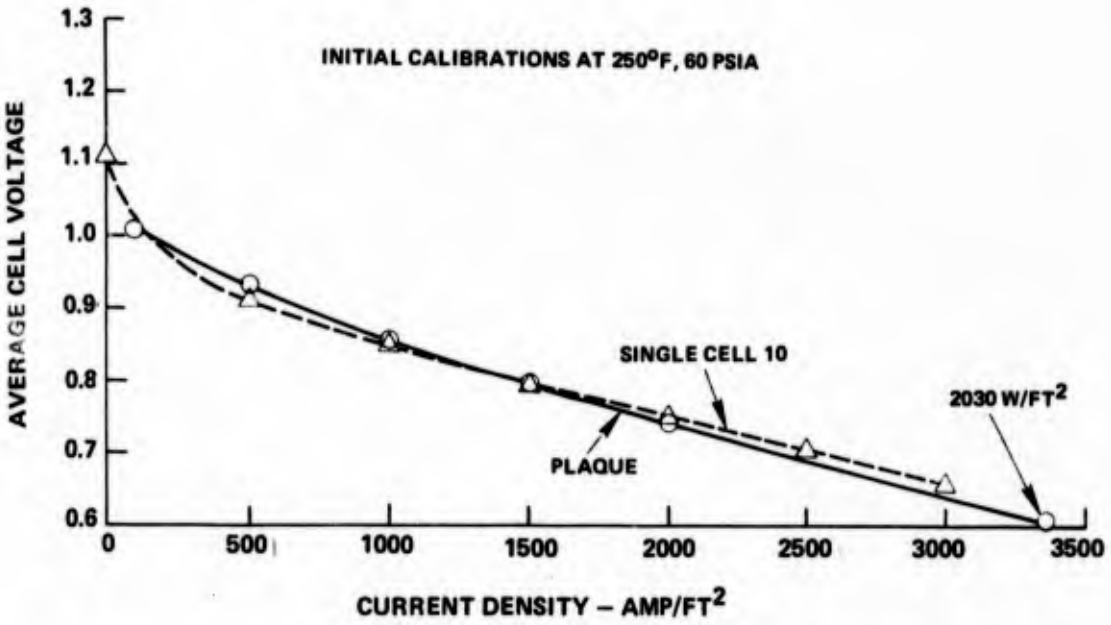

Figure 166 – Comparison of Development Unit 4 and Strip Cell Performance

Calibrations were conducted with normal (Cell 1 at oxygen inlet port) and reversed oxygen flows at 45 psia. These tests showed the average cell performance was somewhat higher with reversed flow than with normal flow. Consequently, the reversed flow pattern was used to begin subsequent testing. A calibration was conducted at 60 psia up to a current density of 3362 ASF. At this level the average cell voltage was 0.603 v., resulting in a power density of 2030 WSF, as shown in Figure 167. Two 30-second water storage missions were run next. The first mission consisted of 15 two-second bursts each followed by 3 seconds at no load. Peak power density achieved during this mission was 2030 WSF at 3670 ASF. Power variation throughout the mission was less than 5 percent and electrode thermocouples indicated that cooler performance was adequate and stable. The second mission consisted of five 6-second bursts each followed by 5 seconds off load. Peak power achieved in this mission was 2050 WSF. During this mission visicorder traces showed a slight decrease in the performance of Cell 4 at the end of a burst.

Next, following a thermal cycle to room temperature to simulated shutdown and restart, two more missions were conducted. Mission No. 3 consisted of three 10-second bursts, each followed by 10 seconds off load. Peak power achieved was again over 2000 WSF; however, midway through the third burst the voltage of Cell 1 went negative. A repeat of this mission with dual oxygen feed showed essentially the same results. Consequently, the unit was shut down and refilled with electrolyte. After restart and diagnostics, which showed the plaque had regained its initial performance level, six 30-second water storage missions were conducted. Starting with two-second bursts, the length of the bursts was increased with each successive mission, ending with two 15-second bursts on mission No. 10. The objective of these missions was to determine whether a slightly higher oxygen purge rate would improve the performance of the poorer cells and to observe, in detail, the oxygen field pressure drop, which seemed to increase during repeated bursts.

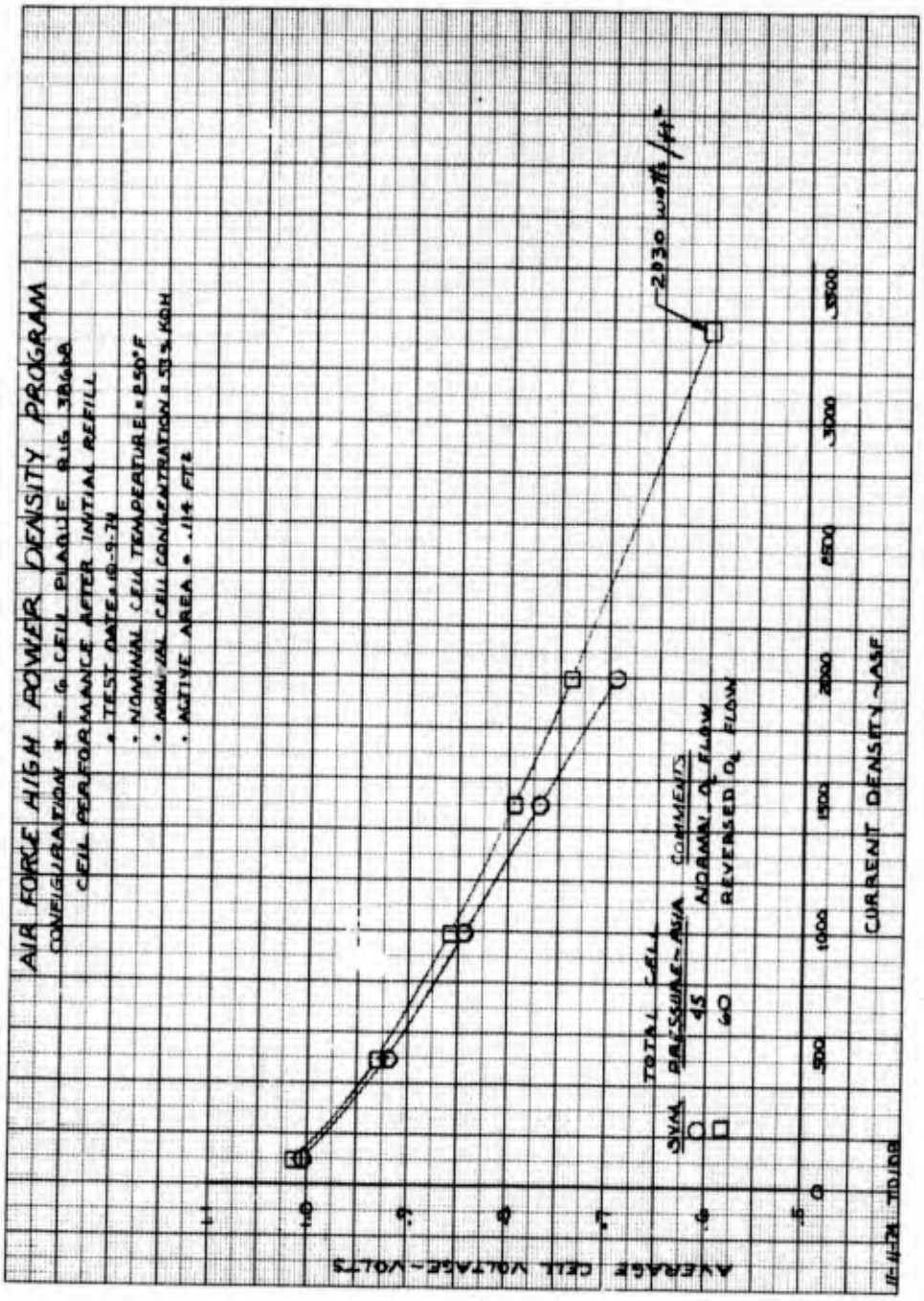

Figure 167 – Development Unit 4 - Performance Calibration to 2030 WSF

In the first mission of this test grouping, No. 5, a peak power density of 2050 WSF was obtained. No problems were encountered with negative cells on this or any of the subsequent missions with longer bursts.

During these missions, oxygen pressure observations, see Figure 168, showed an increasing pressure drop from inlet to exit with each burst. This effect increased with the length of each burst to a value as high as a 10 psi during the longer bursts. It was suspected that the initial pressure differential seen at the beginning of each burst had the effect of causing a hydrogen-oxygen cross pressure which forced electrolyte from the cell into the oxygen field. This in turn led to ever higher pressure drops, and consequently, lower oxygen pressures particularly at the downstream cells. The net effect was a performance loss toward the end of each mission. The next set of missions, Nos. 11 through 17, were conducted with the primary objective of determining if a small oxygen overpressure would counteract this phenomenon. The first three missions, Nos. 11 through 13, were run with normal gas pressures to establish a data baseline and then four additional missions, Nos. 14 through 17, were run with a 3-psi oxygen overpressure at open circuit conditions. The overpressure did serve to reduce the rate of pressure drop and to reduce end-of-burst performance loss. A comparison of the baseline mission performance without overpressure and those with overpressure is shown in Figure 169. Comparison of the 10-second burst mission shows the overpressure ensures stable performance.

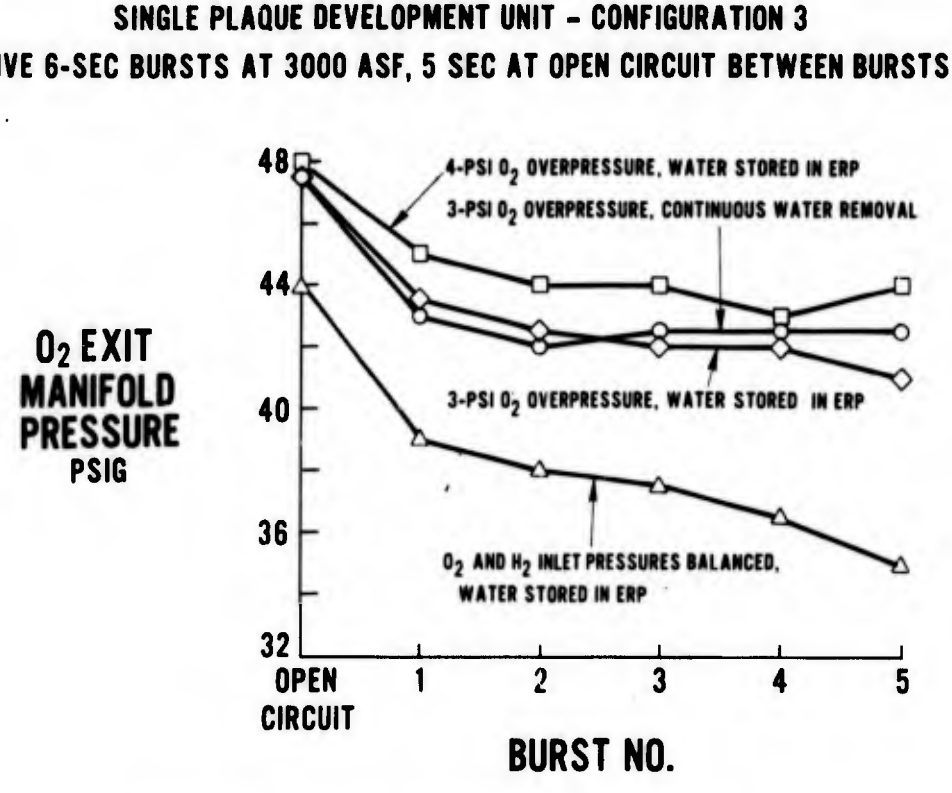

Figure 168 – Oxygen Pressure Drop Observations

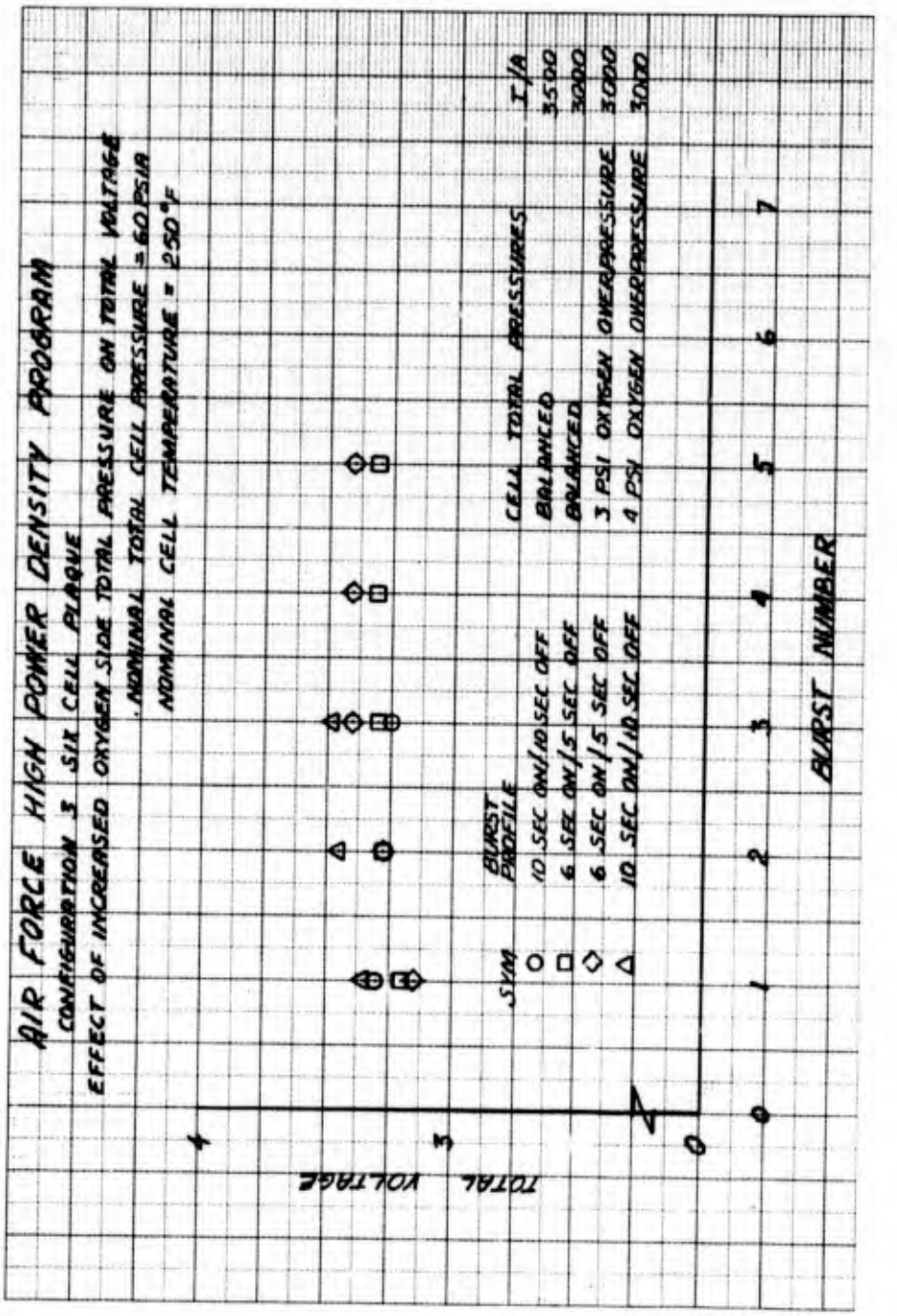

Figure 169 – Performance Stabilized by Overpressure

Following Mission No. 17, the unit was shut down and refilled. Then a final group of 30-second water storage missions, mission No. 18 through 22, were conducted. These were all run at 3000 ASF with a 4-psi oxygen overpressure. Mission No. 22 consisted of one continuous 30-second burst. Even with this single continuous burst no problems were encountered and the plaque showed a slight improvement in performance from start to finish.

The final test was conducted with dynamic water removal and consisted of 30 minutes of continuous cycling between open circuit and 3000 ASF for a total of 165 cycles. Figure 170 shows there was essentially no loss in plaque performance during this period.

After final diagnostics the unit was shut down for inspection. Diagnostics before and after each day of testing revealed a gain in cell IR. This increase in IR appeared almost entirely responsible for the overall loss in performance in the toal test period and is believed to be connected with the electrolyte movement resulting from the oxygen pressure differentials observed during testing.

Post-test inspection showed the following:

- All cooler laminate bonds were in good condition with no evidence of leakage.
- Some corrosion occurred at the oxygen exit port, as shown in Figure 171. This was apparently responsible for some of the increased pressure drop.
- Compression (pinch) was uniform across the entire plaque. (Revealed by uniform nubbin identation depth in electrodes.)
- Corrosion of the laminate strips between cells on the oxygen side; see Figure 171. Products of this corrosion appeared to plug the exit port and contribute to the oxygen pressure drop.
- The hydrogen electrodes and ERP's, as shown in Figure 172, were in good condition. Water take-up tests of the ERP's following teardown showed no change in ERP porosity had occurred.
- The Astrel flow fields were slightly cracked. This did not appear to have had any effect on the development unit performance.
- Laboratory analysis of the electrodes revealed an average loss of 50 mv in cathode activation. The anodes appeared to be somewhat flooded.

During this test the development unit accumulated 58 hours of hot time and 29 hours of load time. Twenty-two 30-second water-storage missions were completed. In addition the unit demonstrated 165 consecutive bursts from open circuit to 3000 ASF with dynamic water removal, the equivalent of 33 missions. Total time accumulated above 3000 ASF was 28 minutes. Six thermal cycles were completed. Table XXXVIII presents a chronology of events during the test.

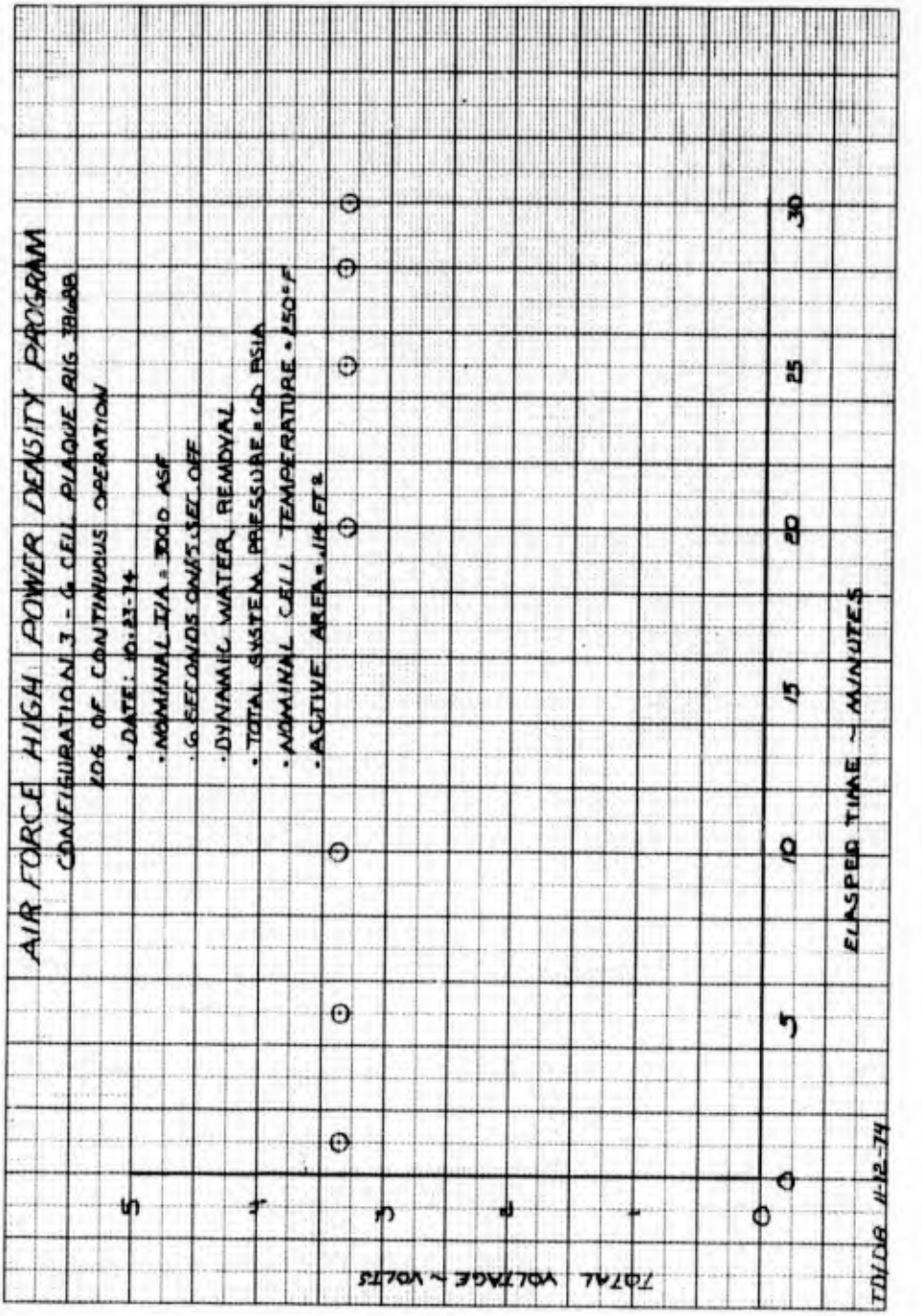

Figure 170 – 165 Cycle Endurance Test

POST-TEST EXAMINATION

H_2 ELECTRODES AND ELECTROLYTE RESERVOIR PLATES

SINGLE-PLAQUE DEVELOPMENT UNIT – CONFIGURATION 3

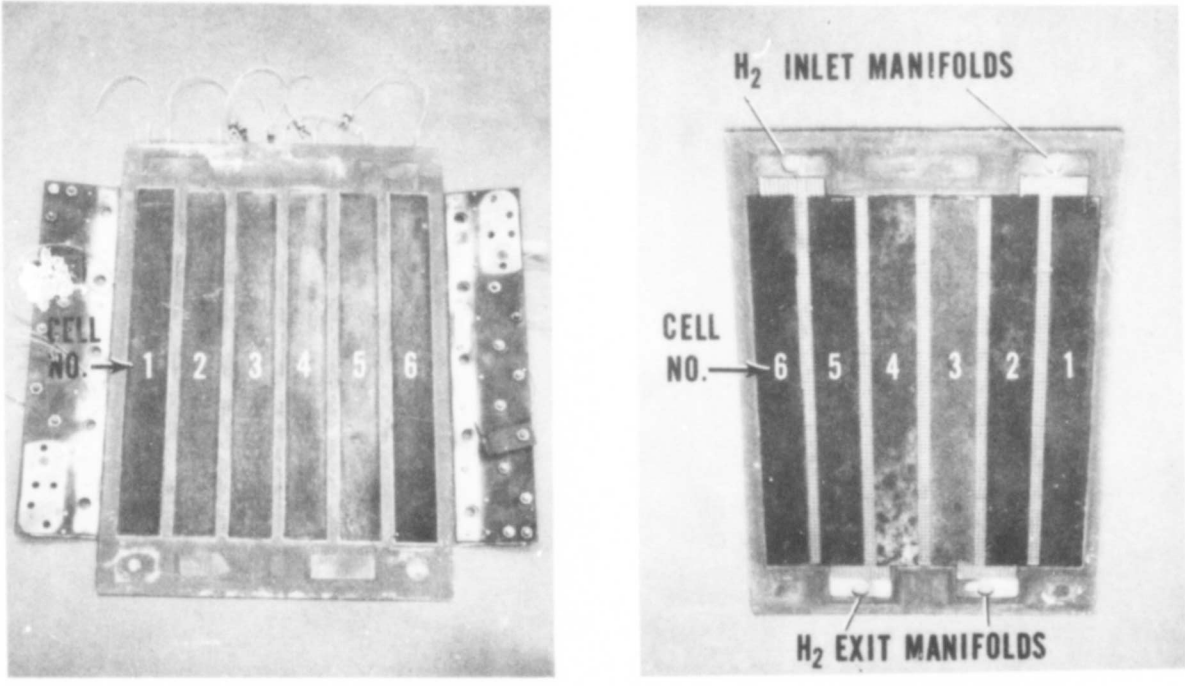

H_2 ELECTRODES

ERP'S

Figure 171 – Development Unit 4 - Hydrogen Side of Plaque

POST-TEST EXAMINATION

O_2 FLOW FIELDS AND O_2 ELECTRODES

SINGLE- PLAQUE DEVELOPMENT UNIT – CONFIGURATION 3

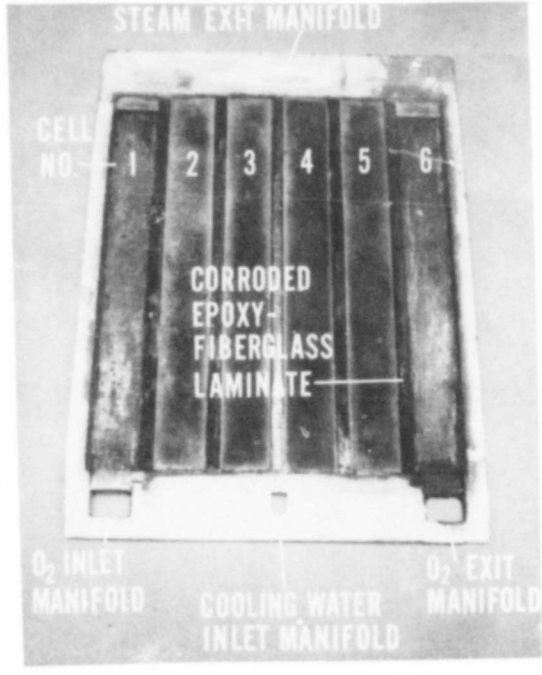

O_2 FLOW FIELDS AND COOLER

(FLOW FIELDS FROM CELLS 1 AND 6 REMOVED)

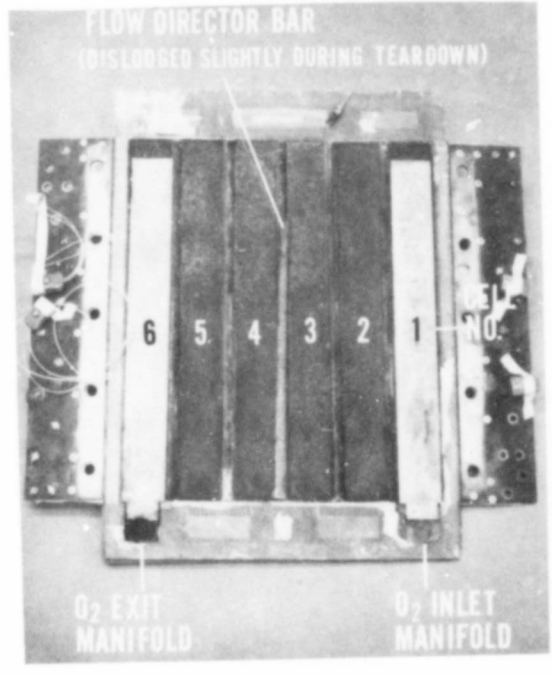

O_2 ELECTRODES

(O_2 FLOW FIELDS COVER CELLS 1 AND 6)

Figure 172 – Development Unit 4 - Oxygen Side of Plaque

TABLE XXXVIII
TEST SUMMARY

DEVELOPMENT UNIT 4 – CONFIGURATION 3
PRODUCT WATER STORED IN ERP EXCEPT AS NOTED

MISSION NO.	MAX. POWER DENSITY, WSF	NOM. CURRENT DENSITY, ASF	DESCRIPTION OF MISSION	O_2 FLOW DIRECTION	O_2 OVER-PRESSURE, PSI	REMARKS
FIRST TEST SERIES						
1	2030	3500	15 BURSTS – 2 SEC ON/3 SEC OFF	REVERSED	0	VOLTAGES STABLE
2	2050		5 BURSTS – 6 SEC ON/5 SEC OFF			
3	> 2000		3 BURSTS – 10 SEC ON/10 SEC OFF			DIDN'T HOLD LOAD
4	> 2000		2 BURSTS – 10 SEC ON/10 SEC OFF	DUAL FEED		
SECOND TEST SERIES						
5	2050	3500	15 BURSTS 2 SEC ON/3 SEC OFF	NORMAL	0	VOLTAGES STABLE
6	2000		7 BURSTS 4 SEC ON/4 SEC OFF			
7	1910		5 BURSTS 6 SEC ON/5 SEC OFF			
8	1930		4 BURSTS 8 SEC ON/8 SEC OFF			CELL 6 DROPPED 30 MV ON LAST BURST
9	1910		3 BURSTS 10 SEC ON/10 SEC OFF			CELLS 4, 5, 6 DROPPED 30 MV ON LAST BURST
10	1850		2 BURSTS 15 SEC ON/15 SEC OFF			CELLS 4, 5, 6 DROPPED 60 MV ON LAST BURST
11	1800		8 BURSTS 4 SEC ON/4 SEC OFF			CELLS 5, 6 DROPPED 30 MV ON LAST BURST
12	1720		5 BURSTS 6 SEC ON/5 SEC OFF			CELLS, 5, 6 DROPPED 20-30 MV ON LAST BURST
13	1710	3000				CELLS 5, 6, DROPPED 10-20 MV ON LAST BURST
14	1780				3	VOLTAGES STABLE
15	1830					
16	1610			REVERSED		CELLS, 1,2,3,4 DROPPED 40-70 MV ON LAST BURST
17	1600			NORMAL		H_2O REMOVED, VOLTAGES STABLE
THIRD TEST SERIES						
18	1960	3000	15 BURSTS – 2 SEC ON/3 SEC OFF	NORMAL	4	VOLTAGES STABLE
19	1940		5 BURSTS – 6 SEC ON/5 SEC OFF			
20	1860		3 BURSTS – 10 SEC ON/10 SEC OFF			
21	1810		2 BURSTS – 15 SEC ON/15 SEC OFF			
22	1660		1 BURST – 30 SEC ON			
23	1660		5 BURSTS – 6 SEC ON/5 SEC OFF			H_2O REMOVED, VOLTAGES STABLE
55	1660		15 BURSTS – 6 SEC ON/5 SEC OFF			

Development Unit 5

The first 12-cell dual-plaque development unit to be tested was of the Configuration 3 design. This unit was similar to the Configuration 3 single plaque in Development Unit 4 except that a 2-mil thick nickel foil was laminated into the oxygen field/cooler assembly rather than a 3-mil thick foil. Use of this thinner separator sheet reduced the units specific weight to 0.67 lb/kw from the 0.69 lb/kw of Development Unit 4. Figure 173 shows a cross section of this dual-plaque development unit. This unit is the basic repeating section of a power-plant cell stack.

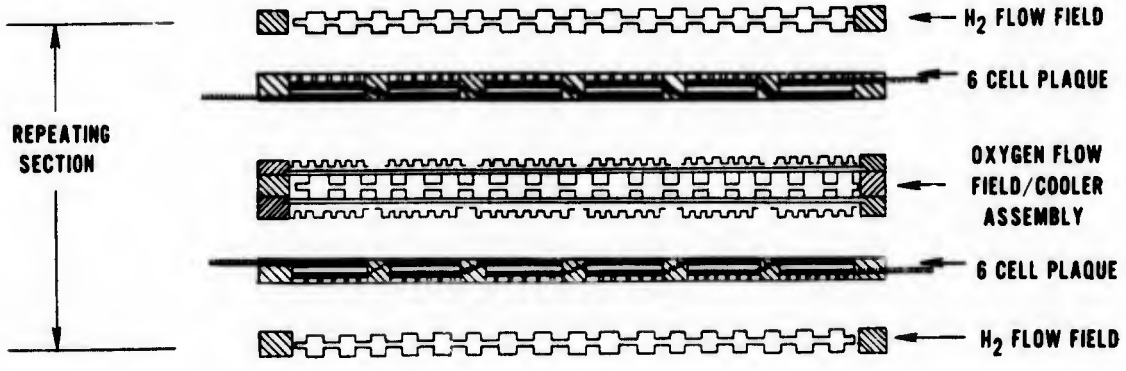

Figure 173 — Cross-Section of 12-Cell Dual Plaque Development Unit

The objectives of this test were to 1) evaluate the basic performance of the dual-plaque configuration and to 2) demonstrate endurance capability, up to 50 thermal cycles.

The initial calibration showed good performance; see Figure 174. The initial steady state calibration was limited to 1000 ASF because of the high hydrogen flow required for product water removal at higher current desnities. This performance was comparable to that demonstrated in single plaque development unit tests. Cell IR readings indicated good pinch distribution throughout both plaques. Following diagnostics a 30-second water storage mission was simulated. The mission consisted of 15 two-second power bursts, each followed by 3 seconds at open circuit. During this mission the peak power generated was 3098 watts at 4482 ASF resulting in a power density of 2265 WSF. As shown in Figure 175, interpolation between this point and the initial calibration curve indicates a power density of 2100 WSF would be obtained at the design current of 3500 ASF. Following the 30-second mission the plaque was shut down as part of the cycling program.

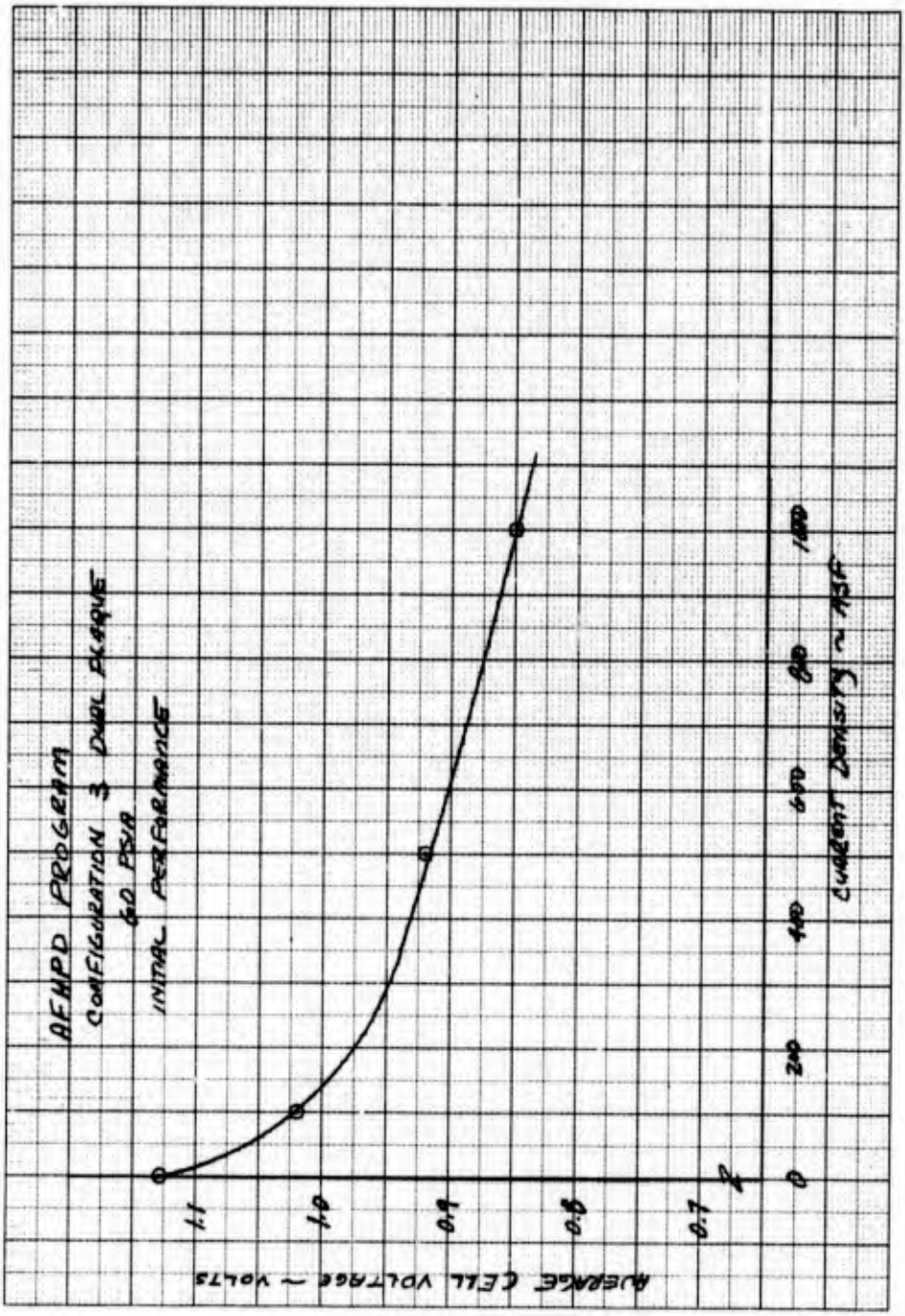

Figure 174 – Development Unit 5 - Performance Calibration to 1000 ASF

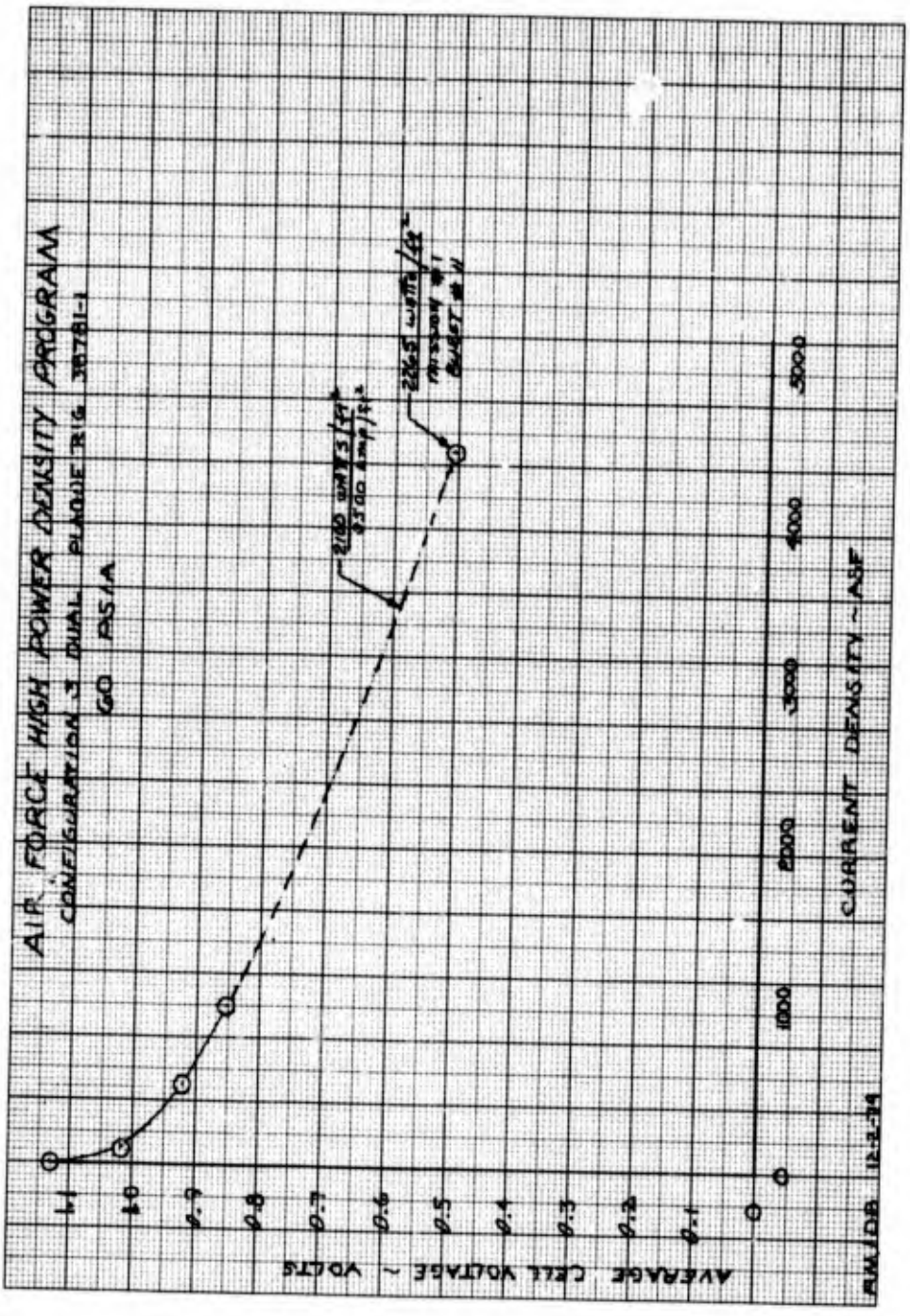

Figure 175 -- Development Unit 5 - Performance Calibration to 4482 ASF

Mission No. 2 repeated the first mission except that the oxygen flow direction was reversed. The oxygen flow direction was alternated from mission to mission in order that all cells see the same type of hydrogen to oxygen over-pressure with time. During the entire program no serious problem was noted with high oxygen pressure drop through the unit. The highest pressure drop noted was 5 psi which was compensated for by setting the O_2 pressure at 2-3 psi over the hydrogen pressure. Peak power observed in this mission was 2930 watts at 3661 ASF. This equals a power density of 2140 WSF. Next, the unit was thermal cycled three times (Cycles 3-5). The third mission profile consisted of 5 six-second bursts, each followed by 5 seconds at open circuit. The first attempt at this mission was terminated after the second burst due to low voltage in Cell 6. In the second run, the hydrogen vent rate was set so that 50 percent of the water produced was removed with the vent stream. This run was made with no problems and demonstrated a peak power density of 1801 WSF at 3430 ASF.

Mission 4 was a repeat of the third with the oxygen flow reversed. The peak power achieved was 1930 WSF at 3485 ASF. Mission 5 consisted of 8 bursts of 4-seconds duration each followed by 4 seconds at open circuit. Peak power was 1880 WSF at 3529 ASF. Following this mission, the unit was shut down for electrolyte refill. After refill and diagnostics Missions 6 and 7 were run. These missions were fifteen 2-second bursts each followed by 3 seconds at open circuit with 50 percent water removal. Mission 6 was run with normal oxygen flow and Mission 7 with reversed oxygen flow. Both missions achieved peak power densities of 2040 WSF; Figure 176 presents a power profile for the unit during Mission 6. There is a rise in average power during the first few bursts. This phenomenon is believed to be due primarily to electrolyte concentration effects. These effects can be alleviated by proper adjustment of the initial concentration. After 3 additional thermal cycles (13-15) Mission 8 was run. This mission was identical to Mission 3 and resulted in a peak power density of 2030 WSF at 3477 ASF. For Missions 9 and 10, 25 percent of the product water was removed in the hydrogen vent stream. Both missions consisted of 5 bursts of 6-seconds duration, each followed by 5 seconds at open circuit. Peak power achieved was 2090 WSF for Mission 9 and 1080 WSF for Mission 10. During Thermal Cycle 27 an oxygen to coolant leak developed and the test was terminated. Figure 177 shows the average cell voltages during this test series and Table XXXIX is a chronology of events during the testing. A total of 66 hours of hot time and 10.7 hours of load time were accumulated including 10, 30 second missions and 27 thermal cycles.

Disassembly of the stack showed several small pinholes through the oxygen steam separator foil in the area of Cell 6 along the outside edge. Similar pinholes were observed along the edge of Cell 1. It is believed that this is evidence that shorting from cell 1 to cell 6 through the dielectric layer eventually caused pinholes to form in the separator foil which led to the oxygen to coolant leakage. This in turn led to reactant crossover in Cell 6. The general condition of the stack was very good except for some cracking and distortion of the Astrel flow fields and polysulfone ERP near the location of the oxygen tank. There was no evidence of significant corrosion either in the intercell spacers or the manifold as had been observed in the Development Unit 5. Except as noted above, all components, including electrodes, ERPs, and flow fields, appeared to be in good condition.

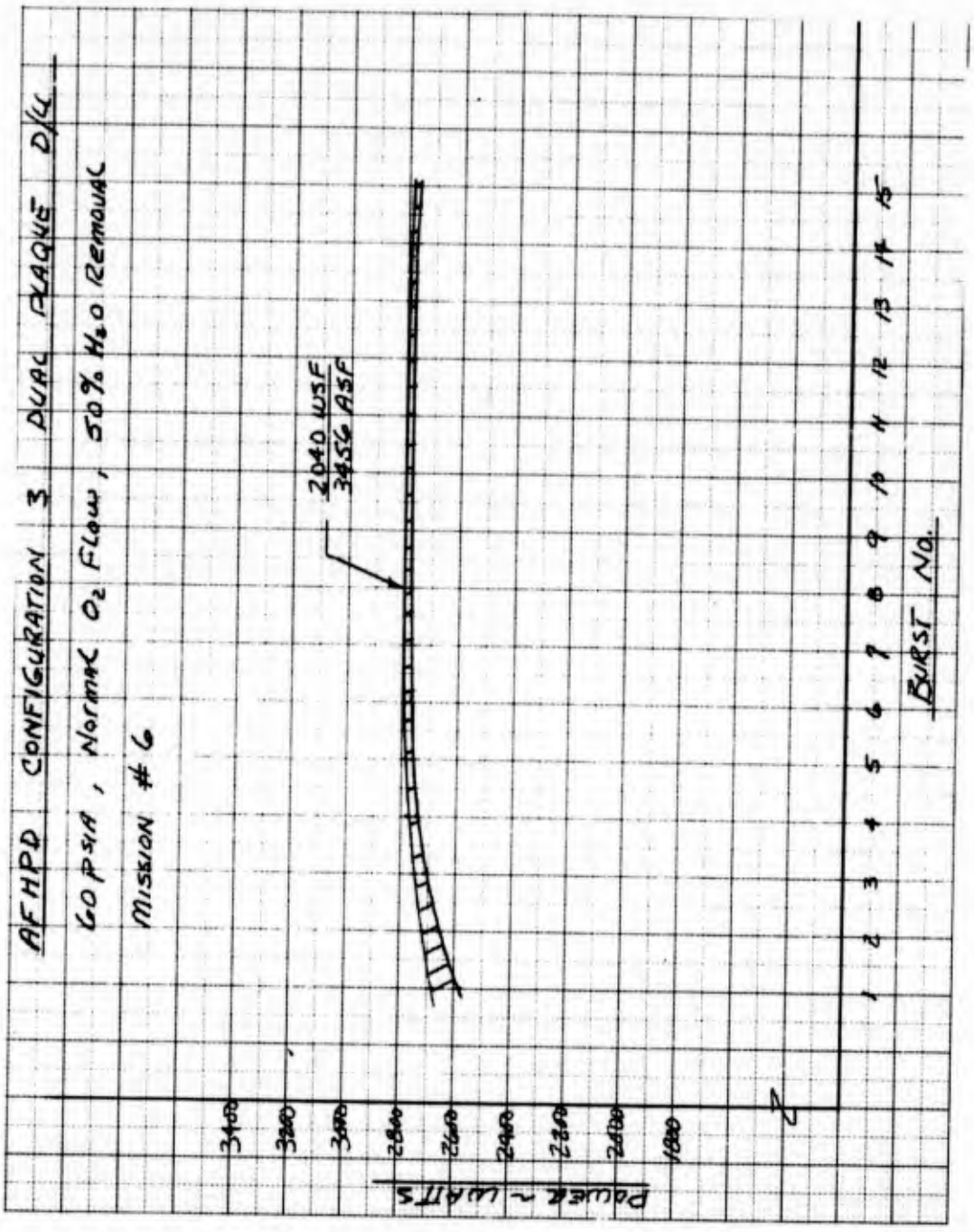

Figure 176 – Development Unit 5 - Power Delivery Profile

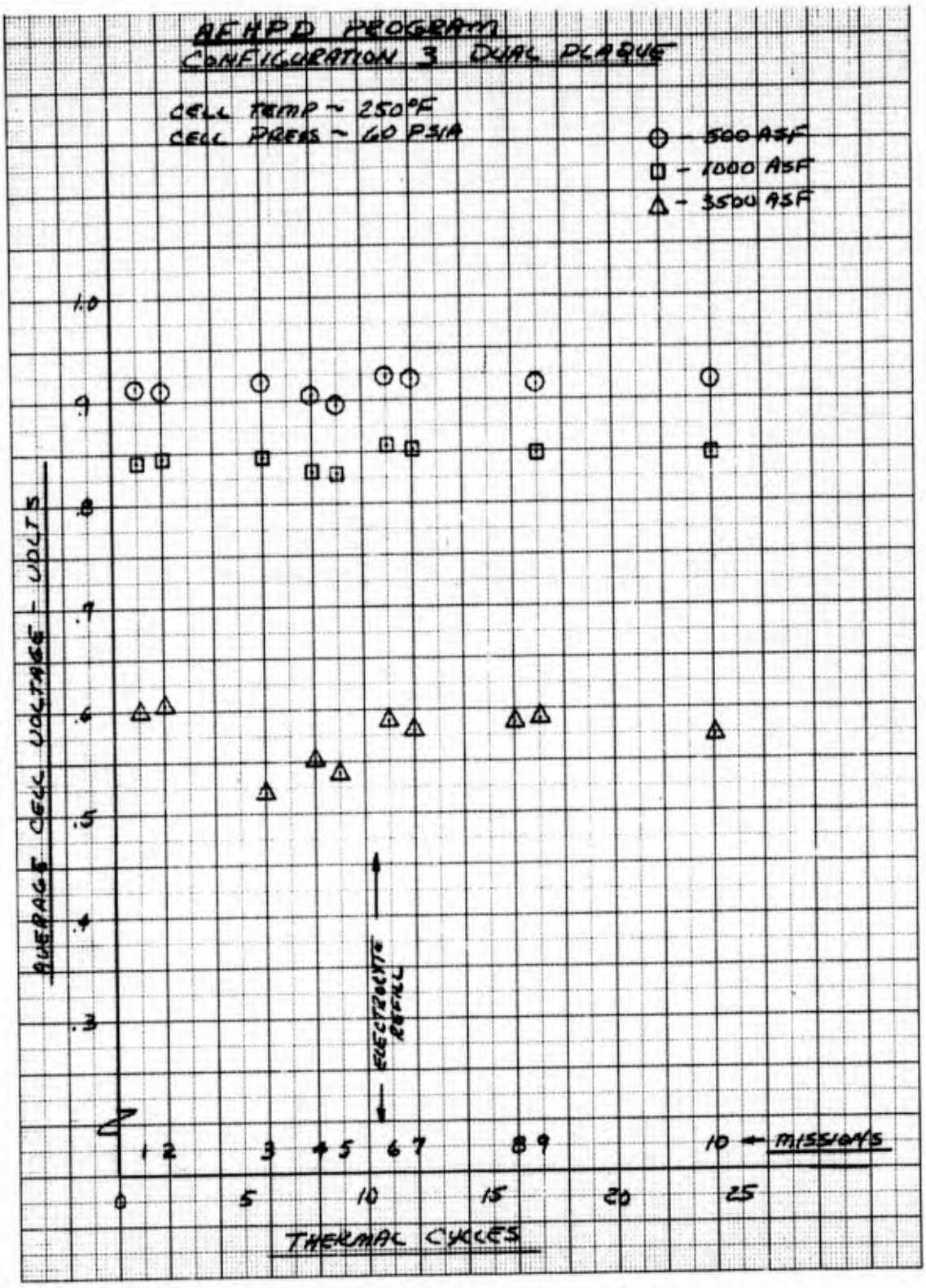

Figure 177 – Development Unit 5 - Average Cell Voltages

TABLE XXXIX
TEST SUMMARY
DEVELOPMENT UNIT 5 – CONFIGURATION 3

Product Water Stored in ERP Except as Noted

Mission No.	Max. Power Density, WSF	Nom. Current Density, ASF	Description of Mission	O_2 Flow Direction	O_2 Over Pressure PSI	Remarks
1	2265	4500	15 Bursts 2 sec on-3 sec off	Normal	2	No water removal
2	2140	3500	15 Bursts 2 sec on-3 sec off	Reversal	2	No water removal
3	1801	3500	5 Bursts 6 sec on-5 sec off	Normal	3	50% water removal
4	1930	3500	5 Bursts 6 sec on-5 sec off	Reversed	3	50% water removal
5	1880	3500	8 Bursts 4 sec on-4 sec off	Reversed	3	50% water removal
6	2040	3500	15 Bursts 2 sec on-3 sec off	Normal	3	50% water removal
7	2040	3500	15 Bursts 2 sec on-3 sec off	Reversed	3	50% water removal
8	2030	3500	5 Bursts 6 sec on-5 sec off	Normal	3	50% water removal
9	2090	3500	5 Bursts 6 sec on-5 sec off	Reversal	3	25% water removal
10	2080	3500	5 Bursts 6 sec on-5 sec off	Normal	3	25% water removal

V CONCLUSIONS

The primary conclusions of the program are:

1) Test demonstrations have shown that no breakthroughs are required to reduce the demonstrated hardware to prototype and then flight-ready powerplants and power systems.

2) Demonstration of power densities to 3000 watts/ft^2 has shown that the Reference System design power density of 2150 watts/ft^2 is realistic and conservative.

3) Test demonstrations have shown that the fuel cell has a useful life of at least 300 missions and probably more than 600 missions.

4) Design studies have shown that the fuel cell is competitive in advanced aircraft installations.

5) Design studies have shown that fuel cell system weight and volume do not increase rapidly as mission energy delivery and duration grow.

6) Test demonstrations and the design studies show the fuel cell possesses significant potential for development of still lighter powerplants and power systems.

APPENDIX A

COOLER THERMAL ANALYSIS

AE/HPD THERMAL ANALYSIS

ASSUMPTIONS:

- ONE-DIMENSIONAL HEAT TRANSFER MODEL
- 6600 BTU/HR-FT^2 HEAT FLUX (BASED ON PLANAR DIMENSION)
- 30% OF HEAT GENERATED AT ANODE
- NEGLECT ELECTRODE ΔT
- K (KOH/MATRIX) = .4 BTU-ft/HR-ft^2-°F
- K (PLASTIC COATING) = 1.7 BTU-IN/HR-ft^2-°F
- K (NICKEL) = 35 BTU-ft/HR-ft^2-°F
- K (ALUMINUM) = 100 BTU-ft/HR-ft^2-°F
- PLANAR HEAT TRANSFER AREA EQUALS COOLER HEAT TRANSFER AREA
- 15 MIL O_2 FIELD DEPTH

AF/IIFD THERMAL ANALYSIS

KNOWN VARIABLES (REQUIRED):

- MATRIX THICKNESS (MILS)
- CONTACT FILM COEFFICIENT (BTU/HR-FT^2-°F)
- OXYGEN PIN COVERAGE (%)
- PLASTIC COATING THICKNESS (MILS)
- THERMAL CONDUCTIVITY OF PIN MAT'L (BTU/HR-FT-°F)
- NUCLEATE BOILING SURFACE COEFFICIENT (C)
- FIN MATERIAL (NICKEL OR ALUMINUM)

AF/HPD THERMAL ANALYSIS

CALCULATION PROCEDURE:

1. DETERMINE MATRIX ΔT FROM CURVE 1
2. DETERMINE CONTACT RESISTANCE ΔT FROM CURVE 2
3. DETERMINE PLASTIC COATING ΔT FROM CURVE 3
4. DETERMINE O_2 PIN ΔT FROM CURVE 4
5. ESTIMATE FIN/BOILING/PLASTIC COATING ΔT RANGE

METHOD 1: NEGLECT FORCED CONVECTION

a. DETERMINE $\frac{1}{h_{plastic}}$ FROM CURVE 5

b. ASSUME $(Q/A)_{EFFECTIVE}$ AND DETERMINE $h_{NUCLEATE\ BOILING}$ FROM CURVE 6.

c. CALCULATE h_{TOT} / FIN THICKNESS (h_{TOT}/ℓ)

WHERE $$\frac{1}{h_{TOT}} = \frac{1}{h_{PLASTIC}} + \frac{1}{h_{NUC.\ BOILING}}$$

D. FIND η_c FROM CURVES 7A OR 7B.

E. DETERMINE EFFECTIVE (Q/A) FROM CURVE 8.

F. COMPARE RESULTING (Q/A) TO ASSUMPTION IN (b.) AND ITERATE, IF NECESSARY

G. CALCULATE $\Delta T = \frac{(Q/A)_{EFFECTIVE}}{h_{TOT}}$

AF/IRFD THERMAL ANALYSIS

METHOD 2: NEGLECT NUCLEATE BOILING EFFECTS AND ASSUME FORCED CONVECTION FILM COEFFICIENT LARGE.

$$\frac{1}{h_{\text{FORCED CONVECTION}}} \cong 0$$

a. DETERMINE $\frac{1}{h_{\text{PLASTIC}}}$ FROM CURVE 5

b. $h_{TOT} \cong h_{\text{PLASTIC}}$

c. FIND η_f FROM CURVE 7A OR 7B

D. DETERMINE EFFECTIVE (Q/A) FROM CURVE 8

E. CALCULATE

$$\Delta T = \frac{(Q/A)_{\text{EFFECTIVE}}}{h_{TOT}}$$

LAMINATED MAG/III COOLER (PCH569)

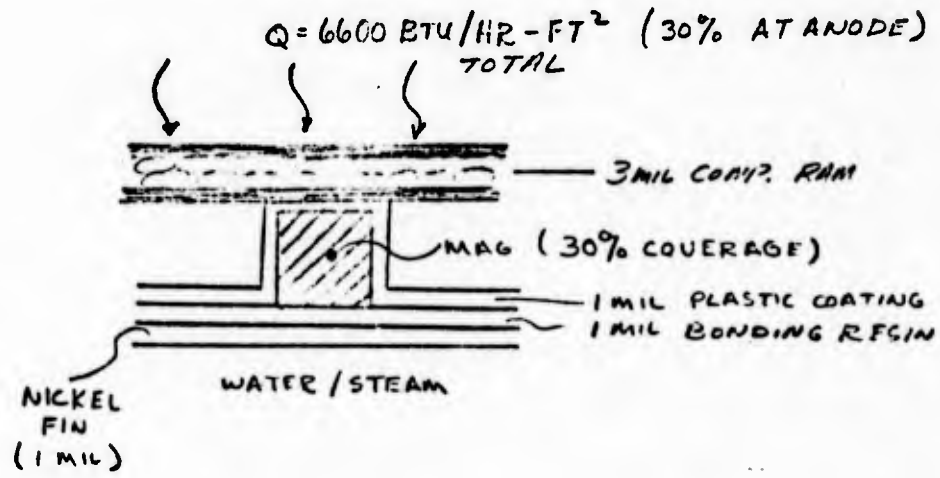

1. MATRIX ΔT = (1.3 °F)
2. Assume $h_{CONTACT}$ = 5000 $\frac{BTU}{HR-ft^2-°F}$ AND 30% O_2 COVERAGE

∴ CONTACT ΔT = (3.2 °F)

3. Assume BONDING RESIN HAS SAME K AS PLASTIC
   ∴ 2 MILS PLASTIC @ 30% COVERAGE

∴ Plastic ΔT = (26 °F)

4. $K_{MAG} \cong$ 40 BTU/HR-ft-°F

∴ ΔT_{FIN} = (.7 °F)

5. No plastic film on nickel fin ⟶ C = .006
   Assume $(Q/A)_{eff}$ = 10.1×10^3
   $h_{TOT} - h_{N.C.}$ = 1.7×10^3
   ℓ_{fin} = 40 mils ⟶ η_f = .27 ⟶ $(Q/A)_e$ = 13.5×10^3

Assume $(Q/A)_c = 12.0 \times 10^3$

$h_T = 1.9 \times 10^3$

$\eta_f = .27 \rightarrow (Q/A)_c = 13.5 \times 10^3$

$$\Delta T = \frac{13.5 \times 10^3}{1.9 \times 10^3} = 7.1^\circ F$$

∴ BOILING ΔT 0 - 7.1 °F

MATRIX	1.3 °F
CONTACT	3.2
PLASTIC	26.0
PIN	.7
BOILING	0.0 - 7.1
	31.2 - 38.3 °F

ELECTROFORMED NICKEL

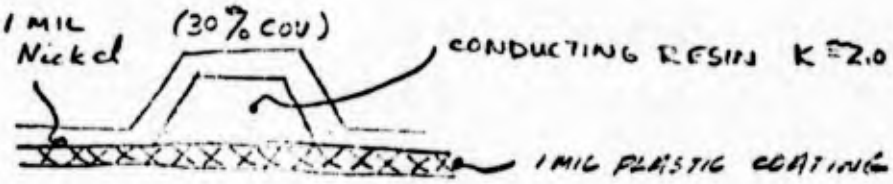

1. MAX. ΔT = 1.3 °F
2. CONTACT ΔT = 3.2 °F
3. $K_{PIN} \sim 2.0 \frac{BTU-ft}{HR-ft^2-°F}$

$$\Delta T_{PIN} = 14\ °F$$

4. $\frac{1}{h_{Plastic}} = .59 \times 10^{-3} \frac{HR-ft^2-°F}{BTU}$

For plastic assume C = .013
Assume $(Q/A)_e = 10^4$

$h_{n.B} = 650$

$$\frac{1}{h_{TOT}} = \frac{1}{650} + .59 \times 10^{-3} = 2.13 \times 10^{-3}$$

$h_{TOT} = 470$

$\eta_f = .5$

$(Q/A)_e = 10.1 \times 10^3 = 1.01 \times 10^4$

For Nuc. Fuel.

$$\Delta T = \frac{10.1 \times 10^3}{.470 \times 10^3} = 21.5\ °F$$

$h_{TOT} = h_{PLASTIC} = 1.7 \times 10^3$

$\eta_f = .27$

$(Q/A)_e = 13.7 \times 10^3$

$$\Delta T = \frac{13.7 \times 10^3}{1.7 \times 10^3} = 8.06\ °F$$

MAXIMUM FORCED CONVECTION

MATRIX	1.3 °F
CONTACT	3.2
PIN	14.0
BOILING	8.1 - 21.5
	26.6 - 40.0 °F

AF/NPD THERMAL ANALYSIS

CURVE I

THERMOFLEX CERAMIC FIBROUS INSULATION

- $K_{(MATRIX)}$ = 1.60 BTU/HR-FT-°F
- 30% HEAT GENERATED AT ANODE (1500 BTU/HR-FT²)
- K (MATRIX AND VOID) = 0.1 BTU/HR-FT-°F

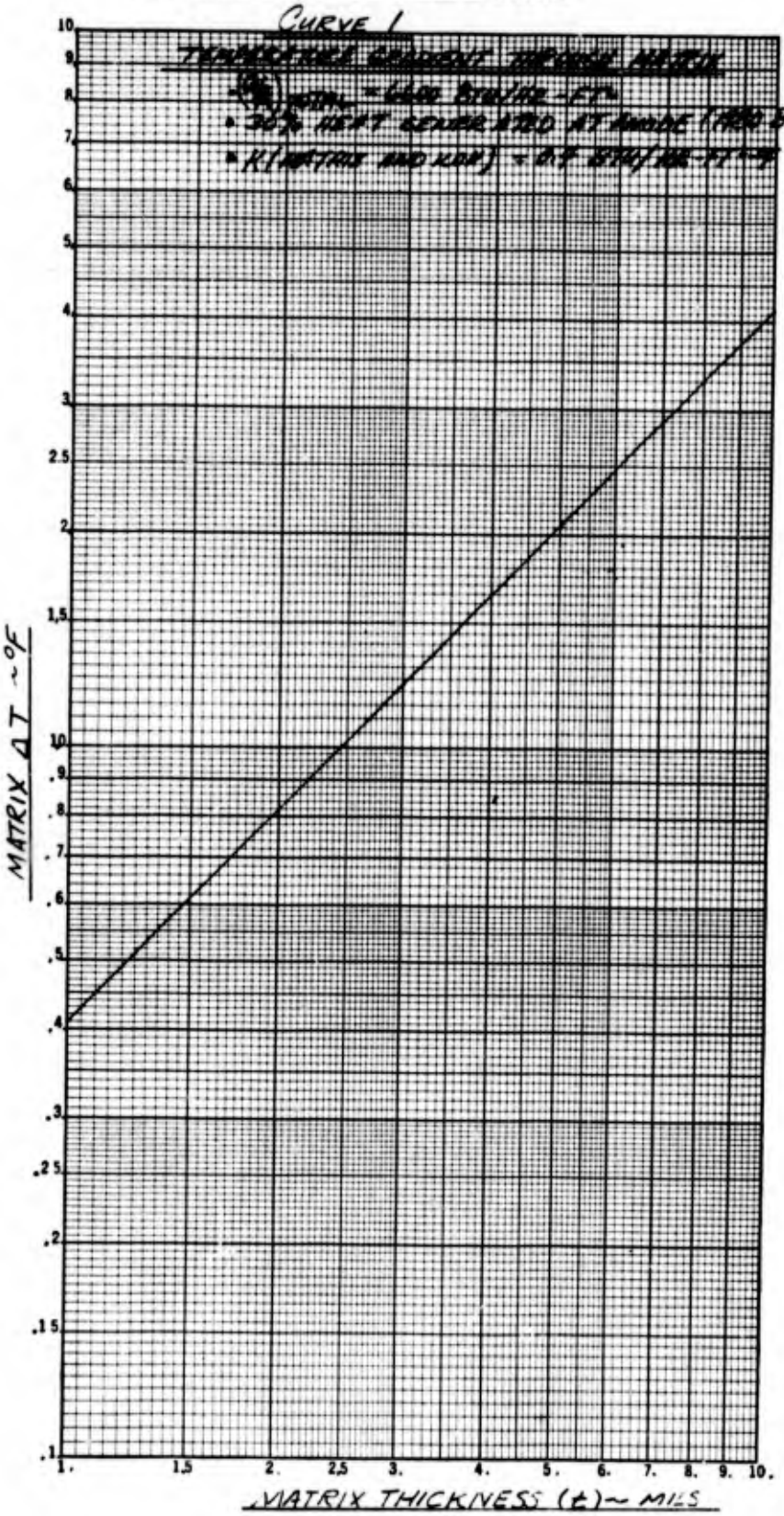

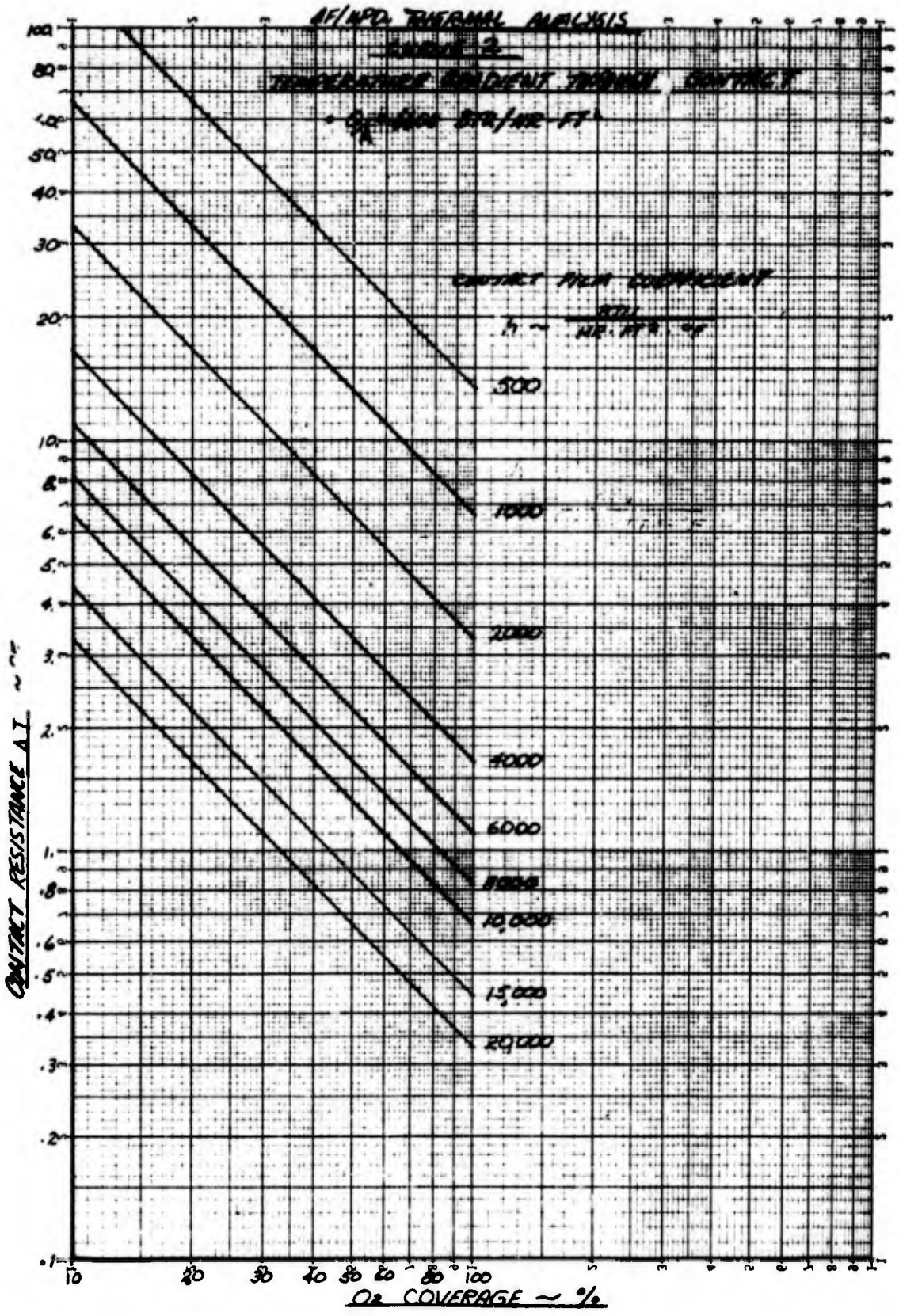
AF/APD THERMAL ANALYSIS
FIGURE 2
TEMPERATURE DROP AT THERMAL CONTACT
CONTACT HEAT COEFFICIENT
500
1000
2000
4000
6000
10,000
15,000
20,000
CONTACT RESISTANCE ΔT
O₂ COVERAGE ~ %

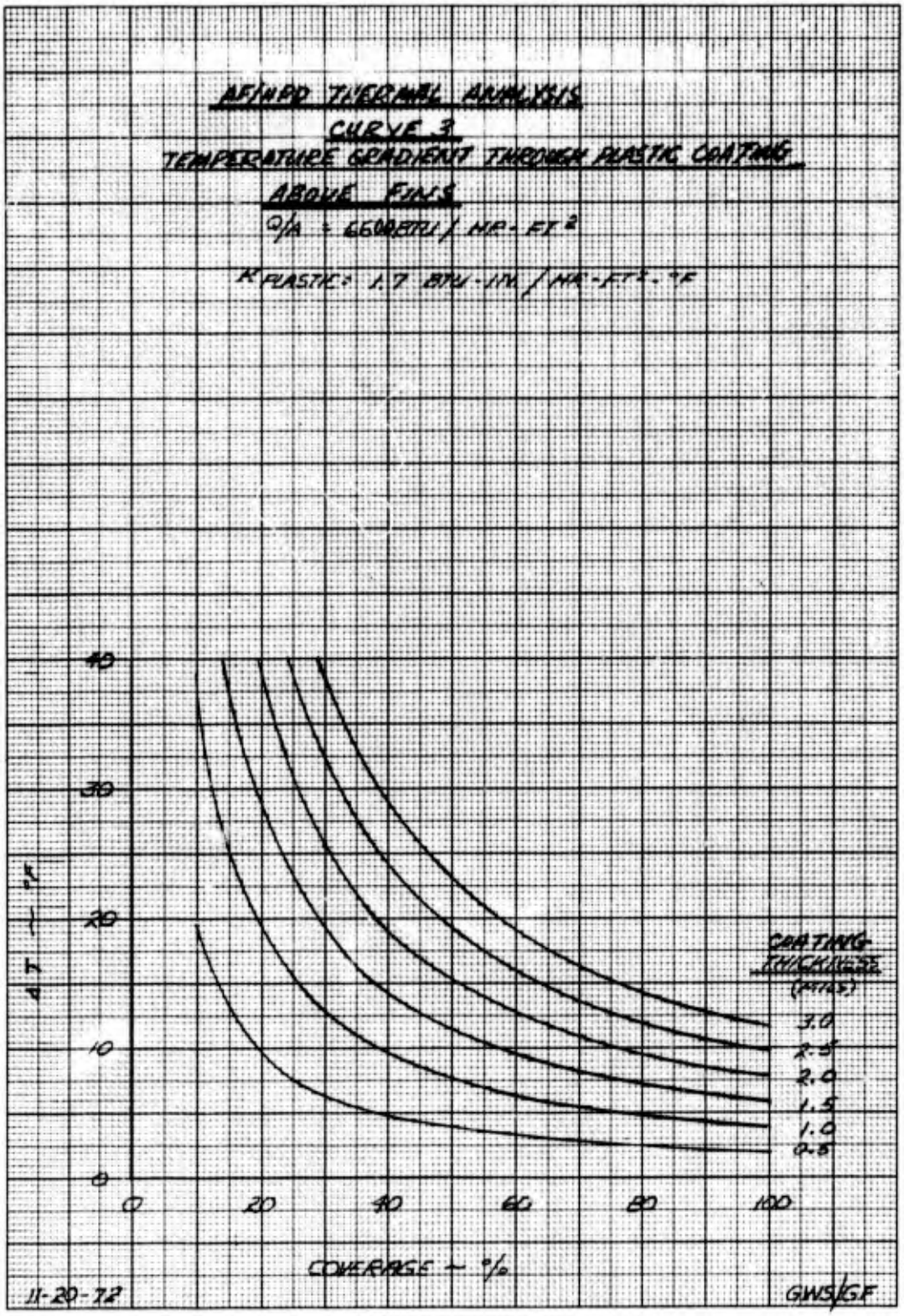
AFWBD THERMAL ANALYSIS
CURVE 3
TEMPERATURE GRADIENT THROUGH PLASTIC COATING
ABOVE FIALS
Q/A = 6600 BTU / HR - FT²
K PLASTIC = 1.7 BTU - IN / HR - FT² - °F
40
30
20
10
0
ΔT °F
0
20
40
60
80
100
COVERAGE - %
COATING THICKNESS (MILS)
3.0
2.5
2.0
1.5
1.0
0.5
11-20-72
GWS/GF

AF/HDD THERMAL ANALYSIS

CURVE 4

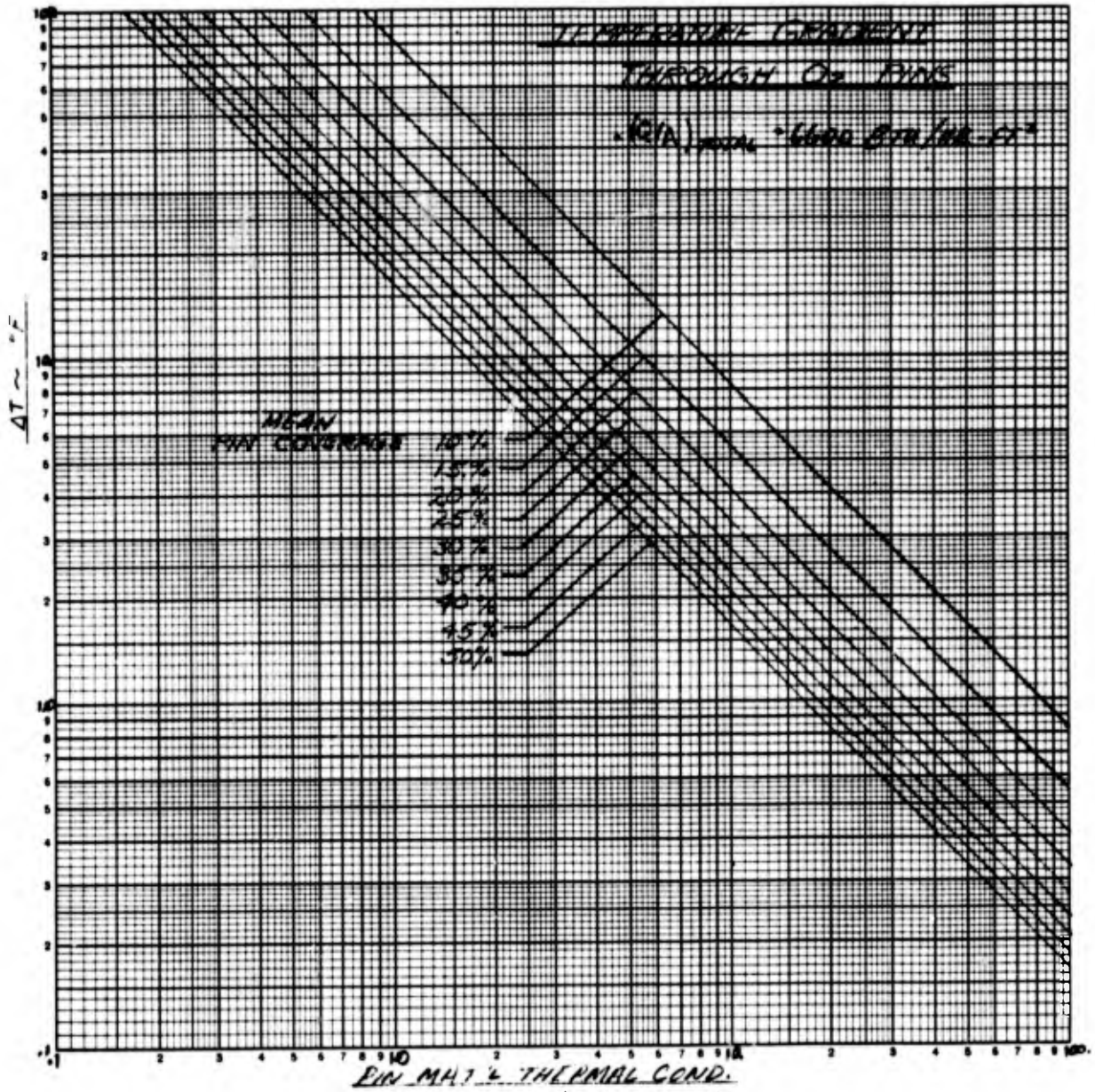

BIN MAT'L THERMAL COND.
(K) ~ BTU - FT / HR - FT² - °F

AF/HPD THERMAL ANALYSIS

CURVE 5

EFFECTIVE FILM COEFFICIENTS FOR PLASTIC FILMS

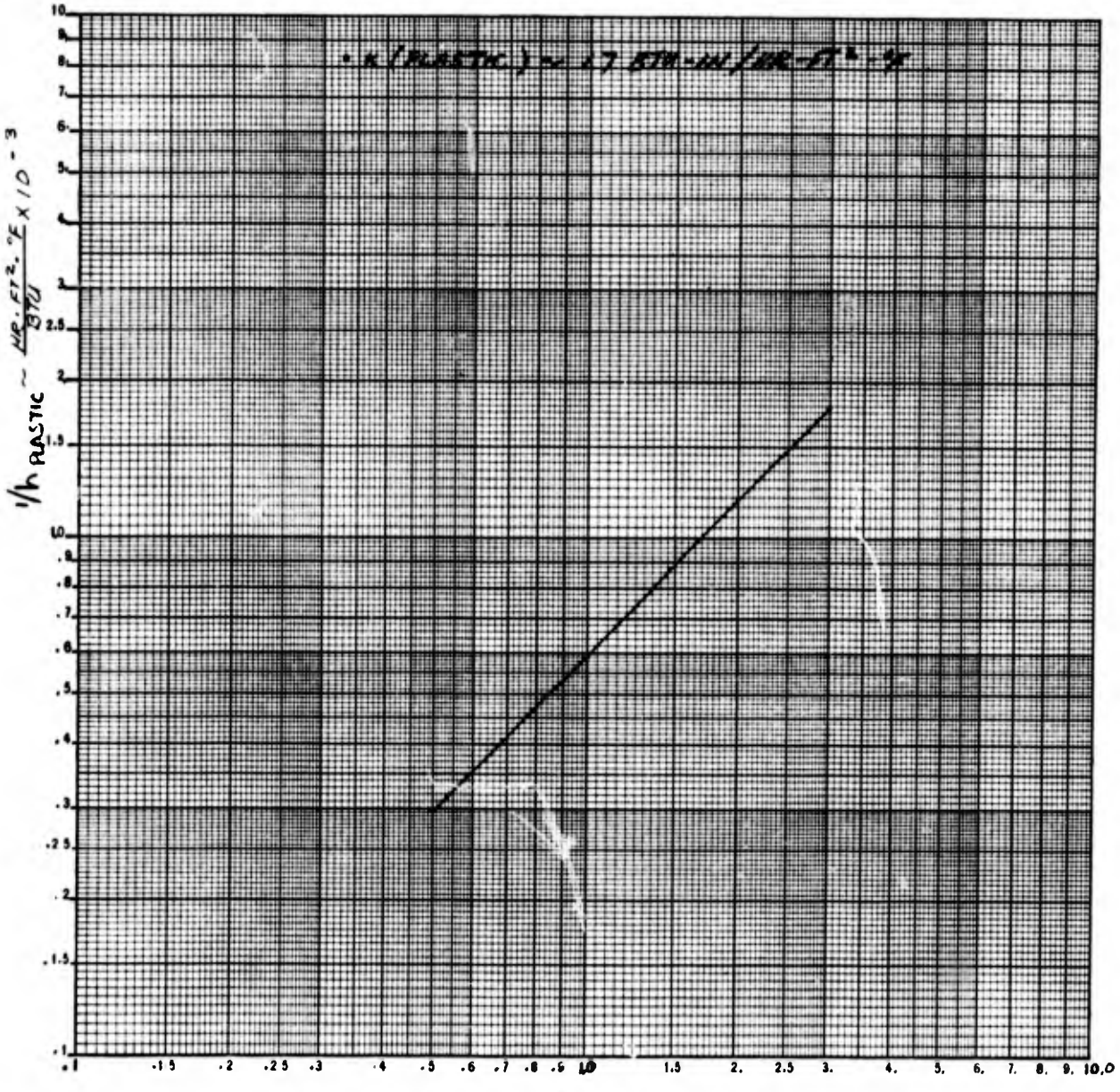

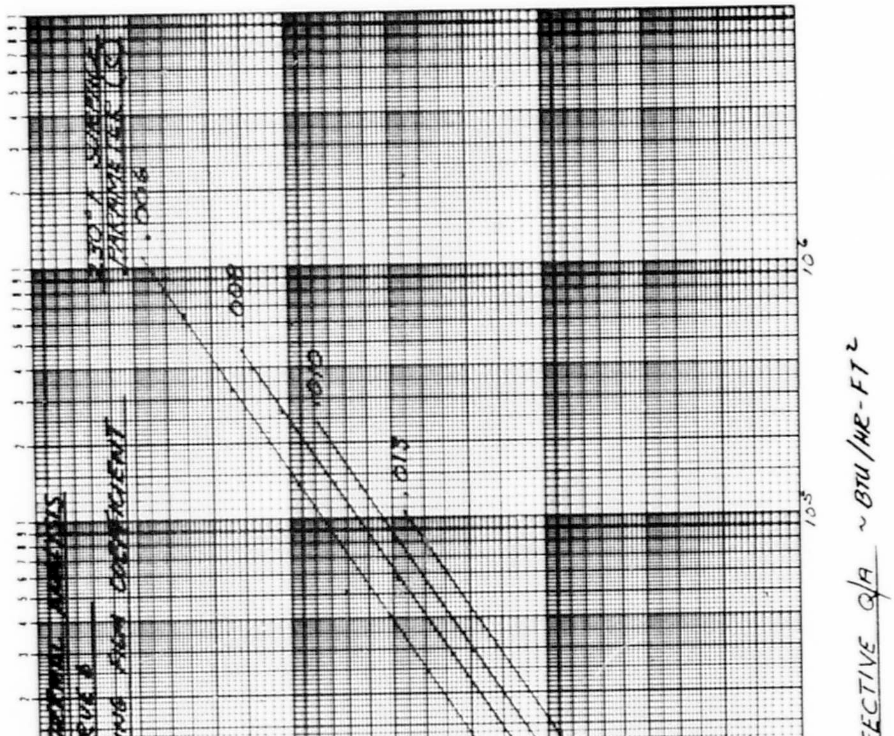
CURVE 8
NUCLEATE BOILING FILM COEFFICIENT
PARAMETER
.008
.010
.013
.018
EFFECTIVE Q/A ~ BTU/HR-FT²
h NUCLEATE BOILING ~ BTU/HR-FT²-°F
10²
10³
10⁴

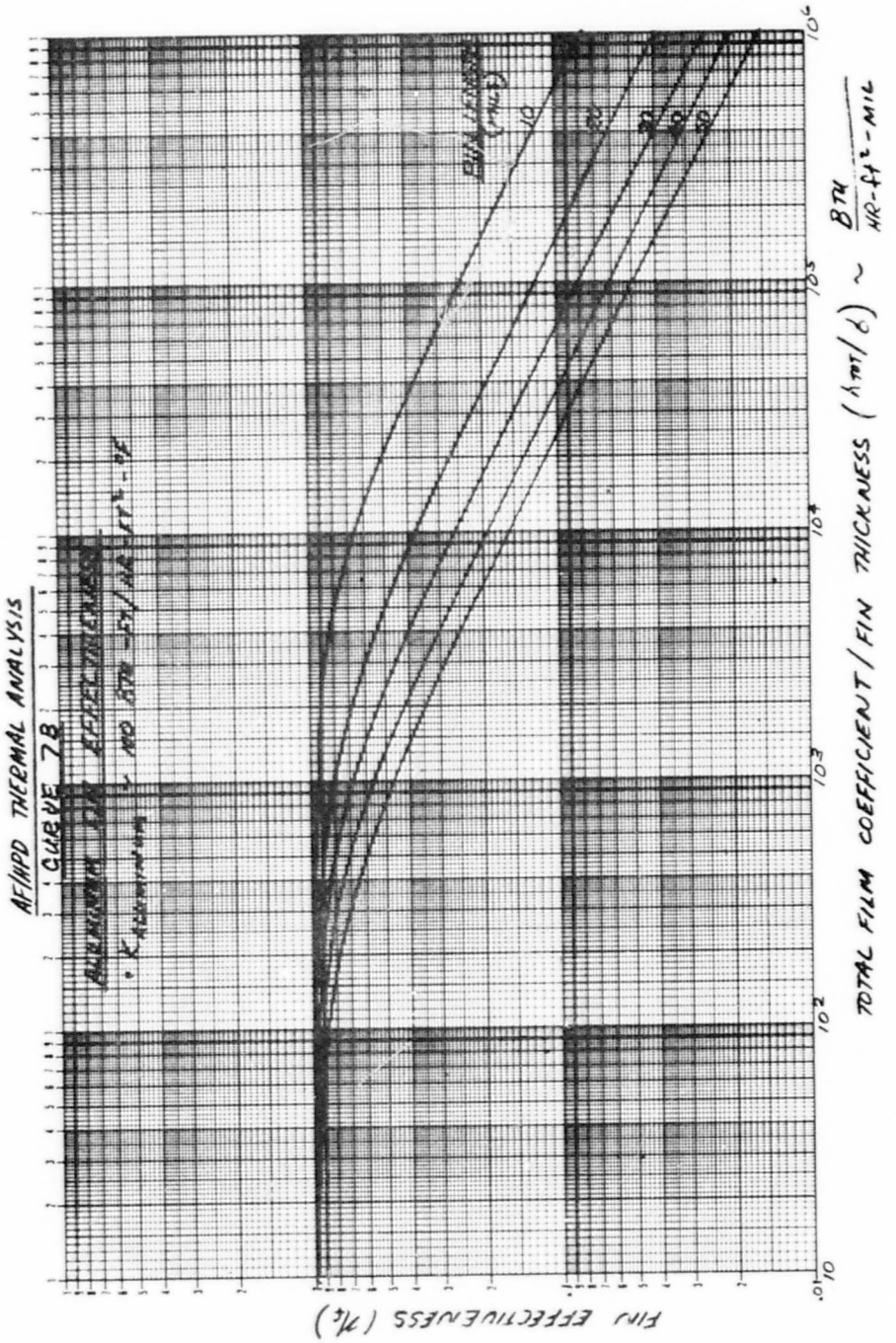
AF/HPD THERMAL ANALYSIS
CURVE 28
FIN EFFECTIVENESS (η_f)
TOTAL FILM COEFFICIENT / FIN THICKNESS (h_tot/δ) ~ BTU/HR-FT²-MIL
10
10²
10³
10⁴
10⁵
10⁶
.01
.1

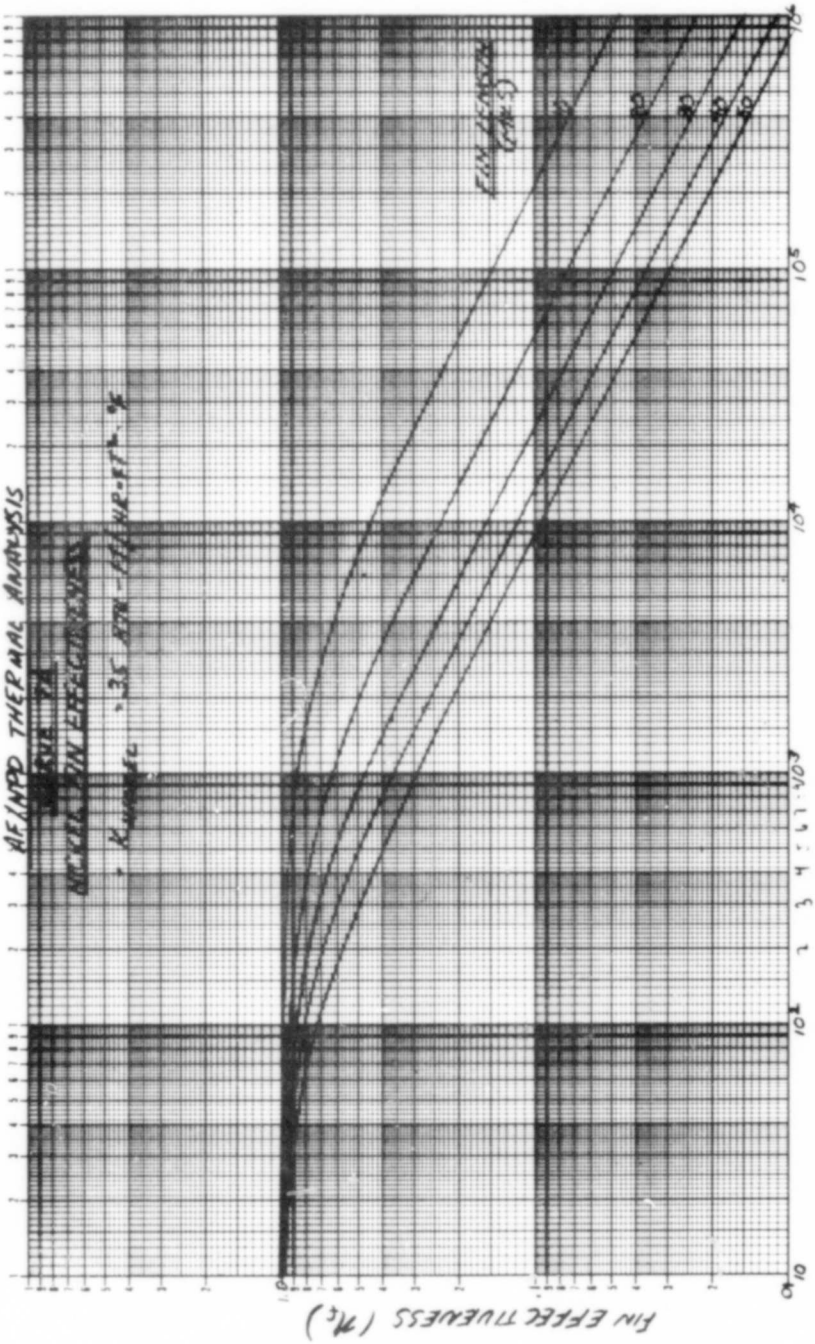
REVISED THERMAL ANALYSIS
FIN EFFECTIVENESS (η_f)
TOTAL FILM COEFFICIENT/FIN THICKNESS (h_T/δ) = BTU / HR-FT²-MIL

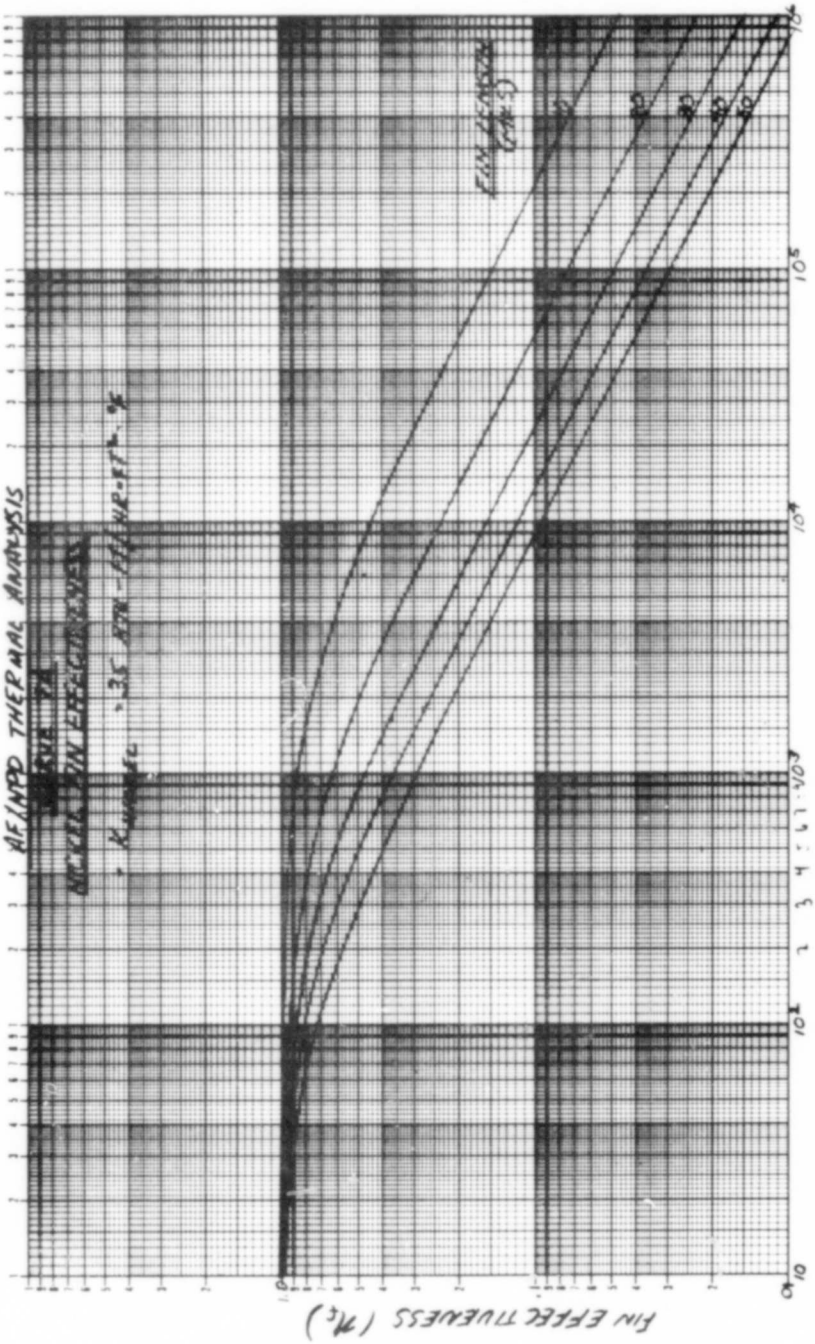
REVISED THERMAL ANALYSIS
FIN EFFECTIVENESS (η_f)
TOTAL FILM COEFFICIENT/FIN THICKNESS (h_T/δ) = BTU / HR-FT²-MIL

APPENDIX B

FUEL CELL RAM-AIR CONDENSER STUDY

DESIGN STUDY #294

FUEL CELL CONDENSER STUDY

PREPARED FOR

PRATT & WHITNEY AIRCRAFT

CONTRACT NUMBER F33615-72-C-13711

JANUARY 10, 1973

DS #294

FUEL CELL CONDENSER STUDY

This study presents weight, size, and drag parameters for an air cooled steam condenser for a single heat load condition but a variety of altitudes and vehicle speeds. This information is to facilitate an evaluation relative to an alternate scheme that uses an expendable coolant.

The design load, identified as Condition 2, requires the condensing of 1.33×10^4 lb/hr. of steam at 230°F saturation temperature and the subcooling of this condensate and a like amount of liquid water (a total of 2.66×10^4 lb/hr.) from 230°F to 215°F. This load amounts to 191,150 Btu/min.

A baseline operating condition was defined for vehicle flight at Mach .9 and 30,000 ft. altitude. In addition to this design condition, cores were sized for three different speeds (Mach .5, .7 and .9) at each of three altitudes (15,000 ft., 30,000 ft. and 45,000 ft.).

At each operating condition four different air flows were assumed. Core weight decreases with increased air flow but ducting weights and drag increase. Since the mission profile of the vehicle and the S.F.C. of its engines are not available, an equivalent take-off weight penalty for the increase in drag cannot be made in this study. In order for others to make this evaluation the results are plotted showing core weight vs. drag at each of the flight conditions considered. See Figures #1, #2 and #3.

At each operating condition the following assumptions were made relative to available pressure:

Available Pressure = $P_{stagnation} - P_{ambient}$

Scoop Loss (80% recovery)	=	20. %
Core Loss	=	60. %
Inlet Header Loss	=	8. %
Outlet Header Loss	=	4.8%
Ducting to Overboard	=	2.4%
Dumping Loss to Ambient	=	4.8%
		100 %

The fins selected for all cores are the same, consisting of a serrated fin on the steam side, .100 in. high, 18 fins per inch, and on the air side a ruffled fin .426 in. high, 27 fins per inch. This high density air fin provides the lowest weight core but not the smallest frontal area. Table I shows the size and weight effect of five cores designed to the same operating condition but using plain straight fins, perforated straight fins, and ruffled fins all 22 fins/inch and ruffled fins at 18 fins/inch and 27 fins/inch.

The total core weight values plotted are calculated based on a fixed ratio between total weight and effective weight. The computer program calculates the weight of the heat transfer surfaces only and does not include such items as closure bars, end plates, headers, flanges, etc. The structural design group calculated the total weight of a core sized for Mach .9, 30,000 ft. The ratio of total to effective core weight of this core was used for all cores.

DS #294

Although no ducting arrangement has been defined for this equipment, its weight is directly chargeable to the steam condenser approach, so approximations were made for the cores designed to the Mach .9, 30,000 ft. and the Mach .7, 45,000 ft. operating conditions to lend perspective to this study. The model presumed for the ducting arrangement is as shown on sketch "A".

The scoop throat is sized to pass the flow at 0.6 of the free stream velocity. Assuming 80% recovery a diffuser length providing a 2Θ of 15° is calculated to match the heat exchanger inlet flange. The outlet duct length is set at 1.5 times the core height. Because of the size of the overboard area it is assumed that a dual overboard exit will be used. Ducting is based on a .060 in. thick wall and flanges are assumed to be .75 in. wide and .25 in. thick. All cross-sectional areas are assumed to be square to simplify calculations and since it represents the smallest periphery and thus the lightest weight for a rectangular shape. Ultimately installation and packaging will determine the most practical shape. The significance of also evaluating drag penalty in making an overall weight study can be shown by its possible effects at one design condition. Figure 4 shows a plot of total core, flange, and ducting weight as a function of drag for the Mach .9, 30,000 ft. operating condition for various "on" time drag penalties. The penalty weights are calculated on the basis of an assumed S.F.C. (specific fuel consumption) of .85 lb. fuel per hour per lb. of thrust. Thus, at this operating condition if the drag is 3460 lbs. for two minutes the fuel needed to overcome this drag is $3460 \text{ lbs.} \times \frac{2 \text{ min.}}{60 \text{ min/hr.}} \times \frac{.85 \text{ lbs. fuel}}{\text{hr.}} =$ 97.8 lbs. of fuel penalty. These weight figures do not include any allowance

for the ram scoop and its advancing and retracting mechanism nor for the overboard louvres. The drag values do not include profile drag penalty nor is there any credit for overboard thrust.

Some visibility of flight performance over a range of Mach Nos. at 15,000, 30,000 and 45,000 ft. altitude is provided by showing the performance of the smallest core (23.8 ft.^{2} face, 394 lb. core, 602 lbs. with ducting), designed for Mach .9, 30,000 ft. and for a large core (44.9 ft.^{2} face, 390 lb. core, 787 lbs. with ducting), designed for Mach .7, 45,000 ft. (See Figures 5 and 6.)

A cross plot of the data of Figure 6 yields condensing capacity as a function of altitude and Mach No. (see Figure 7). Note that as vehicle speed increases, condensing capacity increases until a peak value is reached and then capacity decreases. The cooling air flow rate and the heat transfer coefficient both increase with increasing Mach No. but the cooling air temperature also increases. As speed increases beyond the peak value, the benefit of higher air flow is not sufficient to offset the rising temperature. At higher altitudes the base ambient temperature is lower which is beneficial but this tends to be offset by the lower density. It can be seen on both Figures 5 and 6 that the maximum capacity of a given heat exchanger for the altitudes studied occurs at 30,000 ft.

DS #294

FUEL CELL CONDENSER

TABLE I

Air Side Fin Description		Frontal Area $ft.^2$	Air Flow Length in.	Core Weight lbs.
Plain Straight	22 fins/inch	17.9	8.22	653
Slotted Straight	22 fins/inch	22.5	5.62	561
Ruffled	22 fins/inch	23.1	4.35	443
Ruffled	18 fins/inch	22.5	5.07	465
Ruffled	27 fins/inch	23.8	3.66	424

All of the above cores are designed for the same air flow rate and flight condition. They use the same steam fin and are all .426 in. high on the air side.

DS #294

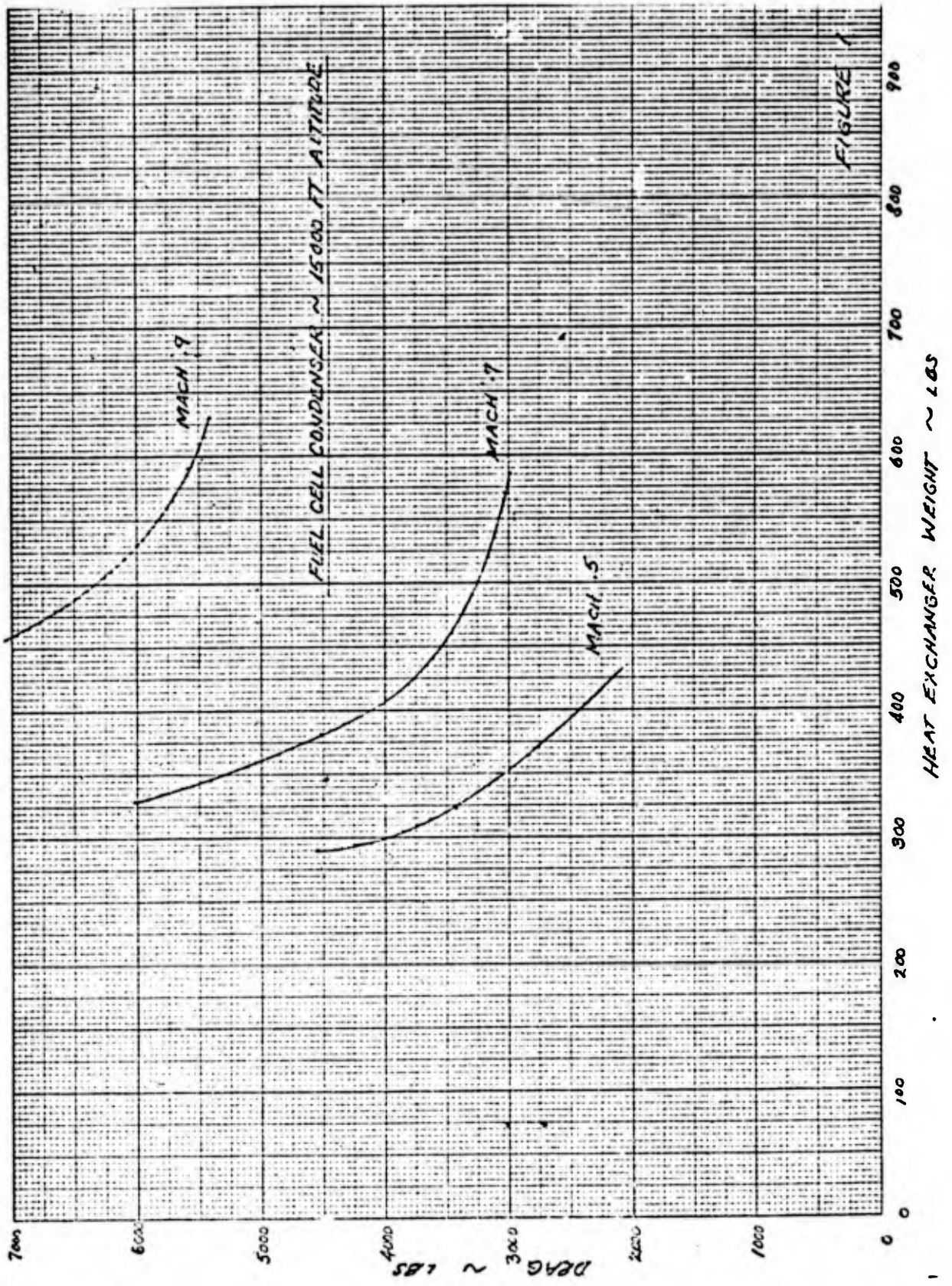

FIGURE 1

DS #294

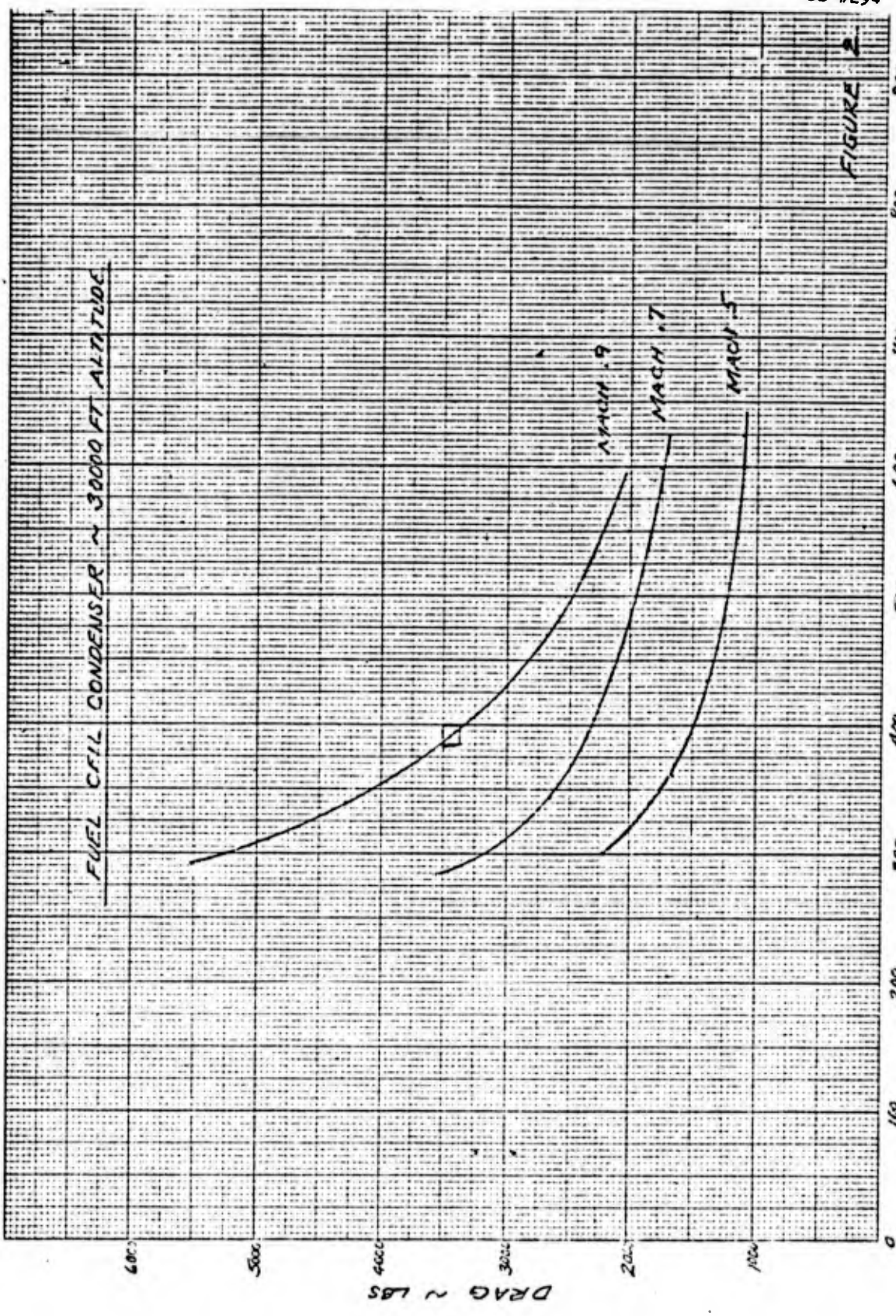

FIGURE 4

DS #294

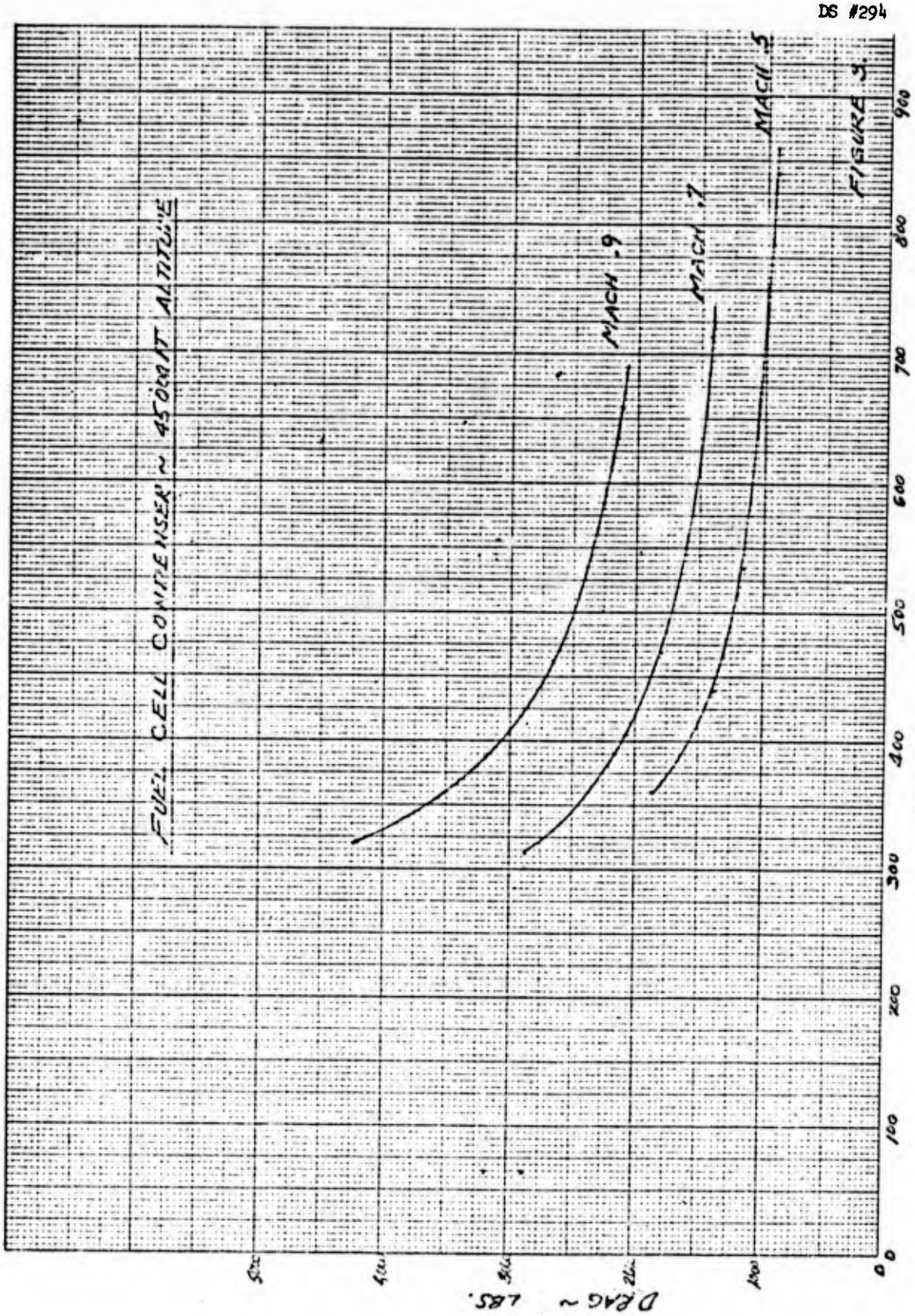

FIGURE 3.

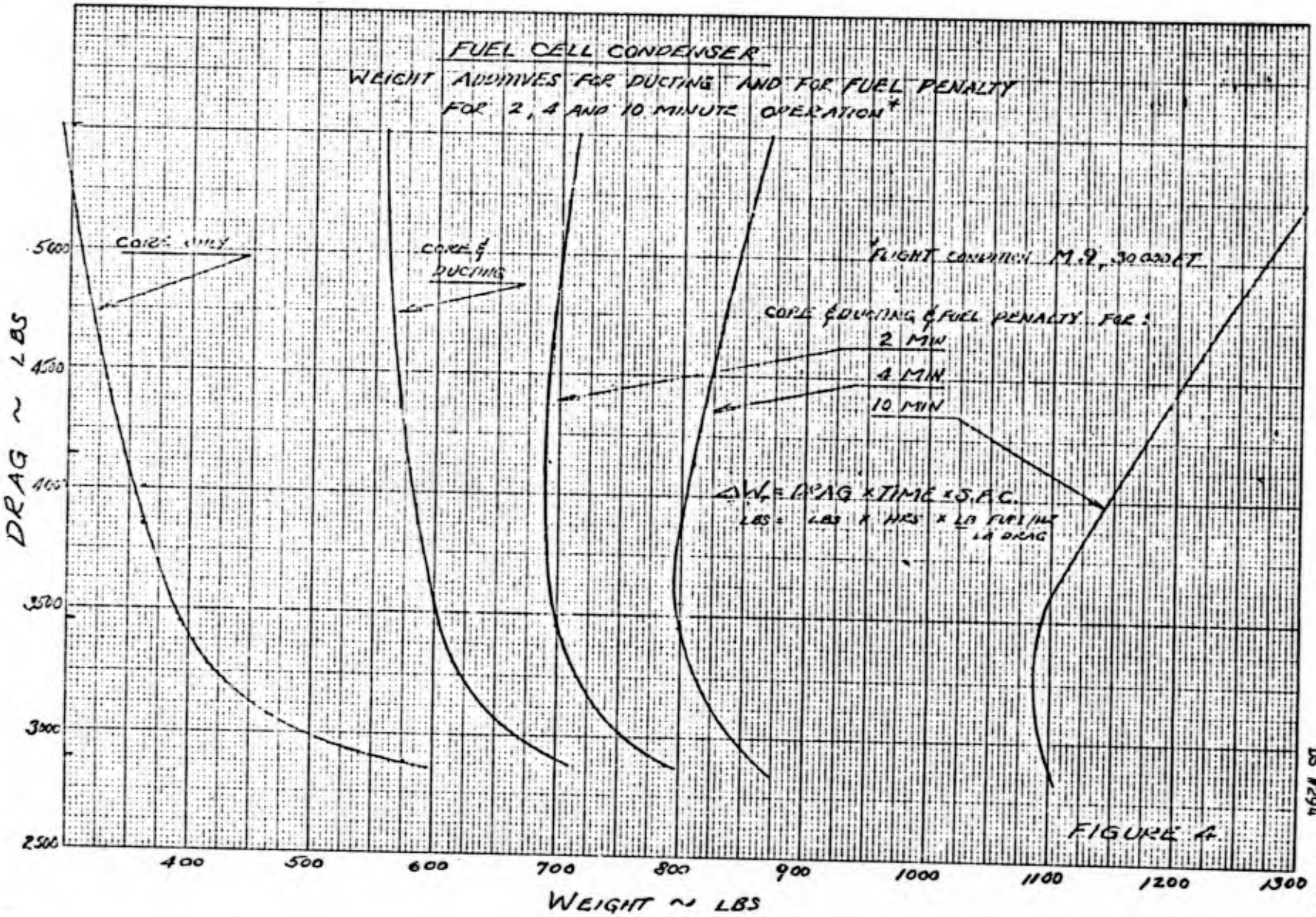
FUEL CELL CONDENSER
WEIGHT ADDITIVES FOR DUCTING AND FOR FUEL PENALTY
FOR 2, 4 AND 10 MINUTE OPERATION*
CORE ONLY
CORE & DUCTING
*FLIGHT CONDITION M.9, 30,000 FT.
CORE & DUCTING & FUEL PENALTY FOR:
2 MIN
4 MIN
10 MIN
ΔW = DRAG × TIME × S.F.C.
LBS = LBS × HRS × LB FUEL/HR / LB DRAG
DRAG ~ LBS
5000
4500
4000
3500
3000
2500
400
500
600
700
800
900
1000
1100
1200
1300
WEIGHT ~ LBS

FIGURE 4

DS #294

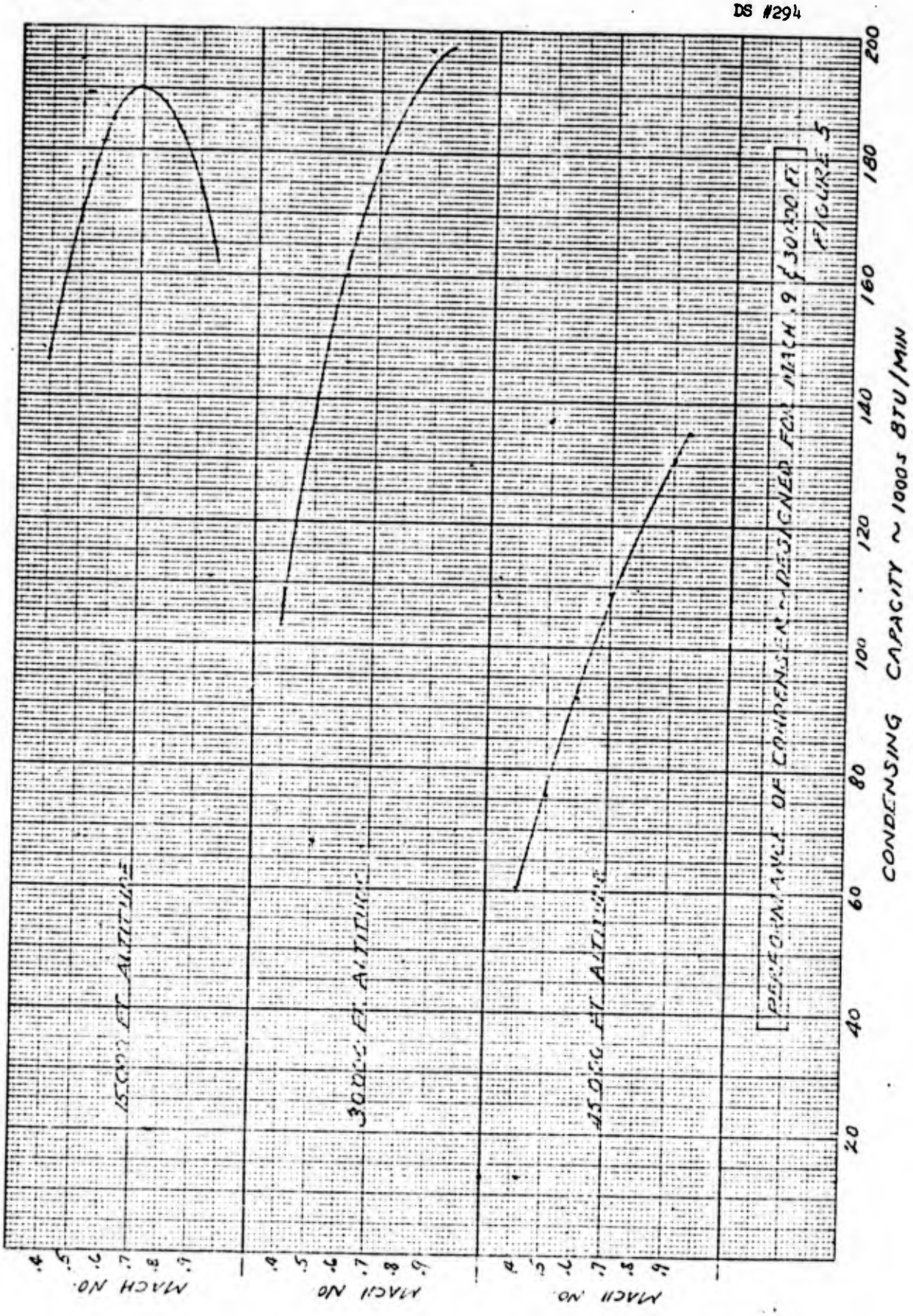
CONDENSING CAPACITY ~ 1000s BTU/MIN
200
180
160
140
120
100
80
60
40
20
PERFORMANCE OF CONDENSER DESIGNED FOR MACH .9 @ 30,000 FT
FIGURE 5
15000 FT ALTITUDE
30000 FT ALTITUDE
45000 FT ALTITUDE
MACH NO.
.4 .5 .6 .7 .8 .9

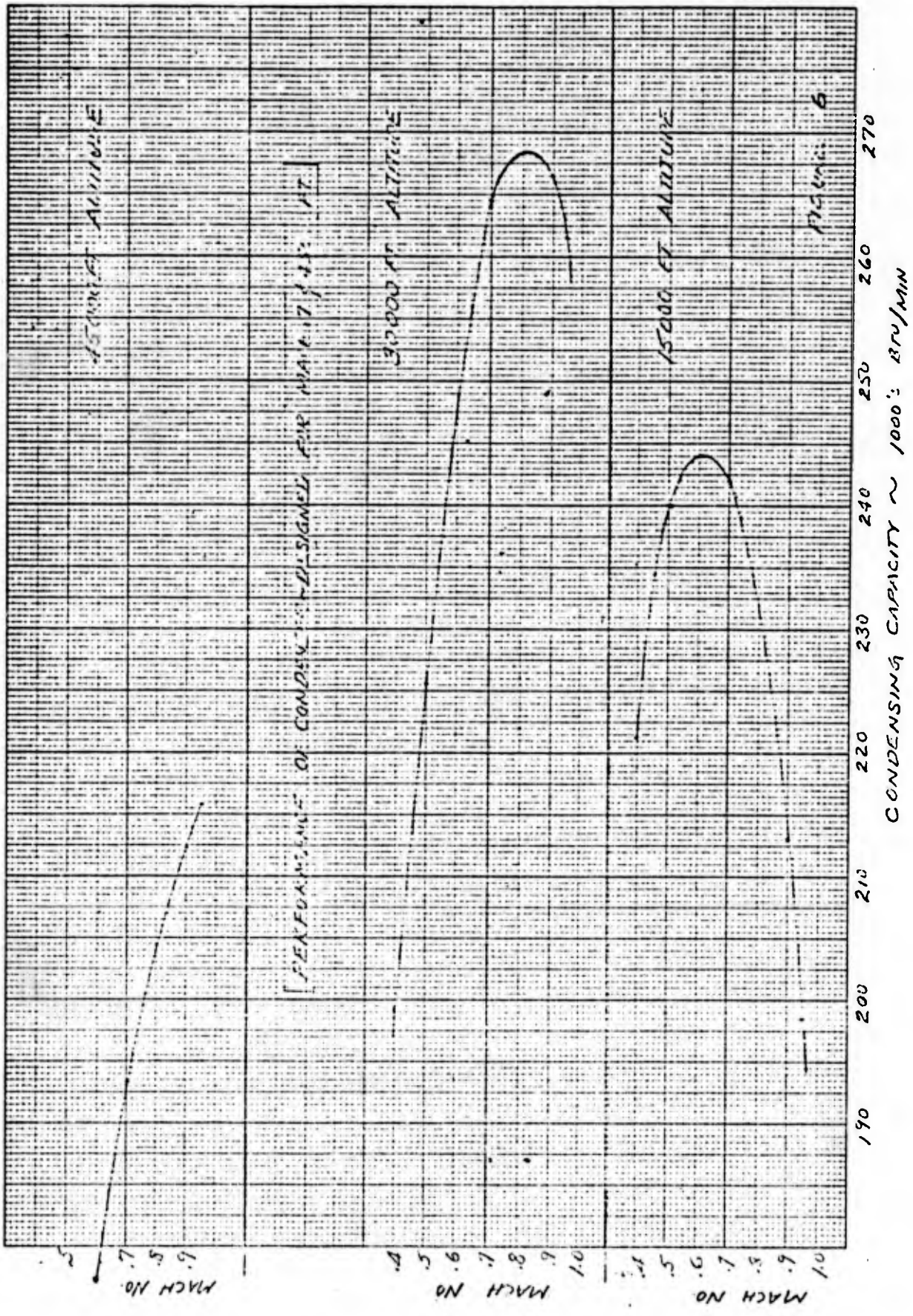
CONDENSING CAPACITY ~ 1000's #V/MIN
190
200
210
220
230
240
250
260
270
MACH NO
.4 .5 .6 .7 .8 .9 1.0
MACH NO
.4 .5 .6 .7 .8 .9 1.0
MACH NO
.5 .6 .7 .8 .9 1.0

DS #294

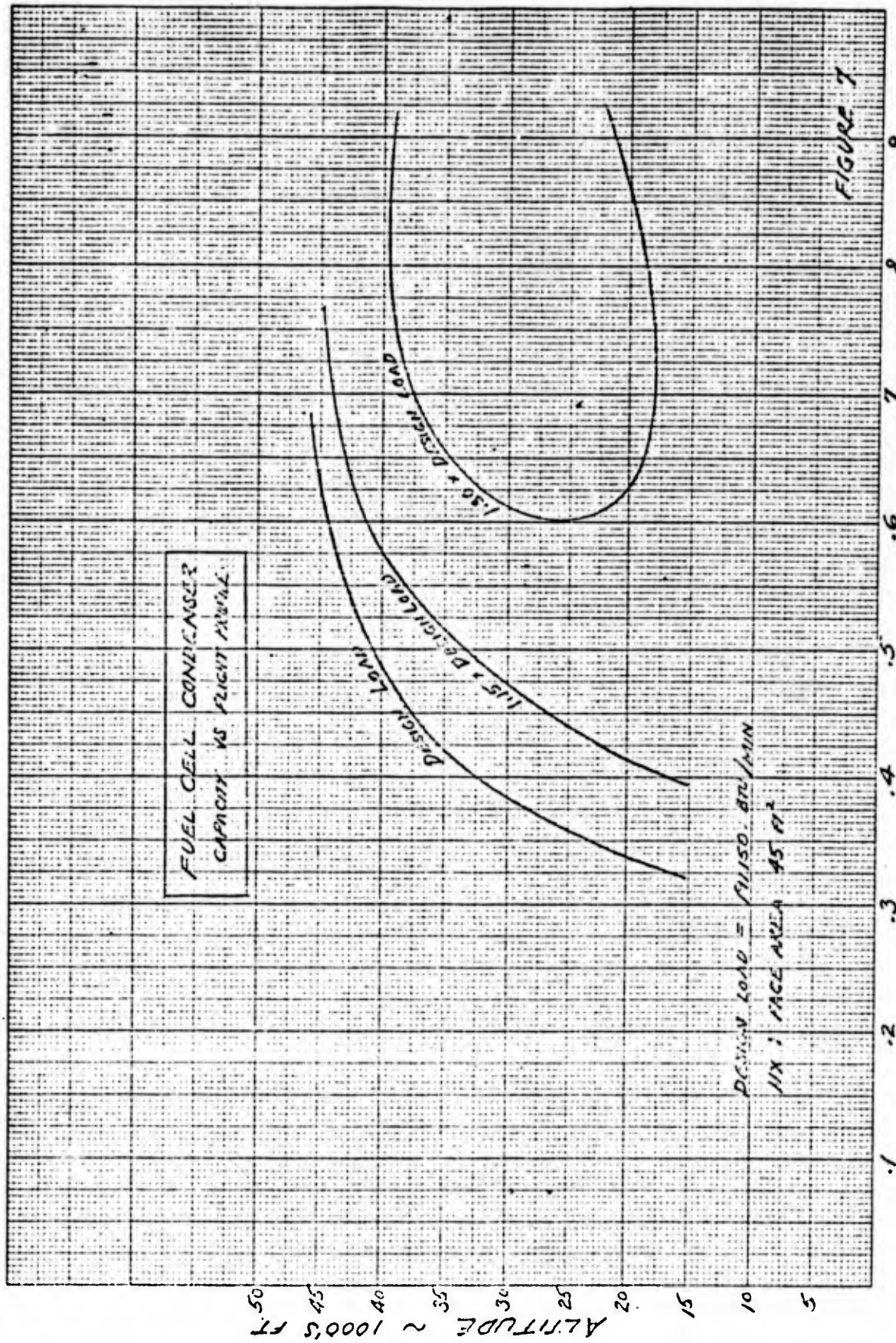

FIGURE 7

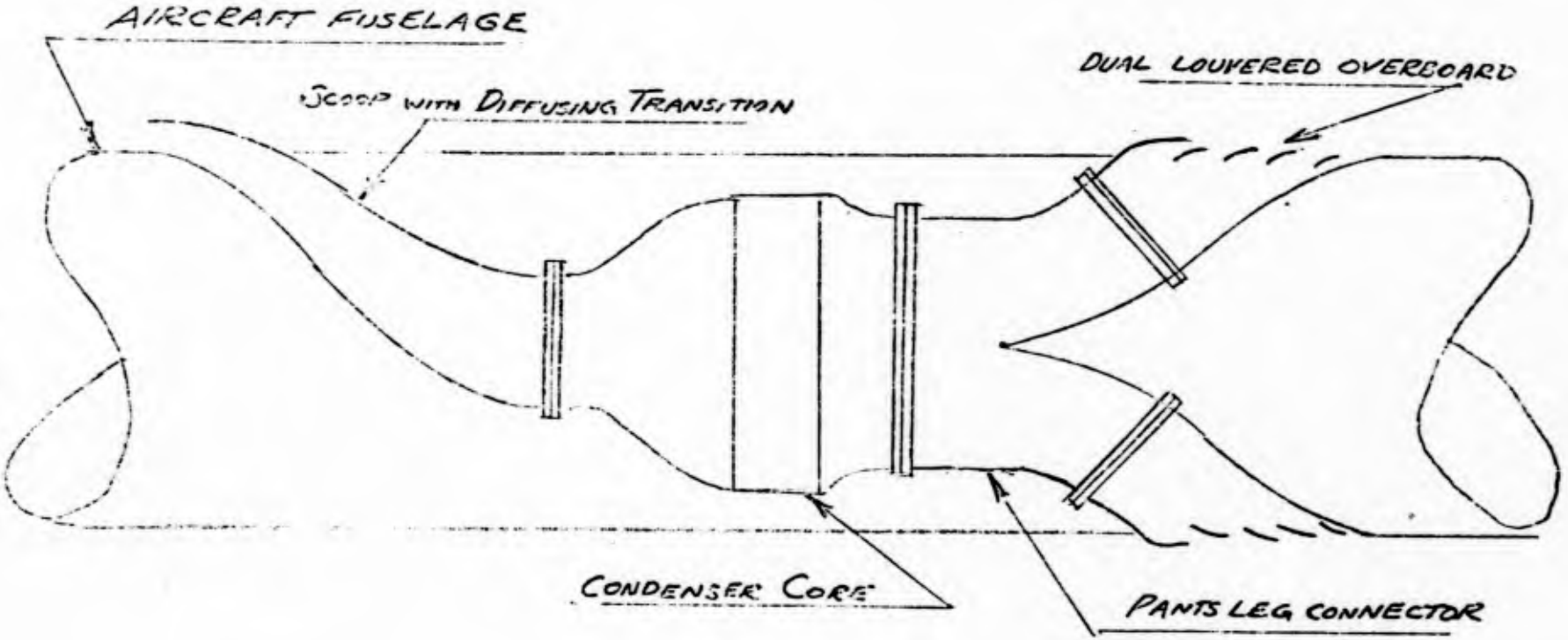

TYPICAL INSTALLATION OF CONDENSER